

Expanding the Arsenal: Development of G-Protein Receptor Kinase 5 Inhibitors Utilizing a Covalent Strategy

by

Rachel Rowlands

A dissertation submitted in partial fulfillment
of the requirements for the degree of
Doctor of Philosophy
(Medicinal Chemistry)
in The University of Michigan
2020

Doctoral Committee:

Professor John J.G. Tesmer, Purdue University, Co-Chair
Research Professor Andrew White, Co-Chair
Professor Heather Carlson
Associate Professor Jolanta Grembecka
Research Associate Professor Peter Scott

Rachel Rowlands

rowlara@umich.edu

ORCID ID: 0000-0001-7135-1447

© Rachel Rowlands 2020

ACKNOWLEDGEMENTS

The work described in this thesis would not be possible without the help of many people. First, I'd like to thank my advisors, Dr. Andrew White and Dr. John Tesmer. Andy took me into his lab as his first student at the University of Michigan and we grew together. He allowed me to learn from my mistakes, guiding me gently towards leading my own project. He has served as an incredible mentor both scientifically and personally over the past five years, and for that I am entirely grateful. John took me on as a novice and trained me to understand the biology behind my chemical campaign. Along the way, he was incredibly patient and pushed me to fight for the things I needed to be successful. I'm so grateful to have worked with two people who have encouraged me to find my own voice as a scientist and were willing to develop me into the academic I am today.

In addition to my advisors, I have to thank the other scientists who have played a role in my technical education, including the scientific staff in the Vahlteich Medicinal Chemistry Core: Dr. Kim Hutchings and Mike Wilson. Kim and Mike have been incredible resources who have not only helped me develop technical skill but created a fun and warm environment in which to learn. I also have to thank former VMCC director Dr. Scott Larsen, who allowed me to work within the core even though I wasn't his student. In short, I'm thankful to have found a truly collegiate environment in which to learn and grow as a scientist.

While advisors do hold sway over the environment, it's the students who worked beside me every day that I really have to thank for their constant encouragement. First, I have to thank the current White Group members: Jake Hitchens and Sherrice Zhang. They have provided countless laughs, jokes and good times. Finishing a PhD isn't always fun and games, but these two have made life so much easier. I also have to thank the original Larsen Lab Boys: Jeffery Zwicker, Brandt Huddle and Dylan Khal. These guys taught me everything they knew, and for that I'm grateful. If I ever missed my own brothers, these three guys were sure to take their place with countless jokes and encouragement.

From the Tesmer lab, I have to thank my close collaborators, M. Claire Cato and Renee Bouley. These ladies made my time in the Tesmer lab so much easier by either helping me sort through the frozen abyss that was the -80 °C freezer or providing a good laugh when biology had

decided not to work that day. Claire has been a great friend and collaborator helping me to write papers and wrap up biology experiments where she was several times faster than me. I also have to thank Tyler Beyett, who trained me in radiometric assays and handling of radioactive materials. Cheers for always double checking whether I was radioactive when I lost my head!

Finally, I have to thank my friends and family. To my Wine Wednesday ladies: Janice Tse, Danielle Santos, Rachel Wright, Rachelle Medhi and Stephanie Scott. You guys have listened to me complain, explain science and stress out. Thanks for the countless fun nights, good food and even better company on this crazy journey. Thanks to my parents, Dave and Anne Rowlands, who have been through every stressed-out phone call about science. Cheers, for always knowing that it would work out in the end. To my siblings, Josh Rowlands, Justin Rowlands and Emily Rowlands, sorry for the years of explaining my science at every holiday dinner or family gathering.

Table of Contents

Acknowledgments	ii
List of Tables	vii
List of Figures	viii
List of Schemes	xi
List of Abbreviations	xii
Abstract	xiv
Chapter 1: Building an Arsenal: The Need for Covalent GRK5 Inhibitors	
1.1 G Protein-Coupled Receptor Kinase 5 is involved in Multiple Disease States.....	1
1.1.1 GRK5 Plays a Dual Role in Neurodegenerative Diseases.....	1
1.1.2 GRK5 Has Been Revealed to Affect Cancer Cell Migration and Treatment Sensitivity.....	2
1.1.3 GRK5 Deficiencies Leads to Insulin Resistance.....	3
1.1.4 GRKs Have a Critical Role in Cardiovascular Diseases.....	3
1.2 Designing GRK5 Inhibitors Utilizing A Covalent Approach.....	7
1.2.1 GRK Homology and Sequence Similarity Presents Challenges for Subfamily Selectivity.....	7
1.2.2 GRK5 Structure – Annotated.....	8
1.2.3 Canonical and Non-Canonical Kinase Drug Design	9
1.3 Covalent Inhibitors Offer a New Path Towards Selective GRK5 Inhibitors.....	11
1.3.1 FDA Approved Tyrosine Kinase Inhibitors Provide a Plan for GRK5 Inhibitor Development.....	11

1.3.2	Cysteine as a Handle for Selective Covalent Inhibition.....	11
1.3.3	Other Amino Acid Handles for Covalent Inhibition.....	13
1.3.4	Reversible Covalent Inhibition is Expanding the Frontier of Covalent Kinase Drug Design.....	13
1.4	Using a Covalent Strategy GRK5 Selectivity over GRK2 Can Be Achieved.....	14
1.4.1	GRK5 Inhibitor Design Strategy.....	14
1.4.2	GRK5/6 Overlay Model Enables Rationale Design.....	16
1.4.3	Known GRK5 Inhibitors Will Serve as Initial Lead Compounds in This Campaign.....	16
1.5	Application of a Covalent Strategy May Yield Ultra Selective GRK5 Inhibitors.....	18
1.5.1	Chapter Breakdowns and Project Flow.....	18
1.6	References.....	18
Chapter 2: Structure-Based Design of Selective, Covalent G-Protein Coupled Receptor Kinase 5 Inhibitors		
2.1	Preface.....	25
2.2	Selectivity Presents a Massive Challenge for Developing GRK5 Inhibitors.....	25
2.3	Pyrrolopyrimidine Analogues can Achieve GRK5 Selectivity through Covalent Engagement	28
2.4	Initial Testing Suggests CCG-265328 Can Improve Contractility in Primary Cardiomyocytes	35
2.5	SAR is Tractable to the 5-methylpyrimidine Series but Does Not Offer Better Potency.....	37
2.6	Synthesis of Compounds.....	39
2.7	Materials, Methods and Synthetic Experimental Data.....	42
Chapter 3: Expanding the Arsenal: Virtual Screening & Validation of the Aminopyridine Scaffold		
3.1	Preface.....	83
3.2	Virtual Screening Mined New Scaffolds for GRK5 Inhibitors.....	83
3.3	Independent Synthesis of Chembl-1607632A Required Route Optimization.....	89
3.4	CCG-265649 Invalidates Chembl-1607632 Lead Compound in Radiometric Assays.....	92
3.5	Invalidation of CCG-265649 Means Abandoning the Series.....	95

3.6 Materials, Methods and Synthetic Experimental Data.....	98
3.7 References.....	113
Chapter 4: Indolinone-Based Covalent, Selective Inhibitors of GRK5	
4.1 Preface.....	117
4.2 Validation of Indolinone-Ullrich 57 Provides a New Scaffold for GRK5 Inhibitor Development.....	117
4.3 Haloketones Produce a Rapid Covalent Interaction with Cys474.....	118
4.4 Filling Lipophilicity Pockets Increases Potency, But Electronics Also Plays a Critical Role.....	123
4.5 The Stereocenter Cannot Be Replaced or Activity Will Be Lost.....	126
4.6 Tandem Mass Spectrometry Confirms Cys474 Engagement.....	128
4.7 Screening of CCG-273463 and CCG-271423 against a Kinase Panel Indicates High Selectivity for This Series.....	130
4.8 Indolinones Do Not Increase Cardiomyocyte Contractility, But They Do Alter Ca ²⁺ Flow.....	131
4.9 Concluding Thoughts on the Indolinone Series.....	133
4.10 Synthesis of Compounds.....	133
4.11 Materials, Methods and Synthetic Experimental Data.....	135
4.12 References.....	159
Chapter 5: Future Directions in the Age of Covalent GRK5 Inhibitors	
5.1 Expanding the SAR of the Indolinone Scaffold Could Offer New Insights.....	161
5.2 Combining Linkers and Covalent Warheads can Rapidly Expand the Current Arsenal.....	164
5.3 Biological Evaluation of GRK5 Inhibitors Can Clarify Role of GRK5 in Cardiovascular Disease.....	166
5.4 Biological Evaluation of GRK5 Inhibitors Can Provide New Treatments for Cancer, and Neurodegenerative Diseases.....	166
5.5 Concluding Remarks.....	167
5.6 References.....	167

List of Tables

Table 2.1 IC50 Values for Pyrrolopyrimidine Compounds.....	29
Table 2.2 IC50 Values for the 5-Methylpyrimidine and Alternative Pyrrolopyrimidine Compounds.....	37
Table 3.1 IC50 Values for Aminopyridine Route Development Compounds.....	92
Table 3.2 IC50 Values for Aminopyridine Compounds.....	93
Table 4.1 IC50 Values for Indolinones With Various Warheads.....	119
Table 4.2 Expanded SAR for Indolinone Series.....	124
Table 4.3 Thermodynamic Solubility of Indolinone Series Analogues.....	126

List of Figures

Figure 1.1 Renin Aldosterone Angiotensin System (RAAS) that happens in response to a drop in blood pressure.....	4
Figure 1.2 Simplified diagram of GPCR desensitization.....	6
Figure 1.3 Sequence homology of the 7 mammalian GRKs, divided by subfamily	8
Figure 1.4 Annotated structure of GRK5 (cyan) shown with CCG-215022 (orange carbons) bound to the active site.....	9
Figure 1.5 Structures of FDA approved covalent TKIs.....	11
Figure 1.6 Selected cysteine targeting covalent modifiers, arranged by reactivity to nucleophiles	12
Figure 1.7 Selected set of lysine (nitrogen) targeting covalent warheads.....	13
Figure 1.8 Selected set of reversible covalent warheads.....	13
Figure 1.9 Cysteine Map, developed from the GRK5 structure (PDB: 4WNK).....	15
Figure 1.10 GRK5 (blue)/GRK6(purple) overlay model with CCG-215022 bound to GRK5 shown in dark blue.....	16
Figure 1.11 Current leads with known GRK2 or GRK5 activity.....	17
Figure 2.1 GSK2163632A and related compounds suggest a route to selective inhibition of GRK5 via covalent modification of Cys474.....	27
Figure 2.2 Time-dependent inhibition of GRK5 by CCG-265328 and CCG-265507 but not CCG-215022.....	31
Figure 2.3 Evidence from intact mass spectrometry for covalent modification of GRK5 by CCG-258903, CCG-264099, and CCG-265328.....	32
Figure 2.4 MS traces for (a) CCG-265041, (b) CCG-265042, (c) CCG-265044, (d) CCG-265267 and (e) CCG-265268 indicate that no meta-substituted material can make a covalent interaction with GRK5.....	33
Figure 2.5 Evidence for GRK5-Cys474 covalent engagement of CCG-265328.....	34
Figure 2.6 GRK5 (gold) with CCG-265328 (pink) bound to the hinge.....	35

Figure 2.7 CCG-265328 can produce similar contractility improvements to that seen with paroxetine in primary cardiomyocytes following isoproterenol (100 nM) induced TAC.....	36
Figure 2.8 Tandem MS/MS data for CCG-265507 indicates that Cys474 is tagged and detected in multiple peptide fragments.....	38
Figure 3.1 Overlay model of GRK5 (blue) and GRK6 (purple). Cys474, located on the AST loop is highlighted in green.....	85
Figure 3.2 Screening funnel used for compilation, filtering and screening of in silico library of enriched compounds.....	86
Figure 3.3 Binding mode for CCG-215022 as seen when crystallized with GRK5 (PDB: 4WNK)	87
Figure 3.4 Lead compound Chembl-1607632 bound to GRK5 (blue)/GRK6 (purple) overlay model.....	88
Figure 3.5 Intact protein mass spectrometry of CCG-265649 (coral), and CCG-265175 (lavender).....	94
Figure 3.6 Alternate binding mode for CCG-270964 (gray) bound to the GRK5(blue)/GRK6 (purple) homology model	95
Figure 3.7 Alternate binding mode for CCG-265649 (orange) shown with the lipophilic pocket of GRK5 (blue).....	96
Figure 3.8 Electrostatic map shown for alternate binding mode of CCG-265649 shown in blue and red	97
Figure 4.1 Intact protein MS for original warheads	120
Figure 4.2 Intact protein MS for haloketones. CCG-273220 (purple) shows labelling in 30 mins.....	122
Figure 4.3 Electrostatic map comparison between GRK5 (Blue) and CCG-273442 (Gold carbons).....	125
Figure 4.4 CCG-273220 (gold carbons) docked into the GRK5 (blue)/GRK6 (purple) model.....	127
Figure 4.5 Tandem MS data shown in the table above indicates that Cys474 is the most predominantly labeled cysteine	128
Figure 4.6 Intact MS of GRK5 and GRK5-C474S with CCG-273220.....	129

Figure 4.7 Kinase selectivity panel for CCG-271423 and CCG-273463.....	130
Figure 4.8 Fractional shortening of cardiomyocytes, both without and with an isoproterenol challenge	132
Figure 5.1 Design analogues which demonstrate a combined strategy for blocking metabolism and maintaining high levels of affinity for GRK5.....	161
Figure 5.2 Pseudo-seven membered ring shown in the structure on the left	162
Figure 5.3 Reversible covalent inhibitor, CCG-273240, and designed analogues.....	163
Figure 5.4 New analogues which possess a linker with a covalent element already in place...	164
Figure 5.5 New enamine and sulfone warheads could be used to explore how to tune reactivity of a covalent warhead.....	165

List of Schemes

Scheme 2.1 Synthetic route to CCG-264099-265328.....	39
Scheme 2.2 Synthetic route to CCG-265041-265268.	40
Scheme 2.3 Synthetic route to CCG-265507 and CCG-265508.....	41
Scheme 2.4 Synthetic route to CCG-265647 and CCG-265648.....	41
Scheme 2.5 Synthesis of non-homologated <i>para</i> -substituted analogues 10 and 11	44
Scheme 2.6 Synthesis of non-homologated <i>meta</i> -substituted analogues	47
Scheme 2.7 Synthesis of saturated analogs 22 and 23	49
Scheme 2.8. Synthetic route to <i>para</i> substituted homologated probes, 33-37	52
Scheme 2.9. Synthetic route for <i>meta</i> homologated compounds 45-49	62
Scheme 3.1 Original synthetic route proposed for Chembl-1607632A (109) and related compounds.....	89
Scheme 3.2 Optimized synthetic route to CCG-265649	91
Scheme 3.3. Original synthetic route to CCG-265649.....	100
Scheme 3.4 Synthetic route to lead compound 109	103
Scheme 3.5. Synthesis of other final compounds using the optimized route.....	106
Scheme 4.1 Synthetic route to CCG-271421-CCG-271442	134
Scheme 4.2 Synthesis of CCG-273180-CCG-359090	134
Scheme 4.3 Synthetic route to indolone materials	136
Scheme 4.4. Synthesis of compound 143-147.....	141

List of Abbreviations

G Protein-Coupled Receptor	GPCR
G Protein-Coupled Receptor Kinase	GRK
Alzheimer's Disease	AD
Parkinson's Disease	PD
Lewis Bodies	LBs
Alpha-synuclein	α -syn
Sporadic Parkinson's Disease	sPD
Casein Kinase	CK
Receptor Tyrosine Kinase	RTK
Receptor Tyrosine Kinase Inhibitor	RTKIs
Triple Negative Breast Cancer	TNBC
GRK5 Knockout	GRK5KO
Histone Deacetylase 6	HDAC6
Sodium-Glucose Co-Transporter 2	SLGT2
Glucagon Like Peptide 1	GLP1
Federal Drug Administration	FDA
Heart Failure	HF
Cardiovascular Diseases	CVDs
American Heart Association	AHA
Angiotensin II Converting Enzyme Inhibitors	ACE Inhibitors
Beta Blockers	β blockers
Renin-Angiotensin-Aldosterone Secretion	RAAS
Myocyte Enhancer Factor 2	MEF2
Adenosine Triphosphate	ATP
Adenosine Diphosphate	ADP
Active Site Tether	AST
Tyrosine Kinase Inhibitors	TKIs

Burton's Tyrosine Kinase	BTK
Epidermal Growth Factor Receptor	EGFR
QT Interval	QT
Hard-Soft Acid-Base Theory	HSAB
Protein Database	PDB
GRK5 Mutant Type Cys474Ser	GRK5-C474S
Tandem Mass Spectrometry	MS/MS
Center for Chemical Genomics	CCG
Transverse Aortic Constriction	TAC
Solubility Forecast Index	SFI
High Throughput Screening	HTS
Pan Assay Interference Compounds	PAINS
Intact Protein Mass Spectrometry	MS
Structure Activity Relationship	SAR
Dimethyl Sulfoxide	DMSO
Targeted Covalent Inhibitors	TCIs
Nucleophilic Aromatic Substitution	SNAr
Platelet-Derived Growth Factor Receptor	PDGFR
Vascular Endothelial Growth Factor Receptor	VEGFR

ABSTRACT

Many cellular events are regulated by G-protein coupled receptors (GPCRs). In order to maintain homeostasis, GPCR kinases (GRKs) selectively recognize and phosphorylate activated GPCRs for internalization. There is growing evidence that both GRK2 and GRK5 have roles in pathological heart failure. Previous work has demonstrated that targeting GRK2 can reduce the amount of receptor desensitization that occurs in cardiomyocytes and increase cardiac output. However, the close homologue GRK5 is equally well expressed in cardiac tissue. Herein, we describe our efforts toward developing selective GRK5 inhibitors using covalent engagement of a non-conserved cysteine to elucidate the role of GRK5 in cardiovascular diseases.

Initially, we had identified a lead compound with a pyrrolopyrimidine scaffold (**GSK2163632**) from the GSK Published Kinase Inhibitor Set that had modest potency for GRK5 and GRK2. Due to the similarity of the hinge region and binding pockets of GRK2 and GRK5, an approach towards building out GRK2 activity had to be based upon non-conserved residues such as Cys474. We used this approach to build covalent, and thereby selective, GRK5 inhibitors. Our initial designs allowed us to identify one strongly covalent inhibitor based on the pyrrolopyrimidine scaffold (**CCG-265328**) which features a weak electrophile and has 90-fold selectivity for GRK5 over GRK2. Previously, engagement of Cys474 was confirmed through tandem MS/MS, suggesting that this covalent interaction is driving selectivity. Structure-activity relationships (SAR) also revealed that linker length and degrees of freedom had less of an effect on covalent engagement than the reactivity of the electrophilic warhead. Additionally, SAR revealed that without a warhead, the modified pyrrolopyrimidine scaffold (**CCG-264561**) had only modest potency.

We tried to improve potency through exploration of two separate scaffolds mined from a virtual screen and the literature respectively. From a virtual screen an aminopyridine compound (ChEMBL-1607632) was independently synthesized and a few analogues were created. We discovered that this scaffold was unviable due to both poor potency ($> 1 \mu\text{M}$) and untransferable SAR.

However, the indolinone scaffold derived from the literature proved a much more tractable option, with low nanomolar potency for the independently synthesized reference compound (**CCG-271421**). Interestingly, the warhead SAR developed in the pyrrolopyrimidine scaffold proved to be intractable. Indeed, the most reactive warheads, the haloketones (**CCG-273220**, **CCG-273463**) were considerably more potent and selective than the pyrrolopyrimidines (**CCG-265328**). In fact, the haloketones (**CCG-273441**) proved to be the most potent and selective covalent GRK5 inhibitors ($IC_{50} = 3.8$ nM, 1300-fold selective over GRK2) to date. Thus, we have demonstrated through development of the pyrrolopyrimidine series (**CCG-265328**) that Cys474 can serve as a covalent handle to convey high levels of selectivity through covalent engagement with a warhead and that this covalent strategy is transferable to different scaffolds known in kinase drug discovery, provided these scaffolds have sufficient inherent potency.

Chapter 1: Building an Arsenal: The Need for Covalent GRK5 Inhibitors

1.1 G Protein-Coupled Receptor Kinase 5 (GRK5) is Involved in Multiple Disease States

G protein-coupled receptor kinases (GRKs) play a crucial role in cellular homeostasis, due to their ability to regulate G protein coupled receptor (GPCR) signaling. Given the importance of their functions, GRKs are often investigated in multiple clinically relevant disease states, such as neurodegenerative disorders, various cancers, diabetes, and cardiovascular diseases.

1.1.1 GRK5 Plays a Dual Role in Neurodegenerative Diseases

G Protein-Coupled Receptor Kinase 5 (GRK5) has been traditionally studied within cardiovascular diseases. However, there is growing evidence the GRK5 is involved in neurodegenerative disorders, such as Alzheimer's Disease (AD) and Parkinson's Disease (PD).

Parkinson's Disease (PD) has hallmark symptoms including involuntary muscular contractions (tremors) and non-motor associated symptoms such as cognitive impairment.¹ Cognitive impairment in PD is associated with increased morbidity and mortality across patient samples.² The pathological process of PD has been linked to development of dementia over time as patients experience degeneration of the basal forebrain cholinergic nuclei, degeneration of the brainstem dopaminergic neurons and the presence of cortical Lewis bodies (LBs).³ Deposition of LBs is strongly associated with α -synuclein (α Syn). α Syn is a soluble protein localized at the presynaptic terminals within the nervous system.^{4,5} Phosphorylation of α Syn at Serine 129 (Ser129) has been identified as an essential step in producing a toxic environment for dopaminergic neurons and leads to aggregation of the protein and eventual deposition of LBs.. This series of events is key to the pathogenesis of sporadic PD (sPD). It has been reported that casein kinase 1 (CK1), CK2 and GRKs can control this event. Of the GRKs, GRK5 has been identified as one of the kinases .

Thus, GRK5 inhibition thereby eliminates the phosphorylation of α Syn which may present a new path towards PD treatment.

Similar to PD, Alzheimer's Disease (AD) is a neurodegenerative disorder characterized by degeneration of neurons leading to progressive memory loss. However, AD is not associated with muscular tremors or loss of muscular tone. Given that the mechanisms which trigger this disorder are complex, treatments which target the underlying mechanisms of AD are rare. However, some of the underlying mechanism is understood. For example, GRK5 has been identified as the kinase responsible for regulating the desensitization of the M2/M4 receptors.⁶

However, it may not be advantageous to target GRK5 as an AD treatment. Recent studies have shown that reduced membrane bound GRK5 increases soluble β -amyloid *in vitro*.^{7,8} Studies have also shown that GRK5 dysfunction mediates tau hyperphosphorylation, leading to accumulation of neurofibrillary tangles within the hippocampus.^{9,10} Taken together, these studies suggest that GRK5 could be an attractive target for PD. However, this path should be approached with caution as its positive effects do not extend to AD.

1.1.2 GRK5 Has Been Revealed to Affect Cancer Cell Migration and Treatment Sensitivity

Various cancers have been some of the hottest targets within the pharmaceutical field for the past twenty years, since the release of the blockbuster drug Gleevec in 2001. Given the rise of drug resistance there is an urgent need to validate new targets and develop new therapeutic agents.

Unsurprisingly, the GRKs have recently become interesting targets for decreasing tumorigenesis and metastasis due to their ability to regulate cellular signaling pathways in a similar fashion to the receptor tyrosine kinases (RTKs). Given the complexity of each system, the exact effect of altering GRK functions must be determined on a case-by-case basis.^{11,12}

Fortunately, there are some RTK inhibitors (RTKIs) which are also active against the GRKs. For example, Sunitinib, a FDA approved RTKI for use in cancer, has been shown to be active against GRK5.¹³ Recent studies have shown that when Sunitinib is used to inhibit GRK5 in triple negative breast cancer (TNBC) cells, lack of GRK5 function limits the migration of TNBC cells to unaffected areas.¹⁴ Such efforts illustrate that GRK5 inhibitors could be used to limit the progression of the cancer. This indirect effect on breast cancer cells extends to more than just metastasis.

In a separate study, GRK5 was studied for its ability to restore potency to Paclitaxel, a frontline cancer treatment, in drug resistant TNBC (MDA-MB-231) cells. GRK5 knockouts

(GRK5KO) were created and then treated with Paclitaxel whereby the cells were shown to have a susceptibility to treatment. This sensitivity to treatment is associated with increased levels of cellular acetylated α -tubulin thereby increasing sensitivity of the TNBC cells to the apoptotic effects of Paclitaxel. Increases in α -tubulin have been linked to decreased histone deacetylase 6 (HDAC6) activity, thus providing evidence that decreases in HDAC6 activity may be key to sensitizing drug resistant TNBC cells to treatment. As GRK5 is known to phosphorylate HDAC5 and HDAC6, there is evidence that GRK5 could be an interesting upstream target to control sensitization of TNBC cells to frontline treatments.¹⁵ Taken together, this evidence suggests that selective GRK5 inhibitors could be effective in multiple combination therapies.

1.1.3 GRK5 Deficiencies Leads to Insulin Resistance

Diabetes is a metabolic disorder that induces hyperglycemia from defects in insulin release or insulin action. Due to complex factors (socio-economic status, genetic pre-disposition, and environment to name a few), this disorder has risen in prevalence worldwide. Experts attribute this public health crisis with the rise of obesity over the past 30 years.^{16,17} While obesity and diabetes are intimately linked, canonical pharmacological efforts to combat obesity have largely been ineffective. However, there is a thriving industry for new diabetes drugs, as long term exposure to second-generation diabetes medications has been linked to a higher risk for cardiovascular events.¹⁸ Other drugs, as part of the fourth-generation of the diabetes arsenal are known to target either the sodium-glucose co-transporter 2 (SLGT2) or glucagon-like peptide 1 (GLP1). Examples approved by the FDA include empagliflozin and liraglutide for use in diabetes patients to reduce cardiovascular risk.¹⁹ Thus, there is an urgent need for a new generation of diabetes drugs which can also treat co-morbid cardiovascular diseases.

Ullrich and coworkers have described a GRK5 inhibitor that has been shown to increase insulin release, thereby providing treatment of diabetes.¹³ As GRK5 is one of the protein kinases known to be highly expressed in cardiovascular tissues and is thought to control cardiomyocyte contractility, this study provides a possible new avenue to treating these two co-morbidities concurrently.

1.1.4 GRKs Have a Critical Role in Cardiovascular Diseases

Cardiovascular disease is the leading cause of death among men and women within the United States.²⁰ Of those effected by cardiovascular disease, about 6.1 million have a type of cardiomyopathy and 6.2 million over the age of 20 years old have heart failure (HF) according to

the American Heart Association.²¹ Indeed, roughly 46% of the adult population have hypertension and 38.2% have high cholesterol, both of which indicate an increased risk for developing more serious CVDs such as heart failure. Currently, there are around 915,000 new cases of heart failure diagnosed each year, according to a 2019 AHA survey.^{21,22} Given these statistics, there is an incredible need to update the current strategies used to treat cardiovascular disease.

Current treatments for HF commonly include the use of angiotensin II converting enzyme

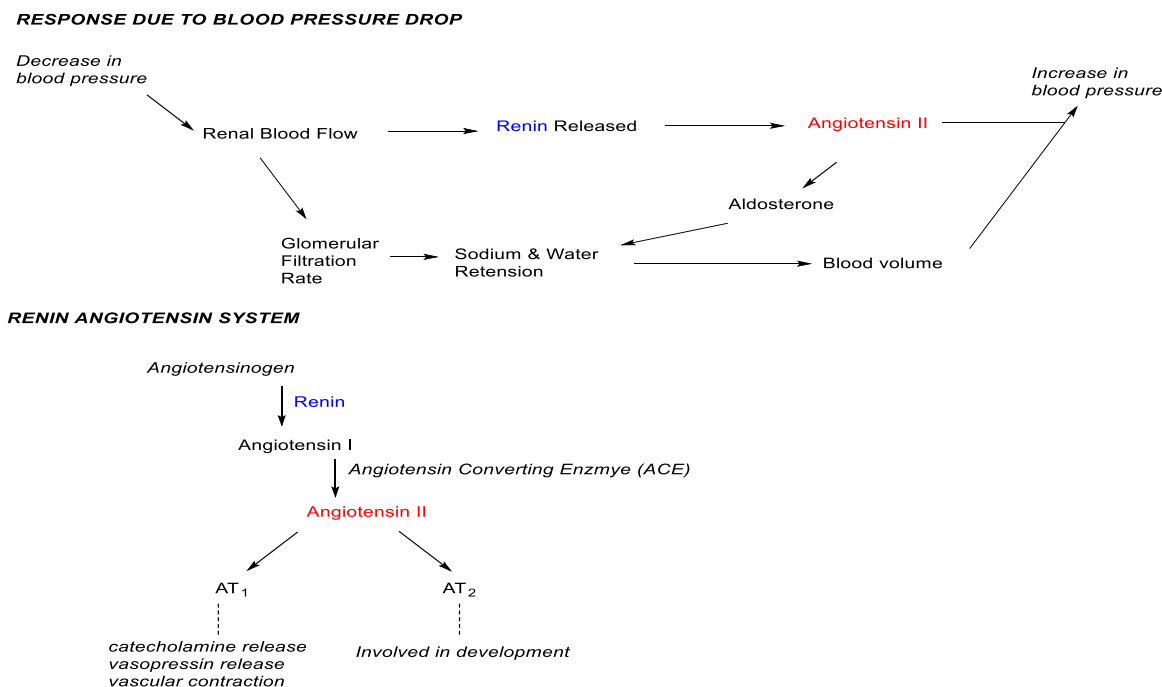


Figure 1.1 Renin Aldosterone Angiotensin system (RAAS) that happens in response to a drop in blood pressure.

inhibitors (ACE inhibitors) and beta blockers (β -blockers). These treatments options are effective for HF management; however, they do not address the underlying mechanism that cause progressive HF. ACE inhibitors work by acting within the Renin-Angiotensin-Aldosterone Secretion (RAAS) system that controls blood pressure. When a drop in blood pressure occurs, the RAAS system triggers a release in renin, which in turn causes ACE to convert Angiotensin I to Angiotensin II. Angiotensin II then goes on to trigger the release of vasopressin causing a restriction of the vasculature and subsequent increase in blood pressure. Thus, ACE inhibitors alter blood pressure by avoiding the release of vassopressins, however, this class of compounds do not counteract underlying contractile dysfunctions, which are key to progressive HF (Figure 1.1).²³

In a properly functioning heart, cardiac performance increases as preload increases. Preloading, as measured by left ventricular pressure is linked to cardiac performance (measured as cardiac output) by the Frank-Starling Law.^{24,25} In HF, the heart can no longer access the proper Frank-Starling mechanism. Instead, at preload, the left ventricle stroke volume is lower than the level observed in a normal functioning left ventricle leading to incomplete ventricular emptying. Consequentially, this residual volume leads to progressive stretching of the myocardial fibers of the left ventricle. As this cycle continues, the volume preloaded for each successive stroke is higher in order to preserve cardiac output. Thus, the muscle workers harder meanwhile the left ventricle fibers continue to stretch until the heart can no longer pump enough volume to maintain cardiac output.^{24,26} Therefore, to break this cycle of progressive ventricularly weakening would be an effective way to treat the underlying mechanism of HF and possibly help to strengthen the stretched left ventricle wall.

Currently, there is a series of compounds, GRK2 inhibitors, which are known to increase cardiomyocyte contractility in this manner that could be used to strengthen the weakened left ventricle wall. Waldschmidt et. al. were able to show that GRK2 inhibitors, such as CCG-215022, can increase cardiomyocyte contractility following a treatment with isoproterenol.^{27,28} This study indicates that GRKs, which are involved in signal mediation within cardiomyocytes, are

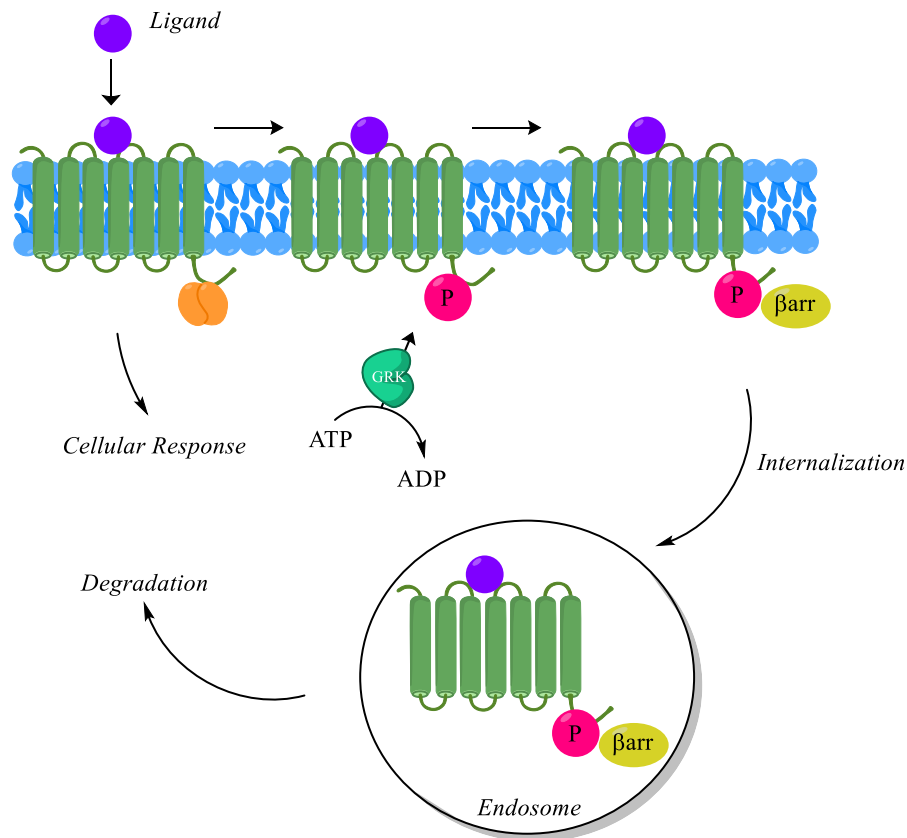


Figure 1.2 Simplified diagram of GPCR desensitization. Catecholamines (purple) bind the GPCR (green), causing the release of the heterotrimeric g-protein complex (orange) thereby inducing cellular signaling. The free GPCR tail is then phosphorylated by GRK2 or GRK5 (lime) (4 phosphates shown here as one ball for simplicity, pink). The phosphorylated GPCR then recruits arrestins (yellow) causing endocytosis. Once endocytosed, the GPCR is then degraded, and therefore removed from the cellular surface.

potentially potent targets for next generation of cardiovascular treatments.

Of the seven known GRKs, GRK2/3 and GRK5/6 are the most ubiquitously expressed, with GRK2 and GRK5 being the most highly expressed within cardiovascular tissues. GRK2 and GRK5 are known to phosphorylate the free C-terminal tail of G protein-coupled receptors (GPCRs) within cardiomyocytes. Cardiac GPCRs are activated by circulating catecholamines (norepinephrine and epinephrine), which causes the release of the heterotrimeric G-protein complex, thereby inducing signal amplification. The free tail of the GPCR is then phosphorylated

by GRK2 or GRK5 triggering the recruitment of arrestins from the cytoplasm that promote receptor endocytosis. Once internalized, GPCRs can either be recycled back to the cellular membrane or degraded. In the case of HF, GPCRs tend to be degraded effectively lowering the number of receptors at the cell surface. A lack of receptors at the cell surface in turn leads to an increase in endogenous ligands (catecholamines) to result in maintained cardiac output (Figure 1.2).²⁹

The work done by Waldschmidt et. al. indicate that by targeting GRK2, cardiac contractility can be improved over time to restore ventricular function.^{27,28,30} However, there is a lack of knowledge as to the exact role of GRK5 within the cardiovascular system. GRK5 is known to act in a similar fashion to GRK2, phosphorylating GPCRs during desensitization. However, GRK5 is unique in that it can use a nuclear translocation domain to cross the nuclear membrane. Once inside the nucleus, GRK5 phosphorylates HDAC5 initiating the transcription of hypertrophic genes through myocyte enhancer factor 2 (MEF2). Thus, GRK5 is implicated in both progressive HF and hypertrophic cardiomyopathy.³¹

Given the role of GRK5 in multiple CVDs, development of a selective GRK5 inhibitor is of interest. Waldschmidt et. al. have tried to create GRK5 inhibitors with limited success. It was shown that GRK5 activity can easily be built out of GRK2 inhibitor scaffolds as GRK5 has a narrow and unaccommodating active site. For this reason, GRK2 activity has been a major block to developing GRK5 selective inhibitors. Canonical structure-based design efforts have failed to produce a truly GRK5 selective inhibitor. Therefore, a new approach is needed to create an arsenal of GRK5 selective inhibitors.

1.2 Designing GRK5 Inhibitors Utilizing A Covalent Approach

1.2.1 GRK Homology and Sequence Similarity Presents Challenges for Subfamily Selectivity

The seven mammalian GRKs are split into three distinct subfamilies. The GRK1 subfamily consists of GRK1 and GRK7, both of which are primarily expressed in ocular tissue. The GRK2 subfamily, also known as the β -adrenergic receptor kinases, consists of GRK2 and GRK3, both of which are expressed ubiquitously. Finally, the GRK4 subfamily consists of GRK4, GRK5 and GRK6. Of these three kinases, GRK5 and GRK6 are expressed ubiquitously, while GRK4 is expressed primarily in sexual organs.³² GRK2 and GRK5 are the most highly expressed GRKs in cardiovascular tissues.³³ Overall, the GRKs are highly similar, with a conserved structural core consisting of the RH domain and the kinase domain. The two domains work in tandem to phosphorylate GPCRs. The RH domain maintains the small lobe of the kinase domain in a state

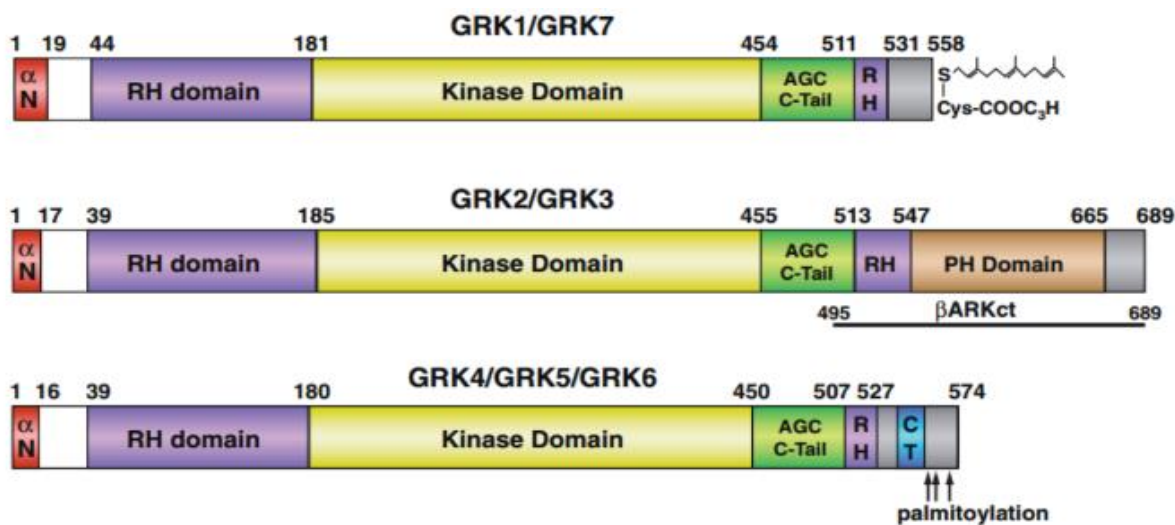


Figure 1.3 Sequence homology of the 7 mammalian GRKs, divided by subfamily.³⁴

that allows phosphorylation by the kinase domain (Figure 1.3, reprinted with permission from Science Direct).³⁴ The kinase domain itself contains the ATP binding pocket whereupon binding ATP, a phosphate can be transferred to the GPCR tail and ADP is released as a product. The C-terminal extension of the GRKs, characteristic of AGC kinases, are variable but these elements are thought to regulate kinase activity in a manner similar to other AGC kinases.^{35,36} Kinase inhibition efforts generally focus on the inhibition of the orthosteric active site (kinase domain).

1.2.2 GRK5 Structure – Annotated

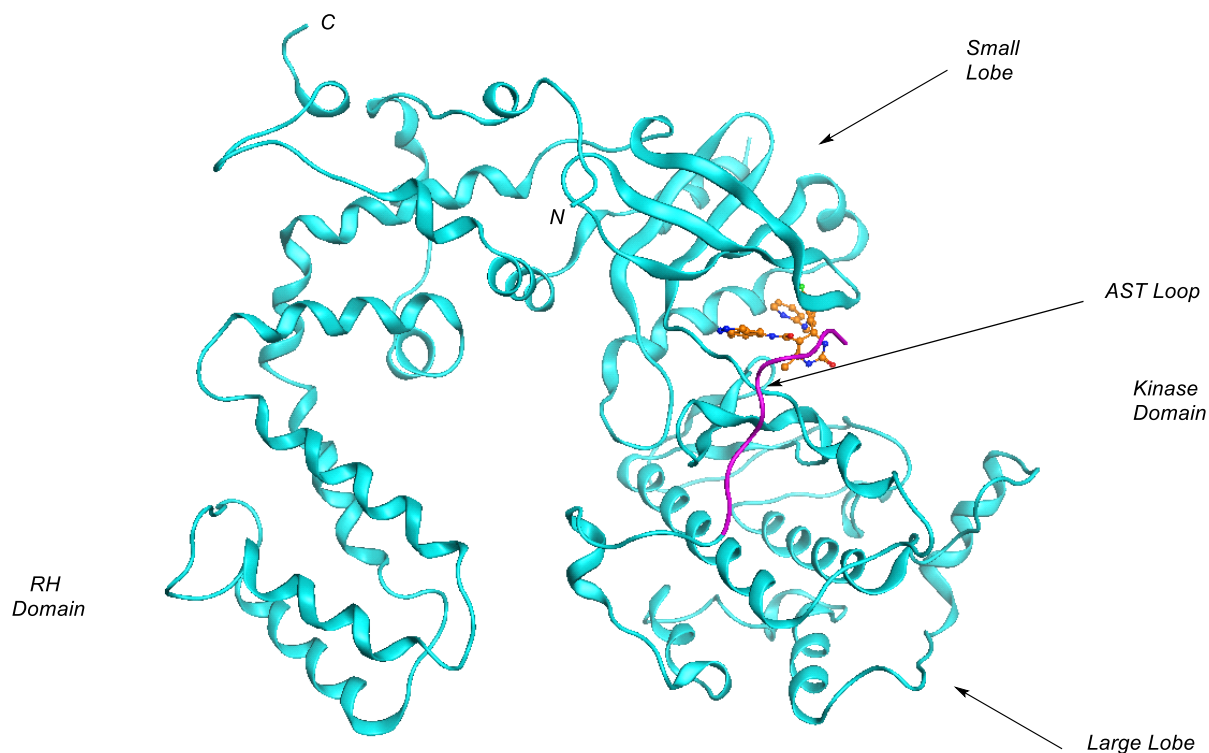


Figure 1.4 Annotated structure of GRK5 (cyan) shown with CCG-215022 (orange carbons) bound to the active site. AST loop highlighted in purple.

Similar to other kinases, GRK5 has a large lobe and a small lobe that are connected via the hinge loop (Figure 1.4). Additionally, there is the activation loop, which does not need to be fully phosphorylated to achieve an active conformation.³⁴ Other key features include the active site tether (AST) loop, a piece of architecture that wraps down over the face of the kinase, passing over the ATP binding pocket when GRK5 adopts a closed, active conformation.

The GRK5 orthosteric site features a narrow and slightly polar binding pocket, with the majority of the hydrophobicity located closest to the hinge loop. Within the binding pocket there are several key features, including the hinge donor and hinge acceptor. Interactions with these two amino acids are key to achieving binding for ATP. Also, within the binding pocket is the Gatekeeper residue, which resides just behind the hinge acceptor, and guards a secondary hydrophobic pocket, herein referred to as the back hydrophobic pocket or deeper hydrophobic pocket. The gatekeeper residue determines the size and shape of this deeper hydrophobic pocket in kinases.³⁷

1.2.3 Canonical and Non-Canonical Kinase Drug Design

Before the introduction of Gleevec (May 2001) kinases were considered to be “undruggable” targets due to the highly conserved nature of the orthosteric binding pocket.³⁸ Since the introduction of Gleevec, there has been a rapid expansion of kinase drug discovery campaigns leading to the creation of numerous kinase inhibitors that fall into four different types.

Type I kinase inhibitors were the first-in-class examples of kinase targeted drugs. Type I kinase inhibitors bind in the orthosteric site and are ATP competitive. There are numerous examples of type I inhibitors that have been approved by the FDA. There is a majority of kinase inhibitors that adhere to this design template, possibly due to the initial bias set by use of phosphorylated kinases in biochemical assays that led the initial kinase drug discovery programs. These inhibitors interact with the hinge donor and acceptor residues in a pattern that mimics the binding pattern of ATP. It is important to note that although the binding pattern is similar to ATP, different scaffolds can be used to achieve this type I architecture. For example, Sunitinib, a FDA approved tyrosine kinase inhibitor (TKI) is a type I kinase inhibitor but features an indolinone scaffold in place of a purine scaffold.³⁹

Type II inhibitors are similar to Type I inhibitors, in that these compounds bind to the ATP site. However, Type II inhibitors exploit structural elements to boost potency and selectivity. Type II inhibitors bind a kinase in the inactive state, with the DFG-out conformation. Having the DFG residues in the “out” conformation results in an opening of the deeper hydrophobic pocket. Filling this secondary hydrophobic pocket with different pendants can lead to greater potency and selectivity for Type II inhibitors. The Type II inhibitor scaffold is exemplified in Gleevec, which features the hydrogen bonds to the α C-helix and the DFG-residues needed to unveil the secondary hydrophobic pocket.^{37,40,41}

Type III and Type IV kinase inhibitors are allosteric in nature.⁴² Type III kinase inhibitors are non-ATP competitive inhibitors as they bind outside the ATP binding pocket, in between the cleft of the large and small kinase lobes adjacent to the orthosteric site. Type IV inhibitors are also not known to bind the orthosteric site of a kinase. Rather, Type IV inhibitors bind outside the cleft and the phosphoacceptor sites.⁴³

These types of kinase inhibitors constitute the canonical set of design templates. Recently, given the rise of resistance-conveying mutations, the development of a new type of kinase inhibitors has appeared with the resurgence of covalent inhibition. These new covalent kinase inhibitors utilize one of the aforementioned design templates but exploit a piece of kinase

architecture prone to chemical interactions to afford ultra-selective compounds. This new strategy has opened the door to developing inhibitors for previously inaccessible targets.

1.3 Covalent Inhibitors Offer a New Path Towards Selective GRK5 Inhibitors

1.3.1 FDA Approved Tyrosine Kinase Inhibitors Provide a Plan for GRK5 Inhibitor Development

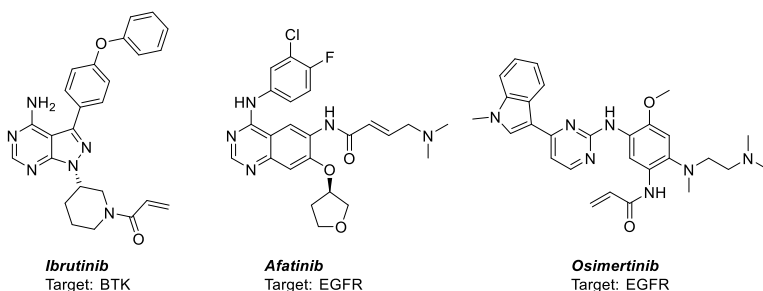


Figure 1.5 Structures of FDA approved Covalent TKIs

A key point in this campaign is the lack of truly GRK5 specific inhibitors. However, there are strategies that can be pursued to achieve GRK5 selectivity, chief among them is covalent inhibition. There are more than 40 FDA-approved covalent

inhibitors currently on the market.⁴⁴ Notable examples include the recent FDA approved Ibrutinib, a covalent inhibitor of BTK which treats non-small cell lung cancer and compounds such as Afatinib and Osimertinib which are FDA-approved inhibitors of EGFR and treat various types of cancer (Figure 1.5). The need for these new covalent inhibitors is driven primarily by the rise of clinical resistance to the original non-covalent inhibitors. For example, Osimertinib was developed from a known non-covalent EGFR inhibitor, and carries a covalent warhead to convey activity against EGFR T790M, the most clinically relevant mutation in EGFR. Osimertinib binds with Cys797, which exists on the hinge loop of the kinase domain, and has been proven to effectively reverse the loss of potency against the EGFR-T790M mutant.⁴⁵⁻⁴⁸ This covalent strategy, targeting a non-conserved cysteine residue within the binding pocket, has grown popular as it allows for minor modifications to an already optimized scaffold to convey large boosts in potency and selectivity as well offering the ability to lower the dose of compound needed to achieve a clinical effect.

1.3.2 Cysteine as a Handle for Selective Covalent Inhibition

Cysteine plays critical roles in protein folding and establishing tertiary protein structure, despite this, the presence of cysteine codons within the genetic code (i.e.. coding genes) is 1.9%, making it a rare, and therefore, ideal handle for covalent interaction.⁴⁴ Targeting a cysteine residue for covalent interaction is not straightforward as its pKa values are highly variable, making it

uncertain whether solvent exposed cysteines will be available for engagement. This variability means that each inhibitor is designed to fulfill one set of conditions for reacting with a specific cysteine and is unlikely to interact with other surface cysteine residues.

This level of selectivity allows the newly constructed covalent inhibitors to have a lower level of toxicity, which has traditionally been one of the most troubling side effects of covalent inhibitors. While idiosyncratic toxicity cannot be predicted *a priori*, the ability to lower the dose of a highly potent and selective inhibitor allows for less toxicity arising from hitting off-targets such as hERG, an ion channel which controls cardiomyocyte contractility (QT).⁴⁹ Therefore, new classes of covalent inhibitors offer an alternative path towards optimized potency, selectivity and resilience against arising clinical resistance.

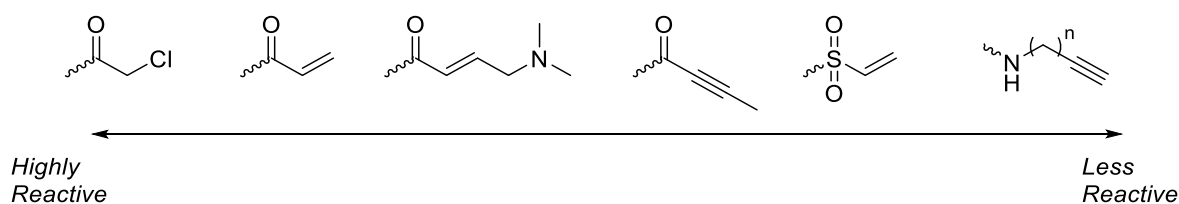


Figure 1.6 Selected cysteine targeting covalent modifiers, arranged by reactivity to nucleophiles.

Conveniently, the warhead design for cysteine engagement has already been fairly well studied by several groups. As hard-soft acid-base theory (HSAB) states that each nucleophile needs a matched electrophile, the warheads for each residue (Cys, Lys, Arg etc.) is highly specific, and sensitive to changes in electrophilicity or strength of the nucleophile.⁵⁰ Covalent warhead design also deals with vector length and angle, as there can be no covalent interaction if the warhead is not within striking distance of the nucleophile (generally between 2.5-5Å) or if the angle of approach does not match the ideal Bürgi-Dunitz angle (107°).⁵¹ Given the various parameters to keep in mind, multiple warheads must be tested for each individual scaffold.

There are a few well known covalent warheads which commonly appear in known covalent inhibitors (Figure 1.6). The most common examples of cysteine specific warheads include classical Michael acceptors such as acrylamides and butynoic amides. Given the utility of the classic acrylamide, new warheads have been designed to act not only as a covalent modifier but also as internal bases. In the case of Afatinib, which features a N,N-dimethylaminobutenoic amide, the terminal dimethyl nitrogen acts as an intermolecular base designed to deprotonate the cysteine nucleophile of the protein to boost reactivity against the electrophile.⁴⁷ This warhead, pioneered by Boehringer Ingelheim, has quickly gained traction as a popular warhead to test in covalent

inhibitor programs as it allows for a boost in reactivity of nucleophile rather than the electrophile. Highly electrophilic Michael acceptors are known to have promiscuous behavior which can lead to idiosyncratic toxicities. Other popular warheads include vinyl sulfones, epoxides and haloketones, which are some of the most reactive warheads designed yet but can offer the same levels of selectivity without altering the nucleophilicity of the targeted cysteine residue, which is useful in targeting cysteines located on flexible pieces of kinase architecture.⁵²⁻⁵⁸

1.3.3 Other Amino Acid Handles for Covalent Inhibition

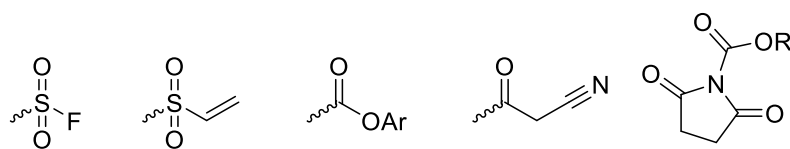


Figure 1.7 Selected set of Lysine (nitrogen) targeting warheads.

Cysteine is not the only amino acid residue used in designing covalent inhibitors. In fact, any amino acid which features a potential

nucleophile can be targeted for covalent engagement, including lysine and arginine, which both feature nitrogen nucleophiles. As these nucleophiles are generally less reactive than cysteine, they require different electrophiles to produce a covalent interaction. Similar to their cysteine counterpart, nitrogen and oxygen specific warheads exist as a common set to be used in developing covalent warheads in a case-by-case manner (Figure 1.7).⁴⁴

1.3.4 Reversible Covalent Inhibition is Expanding the Frontier of Covalent Kinase Drug Design

Perhaps one of the biggest impacts in the revival of covalent inhibitors has been the development of reversible covalent inhibitors. Prior drug discovery efforts have focused on irreversible inhibition, but these compounds can have various issues. Irreversible inhibition means that residence time within the active site is limited by the turn-over time of the protein target. However, it may be advantageous to have a residence time that is shorter than the protein turn-over time, thereby keeping the fraction of unbound drug high enough to increase exposure. In these cases, tunable reversible warheads offer a unique solution. Pioneered by Taunton and co-workers, these reversible warheads can form a covalent interaction with a cysteine residue, but over time

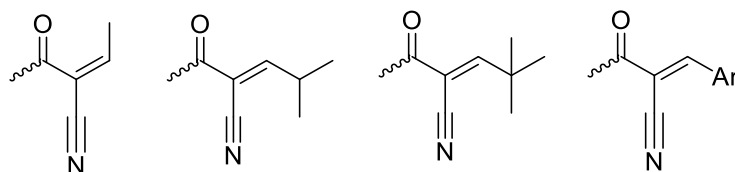


Figure 1.8 Selected set of reversible covalent warheads, as pioneered by Taunton et. al.

and with the addition of a second nucleophile such as water, can reverse this covalent interaction to release the inhibitor.⁵⁹⁻⁶¹ This tunable residence time offers a solution to the problem of rapidly eliminating proteins labelled with irreversible covalent warheads and protein manufacturing, which is a common mechanism of resistance.⁶²

Taunton and co-workers have detailed the impact of various branching pendants on the residence time of reversible covalent warheads. There now exists a set of known tunable reversible warheads that can be employed within covalent inhibitor programs to further expand the arsenal of covalent inhibitors for each case (Figure 1.8).⁵⁹ These reversible covalent warheads are of interest to us as they could be used to mitigate the potential pharmacokinetic toxicities.

1.4 Using a Covalent Strategy GRK5 Selectivity over GRK2 Can Be Achieved

1.4.1 GRK5 Inhibitor Design Strategy

Previous work to validate GRK5 as a pharmacological target have been limited to genetic knockdown or knockout studies.⁶³⁻⁶⁵ Such studies have indicated that GRK5 has utility in many diseases, but a truly selective inhibitor has not been independently confirmed.⁶⁶ Of the known GRK5 inhibitors, few are subfamily selective against GRK2.^{67,68} Perhaps the best example of a GRK5 inhibitor are the pan-GRK2/5 inhibitors, **CCG-215022** and **CCG-258747**, created by Waldschmidt et. al.^{27,28}

Much of the challenge of achieving a GRK5 selective inhibitor hinges on the high level of similarity between the GRK2 and GRK5 active sites. GRK2 and GRK5 share a similar hinge region and have the same residues as the hinge donor and acceptor, Met 266 and Thr 264 respectively. The active site of GRK2 is larger and more hydrophobic than that of GRK5; for this reason, GRK5 activity is easily built out of GRK2 inhibitors.⁶⁹

The aforementioned examples of covalent inhibition use cysteines within the ATP binding site (Figure 1.9). Typically, the sites of covalent engagement have been on the hinge loop (yellow), the roof of the ATP binding pocket (orange) or the P-loop (green). Other sites for covalent binding have included the DFG region (dusty blue). However, GRK5 does not feature a cysteine within the ATP binding pocket. Fortunately, GRK5 does have a non-conserved cysteine close to the ATP binding pocket, Cys474 which is found on the AST loop.⁷⁰ The AST loop (cyan) where Cys474 is located is outside of these zones but is still predicted to be within reach. Additionally, Cys474 is only present in GRK4 subfamily members, making it an ideal candidate for a covalent handle. The easiest way to begin a campaign to build GRK5 covalent inhibitors is through a crystal structure of GRK5 with the covalent handle visualized. Although GRK5 has been crystallized a handful of

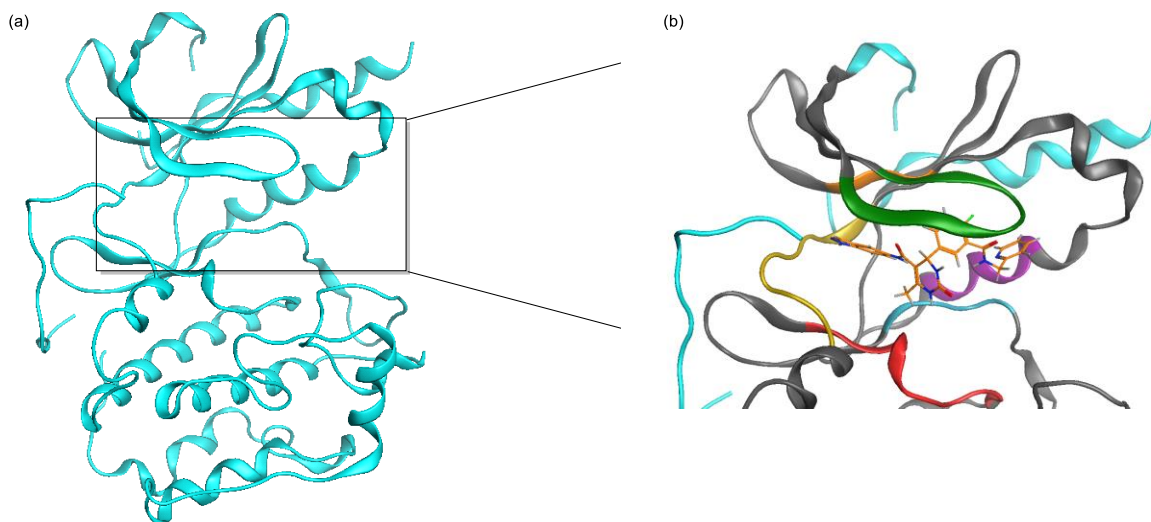


Figure 1.9 Cysteine Map, developed from the GRK5 structure (PDB: 4WNK). (a) full GRK5 structure, (b) ATP binding pocket with CCG-215022 bound (orange carbons), zoomed in view. Previously, covalent inhibitors have been designed to hit cysteines within the active site. Key areas of previous development have included the P-loop (green), the roof of the ATP pocket (orange), the hinge/front loop (yellow), and the DFG region (dusty blue). The AST loop where Cys474 is located is shown in cyan.

times, there are no structures in which Cys474 is visualized.^{71,72} Fortunately, GRK6, a subfamily member, has been crystallized in what is believed to be an active conformation, and Cys474 is visible within this structure (Figure 1.10).⁷¹ This GRK6 structure reveals that the thiol group of Cys474 is located within the flexible active site tether (AST) loop of the kinase domain and is positioned adjacent to the ATP-binding site, at least when the kinase domain adopts a closed, active conformation.

1.4.2 GRK5/6 Overlay Model Enables Rationale Design

An overlay model between GRK5 and GRK6 (PDB entries 4WNK and 3NYN respectively) can guide drug design until a crystal structure of GRK5 bound to a covalent inhibitor can be obtained.^{71,72} The model allows visualization of the covalent handle, Cys474, thereby filling in a crystallographic blind spot. From this point, initial drug discovery efforts could begin, from lead selection to development of advanced chemical probes.

1.4.3 Known GRK5 Inhibitors Will Serve as Initial Lead Compounds in This Campaign

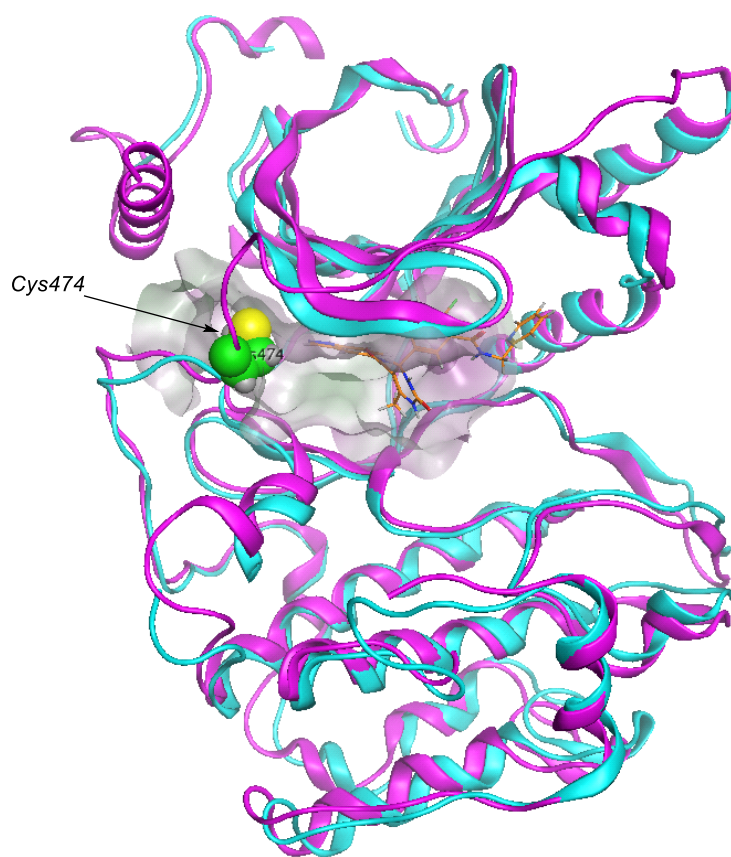


Figure 1.10 GRK5 (blue)/GRK6(purple) overlay model with CCG-215022 bound to GRK5 shown in dark blue. Cys474 (green carbons) is only visible in GRK6, as the AST in GRK5 is not visible. In a closed, active conformation the AST loop positions Cys474 within reach of the active site.

With a model in hand, lead selection for the GRK5 inhibitor campaign can begin. The development of other covalent inhibitors traditionally begins with non-covalent inhibitors that can be modified to carry a covalent warhead.⁷³ The most obvious choice for the GRK5 campaign is CCG-215022, the ligand that was used to obtain the GRK5 crystal structure. CCG-215022 is a known

GRK2/GRK5 inhibitor with mild GRK2 selectivity (GRK2 $K_i = 150$ nM, GRK5 $K_i = 350$ nM, 2-fold GRK2 selective).²⁸ This particular inhibitor features an indazole as the main hinge binding motif and has an optimized pendant that extends into the deeper hydrophobic regions of GRK2 and GRK5. Although this inhibitor has the intrinsic potency needed to run a successful discovery campaign, there remains the issue of appending a covalent warhead. Functionalization at the C3-indazole position would be the ideal position, however the route to achieve this handle would be long and complicated, slowing the pace of design and discovery. Additionally, our initial designs placed these analogues outside the limits imposed by Lipinski's rules.⁷⁴ Although we acknowledge that there are examples of FDA approved drugs that fall outside Lipinski's rule (Ibrutinib among them), these examples are still more the exceptions than the rule. Therefore, new scaffolds that are amenable to carrying a covalent modifier were needed.

Review of the current and historical literature surrounding GRK2 and GRK5 inhibitors gave rise to several new scaffolds that could be amenable to our GRK5 covalent campaign (Figure

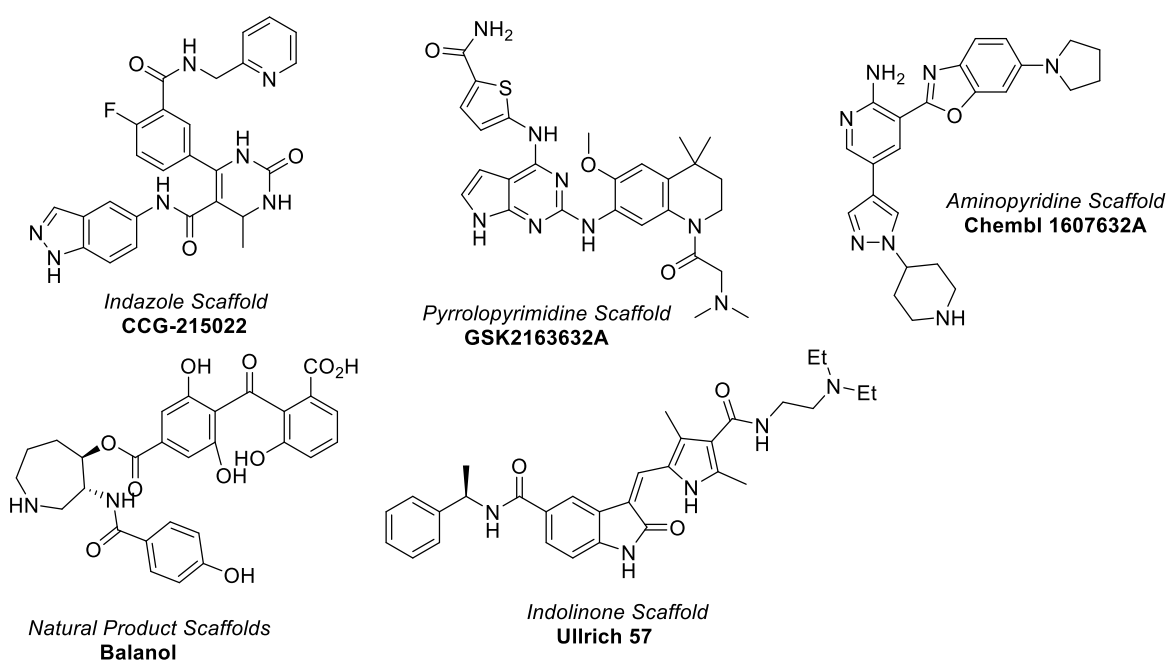


Figure 1.11 Current leads with known GRK2 or GRK5 activity.

1.11).^{13,27,28,66,68} Of these scaffolds, the indazole series is a prominent member, as are the pyrrolopyrimidines (GSK2613632A), that were uncovered in a previous screen conducted by Homan et al. The pyrrolopyrimidine scaffold is known to be privileged in kinase drug discovery, and has been independently validated in have GRK1, GRK2 and GRK5 activity. GSK2613632A

is a potent inhibitor of GRK1 ($K_i = 130$ nM) with more modest potency against GRK2 and GRK5 ($\log IC_{50} = -4.7$, $\log IC_{50} = -5.5$ respectively).⁶⁸

Additional scaffolds with known activity against GRK2 or GRK5 include the aminopyridines (ChEMBL-1607632), natural product derived inhibitors (Balanol) and the indolinone scaffold (Ullrich-57). These scaffolds feature the desired activity, however, there are known drawbacks to these scaffolds. Firstly, the natural product scaffolds, including balanol have long synthetic sequences that are limit the production of potential analogues. The aminopyridine scaffold is known to be privileged in kinase drug discovery, making it a potentially good lead. However, the initial lead, ChEMBL-1607632 needs to be independently validated as it is known to possess activity against common kinase targets, including cMet. The same holds true for the indolinone scaffold lead, Ullrich-57. The indolinone series is derived from a known receptor tyrosine kinase inhibitor (RTKI), Sunitinib. Sunitinib is known to be a pan-RTKI with an FDA black box warning. Thus, these particular lead scaffolds were deprioritized in order to avoid the potential issues that would come along with their development.

1.5 Application of a Covalent Strategy May Yield Ultra Selective GRK5 Inhibitors

1.5.1 Chapter Breakdowns and Project Flow

As it stands, I have used both literature review and virtual screening to uncover three new scaffolds to develop a GRK5 covalent inhibitor program. In Chapter 2, I develop the pyrrolopyrimidines. In Chapter 3, I attempted validation of the aminopyridine scaffold. Chapter 4 describes the development of the indolinone series, wherein I describe the first examples of a nanomolar potency covalent, subfamily selective GRK5 inhibitor, and our efforts to expand this arsenal of GRK5 inhibitors for the treatment of cardiovascular disease.

1.6 References

- (1) Nicoletti, G.; De Luca, V.; Tarantino, P.; Gagliardi, M.; Iannello, G.; Novellino, F.; Morelli, M.; Annesi, G.; Quattrone, A. Role of G-Protein Coupled Receptor Kinase 5 Gene in Cognitive Impairment in Parkinson's Disease. *Psychiatry Res.* **2015**, *230* (3), 975–977. <https://doi.org/10.1016/j.psychres.2015.11.026>.
- (2) Aarsland, D.; Beyer, M. K.; Kurz, M. W. Dementia in Parkinson's Disease. *Curr. Opin. Neurol.* **2008**, *21* (6), 676–682. <https://doi.org/10.1097/WCO.0b013e3283168df0>.
- (3) Harding, A. J.; Halliday, G. M. Cortical Lewy Body Pathology in the Diagnosis of Dementia. *Acta Neuropathol. (Berl.)* **2001**, *102* (4), 355–363. <https://doi.org/10.1007/s004010100390>.
- (4) Dev, K. K.; Hofele, K.; Barbieri, S.; Buchman, V. L.; van der Putten, H. Part II: Alpha-Synuclein and Its Molecular Pathophysiological Role in Neurodegenerative Disease. *Neuropharmacology* **2003**, *45* (1), 14–44. [https://doi.org/10.1016/s0028-3908\(03\)00140-0](https://doi.org/10.1016/s0028-3908(03)00140-0).

- (5) Recchia, A.; Debetto, P.; Negro, A.; Guidolin, D.; Skaper, S. D.; Giusti, P. Alpha-Synuclein and Parkinson's Disease. *FASEB J. Off. Publ. Fed. Am. Soc. Exp. Biol.* **2004**, *18* (6), 617–626. <https://doi.org/10.1096/fj.03-0338rev>.
- (6) Liu, J.; Rasul, I.; Sun, Y.; Wu, G.; Li, L.; Premont, R. T.; Suo, W. Z. GRK5 Deficiency Leads to Reduced Hippocampal Acetylcholine Level via Impaired Presynaptic M2/M4 Autoreceptor Desensitization. *J. Biol. Chem.* **2009**, *284* (29), 19564–19571. <https://doi.org/10.1074/jbc.M109.005959>.
- (7) He, M.; Singh, P.; Cheng, S.; Zhang, Q.; Peng, W.; Ding, X.; Li, L.; Liu, J.; Premont, R. T.; Morgan, D.; et al. GRK5 Deficiency Leads to Selective Basal Forebrain Cholinergic Neuronal Vulnerability. *Sci. Rep.* **2016**, *6* (1), 1–12. <https://doi.org/10.1038/srep26116>.
- (8) Lessel, D.; Muhammad, T.; Tena, T. C.; Moepps, B.; Burkhalter, M. D.; Hitz, M.-P.; Toka, O.; Rentzsch, A.; Schubert, S.; Schalinski, A.; et al. The Analysis of Heterotaxy Patients Reveals New Loss-of-Function Variants of *GRK5*. *Sci. Rep.* **2016**, *6*, srep33231. <https://doi.org/10.1038/srep33231>.
- (9) Singh, P.; Peng, W.; Zhang, Q.; Ding, X.; Suo, W. Z. GRK5 Deficiency Leads to Susceptibility to Intermittent Hypoxia-Induced Cognitive Impairment. *Behav. Brain Res.* **2016**, *302*, 29–34. <https://doi.org/10.1016/j.bbr.2016.01.019>.
- (10) Cheng, S.; Li, L.; He, S.; Liu, J.; Sun, Y.; He, M.; Grasing, K.; Premont, R. T.; Suo, W. Z. GRK5 Deficiency Accelerates β -Amyloid Accumulation in Tg2576 Mice via Impaired Cholinergic Activity. *J. Biol. Chem.* **2010**, *285* (53), 41541–41548. <https://doi.org/10.1074/jbc.M110.170894>.
- (11) Nogués, L.; Palacios-García, J.; Reglero, C.; Rivas, V.; Neves, M.; Ribas, C.; Penela, P.; Mayor, F. G Protein-Coupled Receptor Kinases (GRKs) in Tumorigenesis and Cancer Progression: GPCR Regulators and Signaling Hubs. *Semin. Cancer Biol.* **2018**, *48*, 78–90. <https://doi.org/10.1016/j.semcancer.2017.04.013>.
- (12) Penela, P.; Murga, C.; Ribas, C.; Tutor, A. S.; Peregrín, S.; Mayor, F. Mechanisms of Regulation of G Protein-Coupled Receptor Kinases (GRKs) and Cardiovascular Disease. *Cardiovasc. Res.* **2006**, *69* (1), 46–56. <https://doi.org/10.1016/j.cardiores.2005.09.011>.
- (13) Ullrich, A.; Falcenberg, M.; Örfi, Z.; Kéri, G.; ÖRFI, L.; Horváth, Z.; SZOKOL, B.; DOBOS, J.; NEMES, Z. Indolinone Derivatives as Grk5 Modulators. WO2015022437 A1, February 19, 2015.
- (14) Sommer, A.-K.; Falcenberg, M.; Ljepoja, B.; Fröhlich, T.; Arnold, G. J.; Wagner, E.; Roidl, A. Downregulation of GRK5 Hampers the Migration of Breast Cancer Cells. *Sci. Rep.* **2019**, *9* (1), 1–13. <https://doi.org/10.1038/s41598-019-51923-1>.
- (15) Lagman, J.; Sayegh, P.; Lee, C. S.; Sulon, S. M.; Jacinto, A. Z.; Sok, V.; Peng, N.; Alp, D.; Benovic, J. L.; So, C. H. G Protein-Coupled Receptor Kinase 5 Modifies Cancer Cell Resistance to Paclitaxel. *Mol. Cell. Biochem.* **2019**, *461* (1), 103–118. <https://doi.org/10.1007/s11010-019-03594-9>.
- (16) Prasad, R. B.; Groop, L. Genetics of Type 2 Diabetes—Pitfalls and Possibilities. *Genes* **2015**, *6* (1), 87–123. <https://doi.org/10.3390/genes6010087>.
- (17) International Diabetes Federation - Type 2 diabetes <https://idf.org/aboutdiabetes/type-2-diabetes.html> (accessed Dec 30, 2019).
- (18) O'Brien, M. J.; Karam, S. L.; Wallia, A.; Kang, R. H.; Cooper, A. J.; Lancki, N.; Moran, M. R.; Liss, D. T.; Prospect, T. A.; Ackermann, R. T. Association of Second-Line Antidiabetic Medications With Cardiovascular Events Among Insured Adults With Type 2

- Diabetes. *JAMA Netw. Open* **2018**, *1* (8), e186125–e186125.
<https://doi.org/10.1001/jamanetworkopen.2018.6125>.
- (19) FDA’s Fast Track Designation for Empagliflozin in Heart Failure Points to New Paradigm <https://www.ajmc.com/newsroom/fdas-fast-track-designation-for-empagliflozin-in-heart-failure-points-to-new-paradigm> (accessed Dec 26, 2019).
 - (20) FastStats <https://www.cdc.gov/nchs/fastats/leading-causes-of-death.htm> (accessed Dec 26, 2019).
 - (21) Benjamin Emelia J.; Muntner Paul; Alonso Alvaro; Bittencourt Marcio S.; Callaway Clifton W.; Carson April P.; Chamberlain Alanna M.; Chang Alexander R.; Cheng Susan; Das Sandeep R.; et al. Heart Disease and Stroke Statistics—2019 Update: A Report From the American Heart Association. *Circulation* **2019**, *139* (10), e56–e528.
<https://doi.org/10.1161/CIR.0000000000000659>.
 - (22) Mozaffarian, D.; Benjamin, E. J.; Go, A. S.; Arnett, D. K.; Blaha, M. J.; Cushman, M.; Das, S. R.; Ferranti, S. de; Després, J.-P.; Fullerton, H. J.; et al. Heart Disease and Stroke Statistics—2016 Update: A Report From the American Heart Association. *Circulation* **2015**, CIR.0000000000000350. <https://doi.org/10.1161/CIR.0000000000000350>.
 - (23) Orsborne, C.; Chaggar, P. S.; Shaw, S. M.; Williams, S. G. The Renin-Angiotensin-Aldosterone System in Heart Failure for the Non-Specialist: The Past, the Present and the Future. *Postgrad. Med. J.* **2017**, *93* (1095), 29–37. <https://doi.org/10.1136/postgradmedj-2016-134045>.
 - (24) Delicce, A. V.; Basit, H.; Makaryus, A. N. Physiology, Frank Starling Law. In *StatPearls*; StatPearls Publishing: Treasure Island (FL), 2019.
 - (25) Sequeira, V.; van der Velden, J. Historical Perspective on Heart Function: The Frank–Starling Law. *Biophys. Rev.* **2015**, *7* (4), 421–447. <https://doi.org/10.1007/s12551-015-0184-4>.
 - (26) Schwinger, R. H.; Böhm, M.; Koch, A.; Schmidt, U.; Morano, I.; Eissner, H. J.; Uberfuhr, P.; Reichart, B.; Erdmann, E. The Failing Human Heart Is Unable to Use the Frank-Starling Mechanism. *Circ. Res.* **1994**, *74* (5), 959–969.
<https://doi.org/10.1161/01.RES.74.5.959>.
 - (27) Waldschmidt, H. V.; Homan, K. T.; Cruz-Rodríguez, O.; Cato, M. C.; Waninger-Saroni, J.; Larimore, K. M.; Cannavo, A.; Song, J.; Cheung, J. Y.; Kirchhoff, P. D.; et al. Structure-Based Design, Synthesis, and Biological Evaluation of Highly Selective and Potent G Protein-Coupled Receptor Kinase 2 Inhibitors. *J. Med. Chem.* **2016**, *59* (8), 3793–3807. <https://doi.org/10.1021/acs.jmedchem.5b02000>.
 - (28) Waldschmidt, H. V.; Homan, K. T.; Cato, M. C.; Cruz-Rodríguez, O.; Cannavo, A.; Wilson, M. W.; Song, J.; Cheung, J. Y.; Koch, W. J.; Tesmer, J. J. G.; et al. Structure-Based Design of Highly Selective and Potent G Protein-Coupled Receptor Kinase 2 Inhibitors Based on Paroxetine. *J. Med. Chem.* **2017**, *60* (7), 3052–3069.
<https://doi.org/10.1021/acs.jmedchem.7b00112>.
 - (29) Hanyaloglu, A. C.; von Zastrow, M. Regulation of GPCRs by Endocytic Membrane Trafficking and Its Potential Implications. *Annu. Rev. Pharmacol. Toxicol.* **2008**, *48*, 537–568. <https://doi.org/10.1146/annurev.pharmtox.48.113006.094830>.
 - (30) Brinks, H.; Koch, W. J. Targeting G Protein-Coupled Receptor Kinases (GRKs) in Heart Failure. *Drug Discov. Today Dis. Mech.* **2010**, *7* (2), e129–e134.
<https://doi.org/10.1016/j.ddmec.2010.07.007>.

- (31) Traynham, C. J.; Hullmann, J.; Koch, W. J. “Canonical and Non-Canonical Actions of GRK5 in the Heart.” *J. Mol. Cell. Cardiol.* **2016**, *92* (Supplement C), 196–202. <https://doi.org/10.1016/j.yjmcc.2016.01.027>.
- (32) Gurevich, E. V.; Tesmer, J. J. G.; Mushegian, A.; Gurevich, V. V. G Protein-Coupled Receptor Kinases: More than Just Kinases and Not Only for GPCRs. *Pharmacol. Ther.* **2012**, *133* (1), 40–69. <https://doi.org/10.1016/j.pharmthera.2011.08.001>.
- (33) Lieu, M.; Koch, W. J. GRK2 and GRK5 as Therapeutic Targets and Their Role in Maladaptive and Pathological Cardiac Hypertrophy. *Expert Opin. Ther. Targets* **2019**, *23* (3), 201–214. <https://doi.org/10.1080/14728222.2019.1575363>.
- (34) Homan, K. T.; Tesmer, J. J. Structural Insights into G Protein-Coupled Receptor Kinase Function. *Curr. Opin. Cell Biol.* **2014**, *27*, 25–31. <https://doi.org/10.1016/j.ceb.2013.10.009>.
- (35) Huang, C.; Orban, T.; Jastrzebska, B.; Palczewski, K.; Tesmer, J. J. G. Activation of G Protein-Coupled Receptor Kinase 1 Involves Interactions between Its N-Terminal Region and Its Kinase Domain. *Biochemistry* **2011**, *50* (11), 1940–1949. <https://doi.org/10.1021/bi101606e>.
- (36) Sterne-Marr, R.; Leahey, P. A.; Bresee, J. E.; Dickson, H. M.; Ho, W.; Ragusa, M. J.; Donnelly, R. M.; Amie, S. M.; Krywy, J. A.; Brookins-Danz, E. D.; et al. GRK2 Activation by Receptors: Role of the Kinase Large Lobe and Carboxyl-Terminal Tail. *Biochemistry* **2009**, *48* (20), 4285–4293. <https://doi.org/10.1021/bi900151g>.
- (37) Through the “Gatekeeper Door”: Exploiting the Active Kinase Conformation | Journal of Medicinal Chemistry <https://pubs.acs.org/doi/10.1021/jm901443h> (accessed Dec 30, 2019).
- (38) FDA-approved small-molecule kinase inhibitors: Trends in Pharmacological Sciences [https://www.cell.com/trends/pharmacological-sciences/comments/S0165-6147\(15\)00077-2](https://www.cell.com/trends/pharmacological-sciences/comments/S0165-6147(15)00077-2) (accessed Sep 28, 2019).
- (39) Sun, C. L.; Christensen, J. G.; McMahon, G. Discovery and Development of Sunitinib (SU11248): A Multitarget Tyrosine Kinase Inhibitor of Tumor Growth, Survival, and Angiogenesis. In *Kinase Inhibitor Drugs*; John Wiley & Sons, Ltd, 2009; pp 1–39. <https://doi.org/10.1002/9780470524961.ch1>.
- (40) Noble, M. E. M.; Endicott, J. A.; Johnson, L. N. Protein Kinase Inhibitors: Insights into Drug Design from Structure. *Science* **2004**, *303* (5665), 1800–1805. <https://doi.org/10.1126/science.1095920>.
- (41) Knight, Z. A.; Shokat, K. M. Features of Selective Kinase Inhibitors. *Chem. Biol.* **2005**, *12* (6), 621–637. <https://doi.org/10.1016/j.chembiol.2005.04.011>.
- (42) Fasano, M.; Della Corte, C. M.; Califano, R.; Capuano, A.; Troiani, T.; Martinelli, E.; Ciardiello, F.; Morgillo, F. Type III or Allosteric Kinase Inhibitors for the Treatment of Non-Small Cell Lung Cancer. *Expert Opin. Investig. Drugs* **2014**, *23* (6), 809–821. <https://doi.org/10.1517/13543784.2014.902934>.
- (43) Roskoski, R. Classification of Small Molecule Protein Kinase Inhibitors Based upon the Structures of Their Drug-Enzyme Complexes. *Pharmacol. Res.* **2016**, *103*, 26–48. <https://doi.org/10.1016/j.phrs.2015.10.021>.
- (44) Gehringer, M.; Laufer, S. A. Emerging and Re-Emerging Warheads for Targeted Covalent Inhibitors: Applications in Medicinal Chemistry and Chemical Biology. *J. Med. Chem.* **2018**. <https://doi.org/10.1021/acs.jmedchem.8b01153>.

- (45) Zhang, H. Osimertinib Making a Breakthrough in Lung Cancer Targeted Therapy. *OncoTargets Ther.* **2016**, *9*, 5489–5493. <https://doi.org/10.2147/OTT.S114722>.
- (46) Harbeck, N.; Solca, F.; Gauler, T. C. Preclinical and Clinical Development of Afatinib: A Focus on Breast Cancer and Squamous Cell Carcinoma of the Head and Neck. *Future Oncol.* **2013**, *10* (1), 21–40. <https://doi.org/10.2217/fon.13.244>.
- (47) Keating, G. M. Afatinib: A Review of Its Use in the Treatment of Advanced Non-Small Cell Lung Cancer. *Drugs* **2014**, *74* (2), 207–221. <https://doi.org/10.1007/s40265-013-0170-8>.
- (48) Gayko, U.; Fung, M.; Clow, F.; Sun, S.; Faust, E.; Price, S.; James, D.; Doyle, M.; Bari, S.; Zhuang, S. H. Development of the Bruton's Tyrosine Kinase Inhibitor Ibrutinib for B Cell Malignancies. *Ann. N. Y. Acad. Sci.* **2015**, *1358*, 82–94. <https://doi.org/10.1111/nyas.12878>.
- (49) Danker, T.; Möller, C. Early Identification of HERG Liability in Drug Discovery Programs by Automated Patch Clamp. *Front. Pharmacol.* **2014**, *5*. <https://doi.org/10.3389/fphar.2014.00203>.
- (50) LoPachin, R. M.; Gavin, T.; DeCaprio, A.; Barber, D. S. Application of the Hard and Soft, Acids and Bases (HSAB) Theory to Toxicant–Target Interactions. *Chem. Res. Toxicol.* **2012**, *25* (2), 239–251. <https://doi.org/10.1021/tx2003257>.
- (51) Light, S. H.; Minasov, G.; Duban, M.-E.; Anderson, W. F. Adherence to Bürgi–Dunitz Stereochemical Principles Requires Significant Structural Rearrangements in Schiff-Base Formation: Insights from Transaldolase Complexes. *Acta Crystallogr. D Biol. Crystallogr.* **2014**, *70* (Pt 2), 544–552. <https://doi.org/10.1107/S1399004713030666>.
- (52) Lonsdale, R.; A. Ward, R. Structure-Based Design of Targeted Covalent Inhibitors. *Chem. Soc. Rev.* **2018**, *47* (11), 3816–3830. <https://doi.org/10.1039/C7CS00220C>.
- (53) Ghosh, A. K.; Samanta, I.; Mondal, A.; Liu, W. R. Covalent Inhibition in Drug Discovery. *ChemMedChem* *0* (0). <https://doi.org/10.1002/cmcd.201900107>.
- (54) Lonsdale, R.; Burgess, J.; Colclough, N.; Davies, N. L.; Lenz, E. M.; Orton, A. L.; Ward, R. A. Expanding the Armory: Predicting and Tuning Covalent Warhead Reactivity. *J. Chem. Inf. Model.* **2017**, *57* (12), 3124–3137. <https://doi.org/10.1021/acs.jcim.7b00553>.
- (55) Jackson, P. A.; Widen, J. C.; Harki, D. A.; Brummond, K. M. Covalent Modifiers: A Chemical Perspective on the Reactivity of α,β -Unsaturated Carbonyls with Thiols via Hetero-Michael Addition Reactions. *J. Med. Chem.* **2017**, *60* (3), 839–885. <https://doi.org/10.1021/acs.jmedchem.6b00788>.
- (56) Strelow, J. M. A Perspective on the Kinetics of Covalent and Irreversible Inhibition. *SLAS Discov. Adv. Life Sci. RD* **2017**, *22* (1), 3–20. <https://doi.org/10.1177/1087057116671509>.
- (57) Zhao, Z.; Bourne, P. E. Progress with Covalent Small-Molecule Kinase Inhibitors. *Drug Discov. Today* **2018**, *23* (3), 727–735. <https://doi.org/10.1016/j.drudis.2018.01.035>.
- (58) Chaikuad, A.; Koch, P.; Laufer, S. A.; Knapp, S. The Cysteinome of Protein Kinases as a Target in Drug Development. *Angew. Chem. Int. Ed.* **2018**, *57* (16), 4372–4385. <https://doi.org/10.1002/anie.201707875>.
- (59) Bradshaw, J. M.; Mcfarland, J. M.; Paavilainen, V. O.; Bisconte, A.; Tam, D.; Phan, V. T.; Romanov, S.; Finkle, D.; Shu, J.; Patel, V.; et al. Prolonged and Tunable Residence Time Using Reversible Covalent Kinase Inhibitors. *Nat. Chem. Biol. Camb.* **2015**, *11* (7), 525–531. <http://dx.doi.org/10.1038/nchembio.1817>.
- (60) Krishnan, S.; Miller, R. M.; Tian, B.; Mullins, R. D.; Jacobson, M. P.; Taunton, J. Design of Reversible, Cysteine-Targeted Michael Acceptors Guided by Kinetic and

- Computational Analysis. *J. Am. Chem. Soc.* **2014**, *136* (36), 12624–12630.
<https://doi.org/10.1021/ja505194w>.
- (61) Miller, R. M.; Taunton, J. Chapter Four - Targeting Protein Kinases with Selective and Semipromiscuous Covalent Inhibitors. In *Methods in Enzymology*; Shokat, K. M., Ed.; Protein Kinase Inhibitors in Research and Medicine; Academic Press, 2014; Vol. 548, pp 93–116. <https://doi.org/10.1016/B978-0-12-397918-6.00004-5>.
- (62) Finlay, M. R. V.; Anderton, M.; Ashton, S.; Ballard, P.; Bethel, P. A.; Box, M. R.; Bradbury, R. H.; Brown, S. J.; Butterworth, S.; Campbell, A.; et al. Discovery of a Potent and Selective EGFR Inhibitor (AZD9291) of Both Sensitizing and T790M Resistance Mutations That Spares the Wild Type Form of the Receptor. *J. Med. Chem.* **2014**, *57* (20), 8249–8267. <https://doi.org/10.1021/jm500973a>.
- (63) Gold, J. I.; Martini, J. S.; Hullmann, J.; Gao, E.; Chuprun, J. K.; Lee, L.; Tilley, D. G.; Rabinowitz, J. E.; Bossuyt, J.; Bers, D. M.; et al. Nuclear Translocation of Cardiac G Protein-Coupled Receptor Kinase 5 Downstream of Select Gq-Activating Hypertrophic Ligands Is a Calmodulin-Dependent Process. *PLOS ONE* **2013**, *8* (3), e57324.
<https://doi.org/10.1371/journal.pone.0057324>.
- (64) Gold Jessica I.; Gao Erhe; Shang Xiying; Premont Richard T.; Koch Walter J. Determining the Absolute Requirement of G Protein-Coupled Receptor Kinase 5 for Pathological Cardiac Hypertrophy. *Circ. Res.* **2012**, *111* (8), 1048–1053.
<https://doi.org/10.1161/CIRCRESAHA.112.273367>.
- (65) Hendrickx, J. O.; van Gastel, J.; Leysen, H.; Santos-Otte, P.; Premont, R. T.; Martin, B.; Maudsley, S. GRK5 – A Functional Bridge Between Cardiovascular and Neurodegenerative Disorders. *Front. Pharmacol.* **2018**, *9*.
<https://doi.org/10.3389/fphar.2018.01484>.
- (66) Cho, S. Y.; Lee, B. H.; Jung, H.; Yun, C. S.; Ha, J. D.; Kim, H. R.; Chae, C. H.; Lee, J. H.; Seo, H. W.; Oh, K.-S. Design and Synthesis of Novel 3-(Benzo[d]Oxazol-2-Yl)-5-(1-(Piperidin-4-Yl)-1H-Pyrazol-4-Yl)Pyridin-2-Amine Derivatives as Selective G-Protein-Coupled Receptor Kinase-2 and -5 Inhibitors. *Bioorg. Med. Chem. Lett.* **2013**, *23* (24), 6711–6716. <https://doi.org/10.1016/j.bmcl.2013.10.036>.
- (67) Thal, D. M.; Yeow, R. Y.; Schoenau, C.; Huber, J.; Tesmer, J. J. G. Molecular Mechanism of Selectivity among G Protein-Coupled Receptor Kinase 2 Inhibitors. *Mol. Pharmacol.* **2011**, *80* (2), 294–303. <https://doi.org/10.1124/mol.111.071522>.
- (68) Homan, K. T.; Larimore, K. M.; Elkins, J. M.; Szklarz, M.; Knapp, S.; Tesmer, J. J. G. Identification and Structure-Function Analysis of Subfamily Selective G Protein-Coupled Receptor Kinase Inhibitors. *ACS Chem. Biol.* **2015**, *10* (1), 310–319.
<https://doi.org/10.1021/cb5006323>.
- (69) Waldschmidt, H. V.; Bouley, R.; Kirchhoff, P. D.; Lee, P.; Tesmer, J. J. G.; Larsen, S. D. Utilizing a Structure-Based Docking Approach to Develop Potent G Protein-Coupled Receptor Kinase (GRK) 2 and 5 Inhibitors. *Bioorg. Med. Chem. Lett.* **2018**, *28* (9), 1507–1515. <https://doi.org/10.1016/j.bmcl.2018.03.082>.
- (70) Barf, T.; Kaptein, A. Irreversible Protein Kinase Inhibitors: Balancing the Benefits and Risks. *J. Med. Chem.* **2012**, *55* (14), 6243–6262. <https://doi.org/10.1021/jm3003203>.
- (71) Boguth, C. A.; Singh, P.; Huang, C.; Tesmer, J. J. G. Molecular Basis for Activation of G Protein-coupled Receptor Kinases. *EMBO J.* **2010**, *29* (19), 3249–3259.
<https://doi.org/10.1038/emboj.2010.206>.

- (72) Homan, K. T.; Waldschmidt, H. V.; Glukhova, A.; Cannavo, A.; Song, J.; Cheung, J. Y.; Koch, W. J.; Larsen, S. D.; Tesmer, J. J. G. Crystal Structure of G Protein-Coupled Receptor Kinase 5 in Complex with a Rationally Designed Inhibitor. *J. Biol. Chem.* **2015**, *290* (34), 20649–20659. <https://doi.org/10.1074/jbc.M115.647370>.
- (73) Liu, Q.; Sabnis, Y.; Zhao, Z.; Zhang, T.; Buhrlage, S. J.; Jones, L. H.; Gray, N. S. Developing Irreversible Inhibitors of the Protein Kinase Cysteine. *Chem. Biol.* **2013**, *20* (2), 146–159. <https://doi.org/10.1016/j.chembiol.2012.12.006>.
- (74) Lipinski's Rule of Five - an overview | ScienceDirect Topics
<https://www.sciencedirect.com/topics/pharmacology-toxicology-and-pharmaceutical-science/lipinskis-rule-of-five> (accessed Dec 30, 2019).

Chapter 2: Structure-Based Design of Selective, Covalent G-Protein Coupled Receptor Kinase 5 Inhibitors

2.1 Preface

Ideas and conclusions presented in Chapter 2 appear verbatim in a publication.¹ Design, synthesis and preliminary results for a select set of compounds (CCG258903, CCG258904, CCG262603, CCG264606, CCG263045 and CCG263115) have been published previously in the dissertation for the degree of Doctor of Philosophy (Medicinal Chemistry) from the University of Michigan by Helen Waldschmidt. I performed all additional design and synthesis of compounds CCG264099-265648. In addition to these compounds designed and synthesized, I also generated the GRK5/GRK6 overlay model, performed virtual screening and docking experiments, as well as performed intact protein and tandem mass spectrometry experiments. GRK5 and GRK5-C474S were provided by Renee Bouley, and GRK6 was provided by Kristoff Homan. All other radiometric pharmacological assays including time-dependence experiments were performed by M. Claire Cato. Additional contributions to the analysis of structural-activity relationships were also performed by M. Claire Cato.

2.2 Selectivity Presents a Massive Challenge for Developing GRK5 Inhibitors

There is growing evidence that GRK2 and GRK5 have distinct pathological roles within the failing heart.²⁻⁶ Increased GRK2 levels are thought to mediate the decrease in cell-surface β ARs and the prolonged sympathetic nervous system activation, leading to decreased contractility.³ GRK5 is unique among GRKs in that it undergoes Ca^{2+} -calmodulin-dependent nuclear localization that allows GRK5 to translocate into the nucleus where it phosphorylates histone deacetylase 5 (HDAC), turning on the transcription of hypertrophic genes.⁵ Indeed, cardiac-specific GRK2 knockout mice have improved contractility and increased cell-surface β ARs post-myocardial infarction, and GRK5 knockout mice are protected from cardiac hypertrophy following controlled cardiac stress.⁷ The extent of the functional differences in GRK2 and GRK5 within cardiomyocytes remains to be elucidated, but selective inhibition of each of these kinases would offer the opportunity to further understand their distinct roles in the progression of heart failure. In

addition, the selective inhibition of GRK2 or GRK5 presents the possibility of treating different aspects of heart failure without affecting the entire cardiac regulatory system.

Despite high structural similarity in the active site among GRKs, we have had success in developing potent and selective small molecule inhibitors for the GRK2 subfamily that improve contractility in isolated adult mouse cardiomyocytes, in part because GRK2, and presumably GRK3, adopts a distinct inactive pose from other GRKs and other protein kinases.⁸⁻¹¹ Comparison of GRK2 and GRK5 crystal structures revealed a more spacious ATP-binding pocket in GRK2/3 that was able to accommodate bulkier chemical substituents, which allowed us to build out GRK5 binding.⁸ We have also developed pan GRK-selective compounds (CCG-215022 and CCG-258748) with high nanomolar potency for both GRK2 and GRK5 but thus far we have not been successful in developing GRK5 selective (or GRK4 subfamily selective) inhibitors using the canonical reversible binding model.^{8,9,11} Others have reported GRK4 subfamily selective compounds, but they are also potent inhibitors of other kinase families and have not been independently confirmed.^{12,13}

Examination of the crystal structure of GRK6 in what is believed to be an active conformation (PDB 3NYN) revealed that the thiol group of Cys474, located within the flexible active site tether (AST) loop of the kinase domain, is positioned adjacent to the ATP-binding site, at least when the kinase adopts a more closed conformation (Figure 2.1A).¹⁴ Because this cysteine is unique to GRK4 subfamily members it could be exploited as a handle for covalent inhibition to gain selectivity for GRK5 over GRK2.

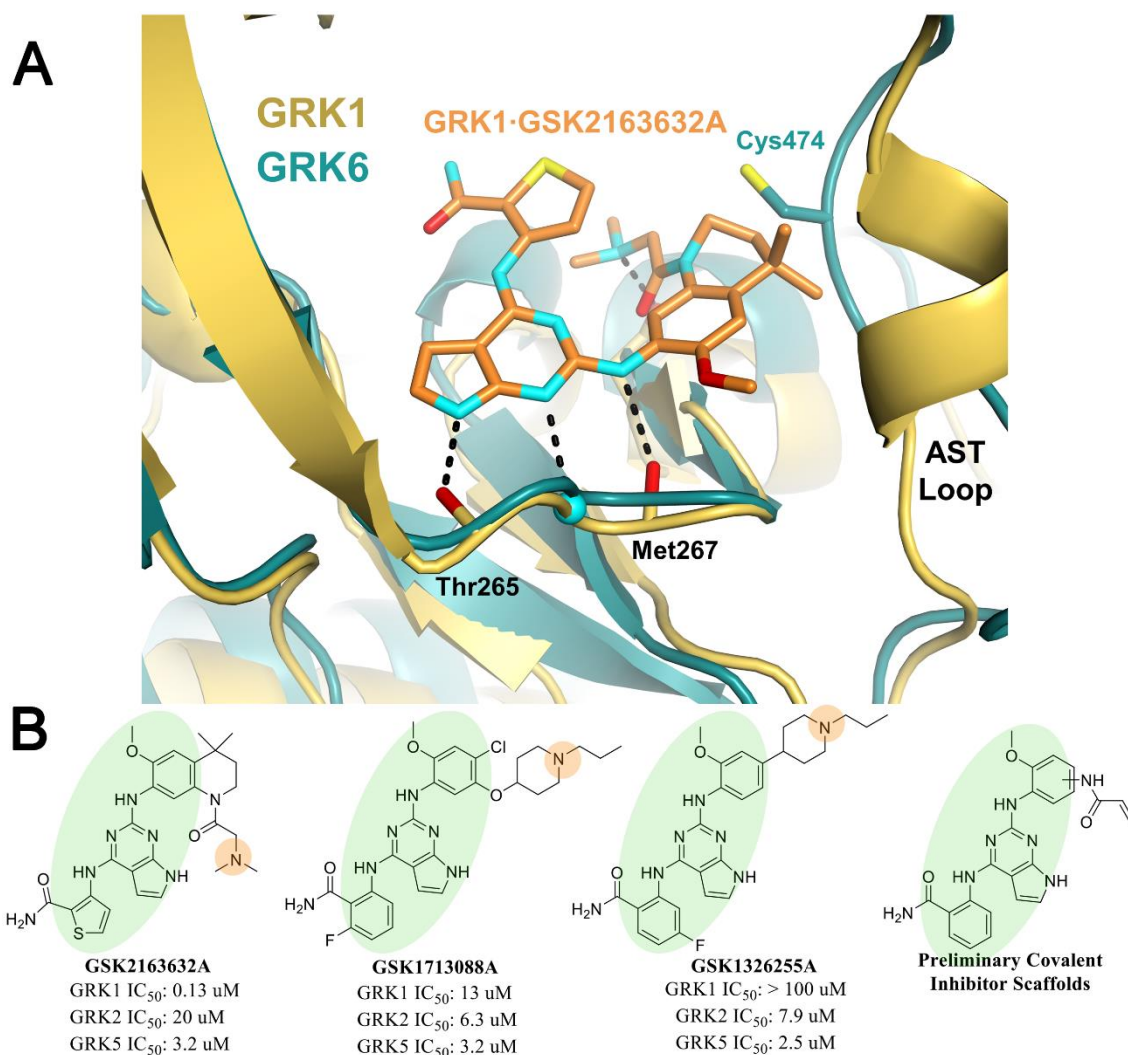


Figure 2.1 GSK2163632A and related compounds suggest a route to selective inhibition of GRK5 via covalent modification of Cys474. (A) GSK2163632A (green) bound to GRK1 (yellow, PDB entry 4PNI) superimposed with the active conformation of GRK6 (blue, PDB entry 3NYN) (B) Previously identified pyrrolopyrimidine based GRK inhibitors and covalent inhibitor design rationale. Green ovals highlight the base of the scaffold that is generally conserved, and orange circles represent a basic nitrogen that was removed except in the case of analogs where it is replicated potentially by a N,N-dimethyl-butenoic amide.

In recent years, the popularity of covalent warheads has risen because they offer the possibility of more potency and selectivity than reversible inhibitors.¹⁵ In particular, specifically targeting non-conserved cysteines in the ATP-binding pocket of kinases has demonstrated utility.^{15–17} The most successful irreversible modifiers have come from designing a reversibly-binding compound with low or sub- μ M affinity to contain a covalent warhead that is within reach and in the proper orientation to interact with the free thiol of a nearby cysteine. The most widely used reaction to achieve irreversible covalent attachment onto a cysteine is a Michael addition using electrophilic warheads such as acrylamides, vinyl sulfones, and alkynes.¹⁷ Recent advances have also been

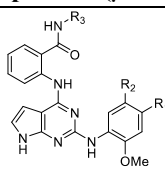
made with the use of an N,N-dimethyl-butenoic amide, which improves solubility and contains an internal base that can deprotonate and activate the thiol group.¹⁷⁻¹⁹

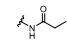
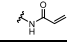
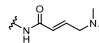
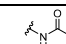
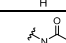
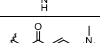
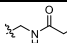
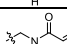
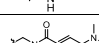
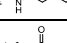
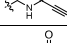
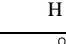
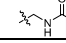
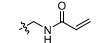
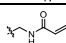
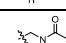
In a previous screen, GSK2163632A was identified as a modestly potent GRK5 inhibitor (IC₅₀ = 3.2 μM) with high potency for GRK1 (IC₅₀ = 130 nM). Two related compounds, GSK1713088A and GSK1326255A (Figure 2.1B), were shown to have similar potency for GRK5 (IC₅₀ = 3.2 and 2.5 μM respectively), but also modest selectivity over both GRK1 and GRK2.²⁰ All three GSK compounds share a common pyrrolopyrimidine core, which binds within the ATP pocket with the nitrogen from the core forming a hydrogen bonds with the hinge of the kinase domain in a donor-acceptor-donor motif, as observed for GSK2163632A in complex with GRK1 (PDB entry 4PNI, Figure 2.1A).¹⁴ We therefore hypothesized that we could append covalent war-heads to the methoxyphenyl of GSK1713088A or GSK1326255A that could react with Cys474 (Figure 2.1B). To avoid a highly substituted ring, we replaced the tertiary amine appendages with our covalent warheads in hopes that the potency gained by the covalent bond would overcome the loss of a hydrogen bond accepted by the tertiary amine. The N,N-dimethyl-butenoic amide warhead would, however, place a basic tertiary amine in a similar position.

2.3 Pyrrolopyrimidine Analogues can Achieve GRK5 Selectivity through Covalent Engagement

We first rationally designed 6 different variants of the GSK inhibitor series with short amide linkers. We overlaid the GRK5 crystal structure (4WNK) with that of the active conformation of GRK6 (3NYN) (Figure 2.1A). Building a covalent warhead *meta* to the aniline (ring C) likely retains the hydrogen bond of the amide carbonyl that GSK2163632A forms with the backbone nitrogen of GRK1-Asp271 (GRK5-Asp270) but this may position the Michael acceptor too distant from Cys474. Alternatively, building the warhead *para* to the aniline would likely hinder the hydrogen bond with Asp271, but may put the Michael acceptor within 1.5 Å of the Cys474 thiol group. However, it is not possible to accurately model these interactions because the degree of kinase domain closure and the conformations of the flexible AST and P loops cannot be predicted a priori. Therefore, both *para* and *meta* substituents were synthesized, including unreactive saturated ethyl amide analogs as negative controls (Table 2.1).

The *para* and *meta* ethyl amide controls, CCG-262604 and CCG-262606 respectively, showed substantially different biochemical results indicating a possible structure-activity-relationship (SAR) cliff. The *para* substituted ethyl amide CCG-262606 appears to saturate the assay, with activity ranging from 5.9 μM at 1 hour to >100 μM at the 4 hour timepoint. This level of activity

Table 1: IC₅₀ Values for Pyrrolopyrimidine Compounds (μM ± SD)


Compound	R ₁	R ₂	R ₃	GRK5 (0 min)	GRK5 (30 min)	GRK5 (60 min)	GRK5 (4 hr)	GRK1 (4 hr)	GRK2 (4 hr)	GRK6 (4 hr)	GRK5 C474S (4 hr)	GRK2/GRK5 [§]	
[‡] GSK 2163632A	1	NA	NA	H	-	-	3.2	0.13	20	-	-	6.2	
[‡] GSK 1713088A	2	NA	NA	H	-	-	3.2	13	6.3	-	-	2	
[‡] GSK 1326255A	3	NA	NA	H	-	-	2.5	>100	7.9	-	-	3	
CCG 262604	4		H	H	>100	>100	>100	-	>100	>100	-	NA	
CCG 258903	5		H	H	59 ± 90	11.3 ± 5	6.2 ± 3	0.22±0.1	>100	>100	0.41±0.2	>100	>450
CCG 263045	6		H	H	0.57±0.5	0.30±0.1	0.35±0.1	-	0.76±0.2	0.68±0.03	-	-	2
CCG 262606	7	H		H	18 ± 10	5.4 ± 8	5.9 ± 4	>100	>100	>100	>100	>100	>17
CCG 258904	8	H		H	20 ± 10	6.3 ± 4	5.5 ± 4	-	>100	39 ± 3	-	-	7
CCG 263115	9	H		H	0.22±0.03	0.26±0.03	0.27±0.03	-	2.1±0.6	2.7±0.2	-	-	10
CCG 264561	16a		H	CH ₃	-	-	-	>100	-	>100	>100	>100	NA
CCG 264099	16b		H	CH ₃	-	-	-	78±20	-	>100	>100	42±40	>1.3
CCG 264629	16c		H	CH ₃	-	-	-	17±10	-	>100	>100	-	>6
CCG 265328	16d		H	CH ₃	>100	-	28±20 [†]	1.1±0.4	-	>100	1.8±2	0.7±1	>90
CCG 265327	16e		H	CH ₃	-	-	-	19±20	-	>100	7.7±6	-	>5
CCG 265041	16f	H		CH ₃	-	-	-	>100	-	2.9±0.6	>100	-	<0.01
CCG 265042	16g	H		CH ₃	-	-	-	22±5	-	3.2±0.8	18±8	-	0.1
CCG 265044	16h	H		CH ₃	-	-	-	4.8±2	-	2.1±2	2.6±2	-	0.4
CCG 265268	16i	H		CH ₃	-	-	-	>100	-	>100	>100	-	NA
CCG 265267	16j	H		CH ₃	-	-	-	7.1±3	-	>100	2.5±3	-	>14

Experimental values derived from this report were run three times in duplicate with the exception of assays involving **5** against GRK5, GRK6, and GRK5-C474S with 4 hr incubations, which were performed two times in duplicate. Inhibitor incubation times are given in parentheses.

[‡]From Homan K. et al.³⁴. Note that these compounds were not assayed after 4 hr incubations and are listed here for comparison purposes only.

[§]Selectivity for GRK5 over GRK2 based on IC₅₀ ratio. The IC₅₀ value for the longest incubation with GRK5 was used for the calculation.

[†] Measured at 100 min.

at the four hour timepoint is consistent with the *meta* substituted ethyl amide CCG-262604 that showed >100 μM inhibition for GRK5 at all timepoints tested. The *para* substituted acrylamide, CCG-258903, exhibited an IC₅₀ of 6.2 μM for GRK5 after one hour of preincubation on ice, with no potency against GRK1 or GRK2. After 4 hr, CCG-258903 showed a convincing increase in potency as a function of time consistent with covalent inhibition, with an IC₅₀ of 0.2 μM (Table 2.1, Figure 2). The >16-fold difference in GRK5 potency for CCG-258903 relative to its non-covalent control CCG-262604 at 1 hour also suggests a covalent mechanism of action. The

compounds also exhibited >450 selectivity over GRK2. The *meta* acrylamide analog CCG-258904 had similar potency for GRK5 at all incubation times with respect to its non-covalent control CCG-262606 suggesting that it is not acting covalently. It also showed no inhibition of GRK1 but modest GRK2 inhibition ($IC_{50} = 39 \mu M$).

Both CCG-263045 and CCG-263115, featuring the N,N-dimethyl-butenoic amide in *para* and *meta* positions, respectively, had increased potency for all three GRKs relative to the acrylamide inhibitors CCG-258903 and CCG-258904, indicating that addition of the basic nitrogen augments potency against all three kinases. The *para* substituted analog, CCG-263045, was predicted to be closer to the AST loop, and thus more likely to form a covalent bond with Cys474. In our time dependent inhibition of GRK5, it shows some improvement from 0 min to 1 hr (GRK5 IC_{50} from 0.57 to 0.35 μM , respectively) but exhibits no selectivity over GRK1 or GRK2 ($IC_{50} = 0.76$ and 0.68 μM , respectively). The *meta* substituted analog, CCG-263115, did not show time dependent GRK5 inhibition (IC_{50} range = 0.22 – 0.27 μM), although it showed ~10-fold selectivity for GRK5 over GRK1 and GRK2 ($IC_{50} = 2.1$ and 2.7 μM , respectively). This difference in GRK selectivity between the *meta* and *para* substituted analogs CCG-263045 and CCG-263115 indicates that the position of the amide linked appendage from the methoxyphenyl ring is one route for gaining GRK5 selectivity. Despite their GRK5 potency CCG-263045 and CCG-263115 were not further pursued due to their lack of selectivity against GRK1 and 2.

We then determined IC_{50} values of the homologated compounds after a 4 hour incubation for GRK2, GRK5, and GRK6 (Table 2.1). GRK6 was included as a positive control for GRK4 subfamily selectivity. As in the non-homologated series, the ethylamide compounds (CCG-264561 and CCG-265041) showed an SAR cliff, with the *para* ethyl amide unable to inhibit any of the GRKs tested. The reactive *para*-substituted series (CCG-264099-265328) were more selective for GRK5/6 over GRK2 than their *meta* analogs with the exception of CCG-265327. GRK5 tolerated both the small substituents of the acrylamide CCG-264099 ($IC_{50} = 78 \mu M$) and vinyl sulfone, CCG-265327 ($IC_{50} = 19 \mu M$) but also the large N,N-dimethyl-butenoic amide of CCG-264629 ($IC_{50} = 17 \mu M$). The *para*-alkyne (CCG-265328) was the most potent and selective GRK5 inhibitor from this series ($IC_{50} = 1.1 \mu M$, 90-fold selectivity over GRK2 after 4 hour incubation). Interestingly, potency for GRK2 was lost for all compounds with the *para*-substitution. It is possible that the slightly longer AST-loop in the GRK2 subfamily allows it to reach further in the

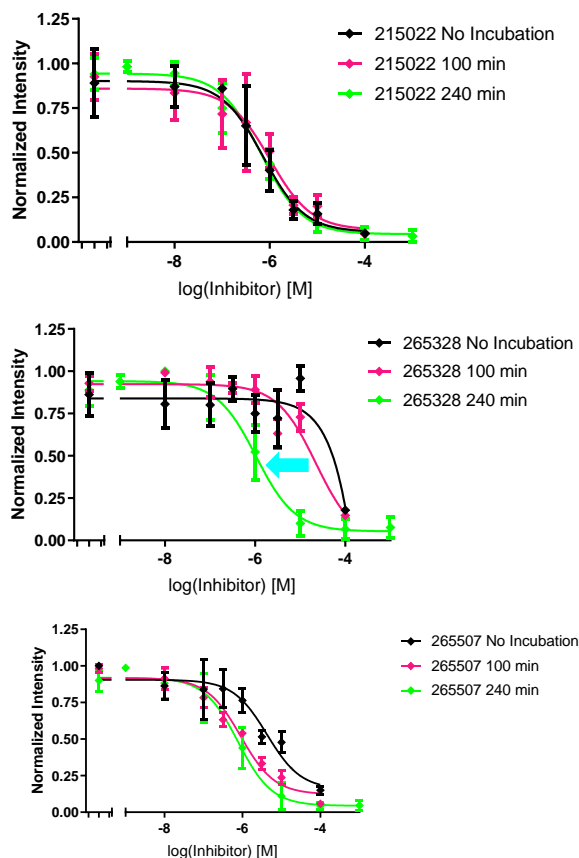


Figure 2.2 Time-dependent inhibition of GRK5 by CCG-265328 and CCG-265507 but not CCG-215022. Compounds were pre-incubated for times of 0 min (black), 100 min (magenta), and 240 min (green). (A) CCG-215022, which has no covalent modifier, does not show a significant change in IC_{50} (380 nM) over time. (B) 5 and (C) CCG-265328 exhibit the expected leftward shift in IC_{50} for covalent inhibitors as pre-incubation times increase, as indicated by the blue arrows. Each curve is the average of either 3 (CCG-215022 and CCG-265328) or 4 (5) experiments. Error bars are standard deviation.

active site, as seen for residues 476-479 in the GRK2-G β γ -GSK180736A co-crystal structure (PDB entry 4PNK), which would collide with substituents in the *para*-position.

Overall, the *meta*-substituted compounds (CCG-265041-265268) tended to have higher potency against GRK5 but lower or even reversed selectivity versus GRK2 (the exception being the vinyl sulfone CCG-265267). Small polar groups, specifically those with hydrogen bond acceptor capability, were well tolerated in GRK5. For example, both CCG-265042 and CCG-265267 inhibited GRK5, but the polar vinyl sulfone of CCG-265267 was more potent (IC_{50} = 7.1 μ M) than the more lipophilic acrylamide of CCG-265042 (IC_{50} = 22 μ M). The *meta*-alkyne (CCG-265268) had no potency for GRK5, suggesting that this more rigid covalent modifier may collide with the P-loop or AST-loop. The CCG-265044 compound had low μ M potency for GRK5.

Of the homologated series, only CCG-265042, CCG-265044 and CCG-265041 showed activity against GRK2. Our modeling suggested that shorter warheads may be more easily accommodated

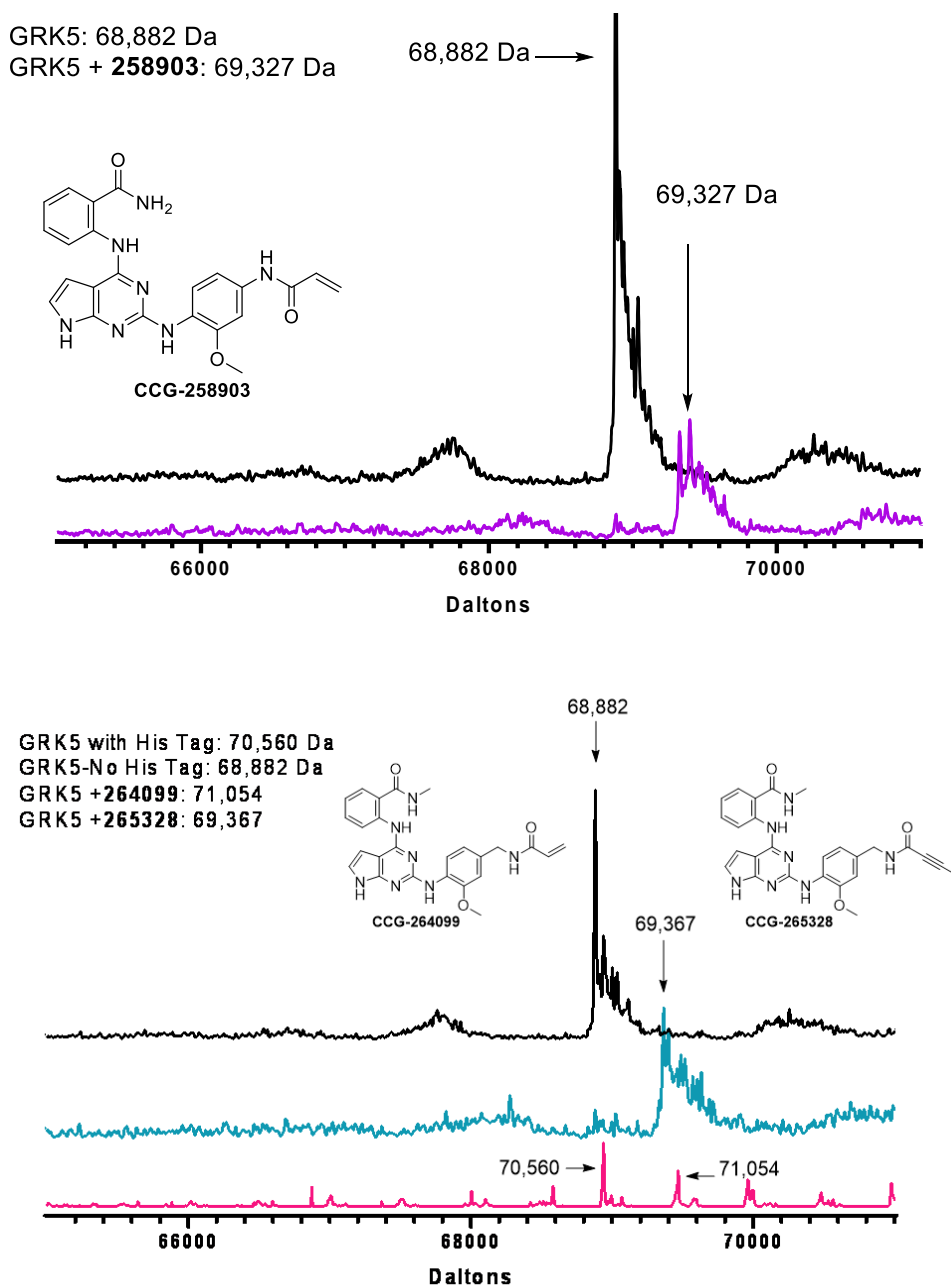


Figure 2.3. Evidence from intact mass spectrometry for covalent modification of GRK5 by CCG-258903, CCG-264099, and CCG-265328. (A) GRK5 only (black trace), GRK5-5 (purple). (B) MS traces for GRK5 (black trace), GRK5-265328 (ocean blue), and GRK5-264099 (pink). The latter trace indicates that 265328 only partially labeled GRK5.

within the shallow GRK2 ribose pocket. All the other *meta*-substituted materials have larger, less flexible warheads. As expected, inhibition of GRK6 was similar to that of GRK5 in most cases, the exception being CCG-265328, which was unable to inhibit GRK6. It is unclear whether this represents true intra-subfamily selectivity or a vagary of the experimental conditions for this combination. The most potent compound CCG-265328 was then additionally tested at 0 and 100 min incubations to assess if there was a time-dependent decrease in IC₅₀, the hallmark of covalent

inhibition. Indeed, CCG-265328 displayed a marked increase in apparent potency as a function of time (Figure 2.2).

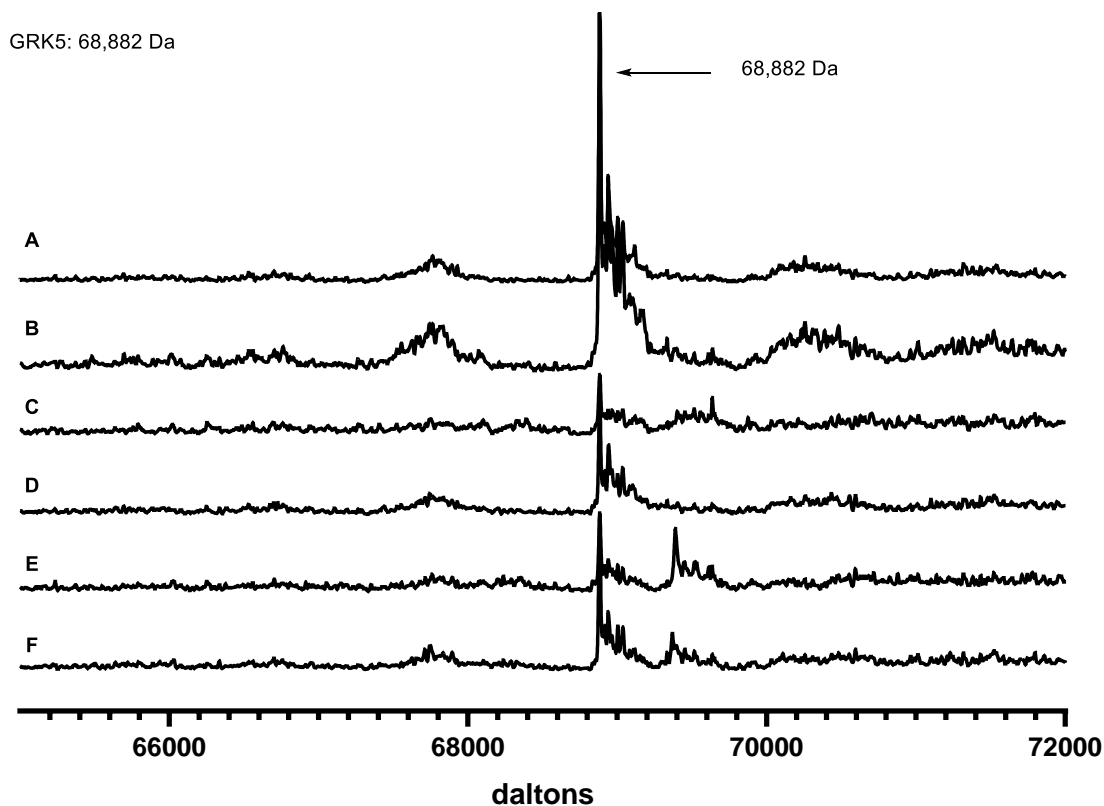


Figure 2.4 MS traces for (a) CCG-265041, (b) CCG-265042, (c) CCG-265044, (d) CCG-265267 and (e) CCG-265268 indicate that no *meta*-substituted material can make a covalent interaction with GRK5.

Further confirmation of covalent inhibition of GRK5 was achieved through intact protein mass spectrometry (MS). Compounds CCG-258903 and CCG-264099-265328 were tested, but only CCG-258903, CCG-264099 and CCG-265328 showed significant amounts of covalent linkage after a three hour incubation (Figure 2.3), consistent with the results of our radiometric assays. Compounds CCG-265041-265268 were also tested but showed no covalent inhibition (Figure 2.4). For CCG-258903, CCG-264099 and CCG-265328, we also tested whether inhibition is affected when Cys474 is mutated to serine (GRK5-C474S). A decrease in GRK5-C474S potency relative to wild-type GRK5 would thus be consistent with a covalent inhibition mechanism. Compound CCG-258903 lost all potency against the mutant protein, whereas CCG-264099 and CCG-265328 retained comparable activity. The reason is unclear, but it is possible that either the intrinsic

GRK5: 68,882 Da
GRK5 + **265328**: 69,367 Da

GRK5 C474S: 68,921 Da
GRK5 C474s + **265328**: 69,405 Da

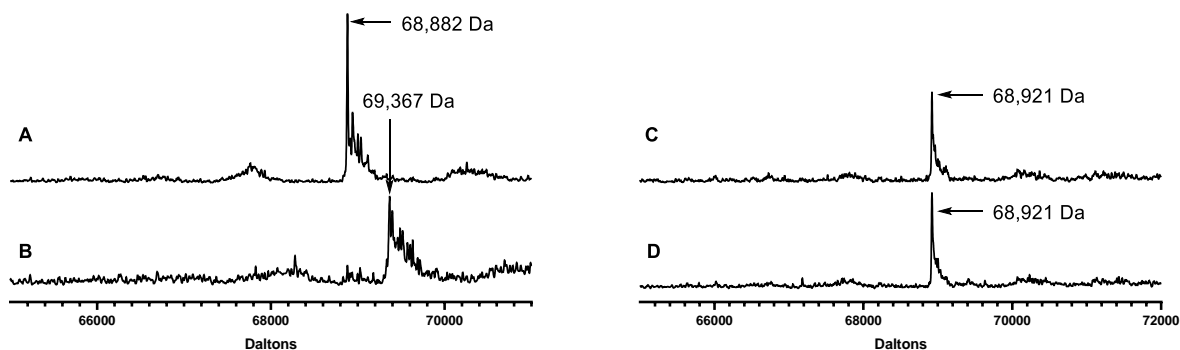


Figure 2.5 Evidence for GRK5-Cys474 covalent engagement of CCG-265328. (A) MS trace for GRK5, (B) MS trace for GRK5 incubated with CCG-**265328** indicating covalent modification, (C) MS trace for GRK5-C474S, (D) MS trace for GRK5-C474S incubated with CCG-265328 indicates that CCG-265328 cannot covalently modify GRK5-C474S. Each peak shown is representative of n = 3 experiments.

reactivity of these compounds is sufficient, or their reactive groups are more optimal oriented to engaged in a non-covalent interaction with an additional hydrogen bond donor on GRK5. However, the base scaffold may also simply bind with high affinity irrespective of covalent attachment. We next tested whether CCG-265328 engaged GRK5 in a covalent bond specifically at Cys474 using intact protein MS and showed that GRK5-C474S mutant does not react (Figure 2.5). Using tandem mass spectrometry (MS/MS) we further observed that CCG-265328 labels Cys474 but also a cysteine located in a solvent-exposed position in its regulator of G protein signaling homology domain, remote from the active site (Figure 2.6). The labeling of Cys54 is

more consistent with a concentration dependent labelling event than with a biologically relevant interaction. As the concentration of CCG-265328 needed to achieve a detectable amount of labelled Cys474 is above 1 mM, it is unsurprising that this extraneous labelling event occurred. In summary, we report the first examples of covalent inhibitors of GRK5, including the first examples of covalent, selective GRK5 inhibitors, CCG-258903 and CCG-265328, with high nM to low μ M potency. We have leveraged the pyrrolopyrimidine scaffold to install *para*-substituted linkers that can interact covalently with the AST from GRK5 but not from GRK2. Additionally, we have shown that Cys474 is selectively targeted by our covalent warheads, validating our design strategy. Moving forward, we aim to further improve the potency of these compounds against GRK5 and GRK6, and to pursue crystal structures of the GRK5/6-258903 and CCG-265328 complexes to confirm their binding poses and the effect of covalent modification on the overall conformation of GRK5. Before examining the effects of our compounds *in vivo* on cardiomyocyte contractility and, ultimately, to parse the role of GRK5 in heart failure, these compounds will also need to be tested for selectivity against other protein kinases.

2.4 Initial Testing Suggests CCG-265328 Can Improve Contractility in Primary Cardiomyocytes

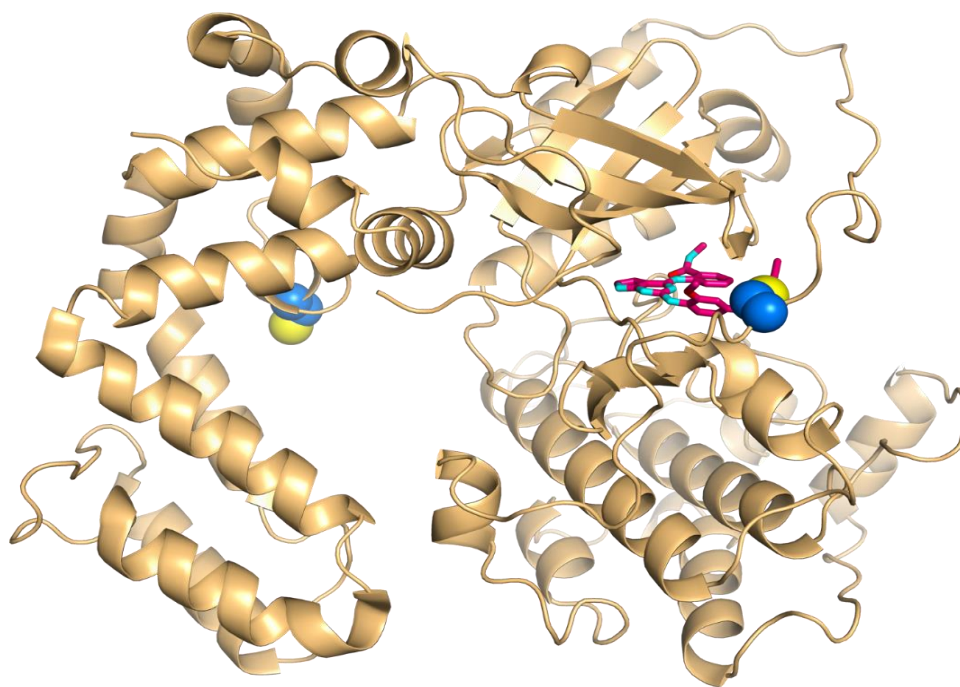


Figure 2.6 GRK5 (gold) with CCG-265328 (pink) bound to the hinge. Cys474 (blue) was tagged by 265328, indicating it is a covalent handle. The more solvent exposed Cys54 (light blue) was also tagged, in a concentration-dependent labelling event.

Validation of CCG-265328 as a compound with high levels of selectivity, and a covalent interaction with Cys474 has opened the door to testing in various disease state models. While

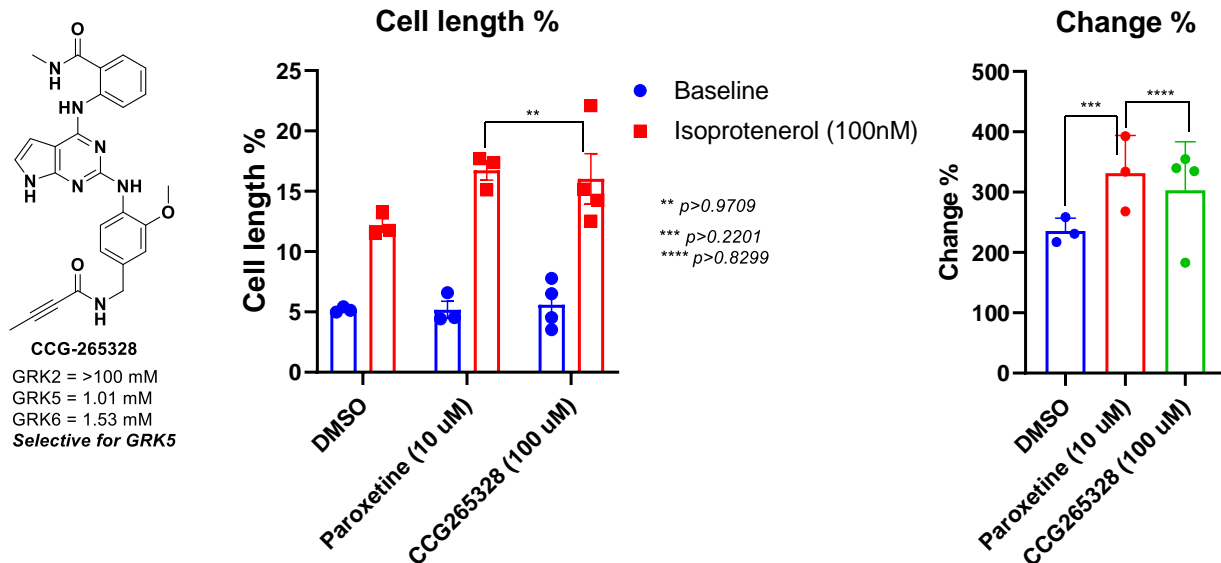


Figure 2.7 CCG-265328 can produce similar contractility improvements to that seen with paroxetine in primary cardiomyocytes following isoproterenol (100 nM) induced TAC. Each bar is an average of 3-4 experiments. Errors bars represent standard deviation.

GRK5 has been implicated in multiple disease states, we are primarily concerned with understanding its role in heart failure. Previously, it has been shown that GRK2 inhibitors can reverse the contractility loss in cardiomyocytes following isoproterenol inducing transverse aortic constriction (TAC). Using this same assay, CCG-265328 was shown to also improve contractility in primary cardiomyocytes at a concentration of 100 μ M. Following isoproterenol, CCG-265328 was able to shorten cardiomyocyte length, indicating that contractility improvement in this model. Cardiomyocytes treated with CCG-265328 had a comparable cell length to those treated with paroxetine, an FDA-approved SSRI compound which is known to improve cardiac function in heart failure (Figure 2.7).⁹ While these results are preliminary, the data does suggest that GRK5 may also play a role in improving cardiomyocyte contractility, independent of the effect seen by inhibiting GRK2. Further work with CCG-265328 can also help to elucidate the full role of GRK5 in heart failure, and other disease states.

2.5 SAR is Tractable to the 5-methylpyrimidine Series, but Does Not Offer Better Potency

Table 2.2: IC₅₀ Values for 5-Methylpyrimidine and Alternative Pyrrolopyrimidine Compounds (μM ± SD)

Compound	R ₁	R ₂	GRK5 (4 hr)	GRK2 (4 hr)	GRK6 (4 hr)	GRK5 C474S (4 hr)
CCG-265507	S1		0.778	> 100	0.755	ND
CCG-265508	S1		> 100	> 100	> 100	ND
CCG-265595	S2	NA	> 100	> 100	> 100	ND
CCG-265596	S2	NA	> 100	> 100	> 100	ND
CCG-265647	S1		> 100	> 100	> 100	ND
CCG-265648	S1		22.1	> 100	> 100	ND

Experimental values derived from this report were run three times in duplicate. Inhibitor incubation times are given in parentheses. Scaffold denotation given as Scaffold 1 (S1) or Scaffold 2 (S2). Activity against GRK5-C474S not determined. Error represents the standard deviation (data not shown).

While the initial series of pyrrolopyrimidine based analogues offers moderate potency, it did allow for the validation of Cys474 as a covalent handle. However, there are pharmacokinetic issues with this series, such as poor solubility which may be limiting the intrinsic potency of these analogues. Our best compound, CCG-265328, had limited solubility (25.8 μM in water). This lack of solubility, when paired with the modest potency of the compound, creates concern about the overall utility of this series. Therefore, we chose to explore analogues which could either increase water solubility, or limit metabolic liabilities thereby increasing exposure time. Our initial change, the addition of a 3-pyridyl pendant, yielded CCG-265596 (Table 2.2). Such a change allows for the lowering of the solubility forecast index (SFI) by way of the cLogP. In this case, pyridyl pendant offer a decrease in cLogP while largely maintaining the properties of the lead compound, CCG-265328. CCG-265596 did display better water solubility (43.2 μM in water) by about 2-fold.

However, we tested within our radiometric assay, this analogue and any analogue featuring a pyridyl pendant in this northern hemisphere are inactive ($K_i > 100 \mu\text{M}$).

One of the other common ways to increase water solubility is to break planarity within the molecule. Following this rule, we synthesized CCG-265507, CCG-265508, CCG-265647 and CCG-265648. Interestingly, we found that CCG-265507, which is the 5-methylpyrimidine equivalent of CCG-265328, does maintain the same level of activity as the original lead compound. Better still, CCG-265507 demonstrated a 12-fold increase in water solubility, thereby validating our rationale design to increase solubility. Additionally, we were able to demonstrate that CCG-265507 maintains the ability to form a covalent adduct with GRK5-C474 through intact and tandem MS (Figure 2.8). A number of cysteines were labeled by CCG-265507 within the tandem MS experiment, however, these labelling events are thought to be concentration dependent. CCG-265507, was shown to label C54, C201, C144, and C297 in addition to the labelling event seen at

Protein FC	Accession	Description	Exp. q-value	Sum PEP S	Coverage	# Peptide	# PSMs	# Unique	# AAs	calc. pl	
High	P34947	G protein-coupled receptor kinase		0	595.461	90	92	3239	33	590	8.1
Confidenc		Annotated Sequence	Modifications	Modificat	Quality	PE Quality	q-#	Protein	# Proteins	# PSMs	Positions in Master Proteins
High		[D].YCSLCDKQPIGRLLFRQFCE.[T]	2xCarbamidomethyl [C5; C]; 1xRowland-2 [C]		0.01133		0	1	1	4	P34947 [53-72]
High		[E].VCACQVRATGKMYACKRLE.[K]	2xCarbamidomethyl [C4; C15]; 1xRowland-2 [C2]		0.20408	0.00866		2	2	1	P34947 [200-218]; GRK_C474S [200-218]
High		[E].LFSACAQSVHE.[Y]	1xRowland-2 [C5]		0.37294	0.00866		1	1	1	P34947 [141-151]
High		[E].ILCGLEDLHRE.[N]	1xRowland-2 [C3]		0.00314		0	1	1	1	P34947 [295-305]
High		[E].AGMLDPPFPVDPRAVYCKD.[V]	1xRowland-2 [C17]		0.24219	0.00866		1	1	1	P34947 [458-476]
High		[D].PPFVDPRAVYCKDVLIDIE.[Q]	1xRowland-2 [C12]		0.26184	0.00866		1	1	1	P34947 [463-481]
High		[E].AGMLDPPFPVDPRAVYCKD.[V]	1xOxidation [M3]; 1xRowland-2 [C17]		0.24019	0.00866		1	1	1	P34947 [458-476]
High		[E].AGMLDPPFPVDPRAVYCKDVLIDIE.[Q]	1xOxidation [M3]; 1xRowland-2 [C17]		0.04949		0	1	1	1	P34947 [458-479]

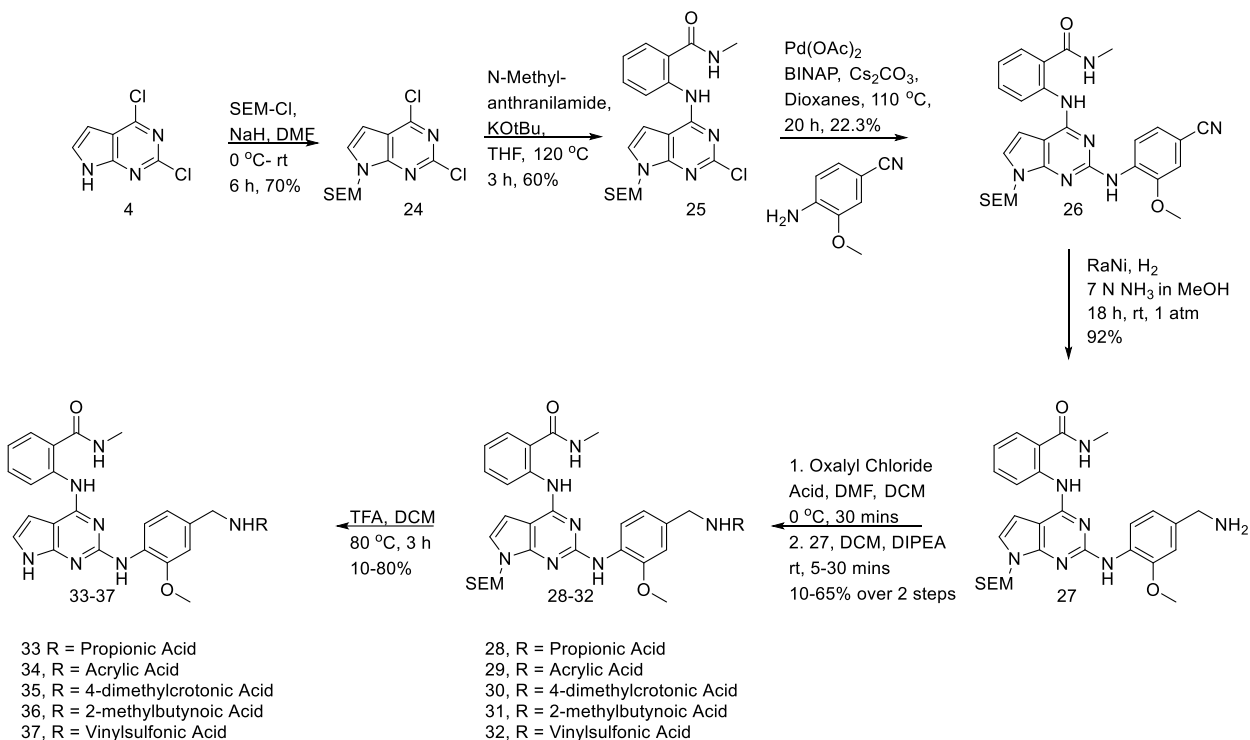
Figure 2.8 Tandem MS/MS data for CCG-265507 indicates that Cys474 is tagged and detected in multiple peptide fragments. Similar to 265328, 265507 also labels more solvent exposed cysteine residues, and due to the high concentration in the sample, at a higher rate than what is observed in the 265328 tandem MS/MS sample.

C474. These cysteine residues are known to be placed at solvent exposed regions of GRK5, suggesting that when CCG-265507 is in excess, in this case there is a 100-fold excess of compound, then solvent exposed regions of the target are also labeled. These data are consistent with concentration dependent labeling event seen in a GRK5-CCG-265328 tandem MS experiment. When GRK5-C474S is used for tandem MS, CCG-265507 cannot form the covalent adduct seen in the GRK5-WT experiment (data not shown). This validates the applicability of our covalent strategy to other more intrinsically potent scaffolds.

However, CCG-265508 and CCG-265647 are inactive, suggesting that potentially the activity of CCG-265507 is driven by covalent engagement of Cys474. Interestingly, CCG-265648, which features a 3-pyridyl in place of the methylbenzylamide featured in CCG-265507, has some intrinsic GRK5 activity, though it is poor ($IC_{50} = 22.1 \mu\text{M}$). This poor activity could be due to low

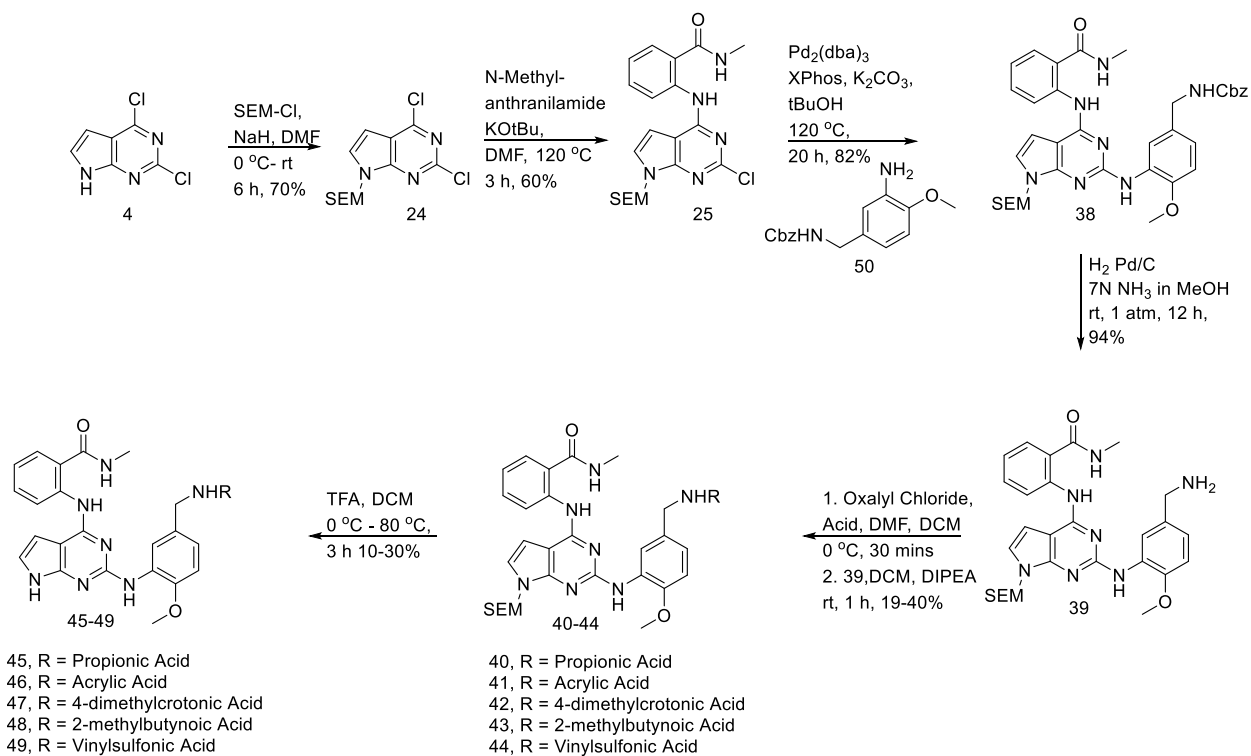
intrinsic potency of the scaffold coupled with covalent interaction at Cys474. Together, these data suggest that the limiting factor for potency of these compounds may be the entropic cost of locking down the flexible AST-loop. We hypothesized that a more intrinsically potent non-covalent scaffold would be able to overcome this entropic cost, and our covalent strategy applied from there.

2.6 Synthesis of Compounds

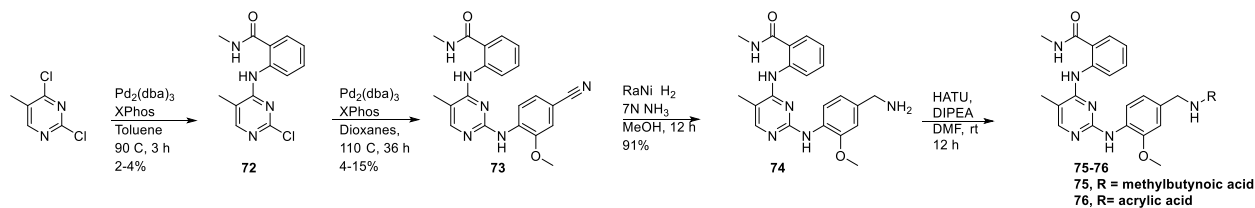


Scheme 2.1 Synthetic route to CCG-264099-265328.

Synthesis of CCG-264099-CCG-265328 starts with the SEM-protection of common intermediate, 2,4-dichloropyrrolopyrimidine, yielding intermediate **24**. The northern hemisphere pendant is then introduced using an SNAr with 2-aminomethylbenzamide to give common intermediate **25**. From **25**, the synthesis of these compounds diverge. For the *para*-substituted materials (CCG-264099-CCG-265328), **25** is submitted to a Buchwald-Hartwig cross-coupling with 4-amino-3-methoxybenzonitrile to give **26**. The benzonitrile is then reduced with Raney nickel to give the free amine **27**. The free amine is then coupled to an appropriate warhead acid to yield **28-32**. Finally, the SEM protecting group is removed to unveil the final products, CCG-264099-265328 (**33-37**).



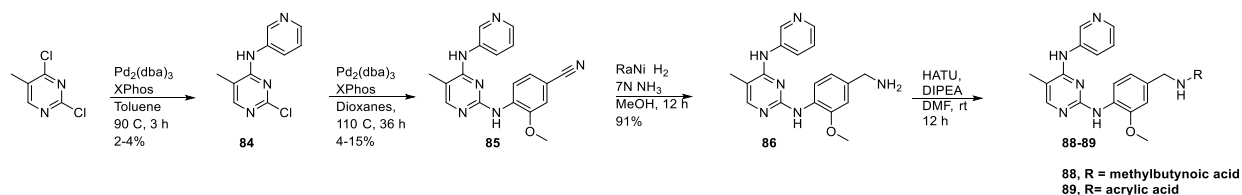
Scheme 2.2 Synthetic route to CCG-265041-265268.



Scheme 2.3 Synthetic route to CCG-265507 and CCG-265508.

In a similar fashion, CCG-265041-265268 are made through a Buchwald-Hartwig cross-coupling of **25** with **50**. **50** is made through a selective reduction of 3-amino-4-methoxybenzamide (**51**), and subsequent selective Cbz-protection of the diamine, **52**. From **38**, the Cbz-protecting group is then removed with hydrogen and palladium on carbon to give the free-amine, **39**. The free amine then undergoes an amide coupling with an appropriate warhead acid to yield **40-44**. The final products CCG-265041-265268 (**45-49**) are then unveiled through acid-catalyzed deprotecting of the SEM-group.

In an abbreviated synthesis, CCG-265507-CCG-265508 were made starting with an SNAr with 2,4-dichloro-5-methylpyrimidine and 2-aminomethylbenzamide to give **72**. **72** is then submitted to an optimized Buchwald cross-coupling with 3-methoxy-4-aminobenzonitrile to give **73**. From **73**, the free amine **74** is accessed through reduction with Raney Nickel. Finally, CCG-265507 and CCG-265508 (**75** and **76** respectively) are then accessed through an amide coupling catalyzed by HATU. In economical form, this synthetic route had no additional protecting groups to be removed, allowing a faster, stream-lined synthesis.



Scheme 2.4 Synthetic route to CCG-265647 and CCG-265648.

Access to the starting materials for CCG-265647 and CCG-265648 proved more difficult due to the highly electron-rich nature of the pendants. 3-aminopyridine is used in a Buchwald cross-coupling to produce **84**. Then, a subsequent Buchwald cross-coupling is used to install the 3-methoxy-4-aminobenzonitrile linker to give **85**. The free amine, **86**, is then accessed through reduction by Raney Nickel. Finally, CCG-265647 and CCG-265648 (**88** and **89** respectively) are accessed through an amide coupling with an appropriate acid starting material.

2.7 Materials, Methods and Synthetic Experimental Data

General Chemistry: All reagents from commercial sources were used without further purification unless otherwise noted. ¹H-NMR spectra were taken in DMSO-d₆, MeOD or CDCl₃ at room temperature on Varian MR 400 MHz; Varian Vnmrs 500 MHz; and Varian Vnmrs 700 MHz instruments. The reported chemical shifts for the ¹H-NMR spectra were recorded in parts per million (ppm) on the δ scale from an internal tetramethylsilane (TMS) standard (0.0 ppm). Small molecule mass spectrometry data was measured using a Waters Corporation Micromass LCT or Agilent6230 Q-TOF instrument. HPLC was used to determine purity of compounds on an Agilent 1100 series with an Agilent Zorbax Eclipse Plus-C18 column. A gradient of 10-90% acetonitrile/water over 6 min followed by 90% acetonitrile/water for 7 min was used with detection at 254 nm.

Intact Protein MS and Tandem MS/MS: Intact protein MS was acquired with a Phenomenex C4 column paired with an Agilent 6545 Q-TOF LC/MS. For intact MS and Tandem MS, all samples were prepared with 20 μM GRK in assay buffer (see below), 1 mM compound, and incubated at 4 °C for 3 hr before being quenched with 1.0 μL of formic acid. In Tandem MS/MS, we chose Glu-C as the restricting enzyme to avoid small fragments with mass-to-charge ratios below the limit of detection of our instrument.¹ All samples were digested with Glu-C sequencing enzyme, procured from Sigma Aldrich (Roche Life Sciences subsidiary) and used without further purification. MS/MS experiments were run on a nano-LC (Dionex RSLC-nano) with an Orbitrap Fusion Tribrid ETD mass spectrometer. This work was conducted by the Proteomics Resource Facility at the University of Michigan.

Inhibition Assays: For compounds **10-23**, IC₅₀ values for human GRK5, bovine GRK2, and bovine GRK1 were determined using a radiometric assay as follows. 50 nM GRK was incubated with 500 nM porcine brain tubulin (Cytoskeleton) and 0 - 333 μM inhibitor in 20 mM HEPES pH 7.0, 2 mM MgCl₂, 0.025% dodecylmaltoside (DDM), 3% DMSO for 20-30 min for GRK1 and 2 and 0-1 hr for GRK5, as denoted in **Table 1**, on ice, prior to initiation with the addition of 5 μM ATP supplemented with radioactive [³²P]-ATP (PerkinElmer Life Sciences). Reactions were quenched at 5 min by addition of 6 μL of 4X SDS gel loading dye to the 6 μL reactions. 8 μL samples were separated on a 4-15% Criterion TGX precast gel (Bio-Rad). Experiments were performed with an n = 3 in duplicate.

For the remaining compounds CCG-264099-265328, IC₅₀ values for human GRK5, bovine GRK2, bovine GRK6, and bovine GRK5-C474S were similarly determined with the following differences. Inhibitors were assessed over the range of 1 nM–1 mM in 20 mM HEPES pH 7.5, 10 mM NaCl, 10 mM MgCl₂, 2 mM DTT after a 4 hr incubation at room temperature prior to reaction initiation with ATP. Reactions were

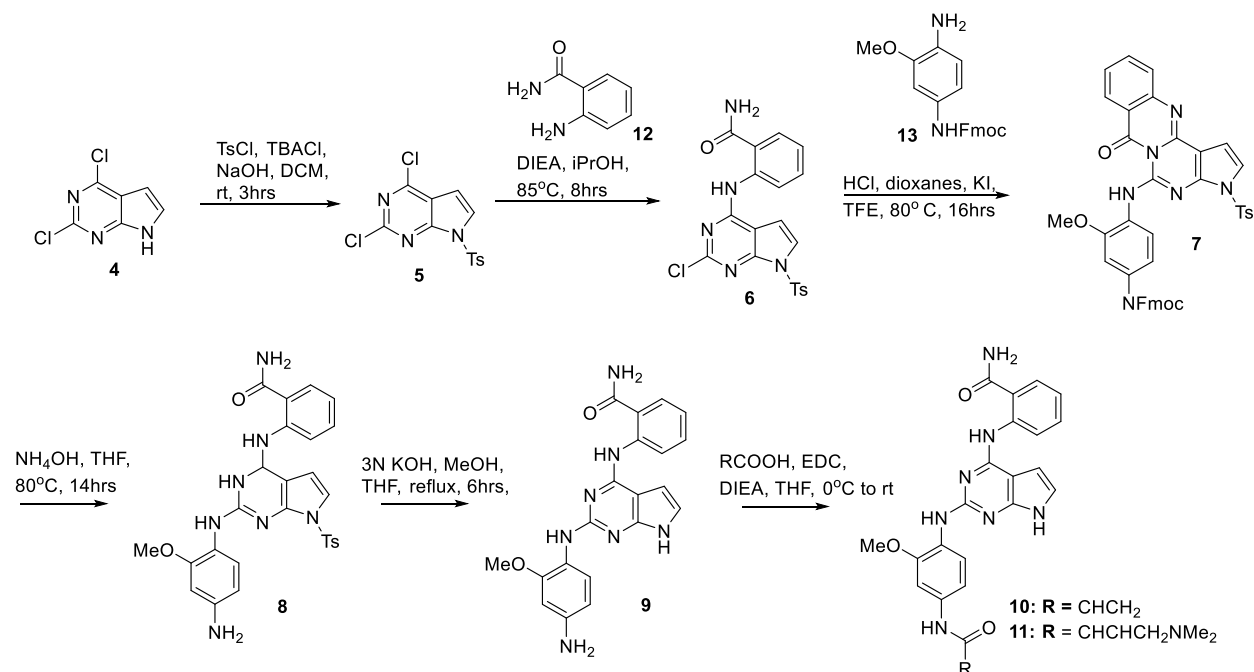
quenched at 8 min by transferring 10 μ L reaction into 5 μ L 4X SDS gel loading dye. 10 μ L samples were separated on a 4-15% Criterion TGX precast gel. These conditions were also used to assess compound **10** for GRK5 (4 hr), GRK2, and GRK5-C474S but with the addition of 3% DMSO (final) to the incubation buffer. Experiments were performed with an n = 3 except for assays involving **5** against GRK5, GRK6, and GRK5-C474S with 4 hr incubations, which were performed 4 times.

For compounds CCG-258903 and CCG-265328, IC₅₀ values were also determined when opsin was used as the substrate. 50 nM of GRK5 were preincubated with 0-750 μ M inhibitor in buffer containing 20 mM HEPES pH 7.0, 2 mM MgCl₂, 0.025% dodecylmaltoside (DDM), 3% DMSO for 0, 30, 60 or 240 min. Rhodopsin in the rod outer segment was exposed to the light for approximately 3 min right before phosphorylation. 5 μ M ATP supplemented with radioactive [γ -³²P]-ATP (PerkinElmer Life Sciences) was added to initiate the reaction. Reactions were quenched at 5 min by addition of 10 μ L of 4X SDS gel loading dye to the 20 μ L reactions. 12 μ L samples were separated on a 4-15% Criterion TGX precast gel (Bio-Rad). Experiments were performed with an n = 2 for compound **5** and n=3 for compound **16d**.

Gels were dried, exposed to a storage phosphor screen overnight, and scanned using a Typhoon scanner. Bands corresponding to phosphorylated tubulin were quantified using ImageQuant, plotted as a function of log[inhibitor], and fit to the three-parameter log(inhibitor) vs. response model in GraphPad Prism 7.03 to determine the IC₅₀, and mean and standard deviation values were calculated using the column statistics function of GraphPad Prism 7.03.

Standard control compounds are run during each assay to assess consistency across time, experimenters, and subtle changes in assay conditions that are sometimes required to keep some of the compounds soluble and disperse (such as through addition of DDM or 3% DMSO). Paroxetine, GSK180736A, and CCG215022 were used as controls for compounds CCG-258903-262606, and CCG215022 for compounds CCG-264099-265328.

Synthetic Protocols:



Scheme 2.5: Synthesis of non-homologated *para*-substituted analogues **10** and **11**.

2,4-dichloro-7-tosyl-7H-pyrrolo[2,3-d]pyrimidine (5): To a 100 mL round bottom flask was added 2,4-dichloro-7H-pyrrolo[2,3-d]pyrimidine **4** (1.0 g, 5.32 mmol), 4-methylbenzene-1-sulfonyl chloride (1.12 g, 5.85 mmol), tetra-butyl ammonium chloride (0.07 g, 0.27 mmol), and dichloromethane (20 mL). Then 6N sodium hydroxide (2.66 mL, 15.96 mmol) was added dropwise. The slurry was stirred at room temperature vigorously for 1.5 hours going from cloudy to clear. The reaction was then diluted with water and the layers were separated. The organic layer was washed with NaCl (1x), and then dried with MgSO₄. The MgSO₄ was filtered off and the filtrate was then concentrated. The resulting off white solid was purified using 100% dichloromethane to give the title compound as a white solid (1.64 g, 4.79 mmol, 89% yield). ¹H NMR (500 MHz, DMSO-d₆) δ 8.13 (d, J = 4.0 Hz, 1H), 8.07 – 8.01 (m, 2H), 7.51 (d, J = 8.2 Hz, 2H), 6.99 (d, J = 4.1 Hz, 1H), 2.39 (s, 4H). HPLC (gradient A): retention time = 8.207 min; purity = 98%.

2-((2-chloro-7-tosyl-7H-pyrrolo[2,3-d]pyrimidin-4-yl)amino)benzamide (6): To a 100 mL round bottom flask was added 2,4-dichloro-7-tosyl-7H-pyrrolo[2,3-d]pyrimidine **5** (0.93 g, 2.72 mmol) and 2-aminobenzamide **S7** (1.48 g, 10.88 mmol). Isopropanol (16 mL) and di-isopropylethylamine (2.38 mL, 13.6 mmol) were then added and the reaction was heated to reflux at 85 °C. All solids went into solution upon heating. After refluxing overnight, the reaction was cooled down and the resulting white precipitate was filtered off and washed with additional isopropanol to give the title compound (1.10 g, 2.49 mmol, 92% yield). ¹H NMR (400 MHz, DMSO-d₆) δ 12.34 (s, 1H), 8.50 – 8.43 (m, 1H), 8.32 (s, 1H), 8.00 (d, J = 8.2 Hz, 2H), 7.85 (d, J = 7.9 Hz, 1H), 7.81 (s, 1H), 7.77 (d, J = 3.9 Hz, 1H), 7.59 (t, J = 7.9 Hz, 1H), 7.49 (d, J

= 8.1 Hz, 2H), 7.19 (t, $J = 7.6$ Hz, 1H), 6.70 (d, $J = 4.0$ Hz, 1H), 2.38 (s, 3H). HPLC (gradient A): retention time = 7.890 min; purity = 99%.

5-((4-amino-2-methoxyphenyl)amino)-3-tosylpyrrolo[2',3':4,5]pyrimido[6,1-b]quinazolin-7(3H)-one (**7**): To a 100 mL pressure vessel was added 2-((2-chloro-7-tosyl-7H-pyrrolo[2,3-d]pyrimidin-4-yl)amino)benzamide **6** (0.221 g, 0.500 mmol), (9H-fluoren-9-yl)methyl (4-amino-3-methoxyphenyl)carbamate **13** (0.189 g, 0.525 mmol), 4M HCl in dioxanes (0.50 mL, 2.0 mmol), potassium iodide (0.01 g, 0.06 mmol), and trifluoroethanol (10 mL). The sealed reaction was then heated overnight at 90 °C. The following day the reaction was cooled to room temperature and then a light yellow/orange solid was filtered off and taken as is to the next step.

2-((2-((4-amino-2-methoxyphenyl)amino)-7-tosyl-4,7-dihydro-3H-pyrrolo[2,3-d]pyrimidin-4-yl)amino)benzamide (**8**): To a 50 mL pressure vessel was added crude *5-((4-amino-2-methoxyphenyl)amino)-3-tosylpyrrolo[2',3':4,5]pyrimido[6,1-b]quinazolin-7(3H)-one* **7** (0.264 g, 0.50 mmol), 28% ammonium hydroxide in water (10 mL), and THF (10mL). The sealed reaction was heated to 60 °C overnight. After cooling the reaction was diluted with dichloromethane and water. The layers were separated, and the organic layer was washed with NaCl (2x) and then dried over sodium sulfate. The sodium sulfate was filtered off and the filtrate was concentrated. The resulting orange solid was purified using 0-10% MeOH/DCM to give the title compound as a white solid (0.120 g, 0.065 mmol, 44% yield over two steps). ¹H NMR (400 MHz, DMSO-*d*₆) δ 12.12 (s, 1H), 8.80 (s, 1H), 8.31 (s, 1H), 7.93 (d, $J = 7.8$ Hz, 2H), 7.84 – 7.80 (m, 1H), 7.75 (s, 1H), 7.36 (d, $J = 8.1$ Hz, 3H), 7.33 (d, $J = 4.0$ Hz, 1H), 7.02 (t, $J = 7.6$ Hz, 1H), 6.46 (d, $J = 4.0$ Hz, 1H), 6.38 (d, $J = 2.2$ Hz, 1H), 6.32 – 6.24 (m, 1H), 5.02 (s, 2H), 3.70 (s, 3H), 2.36 (s, 3H). HPLC (gradient A): retention time = 5.711 min; purity = 94%.

2-((2-((4-amino-2-methoxyphenyl)amino)-4,7-dihydro-3H-pyrrolo[2,3-d]pyrimidin-4-yl)amino)benzamide (**9**): To a 50 mL round bottom flask was added 2-((2-((4-amino-2-methoxyphenyl)amino)-7-tosyl-4,7-dihydro-3H-pyrrolo[2,3-d]pyrimidin-4-yl)amino)benzamide **8** (0.315 g, 0.579 mmol) followed by THF (10 mL), MeOH (2 mL), and 3N potassium hydroxide (6.0 mL). The reaction was stirred, refluxing, at 65 °C overnight. After cooling the organic solvents were concentrated off and then the reaction was diluted with ethyl acetate. The layers were then separated, and the organic layer was washed with NaCl (1x) and dried over sodium sulfate. The sodium sulfate was then filtered off and the resulting filtrate was concentrated and purified using 0% - 8% MeOH/DCM to give the title compound as a slightly grey solid (0.132 g, 0.339 mmol, 59% yield). ¹H NMR (400 MHz, DMSO-*d*₆) δ 11.95 (s, 1H), 11.19 (s, 1H), 8.97 (d, $J = 8.5$ Hz, 1H), 8.28 (s, 1H), 7.88 – 7.77 (m, 1H), 7.77 – 7.65 (m, 1H), 7.52 (d, $J = 8.3$ Hz, 1H), 7.41 (t, $J = 7.9$ Hz, 1H), 7.29 (s, 1H), 6.98 (t, $J = 7.5$ Hz, 1H), 6.91 (dd, $J = 3.4, 2.2$ Hz, 1H), 6.33 (d, $J = 2.3$ Hz, 1H), 6.22 (dd, $J = 3.5, 1.9$ Hz, 1H), 6.18 (dd, $J = 8.4, 2.3$ Hz, 1H), 4.91 (s, 2H), 3.71 (s, 3H). HPLC (gradient A): retention time = 4.120 min; purity =

84%.

2-((2-((4-acrylamido-2-methoxyphenyl)amino)-7H-pyrrolo[2,3-d]pyrimidin-4-yl)amino)benzamide (**10**, **CCG-258903**): In a 25 mL flask 2-((2-((4-amino-2-

methoxyphenyl)amino)-7H-pyrrolo[2,3-d]pyrimidin-4-yl)amino)benzamide **9** (0.10 g, 0.257 mmol) was dissolved in THF (6.0 mL). Diisopropylethylamine (0.134 mL, 0.770 mmol) and 1-ethyl-3-(3-dimethylaminopropyl)carbodiimide hydrochloride (0.098 g, 0.512 mmol) were then added and the reaction was stirred ten minutes and cooled to 0 °C. Acrylic acid (0.02 mL, 0.282 mmol) was then added and the reaction was allowed to warm to room temperature and stir overnight. Water was added to quench the reaction and then ethyl acetate was added to extract the organics. The layers were separated, and the organic layer was washed with NaHCO₃ (1x), dried over magnesium sulfate, and concentrated. The resulting residue was purified using flash chromatography (0 – 10% MeOH/DCM) to give a light yellow solid as the desired compound

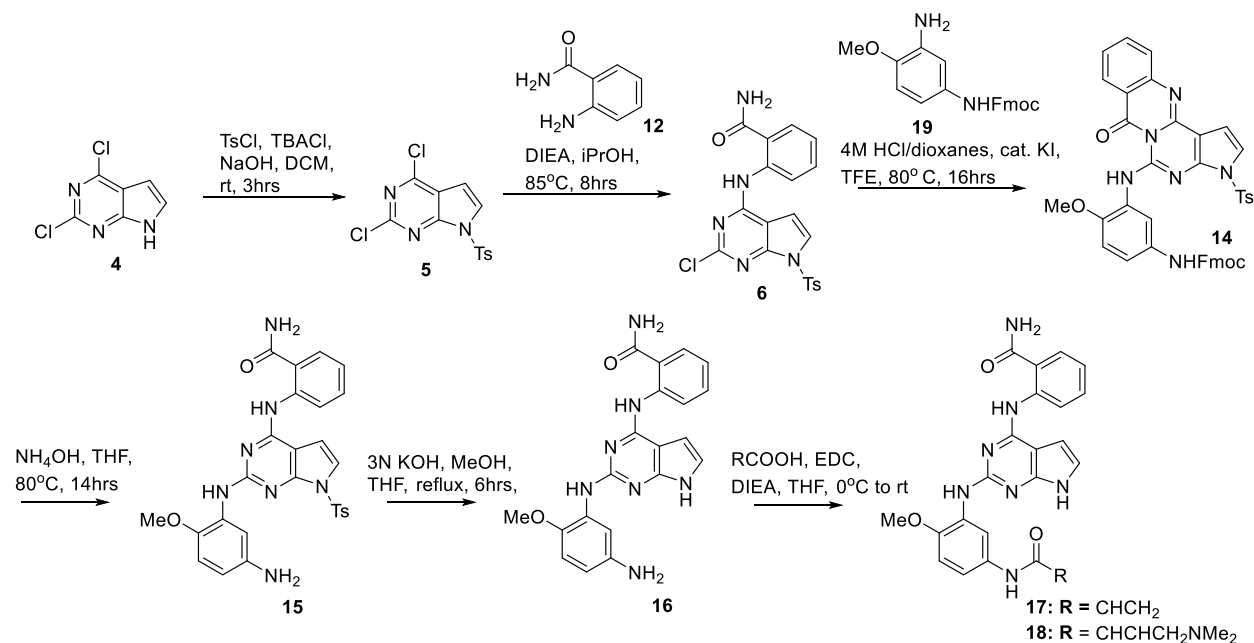
(0.0107 g, 0.024 mmol, 10% yield). ¹H NMR (400 MHz, DMSO-*d*₆) δ 11.99 (s, 1H), 11.36 (s, 1H), 10.10 (s, 1H), 8.93 (d, *J* = 8.5 Hz, 1H), 8.30 (s, 1H), 8.20 (d, *J* = 8.7 Hz, 1H), 7.83 (d, *J* = 7.7 Hz, 1H), 7.74 (s, 1H), 7.56 – 7.43 (m, 3H), 7.24 – 7.16 (m, 1H), 7.07 – 6.97 (m, 2H), 6.44 (dd, *J* = 17.0, 10.1 Hz, 1H), 6.32 – 6.20 (m, 2H), 5.78 – 5.70 (m, 1H), 3.85 (s, 3H). HPLC

(gradient A): retention time = 4.987 min; purity = 95%. Molecular formula: C₂₃H₂₁N₇O₃, Mass Calc: 443.17, ESI-MS Found: 444.1626 [M+1]

(E)-2-((2-((4-(4-(dimethylamino)but-2-enamido)-2-methoxyphenyl)amino)-7H-pyrrolo[2,3-

d]pyrimidin-4-yl)amino)benzamide (**11**, **CCG-263045**): In a 25 mL flask 2-((2-((4-amino-2-methoxyphenyl)amino)-7H-pyrrolo[2,3-d]pyrimidin-4-yl)amino)benzamide **9** (0.137 g, 0.352 mmol) was dissolved in THF (6.0 mL). Diisopropylethylamine (0.246 mL, 0.141 mmol) and 1-ethyl-3-(3-dimethylaminopropyl)carbodiimide hydrochloride (0.108 g, 0.563 mmol) were then added and the reaction was stirred ten minutes and cooled to 0 °C. *Trans*-4-dimethylaminocrotonic acid hydrochloride (0.070 g, 0.422 mmol) was then added and the reaction was allowed to warm to room temperature and stir overnight. Water was added to quench the reaction and then ethyl acetate was added to extract the organics. The layers were separated, and the organic layer was washed with NaCl (1x), dried over magnesium sulfate, and concentrated. The resulting residue was purified using flash chromatography (5 – 10% MeOH/DCM) to give a light brown solid as the desired compound (0.017 g, 0.034 mmol, 10% yield). ¹H NMR (400 MHz, DMSO-*d*₆) δ 11.99 (s, 1H), 11.36 (s, 1H), 10.02 (s, 1H), 8.94 (dd, *J* = 8.4, 1.2 Hz, 1H), 8.30 (s, 1H), 8.17 (d, *J* = 8.7 Hz, 1H), 7.83 (dd, *J* = 8.1, 1.6 Hz, 1H), 7.75 (s, 1H), 7.56 – 7.42 (m, 3H), 7.17 (dd, *J* = 8.7, 2.1 Hz, 1H), 7.07 – 6.96 (m, 2H), 6.72 (dt, *J* = 15.4, 5.9 Hz, 1H), 6.31 – 6.24 (m, 2H), 3.84 (s, 3H), 3.10 – 3.03 (m, 2H), 2.19 (s, 6H). HPLC (gradient A): retention time

= 4.305 min; purity = 97%. Molecular Formula: C₂₆H₂₈N₈O₃, Mass Calc: 500.23, ESI-MS Found: 501.2343 [M+1]



Scheme 2.6: Synthesis of non-homologated *meta*-substituted analogues.

(9H-fluoren-9-yl)methyl (4-methoxy-3-((7-oxo-3-tosyl-3,7-dihydropyrrolo[2',3':4,5]pyrimido[6,1-b]quinazolin-5-yl)amino)phenyl)carbamate (**14**): To a 100 mL pressure vessel was added 2-((2-chloro-7-tosyl-7H-pyrrolo[2,3-d]pyrimidin-4-yl)amino)benzamide **6** (0.60 g, 1.36 mmol), (9H-fluoren-9-yl)methyl (3-amino-4-methoxyphenyl)carbamate **19** (0.515 g, 1.43 mmol), 4M HCl in dioxanes (1.36 mL, 5.44 mmol), potassium iodide (0.04 g, 0.24 mmol), and trifluoroethanol (40 mL). The sealed reaction was then heated overnight at 90 °C. The following day the reaction was cooled to room temperature and then diluted with water and an excessive amount of dichloromethane (~100 mL, otherwise an emulsion will form). The layers were separated and the organic was washed with NaCl (1x) and dried with sodium sulfate. The sodium sulfate was then filtered off and the filtrate was concentrated to give a light yellow/orange solid which was taken as is to the next step.

(9H-fluoren-9-yl)methyl (4-methoxy-3-((7-oxo-3-tosyl-3,7-dihydropyrrolo[2',3':4,5]pyrimido[6,1-b]quinazolin-5-yl)amino)phenyl)carbamate (**15**): To a 100 mL pressure vessel was added (9H-fluoren-9-yl)methyl (4-methoxy-3-((7-oxo-3-tosyl-3,7-dihydropyrrolo[2',3':4,5]pyrimido[6,1-b]quinazolin-5-yl)amino)phenyl)carbamate **14** (1.02 g, 1.36 mmol), 28% ammonium hydroxide in water (20 mL), and THF (20mL). The reaction was heated in a sealed pressure vessel to 60 °C overnight. After cooling the reaction was diluted with ethyl acetate and water. The layers were separated, and the organic layer was washed with NaCl (2x) and then dried of sodium sulfate. The sodium sulfate was filtered off and the filtrate was

concentrated. The resulting orange solid was triturated in dichloromethane to give the title compound as an off white solid (0.378 g, 0.70 mmol, 51% yield over two steps). ¹H NMR (400 MHz, DMSO-d₆) δ 12.13 (s, 1H), 8.76 (dd, J = 8.5, 1.1 Hz, 1H), 8.31 (s, 1H), 8.03 – 7.97 (m, 2H), 7.93 (s, 1H), 7.83 (dd, J = 8.0, 1.5 Hz, 1H), 7.76 (s, 1H), 7.49 (ddd, J = 8.6, 5.7, 1.5 Hz, 2H), 7.41 (d, J = 4.0 Hz, 1H), 7.38 (d, J = 8.2 Hz, 2H), 7.09 – 7.02 (m, 1H), 6.81 (d, J = 8.6 Hz, 1H), 6.53 (d, J = 4.0 Hz, 1H), 6.37 (dd, J = 8.5, 2.7 Hz, 1H), 4.55 (s, 2H), 3.72 (s, 3H), 2.34 (s, 3H). HPLC (gradient A): retention time = 5.850 min; purity = 88%.

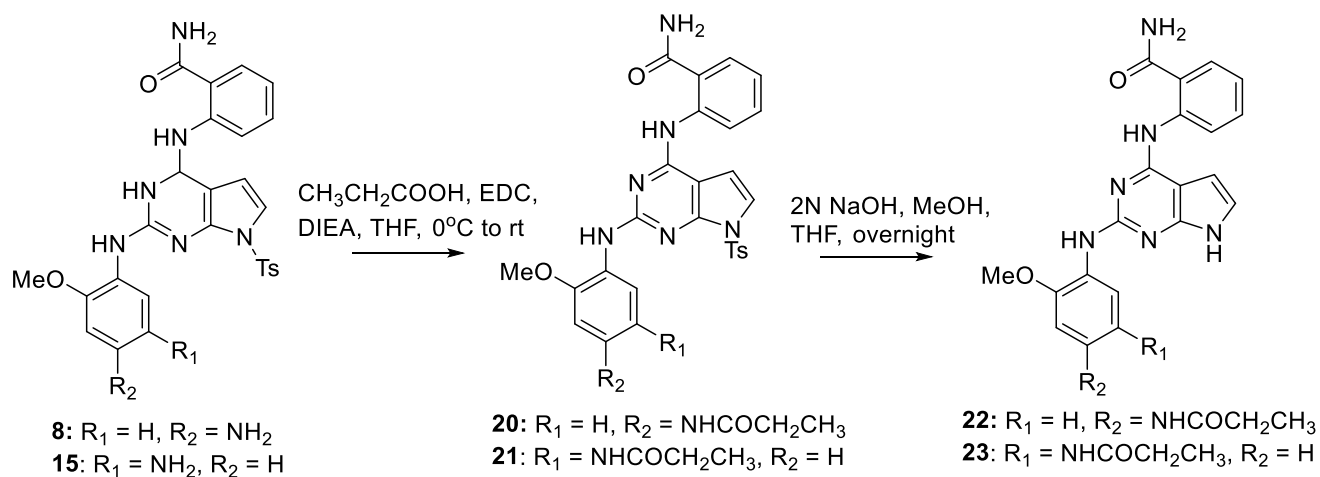
2-((2-((5-amino-2-methoxyphenyl)amino)-4,7-dihydro-3H-pyrrolo[2,3-d]pyrimidin-4-

yl)amino)benzamide (16): To a 25 mL round bottom flask was added (9H-fluoren-9-yl)methyl (4-methoxy-3-((7-oxo-3-tosyl-3,7-dihydropyrrolo[2',3':4,5]pyrimido[6,1-b]quinazolin-5-yl)amino)phenyl)carbamate **15** (0.158 g, 0.291 mmol), methanol (2 mL), 3N potassium hydroxide (2 mL) and THF (4.5 mL). The reaction was heated to 65 °C and stirred overnight for two days. The reaction was then cooled, and the organic layers were concentrated off. The resulting suspension in the aqueous layer was then filtered off to give adequately pure compound (0.082 mg, 72% yield). ¹H NMR (500 MHz, DMSO-d₆) δ 11.99 (s, 1H), 11.33 (s, 1H), 8.97 (d, J = 8.1 Hz, 1H), 8.28 (s, 1H), 7.83 (dd, J = 8.0, 1.5 Hz, 1H), 7.72 (s, 1H), 7.59 – 7.49 (m, 2H), 7.39 (s, 1H), 7.06 – 6.97 (m, 2H), 6.73 (d, J = 8.6 Hz, 1H), 6.29 (dd, J = 3.5, 1.9 Hz, 1H), 6.21 (dd, J = 8.5, 2.7 Hz, 1H), 4.47 (s, 2H), 3.74 (s, 3H). HPLC (gradient A): retention time = 4.166 min; purity = 91%.

2-((2-((5-acrylamido-2-methoxyphenyl)amino)-7H-pyrrolo[2,3-d]pyrimidin-4-yl)amino)benzamide (17,

CCG-258904): In a 25 mL flask *2-((2-((5-amino-2-methoxyphenyl)amino)-7H-pyrrolo[2,3-d]pyrimidin-4-yl)amino)benzamide 16* (0.088 g, 0.226 mmol) was dissolved in THF (6.0 mL). Diisopropylethylamine (0.12 mL, 0.678 mmol) and 1-Ethyl-3-(3 dimethylaminopropyl)carbodiimide hydrochloride (0.087 g, 0.452 mmol) were then added and the reaction was stirred ten minutes and cooled to 0 °C. Acrylic acid (0.017 mL, 0.249 mmol) was then added and the reaction was allowed to warm to room temperature and stir overnight. Water was added to quench the reaction and then ethyl acetate was added to extract the organics. The layers were separated, and the organic layer was washed with NaCO₃ (1x), dried over magnesium sulfate, and concentrated. The resulting residue was subjected to flash chromatography (5 – 10% MeOH/DCM) and then purified using reverse phase chromatography (30 – 60% Acetonitrile/Water) to give the desired compound as a light yellow solid (0.012 g, 0.026 mmol, 12% yield). ¹H NMR (500 MHz, DMSO-d₆) δ 12.05 (s, 1H), 11.44 (s, 1H), 10.05 (s, 1H), 8.94 (d, J = 8.4 Hz, 1H), 8.28 (d, J = 2.8 Hz, 2H), 7.82 (dd, J = 7.9, 1.6 Hz, 1H), 7.73 (s, 1H), 7.59 (s, 1H), 7.44 – 7.36 (m, 2H), 6.98 (q, J = 7.1, 5.9 Hz, 3H), 6.45 (dd, J = 17.0, 10.2 Hz, 1H), 6.29 (d, J = 3.5 Hz, 1H), 6.22 (dd, J = 17.0, 2.1 Hz, 1H), 5.71 (dd, J = 10.0, 2.1 Hz, 1H), 3.84 (s, 3H). HPLC (gradient A): retention time = 4.921 min; purity = 93%. Molecular Formula: C₂₃H₂₁N₇O₃, Mass Calc: 443.17, ESI-MS Found: 444.1630 [M+1].

(*E*)-2-((2-((4-(4-(dimethylamino)but-2-enamido)-2-methoxyphenyl)amino)-7*H*-pyrrolo[2,3-*d*]pyrimidin-4-yl)amino)benzamide (**18**, CCG-263115): In a 25 mL flask 2-((2-((5-amino-2-methoxyphenyl)amino)-7*H*-pyrrolo[2,3-*d*]pyrimidin-4-yl)amino)benzamide **16** (0.073 g, 0.187 mmol) was dissolved in THF (4.0 mL). Diisopropylethylamine (0.10 mL, 0.561 mmol) and 1-ethyl-3-(3-dimethylaminopropyl)carbodiimide hydrochloride (0.047 g, 0.243 mmol) were then added and the reaction was stirred ten minutes and cooled to 0 °C. *Trans*-4-dimethylaminocrotonic acid hydrochloride (0.034 g, 0.206 mmol) was then added and the reaction was allowed to warm to room temperature and stir three hours. Water was added to quench the reaction and then ethyl acetate was added to extract the organics. The layers were separated, and the organic layer was washed with NaCl (1x), dried over magnesium sulfate, and concentrated. The resulting residue was purified using flash chromatography (5 – 10% MeOH/DCM) to give a light brown solid as the desired compound (0.012 g, 0.024 mmol, 13% yield). ¹H NMR (500 MHz, DMSO-*d*₆) δ 12.07 (s, 1H), 11.34 (s, 1H), 9.88 (s, 1H), 8.94 (dd, *J* = 8.6, 1.2 Hz, 1H), 8.30 (s, 1H), 8.24 (d, *J* = 2.5 Hz, 1H), 7.82 (dd, *J* = 7.9, 1.6 Hz, 1H), 7.74 (s, 1H), 7.60 (s, 1H), 7.43 – 7.34 (m, 2H), 7.05 – 6.94 (m, 3H), 6.75 – 6.65 (m, 1H), 6.30 – 6.22 (m, 2H), 3.83 (s, 3H), 3.04 (dd, *J* = 6.1, 1.6 Hz, 2H), 2.18 (s, 6H). HPLC (gradient A): retention time = 4.353 min; purity = 93%. Molecular Formula: C₂₆H₂₈N₈O₃, Mass Calc: 500.23, ESI-MS Found: 501.2356 [M+1]



Scheme 2.7 Synthesis of saturated analogs **22** and **23**.

2-((2-((2-methoxy-4-propionamidophenyl)amino)-7-tosyl-7*H*-pyrrolo[2,3-*d*]pyrimidin-4-yl)amino)benzamide (**20**): To a 25 mL round bottom flask was added 2-((2-((4-amino-2-methoxyphenyl)amino)-7-tosyl-4,7-dihydro-3*H*-pyrrolo[2,3-*d*]pyrimidin-4-yl)amino)benzamide **8** (0.070 g, 0.128 mmol), 1-ethyl-3-(3-dimethylaminopropyl)carbodiimide hydrochloride (0.049 g, 0.258 mmol), diisopropylethylamine (0.068 mL, 0.387 mmol), and THF (4.0 mL). The reaction was cooled to 0 °C and then stirred for ten minutes before adding propionic acid (0.012 mL, 0.155 mmol). The reaction was further

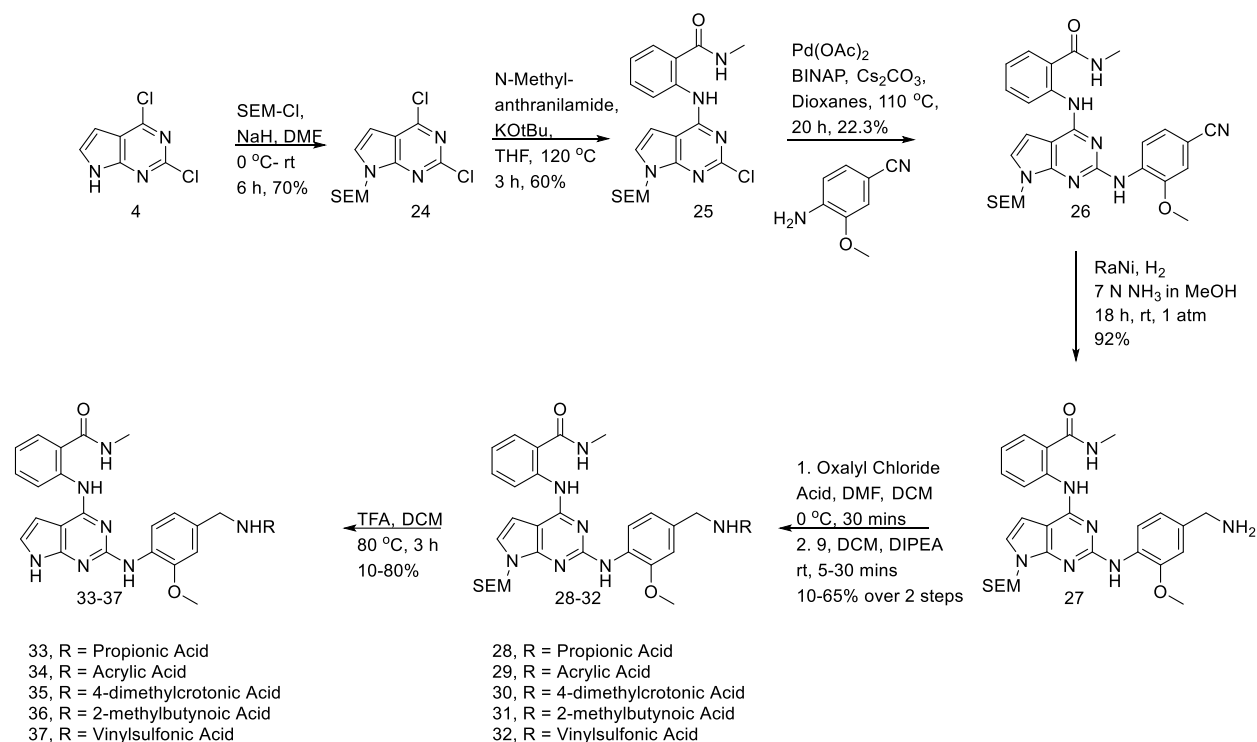
stirred overnight. Water was added to quench the reaction and then the reaction was further diluted with ethyl acetate. The two layers were separated. The organic layer was washed with 10% citric acid (1x), NaCl (2x), and then dried with sodium sulfate. The sodium sulfate was then filtered off and the filtrate was concentrated. The resulting residue was purified using 0 – 5% methanol/dichloromethane to give the title compound as a light pink solid (0.022 g, 0.041 mmol, 32% yield). ¹H NMR (400 MHz, DMSO-*d*₆) δ 12.12 (s, 1H), 9.88 (s, 1H), 8.75 (d, *J* = 8.4 Hz, 1H), 8.31 (s, 1H), 8.04 (s, 1H), 7.94 (d, *J* = 8.1 Hz, 3H), 7.82 (dd, *J* = 8.0, 1.6 Hz, 1H), 7.76 (s, 1H), 7.50 (d, *J* = 2.1 Hz, 1H), 7.48 – 7.34 (m, 4H), 7.20 (dd, *J* = 8.6, 2.1 Hz, 1H), 7.10 – 7.02 (m, 1H), 6.52 (d, *J* = 4.0 Hz, 1H), 3.81 (s, 3H), 2.41 – 2.30 (m, 5H), 1.12 (t, *J* = 7.6 Hz, 3H). HPLC (gradient A): retention time = 7.312 min; purity = 94%.

2-((2-((2-methoxy-5-propionamidophenyl)amino)-7-tosyl-7H-pyrrolo[2,3-d]pyrimidin-4-yl)amino)benzamide (21): To a 25 mL round bottom flask was added (9H-fluoren-9-yl)methyl (4-methoxy-3-((7-oxo-3-tosyl-3,7-dihydropyrrolo[2',3':4,5]pyrimido[6,1-b]quinazolin-5-yl)amino)phenyl)carbamate **15** (0.100 g, 0.184 mmol), 1-Ethyl-3-(3-dimethylaminopropyl)carbodiimide hydrochloride (0.071 g, 0.368 mmol), diisopropylethylamine (0.096 mL, 0.552 mmol), and THF (4.0 mL). The reaction was cooled to 0 °C and then stirred for ten minutes before adding propionic acid (0.017 mL, 0.221 mmol). The reaction was further stirred overnight. Water was added to quench the reaction and then the reaction was further diluted with ethyl acetate. The two layers were separated. The organic layer was washed with 10% citric acid (1x), NaCl (2x), and then dried with sodium sulfate. The sodium sulfate was then filtered off and the filtrate was concentrated. The resulting residue was purified using 0 – 5% isopropanol/dichloromethane to give the title compound as a white solid (0.065 g, 0.108 mmol, 59% yield). ¹H NMR (400 MHz, DMSO-*d*₆) δ 12.20 (s, 1H), 9.71 (s, 1H), 8.71 (d, *J* = 8.4 Hz, 1H), 8.32 (s, 1H), 8.26 (s, 1H), 7.97 (d, *J* = 8.2 Hz, 2H), 7.93 (d, *J* = 2.5 Hz, 1H), 7.82 (dd, *J* = 8.0, 1.5 Hz, 1H), 7.77 (s, 1H), 7.39 (d, *J* = 4.0 Hz, 1H), 7.38 – 7.28 (m, 4H), 7.07 – 6.99 (m, 2H), 6.50 (d, *J* = 4.0 Hz, 1H), 3.79 (s, 3H), 2.34 (s, 3H), 2.29 (q, *J* = 7.6 Hz, 2H), 1.07 (t, *J* = 7.6 Hz, 3H). HPLC (gradient A): retention time = 7.195 min; purity = 93%.

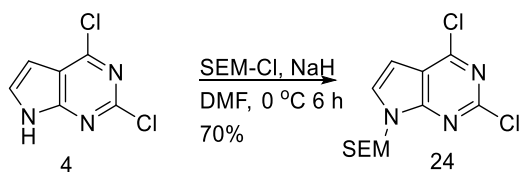
2-((2-((2-methoxy-4-propionamidophenyl)amino)-7H-pyrrolo[2,3-d]pyrimidin-4-yl)amino)benzamide (22, CCG-262604): In a 25 mL round bottom flask a suspension of 2-((2-((2-methoxy-4-propionamidophenyl)amino)-7-tosyl-7H-pyrrolo[2,3-d]pyrimidin-4-yl)amino)benzamide (0.022 g, 0.037 mmol), MeOH (1.0 mL), THF (4.0 mL), and 2N NaOH (4.0mL) was stirred overnight becoming clearer. The reaction was diluted with ethyl acetate and water. The layers were separated and the organic was washed with NaCl (1x), dried over MgSO₄, and concentrated. The resulting crude residue was purified using 5% - 10% MeOH/DCM and then further purified by recrystallizing from 15% MeOH/DCM overnight (~ 1.5 mL) to give the title compound as an off white solid (0.013 g, 0.029 mmol, 78% yield). ¹H NMR (400 MHz, DMSO-*d*₆) δ 11.99 (s, 1H), 11.34 (s, 1H), 9.79 (s, 1H), 8.93 (d, *J* = 8.5 Hz, 1H), 8.30 (s, 1H), 8.13 (d, *J* = 8.6 Hz, 1H), 7.83 (d, *J* = 8.0 Hz,

1H), 7.75 (s, 1H), 7.53 – 7.40 (m, 3H), 7.10 (d, $J = 8.7$ Hz, 1H), 7.05 – 6.95 (m, 2H), 6.28 (s, 1H), 3.82 (s, 3H), 2.31 (q, $J = 8.5, 7.5$ Hz, 2H), 1.09 (t, $J = 7.5$ Hz, 3H). HPLC (gradient A): retention time = 4.906 min; purity = 95%. Molecular Formula: $C_{23}H_{23}N_7O_3$, Mass Calc: 445.19, ESI-MS Found: 446.1926 [M+1]

2-((2-((2-methoxy-5-propionamidophenyl)amino)-7H-pyrrolo[2,3-d]pyrimidin-4-yl)amino)benzamide (**23**, **CCG-262606**): In a 25 mL flask 2-((2-((2-methoxy-5-propionamidophenyl)amino)-7-tosyl-7H-pyrrolo[2,3-d]pyrimidin-4-yl)amino)benzamide 128 (0.062 g, 0.104 mmol) was suspended in 1,4-dioxanes (5.0 mL) and 2N NaOH (5.0 mL) and the reaction was stirred vigorously. After 2 hours the reaction was still cloudy and THF (3 mL) and MeOH (1 mL) were then added and the reaction was stirred overnight. The organics were then concentrated off and the pH was lowered with concentrated HCl at which point a new side product formed. Assuming it was the cyclized lactam the compound was then stirred in a sealed reaction vessel with 28% NH_4OH (4 mL) and THF (4 mL) at 40 °C for four hours, concentrated, and extracted with ethyl acetate (disappearance of the side product was observed confirming likelihood of it being the cyclized lactam). The organic was then washed with NaCl (1x), dried over $MgSO_4$, and concentrated. The resulting residue was then purified on flash chromatography using a gradient of 0 – 5% MeOH/DCM to afford the desired product as a pale yellow solid (0.036 mg, 0.081 mmol, 78% yield). ¹H NMR (400 MHz, DMSO- d_6) δ 12.07 (s, 1H), 11.33 (s, 1H), 9.65 (s, 1H), 8.97 – 8.90 (m, 1H), 8.30 (s, 1H), 8.15 (d, $J = 2.5$ Hz, 1H), 7.83 (d, $J = 7.9$ Hz, 1H), 7.75 (s, 1H), 7.58 (s, 1H), 7.39 (t, $J = 7.8$ Hz, 1H), 7.30 (dd, $J = 8.8, 2.5$ Hz, 1H), 7.04 – 6.92 (m, 3H), 6.29 (dd, $J = 3.5, 1.9$ Hz, 1H), 3.82 (s, 3H), 2.27 (q, $J = 7.6$ Hz, 2H), 1.07 (t, $J = 7.6$ Hz, 3H). HPLC (gradient A): retention time = 4.927 min; purity = 95% Molecular Formula: $C_{23}H_{23}N_7O_3$, Mass Calc: 445.19, ESI-MS Found: 446.1938 [M+1]



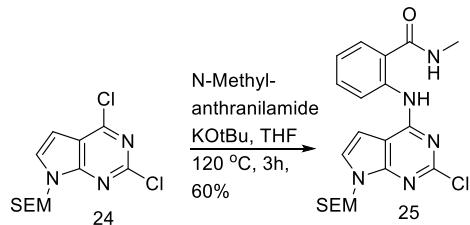
Scheme 2.8. Synthetic route to *para* substituted homologated probes, **33-37**.



2,4-Dichloro-7-((2-(trimethylsilyl)ethoxy)methyl)-7H-pyrrolo[2,3-d]pyrimidine (24)

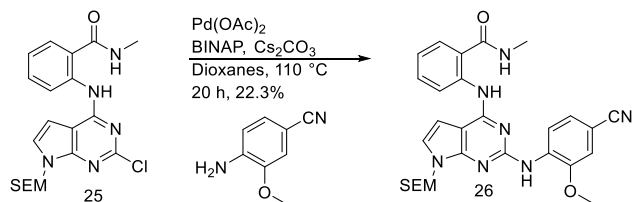
To a flame dried flask were added 5.0002 g (30 mmol) of 2,4-dichloro-7H-pyrrolo[2,3-d]pyrimidine (**4**), dissolved in 60 mL of DMF. The solution was cooled to 0 °C, and 666.3 mg of NaH (60% dispersion in mineral oil, 27.76 mmol, 0.9 equiv) were added portion wise. The solution was allowed to stir at room temperature for 30 min, then cooled back to 0 °C and 6.0 mL of SEM-Cl (30 mmol) then added. The solution was then allowed to warm to rt and stirred for 6 h. The reaction was quenched with 500 mL of brine and then extracted with EtOAc (3 x 150 mL). The combined organic layers were washed with brine (1 x 150 mL) and then dried over MgSO₄. The solvent was removed under pressure, and the yellow residue was taken up in hexanes. The solution was run through a silica plug, eluting with a gradient of hexanes to 5% EtOAc/hexanes. The solvent was removed under pressure to yield a white solid. Yield: 6.9200 g, 70% HPLC: 8.948 min, Molecular Formula: C₁₂H₁₇Cl₂N₃O₃Si, Mass Calc: 317.05, ESI MS-Found: 318 [M+1],

purity: 99% ¹H NMR (500 MHz, Chloroform-d) δ 7.38 (d, J = 3.7 Hz, 1H), 6.68 (d, J = 3.7 Hz, 1H), 5.61 (s, 2H), 3.67 – 3.59 (m, 2H), 1.00 – 0.88 (m, 2H), -0.03 (s, 9H). ¹³C NMR (126 MHz, cdcl3) δ 160.97, 152.57, 152.11, 129.20, 116.16, 100.82, 94.05, 66.74, 26.96, -1.72.



2-((2-Chloro-7-((2-(trimethylsilyl)ethoxy)methyl)-7H-pyrrolo[2,3-d]pyrimidin-4-yl)amino)-N-methylbenzamide (25)

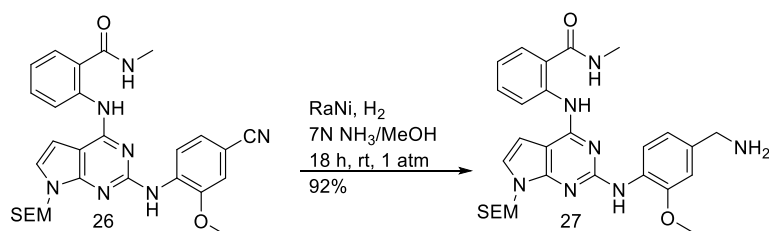
A flask was charged with 1.000 g of **24** (3 mmol, 1 equiv.), 501.1 mg of 2-amino-N-methylbenzamide (3 mmol, 1 equiv.), and 16 mL of THF. The resulting solution was cooled to 0 °C and 702.1 mg of KOtBu (6.0 mmol, 2 equiv.) were added to form an orange solution which was heated to 120 °C for 3 h. The solution was cooled to rt and quenched with water, extracted with EtOAc (3 x 100 mL) and the combined organic layers were washed with brine (1 x 50mL). The organic layer was dried over Na₂SO₄, filtered and concentrated in vacuo and purified by column chromatography eluting with 60% EtOAc/Hexanes to afford an off white solid. Yield: 802.0 mg, 60% HPLC: 8.96 min, Molecular Formula: C₂₀H₂₆ClN₅O₂Si, Mass Calc: 431.15, ESI-MS-Found: 432 [M+1], purity: 92% ¹HNMR (500 MHz, DMSO-d₆) δ 12.06 (s, 1H), 8.80 (d, J = 5.0 Hz, 1H), 8.63 (d, J = 8.4 Hz, 1H), 7.79 (d, J = 7.9 Hz, 1H), 7.58 (t, J = 7.9 Hz, 1H), 7.51 (d, J = 3.5 Hz, 1H), 7.16 (t, J = 7.6 Hz, 1H), 6.56 (d, J = 3.5 Hz, 1H), 5.51 (s, 2H), 3.52 (t, J = 8.0 Hz, 2H), 2.82 (d, J = 4.4 Hz, 3H), 0.84 (t, J = 8.1 Hz, 2H), -0.08 (s, 9H). ¹³CNMR (126 MHz, dmsO) δ 169.60, 153.90, 152.61, 151.34, 140.04, 132.42, 128.62, 127.74, 122.56, 121.28, 121.13, 103.84, 98.70, 72.98, 66.03, 40.50, 40.34, 40.17, 40.00, 39.83, 39.67, 39.50, 26.82, 17.53, -0.96.



2-((2-((4-Cyano-2-methoxyphenyl)amino)-7-((2-(trimethylsilyl)ethoxy)methyl)-7H-pyrrolo[2,3-d]pyrimidin-4-yl)amino)-N-methylbenzamide (26)

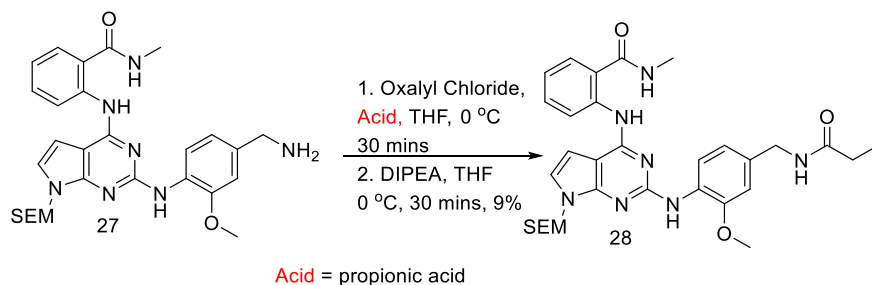
Compound **26** was prepared using protocols described in the literature.² A flame dried three neck flask was charged with 201.1 mg of **25** (0.463 mmol, 1 equiv.), 795.6 mg of Cs₂CO₃ (2.32 mmol, 5 equiv.), 60.3 mg of BINAP, racemic (0.00927 mmol, 0.2 equiv.), Pd(OAc)₂ (0.1 equiv., 5 mol%), and 84.1 mg of 4-amino-3-

methoxybenzonitrile (0.555 mmol 1.2 equiv.). The mixture was degassed with three cycles of evacuation and back filled with nitrogen and 4 mL of dioxanes added. The solution was further degassed with an additional 4 cycles of evacuation and back filled with nitrogen, then heated to 110 °C for 20 h. The reaction mixture was passed through a pad of celite, washing with EtOAc and purified by column chromatography eluting with 50% EtOAc/Hexanes to afford a dark red solid 56.2 mg, 22.3% HPLC: 8.912 min, Molecular Formula: C₂₈H₃₃N₇O₃Si, Mass Calc: 543.24 ESI-MS-Found: 544.17 [M+1], purity: 90% ¹H NMR (500 MHz, Chloroform-d) δ 11.19 (s, 1H), 8.86 (dd, J = 8.5, 5.7 Hz, 2H), 7.78 (s, 1H), 7.56 – 7.49 (m, 2H), 7.10 – 7.05 (m, 2H), 7.01 (d, J = 3.6 Hz, 1H), 6.64 (d, J = 3.7 Hz, 1H), 5.56 (s, 2H), 3.62 – 3.57 (m, 2H), 3.05 (d, J = 4.8 Hz, 3H), 0.98 – 0.92 (m, 2H), -0.07 (d, J = 1.0 Hz, 9H). ¹³CNMR (126 MHz, dmsO) δ 169.62, 163.07, 158.90, 153.91, 152.63, 151.36, 140.05, 132.42, 128.63, 127.73, 123.88, 122.57, 118.65, 117.79, 103.85, 98.72, 72.99, 66.05, 26.83, 17.53, -0.96.



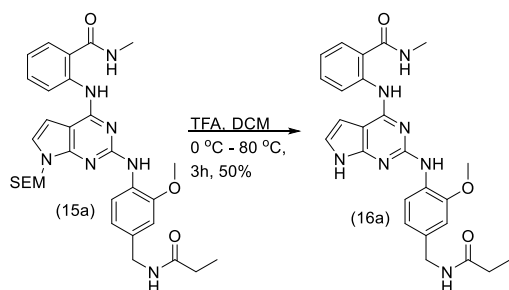
2-((2-((4-(Aminomethyl)-2-methoxyphenyl)amino)-7-((2-(trimethylsilyl)ethoxy)methyl)-7H-pyrrolo[2,3-d]pyrimidin-4-yl)amino)-N-methylbenzamide (27)

To a dried flask were added 270.2 mg of **26** and 10 mL (13 mmol) of 7N methanolic ammonia.³ The solution was degassed with three rounds of evacuation and back filled with nitrogen. RaNi (slurry in water) was added and the mixture was further degassed with three rounds of evacuation and back filled with nitrogen. The atmosphere was then replaced with hydrogen and allowed to stir under H₂ for 6 h. Once complete, H₂ atmosphere was removed and the solution was passed through a pad of celite, washing with methanolic ammonia. The solvent was removed under pressure to give a light green solid, 250 mg, 92%. HPLC: 6.331 min, Molecular Formula: C₂₈H₃₇N₇O₃Si, Mass Calc: 547.27 ESI-MS-Found: 548.2719 [M+1], purity: 97%. ¹H NMR (500 MHz, DMSO-d₆) δ 11.76 (s, 1H), 8.82 (dq, J = 30.6, 7.9 Hz, 2H), 8.41 (dd, J = 32.4, 24.4 Hz, 1H), 7.81 (q, J = 15.7, 10.9 Hz, 1H), 7.70 – 7.59 (m, 1H), 7.54 (dt, J = 25.5, 12.4 Hz, 1H), 7.21 (s, 1H), 7.15 – 7.05 (m, 2H), 6.93 (dt, J = 22.3, 10.2 Hz, 1H), 6.46 (s, 1H), 5.49 (d, J = 18.2 Hz, 2H), 4.08 – 4.04 (m, 2H), 3.90 (d, J = 25.2 Hz, 3H), 3.62 – 3.54 (m, 3H), 2.86 (s, 3H), 0.93 – 0.87 (m, 2H), -0.08 (d, J = 10.4 Hz, 9H). ¹³CNMR (126 MHz, dmsO) δ 170.66, 169.78, 155.97, 153.45, 152.36, 148.46, 141.03, 134.79, 132.16, 128.36, 126.19, 124.07, 121.24, 121.13, 119.91, 119.23, 117.65, 113.43, 108.23, 99.45, 98.55, 72.40, 65.67, 60.11, 56.03, 26.68, 17.46, -1.09.



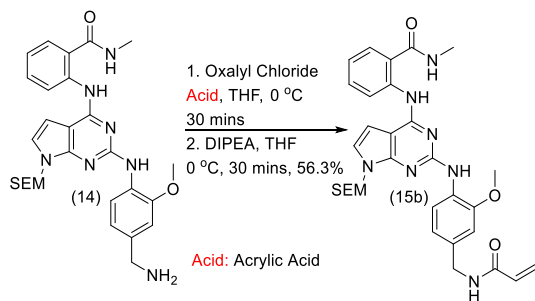
2-((2-((2-methoxy-4-(propionamidomethyl)phenyl)amino)-7-((2-(trimethylsilyl)ethoxy)methyl)-7H-pyrrolo[2,3-d]pyrimidin-4-yl)amino)-N-methylbenzamide (28)

A dried flask was charged with 0.02 mL of propionic acid (0.0913 mmol, 1 equiv), 2 drops of DMF, and 2 mL of DCM (40 mmol). The mixture was cooled to 0 °C and 0.04 mL of oxalyl chloride (5 equiv., 0.5 mmol) were added. The mixture was allowed to warm to rt and stir for 1 h. Once complete, the solvent was removed under pressure and the light green residue was rinsed with DCM (3 x 10 mL). The green residue was then taken up in DCM (2 mL, 40 mmol), and the mixture was cooled back to 0 °C. At 0 °C were added 0.1 mL of DIPEA (0.0913 mmol, 1.0 equiv.), and 50.4 mg of **27** (1 equiv, 0.09 mmol). The solution was warmed to rt for 3 h. Once complete the solvent was removed. The dark yellow residue was purified by preparatory TLC plate (EtOAc/1% MeOH). The band containing the desired material was collected, and the material was eluted off silica gel with acetone. The solvent was removed to give a light yellow solid, 5 mg, 9%. HPLC: 7.04 min, Molecular Formula: C₃₁H₄₁N₇O₄Si, Mass Calc: 603.30 ESI-MS-Found: 604 [M+1], purity: 90%. ¹HNMR (700 MHz, DMSO-d₆) δ 11.69 (s, 1H), 8.82 – 8.78 (m, 1H), 8.75 (d, J = 4.8 Hz, 1H), 8.33 (d, J = 8.1 Hz, 1H), 8.22 (t, J = 5.8 Hz, 1H), 7.95 (s, 1H), 7.75 (dd, J = 7.9, 1.6 Hz, 1H), 7.63 (s, 1H), 7.52 – 7.46 (m, 1H), 7.18 (d, J = 3.6 Hz, 1H), 7.07 (td, J = 7.7, 1.2 Hz, 1H), 6.94 (d, J = 1.8 Hz, 1H), 6.83 (dd, J = 8.2, 1.8 Hz, 1H), 6.41 (d, J = 3.6 Hz, 1H), 5.47 (s, 2H), 4.24 (d, J = 5.9 Hz, 2H), 3.87 (s, 3H), 3.57 – 3.51 (m, 2H), 2.82 (d, J = 4.5 Hz, 3H), 2.15 (q, J = 7.6 Hz, 2H), 1.04 (t, J = 7.6 Hz, 3H), 0.89 – 0.84 (m, 2H), -0.10 (s, 9H). ¹³CNMR (176 MHz, dmsO) δ 173.25, 169.89, 162.79, 156.06, 153.56, 152.46, 148.64, 141.08, 133.36, 132.27, 128.68, 124.24, 121.39, 120.11, 119.49, 118.29, 110.20, 99.53, 98.65, 72.54, 65.79, 56.15, 42.47, 29.04, 26.81, 17.58, 10.55, -0.95.



2-((2-((2-methoxy-4-(propionamidomethyl)phenyl)amino)-7H-pyrrolo[2,3-d]pyrimidin-4-yl)amino)-N-methylbenzamide (**33**, CCG-264561)

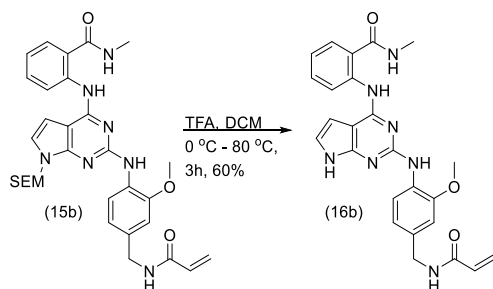
A dried flask was charged with 5 mg of **28** (8 μ mol, 1.0 equiv), and 2 mL of DCM. The solution was cooled to 0 °C, and 0.08 mL of TFA (25 equiv., 0.2 mmol) were added in one portion. The solution was warmed to 80 °C and stirred until complete. Once complete, the solvent was removed, and the residue was rinsed with DCM (3 x 5 mL). The yellow residue was then purified by preparatory TLC plate (1% MeOH/EtOAc). The band containing the desired material was collected, and the material was washed off silica gel with MeOH. The solvent was removed to give a light yellow oil, 2.0 mg, 50%. HPLC: 4.99 min, Molecular Formula: C₂₅H₂₇N₇O₃, Mass Calc: 473.22 ESI-MS-Found: 474 [M+1], purity: 92% ¹HNMR (700 MHz, DMSO-d₆) δ 11.68 (s, 1H), 8.80 (d, J = 8.3 Hz, 1H), 8.75 (d, J = 5.1 Hz, 1H), 8.28 (d, J = 7.9 Hz, 1H), 8.23 (s, 1H), 7.75 (d, J = 7.7 Hz, 1H), 7.60 (s, 1H), 7.47 (t, J = 7.9 Hz, 1H), 7.13 (d, J = 3.6 Hz, 1H), 7.06 (t, J = 7.5 Hz, 1H), 6.93 (s, 1H), 6.84 (d, J = 8.1 Hz, 1H), 6.46 (t, J = 7.3 Hz, 1H), 6.38 (d, J = 3.6 Hz, 1H), 4.24 (d, J = 5.9 Hz, 2H), 3.86 (d, J = 4.3 Hz, 3H), 2.82 (d, J = 4.5 Hz, 3H), 2.16 (dd, J = 10.7, 4.7 Hz, 2H), 1.05 (t, J = 7.6 Hz, 3H). ¹³CNMR (176 MHz, dmso) δ 173.25, 169.89, 162.79, 156.06, 153.56, 152.46, 148.64, 141.08, 133.36, 132.27, 128.68, 124.24, 121.39, 120.11, 119.49, 118.29, 110.20, 99.53, 92.08, 56.15, 42.47, 29.04, 26.81, 10.55.



2-((2-((4-(acrylamidomethyl)-2-methoxyphenyl)amino)-7H-pyrrolo[2,3-d]pyrimidin-4-yl)amino)-N-methylbenzamide (**39**)

A dried flask was charged with 0.05 mL of acrylic acid (0.219 mmol, 1 equiv), 2 drops of DMF and 2 mL of THF (0.1 molar). The mixture was cooled to 0 °C and 0.1 mL of oxalyl chloride (1.14 mmol, 5.1 equiv) were added. The solution was allowed to warm to rt for 1 h. Once complete, the solvent was removed under

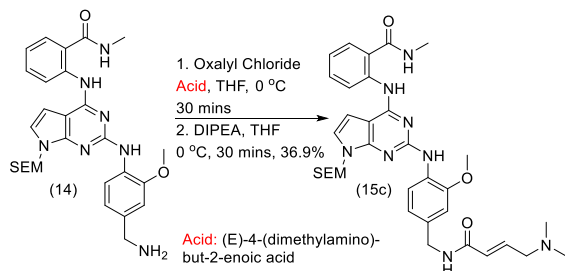
pressure and the light green residue was rinsed with DCM (3 x 10 mL). The light green residue was then taken up in DCM (5 mL, 40 mmol) and cooled to 0 °C. At 0 °C, 120 mg of **27** (0.219 mmol, 1 equiv) and 0.1 mL of DIPEA (0.57 mmol, 2.6 equiv) were added. The solution warmed to rt and stirred until reaction was complete. Once complete, the solvent was removed, evaporating product onto silica gel. The material was purified by column chromatography (EtOAc/Hex). The major product was eluted in MeOH and collected to give a light yellow solid, 70.6 mg, 53.6%. HPLC: 7.24 min, Molecular Formula: C₃₁H₃₉N₇O₄Si, Mass Calc: 601.28 ESI-MS-Found: 674 [M+Acrylic Acid], purity: 90%. ¹HNMR (700 MHz, DMSO-d₆) δ 11.71 (d, J = 4.9 Hz, 1H), 8.80 (dt, J = 8.5, 3.0 Hz, 1H), 8.75 (q, J = 4.4 Hz, 1H), 8.55 (t, J = 5.9 Hz, 1H), 8.35 (d, J = 8.0 Hz, 1H), 7.95 (s, 1H), 7.76 (dt, J = 8.0, 2.0 Hz, 1H), 7.64 (s, 1H), 7.49 (ddd, J = 8.5, 7.1, 1.5 Hz, 1H), 7.20 – 7.17 (m, 1H), 7.10 – 7.04 (m, 1H), 6.97 (d, J = 1.8 Hz, 1H), 6.86 (dd, J = 8.2, 1.8 Hz, 1H), 6.42 (dd, J = 3.6, 1.6 Hz, 1H), 6.33 – 6.27 (m, 1H), 6.17 – 6.12 (m, 1H), 5.47 (s, 2H), 4.34 (t, J = 6.0 Hz, 2H), 3.87 (d, J = 4.5 Hz, 3H), 3.58 – 3.51 (m, 2H), 2.82 (d, J = 4.4 Hz, 3H), 0.88 – 0.84 (m, 2H), -0.10 (s, 9H). ¹³CNMR (176 MHz, dmsO) δ 169.38, 164.43, 162.26, 155.53, 153.05, 151.94, 148.15, 140.58, 132.31, 131.76, 128.36, 127.95, 125.19, 123.73, 120.87, 120.76, 119.57, 119.28, 119.10, 109.93, 99.06, 98.14, 72.04, 65.29, 55.67, 42.21, 26.29, 17.08, -1.46.



2-((2-((4-(acrylamidomethyl)-2-methoxyphenyl)amino)-7H-pyrrolo[2,3-d]pyrimidin-4-yl)amino)-N-methylbenzamide (34, CCG-264099)

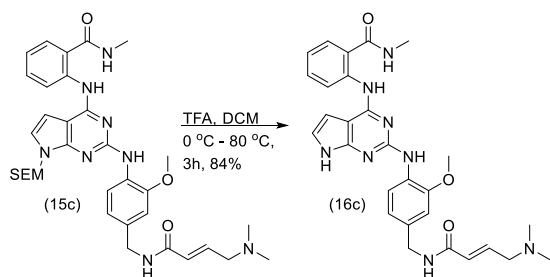
A dried flask was charged with 10 mg of **29** (0.008 mmol, 1.0 equiv), and 2 mL of DCM (4 mmol). The solution was cooled to 0 °C, and 0.20 mL of TFA (150 equiv.) were added in one portion. The dark red solution warmed to 80 °C for 3 h. Once complete, the mixture was cooled to rt and quenched with saturated K₂CO₃ in MeOH. The mixture was then extracted with DCM (3 x 30 mL) and the combined organic layers were washed with brine (1 x 30 mL). The organic layer was dried over MgSO₄ and then purified by preparatory TLC plate (50% EtOAc/Hex with 5% MeOH) to yield a white solid, 4.7 mg, 60%. HPLC: 5.750 min, Molecular Formula: C₂₅H₂₅N₇O₃, Mass Calc: 471.20 ESI-MS-Found: 472 [M+1], purity: 96%. ¹HNMR (700 MHz, DMSO-d₆) δ 11.43 (s, 1H), 10.72 (s, 1H), 8.78 (d, J = 8.8 Hz, 1H), 8.55 (t, J = 5.8 Hz, 1H), 8.22 (d, J = 8.1 Hz, 1H), 7.97 (dd, J = 8.0, 1.6 Hz, 1H), 7.61 – 7.56 (m, 2H), 7.10 (t, J = 7.9 Hz, 1H), 7.03 (dd, J = 3.5, 2.2 Hz, 1H), 6.96 (d, J = 1.8 Hz, 1H), 6.85 (dd, J = 8.2, 1.8 Hz, 1H), 6.40 (dd, J = 3.5, 1.9 Hz, 1H), 6.33 – 6.24 (m, 1H), 6.14 (dd, J = 17.1, 2.3 Hz, 1H), 5.62 (dd, J = 10.2, 2.2 Hz, 1H), 4.33 (d, J =

5.9 Hz, 2H), 3.86 (d, J = 8.8 Hz, 6H).. ¹³CNMR (176 MHz, dmsO) δ 168.98, 164.94, 155.90, 153.28, 152.97, 149.14, 142.41, 134.50, 133.02, 132.25, 131.05, 128.99, 125.74, 121.55, 121.40, 121.11, 119.83, 116.30, 110.55, 99.56, 97.82, 56.17, 42.78, 26.29, 17.08.



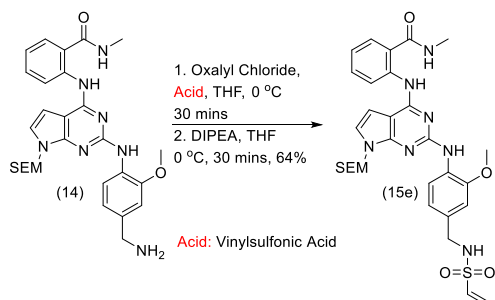
(E)-2-((2-((4-((4-(dimethylamino)but-2-enamido)methyl)-2-methoxyphenyl)amino)-7-((2-(trimethylsilyl)ethoxy)methyl)-7H-pyrrolo[2,3-d]pyrimidin-4-yl)amino)-*N*-methylbenzamide
(30)

A dried flask was charged with 29.7 mg of *(E)*-4-(dimethylamino)but-2-enoic acid (1.0 equiv., 0.219 mmol), 3 drops of DMF, and 2 mL of THF (0.1 molar). . The mixture was cooled to 0 °C and 0.02 mL of oxalyl chloride (1.1 equiv., 0.241 mmol) were added. The solution was warmed to rt and allowed for 1 h. Once complete, the solvent was removed under pressure and the light green residue was rinsed with DCM (3 x 10 mL). The light green residue was then taken up in THF (5 mL, 40 mmol) and cooled to 0 °C. At 0 °C were added 120.0 mg of **27** (0.219 mmol, 1.0 equiv) and 0.1 mL of DIPEA (2.6 equiv., 0.57 mmol). The mixture was warmed to rt and stirred until reaction was complete. Once complete, the solvent was removed, evaporating product onto silica gel. The material was purified by column chromatography (30-50% EtOAc/Hex). The major product was collected, and the solvent was removed under pressure to give a light yellow solid, 53.2 mg, 36.9% HPLC: 7.288 min, Molecular Formula: C₃₄H₄₆N₈O₄Si, Mass Calc: 658.34 ESI-MS-Found: 659.3460 [M+H], purity: 80%. ¹HNMR (700 MHz, Chloroform-d) δ 8.91 (dd, J = 11.7, 8.4 Hz, 2H), 8.64 – 8.60 (m, 2H), 8.10 (dd, J = 20.4, 7.9 Hz, 1H), 7.66 (s, 1H), 7.64 (d, J = 8.1 Hz, 2H), 7.28 (d, J = 1.9 Hz, 1H), 7.20 (t, J = 7.3 Hz, 2H), 7.00 (s, 1H), 6.99 (d, J = 2.0 Hz, 1H), 6.98 (s, 1H), 6.83 (d, J = 1.7 Hz, 1H), 6.32 (d, J = 7.7 Hz, 1H), 5.97 (d, J = 15.3 Hz, 1H), 5.53 (s, 2H), 4.47 (d, J = 5.6 Hz, 2H), 3.91 (s, 3H), 3.55 (dt, J = 8.3, 2.2 Hz, 3H), 3.07 (dd, J = 6.2, 1.6 Hz, 2H), 3.02 (d, J = 4.7 Hz, 3H), 2.18 (s, 6H), 0.88 (t, J = 6.9 Hz, 2H), -0.09 (s, 9H). ¹³CNMR (176 MHz, cdCl₃) δ 168.97, 167.63, 166.29, 155.12, 151.63, 147.90, 143.92, 143.34, 132.23, 130.15, 128.90, 122.70, 121.88, 120.48, 118.89, 117.88, 117.18, 116.44, 111.80, 104.18, 100.23, 87.02, 66.28, 63.24, 55.93, 49.42, 44.04, 26.99, 23.95, -1.29.



(*E*)-2-((2-((4-((4-(dimethylamino)but-2-enamido)methyl)-2-methoxyphenyl)amino)-7*H*-pyrrolo[2,3-*d*]pyrimidin-4-yl)amino)-*N*-methylbenzamide (**35**):

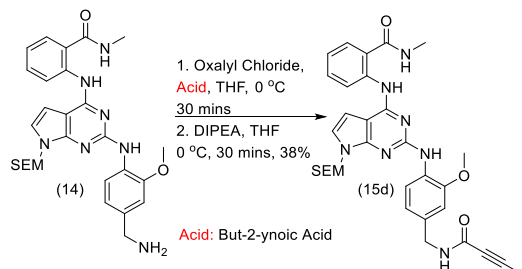
Compound **16c** was synthesized using the protocol described for **30**. Yields a bright yellow solid, 40.5 mg, 84%. HPLC: 4.72 min, Molecular Formula: C₂₈H₃₂N₈O₃, Mass Calc: 528.26 ESI-MS-Found: 559 [M+MeOH], purity: 95%. ¹HNMR (700 MHz, DMSO-*d*₆) δ 11.69 (s, 2H), 8.81 (d, *J* = 8.4 Hz, 1H), 8.75 (s, 1H), 8.32 – 8.28 (m, 2H), 7.76 (d, *J* = 8.0 Hz, 1H), 7.60 (s, 1H), 7.48 (t, *J* = 7.7 Hz, 1H), 7.14 (d, *J* = 3.3 Hz, 1H), 7.07 (t, *J* = 7.3 Hz, 1H), 6.94 (s, 1H), 6.85 (d, *J* = 8.1 Hz, 1H), 6.46 (s, 1H), 6.39 (d, *J* = 3.4 Hz, 1H), 4.25 – 4.21 (m, 2H), 3.87 (s, 3H), 3.06 (m, 2H), 2.83 (d, *J* = 4.4 Hz, 3H), 2.18 (s, 6H). ¹³CNMR (176 MHz, *dms*_o) δ 168.73, 167.68, 166.40, 155.97, 150.40, 147.03, 144.02, 143.35, 132.93, 130.30, 128.36, 122.80, 121.68, 120.05, 118.89, 117.96, 117.13, 116.36, 111.84, 99.30, 91.72, 63.80, 60.57, 55.97, 46.71, 43.98, 26.73.



2-((2-((2-methoxy-4-(vinylsulfonamidomethyl)phenyl)amino)-7-((2-(trimethylsilyl)ethoxy)methyl)-7*H*-pyrrolo[2,3-*d*]pyrimidin-4-yl)amino)-*N*-methylbenzamide (**31**)

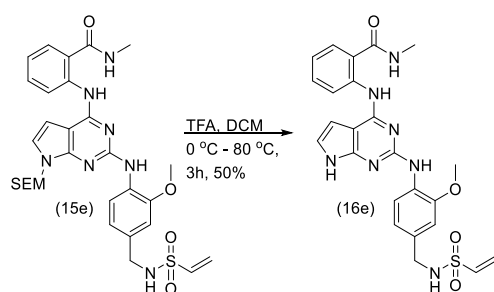
Compound **31** was synthesized using the protocol described for **28**. Yields a yellow solid, 15 mg, 64%. HPLC: 7.163 min, Molecular Formula: C₃₀H₃₉N₇O₅SSi, Mass Calc: 637.25, ESI-MS-Found: 638 [M+1], purity: 95% ¹HNMR (700 MHz, Chloroform-*d*) δ 11.61 (s, 1H), 8.93 (d, *J* = 8.5 Hz, 1H), 8.29 (s, 1H), 8.10 (d, *J* = 7.2 Hz, 1H), 8.05 (s, 2H), 7.75 (m, 1H), 7.54 (m, 1H), 7.42 (m, 1H), 7.36 (s, 1H), 7.22 (d, *J* = 8.2 Hz, 1H), 7.05 (d, *J* = 9.2 Hz, 2H), 6.97 (m, 2H), 6.25 (m, 2H), 6.05 (d, *J* = 9.0 Hz, 1H), 5.80 (d, *J* = 10.0 Hz, 1H), 5.57 (s, 2H), 3.87 (d, *J* = 13.2 Hz, 3H), 3.54 (m, 2H), 3.36 (s, 2H), 3.04 (d, *J* = 5.1 Hz, 3H), 0.85 (m, 2H), -0.08 (s, 9H). ¹³CNMR (176 MHz, *cdcl*₃) δ 168.42, 167.74, 154.59, 151.23, 147.52, 144.10, 135.80,

133.05, 132.47, 130.63, 128.35, 123.63, 119.80, 119.02, 117.86, 117.16, 116.42, 110.90, 103.45, 100.62, 86.55, 66.35, 56.77, 45.81, 26.52, 23.88, -1.64.



2-((2-((4-(but-2-ynamidomethyl)-2-methoxyphenyl)amino)-7H-pyrrolo[2,3-d]pyrimidin-4-yl)amino)-N-methylbenzamide (32)

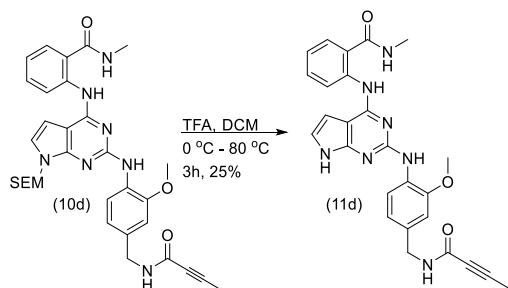
Compound **32** was synthesized using the protocol described for **28**. Yields a light yellow solid, 15 mg, 38%. HPLC: 7.15 min, Molecular Formula: C₃₂H₃₉N₇O₄Si, Mass Calc: 613.28, ESI-MS-Found: 614 [M+1], purity: 80% ¹H NMR (700 MHz, Chloroform-d) δ 11.09 (s, 1H), 8.91 (d, J = 8.4 Hz, 1H), 8.64 (d, J = 8.2 Hz, 1H), 8.21 (s, 1H), 7.51 (d, J = 7.7 Hz, 1H), 7.49 (t, J = 6.2 Hz, 1H), 7.01 (t, J = 7.5 Hz, 1H), 6.94 (d, J = 3.6 Hz, 1H), 6.87 (dd, J = 8.3, 1.8 Hz, 1H), 6.82 (d, J = 1.9 Hz, 1H), 6.60 (d, J = 3.5 Hz, 1H), 6.49 (d, J = 5.6 Hz, 1H), 6.39 (d, J = 5.4 Hz, 1H), 5.53 (s, 2H), 4.42 (d, J = 5.7 Hz, 1H), 3.92 (s, 3H), 3.51 – 3.43 (m, 3H), 2.99 (s, 3H), 1.93 (s, 3H), 0.94 (t, J = 8.2 Hz, 2H), -0.08 (s, 9H). ¹³C NMR (176 MHz, cdcl₃) δ 170.35, 156.89, 155.81, 153.79, 152.77, 149.75, 147.90, 141.29, 132.28, 130.27, 129.29, 126.79, 122.71, 121.86, 121.11, 120.53, 118.22, 109.83, 99.59, 83.75, 66.30, 55.94, 49.28, 27.01, 17.83, 3.84, -1.29.



2-((2-((2-methoxy-4-(vinylsulfonamidomethyl)phenyl)amino)-7H-pyrrolo[2,3-d]pyrimidin-4-yl)amino)-N-methylbenzamide (37)

Compound **37** was synthesized using the protocol described for **34**. Yields a yellow solid, 6 mg, 50% HPLC: 5.7 min, Molecular Formula: C₂₄H₂₅N₇O₄S, Mass Calc: 507.17 ESI-MS-Found: 508 [M+1], purity: 95% ¹H NMR (700 MHz, Chloroform-d) δ 11.60 (d, J = 18.4 Hz, 2H), 9.47 (d, J = 2.3 Hz, 1H), 9.10 (s, 1H), 8.91 (d, J = 9.1 Hz, 1H), 8.44 (d, J = 7.7 Hz, 1H), 7.85 (s, 1H), 7.80 (d, J = 8.6 Hz, 1H), 7.56 (s, 1H), 7.50

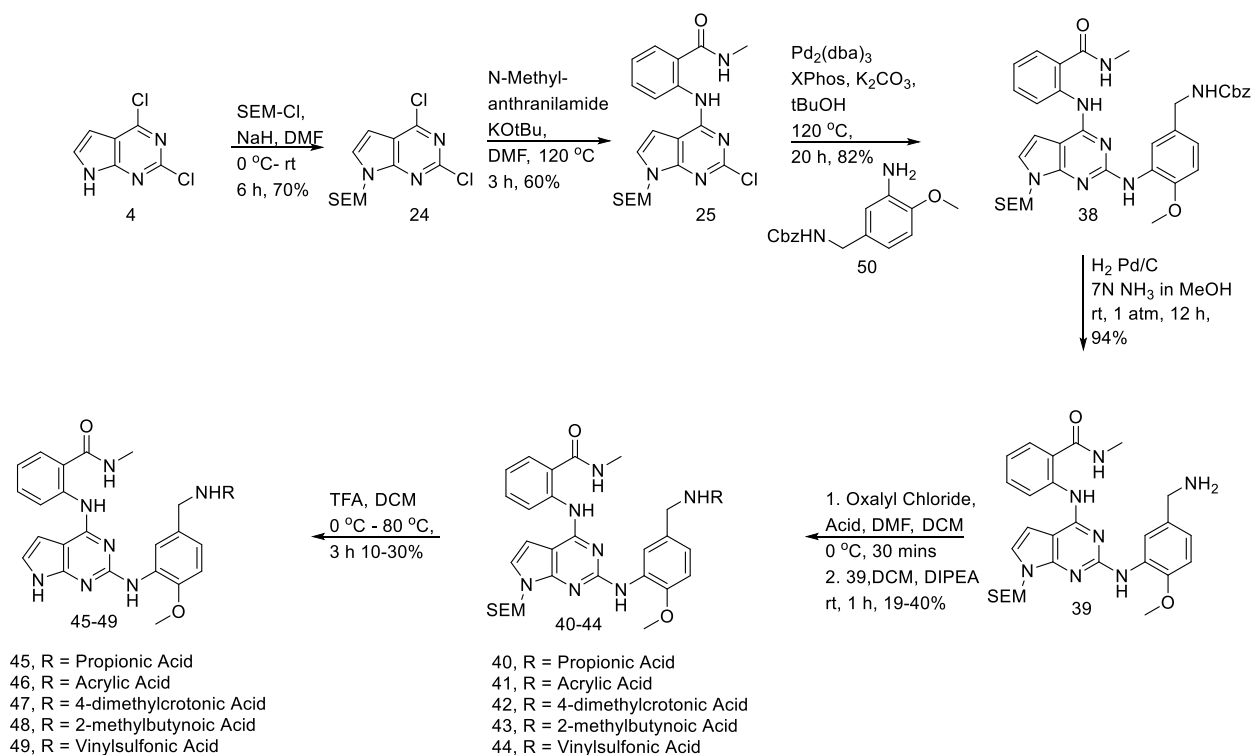
–7.47 (m, 1H), 7.45 (s, 1H), 7.19 (s, 2H), 7.14 (s, 2H), 7.10 (s, 1H), 7.06 (s, 2H), 6.67 (d, J = 19.8 Hz, 1H), 6.28 (s, 1H), 5.65 (s, 1H), 3.86 (s, 3H), 3.35 (d, J = 2.7 Hz, 2H), 3.04 (d, J = 4.4 Hz, 3H). ¹³CNMR (176 MHz, dmsO) δ 168.35, 167.93, 155.05, 150.76, 147.84, 143.92, 135.24, 132.83, 132.37, 130.53, 128.35, 121.68, 119.90, 118.68, 117.80, 117.14, 116.46, 111.78, 99.28, 91.81, 56.08, 47.41, 25.80.



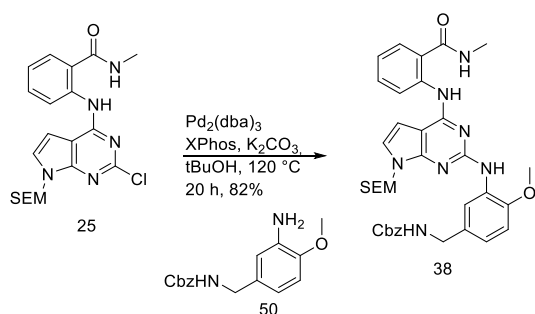
2-((2-((4-(but-2-ynamidomethyl)-2-methoxyphenyl)amino)-7H-pyrrolo[2,3-d]pyrimidin-4-yl)amino)-N-methylbenzamide (36)

Compound **36** was synthesized using the protocol described for **34**. Yields a white solid, 10 mg, 25% HPLC: 5.3 min, Molecular Formula: C₂₆H₂₅N₇O₃, Mass Calc: 483.20 ESI-MS-Found: 484 [M+1], purity: 95%. ¹HNMR (700 MHz, DMSO-d₆) δ 11.64 (s, 1H), 11.37 (s, 1H), 8.95 (t, J = 6.2 Hz, 1H), 8.84 (d, J = 8.4 Hz, 1H), 8.73 (d, J = 4.6 Hz, 1H), 8.23 (d, J = 8.1 Hz, 1H), 7.75 (d, J = 7.8 Hz, 1H), 7.53 (s, 1H), 7.49 (t, J = 7.9 Hz, 1H), 7.05 (t, J = 7.5 Hz, 1H), 7.01 (d, J = 3.3 Hz, 1H), 6.93 (s, 1H), 6.81 (d, J = 8.1 Hz, 1H), 6.33 (s, 1H), 4.25 (d, J = 6.1 Hz, 2H), 3.86 (s, 3H), 2.83 (d, J = 4.4 Hz, 3H), 1.97 (d, J = 1.1 Hz, 3H). ¹³CNMR (176 MHz, cdcl₃) δ 170.17, 156.71, 155.63, 153.61, 153.23, 152.59, 149.57, 147.72, 141.11, 132.10, 130.09, 129.11, 126.61, 122.53, 121.68, 120.93, 120.35, 120.02, 118.04, 109.65, 99.41, 55.76, 44.03, 26.83, 3.66.

Synthesis of 45-49



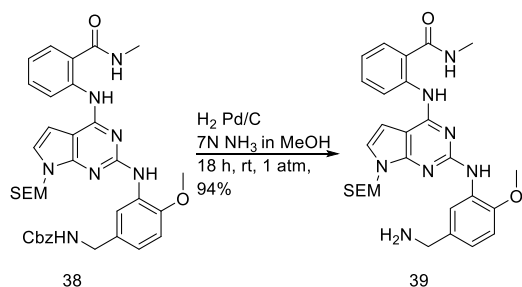
Scheme 2.9. Synthetic route for *meta* homologated compounds **45-49**.



Benzyl-(4-methoxy-3-(((2-(methylcarbamoyl)phenyl)amino)-7-((2-(trimethylsilyl)ethoxy)methyl)-7H-pyrrolo[2,3-d]pyrimidin-2-yl)amino)benzyl)carbamate (38)

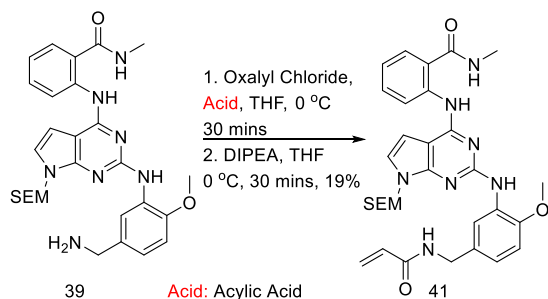
A flame dried three neck flask was charged with 90.0 mg of **25** (0.21 mmol, 1.0 equiv), 68.2 mg of K_2CO_3 (0.42 mmol, 2 equiv.), 5.5 mg of XPhos (0.012 mmol, 0.055 equiv), 2.1 mg of $Pd_2(dba)_3$ (0.002 mmol, 0.01 equiv) and 4 mL of tBuOH. The mixture was degassed with 8 cycles of evacuation and back filled with nitrogen. The solution was heated to 110 °C for 20 h. Once complete, the solution was passed through a pad of celite, and purified by column chromatography (eluting with 50% EtOAc/Hexanes). The solvent was removed under pressure to give a dark red solid, 120.0 mg, 82% HPLC: 8.109 min, Molecular Formula: $C_{36}H_{43}N_7O_5Si$, Mass Calc: 681.31 ESI-MS-Found: 682 [M+1], purity: 97% 1H NMR (700 MHz, $CDCl_3$ -d)

δ 11.03 (s, 1H), 8.84 (d, $J = 8.4$ Hz, 1H), 8.69 (s, 1H), 7.55 (s, 1H), 7.46 (t, $J = 8.1$ Hz, 1H), 7.42 (d, $J = 7.8$ Hz, 1H), 7.33 (dd, $J = 13.1, 5.8$ Hz, 4H), 7.31 – 7.27 (m, 1H), 6.96 – 6.91 (m, 2H), 6.82 (q, $J = 8.5$ Hz, 2H), 6.59 (d, $J = 3.7$ Hz, 1H), 6.41 (q, $J = 4.6$ Hz, 1H), 5.49 (s, 2H), 5.13 (s, 2H), 4.33 (d, $J = 5.7$ Hz, 2H), 3.90 (s, 3H), 3.59 – 3.54 (m, 2H), 2.96 (d, $J = 4.8$ Hz, 3H), 0.93 (t, $J = 8.2$ Hz, 2H), -0.09 (s, 9H). ^{13}C NMR (176 MHz, CDCl_3) δ 170.45, 156.52, 155.88, 153.86, 152.88, 147.15, 141.32, 136.93, 132.19, 130.89, 128.72, 128.28, 128.23, 127.02, 122.90, 121.81, 121.24, 120.55, 119.57, 117.59, 109.96, 100.38, 99.59, 66.33, 56.06, 45.65, 27.03, 17.88, -1.21.



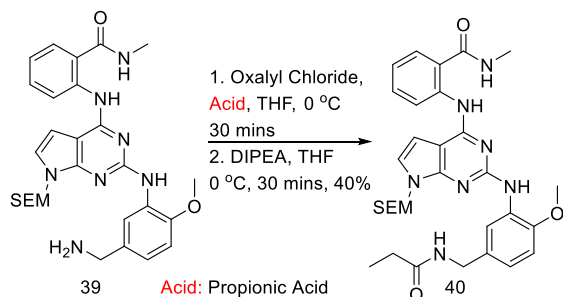
2-((2-((5-(aminomethyl)-2-methoxyphenyl)amino)-7-((2-(trimethylsilyl)ethoxy)methyl)-7H-pyrrolo[2,3-d]pyrimidin-4-yl)amino)-N-methylbenzamide (39)

A dried flask was charged with 120 mg of **38** (0.176 mmol, 1.0 equiv) and 3 mL of 7N NH_3 in MeOH. The solution was degassed with three rounds of evacuation and back filled with nitrogen, and then RaNi (slurry in water), was added. The solution was further degassed by three cycles of evacuation and back fill with nitrogen. The atmosphere was replaced with hydrogen, and the mixture was stirred for 12 hours. Once complete, the atmosphere was removed and then solution was passed through a pad of celite. The solvent was removed to yield a green solid, 91.8 mg, 93.5%. Molecular Formula: $\text{C}_{28}\text{H}_{37}\text{N}_7\text{O}_3\text{Si}$, Mass Calc: 547.27 ESI-MS-Found: 548 [M+1], HPLC: 6.241min, purity: 98.2%. ^1H NMR (500 MHz, Chloroform-d) δ 10.61 (s, 1H), 8.55 – 8.48 (m, 1H), 8.44 (d, $J = 8.0$ Hz, 1H), 8.36 (s, 1H), 7.56 (d, $J = 10.3$ Hz, 1H), 7.50 (s, 1H), 7.42 (d, $J = 8.6$ Hz, 1H), 7.10 (d, $J = 7.5$ Hz, 1H), 7.03 (s, 1H), 7.01 – 6.96 (m, 1H), 6.91 (dd, $J = 10.3, 7.4$ Hz, 2H), 6.80 (d, $J = 8.1$ Hz, 1H), 6.71 (t, $J = 9.6$ Hz, 1H), 6.47 (d, $J = 9.9$ Hz, 1H), 5.51 (s, 2H), 3.89 – 3.84 (m, 3H), 3.55 (t, $J = 8.4$ Hz, 2H), 3.03 – 2.93 (m, 3H), 0.96 – 0.89 (m, 2H), -0.07 (d, $J = 2.7$ Hz, 9H). ^{13}C NMR (176 MHz, cdCl_3) δ 169.94, 155.53, 153.31, 152.31, 140.77, 131.64, 126.52, 122.13, 121.28, 120.51, 119.78, 117.79, 109.92, 99.67, 99.06, 77.03, 77.00, 76.84, 76.82, 76.66, 76.64, 72.21, 65.78, 55.36, 26.43, 17.33, 13.86, -0.33, -1.75, -1.78. (126 MHz, cdCl_3) δ 168.39, 167.61, 155.35, 153.84, 147.88, 144.63, 140.11, 133.00, 131.50, 130.70, 128.22, 121.92, 120.22, 119.20, 118.07, 116.49, 114.73, 103.48, 99.40, 86.60, 66.10, 55.72, 41.14, 26.69, 17.66, -1.46.



2-((2-((5-(acrylamidomethyl)-2-methoxyphenyl)amino)-7-((2-(trimethylsilyl)ethoxy)methyl)-7H-pyrrolo[2,3-d]pyrimidin-4-yl)amino)-N-methylbenzamide (41)

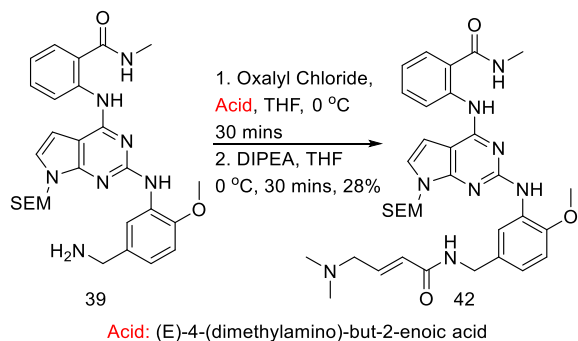
Compound **41** was synthesized using the protocol described for **28**. Yields a light yellow residue, 13.9 mg, 19%. HPLC: 7.104 min, Molecular Formula: C₃₁H₃₉N₇O₄Si, Mass Calc: 601.28 ESI-MS-Found: 602.2900 [M+1], purity: 74.4%. ¹HNMR (700 MHz, CDCl₃) δ 11.03 (s, 1H), 8.81 (s, 1H), 8.65 (s, 1H), 7.50 – 7.45 (m, 2H), 7.01 (q, J = 8.1, 7.6 Hz, 1H), 6.93 (t, J = 3.7 Hz, 1H), 6.85 (d, J = 8.5 Hz, 1H), 6.83 (d, J = 8.2 Hz, 1H), 6.60 – 6.55 (m, 2H), 6.31 (dd, J = 3.0, 1.8 Hz, 1H), 6.28 (dd, J = 2.8, 1.8 Hz, 1H), 5.66 (dd, J = 10.5, 2.0 Hz, 1H), 5.62 (dd, J = 10.3, 1.6 Hz, 1H), 5.51 (s, 2H), 4.44 (dd, J = 9.8, 5.6 Hz, 2H), 3.91 (d, J = 2.7 Hz, 3H), 3.59 – 3.55 (m, 2H), 3.01 (d, J = 3.7 Hz, 3H), 0.96 – 0.89 (m, 2H), -0.08 (d, J = 9.7 Hz, 9H). ¹³CNMR (176 MHz, cdcl₃) δ 170.30, 165.28, 155.82, 153.81, 150.34, 147.14, 143.85, 132.16, 131.02, 130.18, 127.82, 127.71, 126.58, 122.87, 121.85, 119.99, 118.04, 117.18, 116.36, 110.04, 99.67, 86.17, 66.30, 56.00, 44.21, 27.00, -1.29.



2-((2-((2-methoxy-5-(propionamidomethyl)phenyl)amino)-7-((2-(trimethylsilyl)ethoxy)methyl)-7H-pyrrolo[2,3-d]pyrimidin-4-yl)amino)-N-methylbenzamide (40)

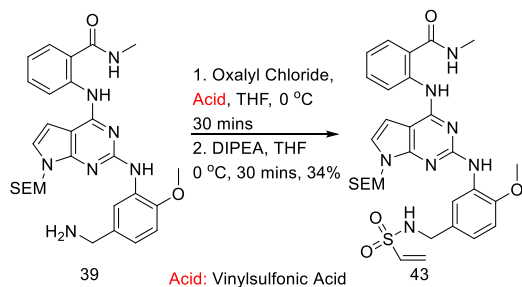
Compound **40** was synthesized using the protocol described for **28**. Yields a light yellow residue, 20 mg, 40%. HPLC: 6.781 min, Molecular Formula: C₃₁H₄₁N₇O₄Si, Mass Calc: 603.30 ESI-MS-Found: 603.3219 [M+1], purity: 99% ¹HNMR (500 MHz, Chloroform-d) δ 11.13 (s, 1H), 8.88 (d, J = 8.4 Hz, 1H), 8.61 (d, J = 8.2 Hz, 1H), 7.99 (s, 1H), 7.54 (s, 1H), 7.50 (d, J = 7.9 Hz, 2H), 7.00 (t, J = 7.6 Hz, 1H), 6.94 (d, J = 3.6 Hz, 1H), 6.87 (d, J = 8.3 Hz, 1H), 6.82 (s, 1H), 6.71 (d, J = 8.0 Hz, 1H), 6.64 (d, J = 1.9 Hz, 1H), 6.62 (s, 1H), 6.60 (t, J = 3.8 Hz, 2H), 6.53 (d, J = 5.7 Hz, 1H), 5.53 (s, 2H), 4.28 (d, J = 5.5 Hz, 3H), 3.91 (s, 3H),

3.59 (t, J = 8.2 Hz, 2H), 3.01 (d, J = 4.7 Hz, 3H), 2.80 (s, 2H), 2.24 (dq, J = 18.6, 7.6 Hz, 2H), 1.18 (dt, J = 15.0, 7.6 Hz, 3H), 0.94 (t, J = 8.2 Hz, 2H), -0.07 (s, 9H).¹³CNMR (126 MHz, cdcl₃) δ 173.53, 170.13, 162.56, 153.57, 152.35, 147.76, 146.72, 140.95, 136.35, 132.00, 130.94, 130.38, 129.69, 126.73, 122.55, 121.67, 121.03, 120.14, 118.19, 117.76, 114.49, 110.29, 109.65, 100.00, 99.45, 72.58, 66.11, 55.52, 43.36, 26.78, 17.64, 9.83, -1.49.



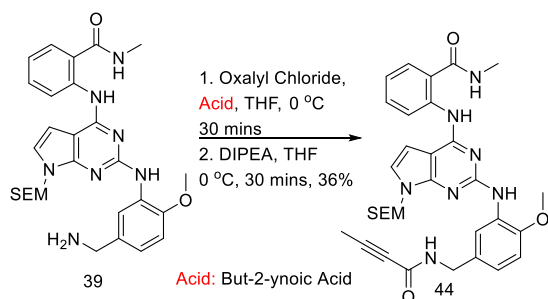
(E)-2-((2-((5-((4-(dimethylamino)but-2-enamido)methyl)-2-methoxyphenyl)amino)-7-((2-(trimethylsilyl)ethoxy)methyl)-7H-pyrrolo[2,3-d]pyrimidin-4-yl)amino)-N-methylbenzamide (**42**)

Compound **42** was synthesized using the protocol described for **28**. Yields a light yellow residue, 20 mg, 28%. HPLC: 7.65 min, Molecular Formula: C₃₄H₄₆N₈O₄Si, Mass Calc: 658.34 ESI-MS-Found: 662 [M+4], purity: 85%. ¹HNMR (700 MHz, Chloroform-d) δ 10.87 (s, 1H), 8.78 (d, J = 8.3 Hz, 1H), 8.70 – 8.65 (m, 1H), 7.57 (s, 1H), 7.49 (d, J = 7.7 Hz, 2H), 7.23 (d, J = 6.5 Hz, 1H), 7.03 (t, J = 7.6 Hz, 1H), 6.96 (d, J = 3.6 Hz, 1H), 6.85 (d, J = 3.0 Hz, 2H), 6.60 (d, J = 3.5 Hz, 1H), 6.44 (d, J = 5.5 Hz, 1H), 5.54 (s, 2H), 4.40 (d, J = 5.8 Hz, 2H), 3.93 (s, 3H), 3.60 – 3.55 (m, 2H), 3.03 (d, J = 4.8 Hz, 3H), 0.94 (ddd, J = 10.9, 7.6, 3.2 Hz, 2H), -0.08 (s, 9H).¹³CNMR (176 MHz, cdcl₃) δ 169.99, 160.06, 156.21, 155.36, 153.45, 152.51, 146.93, 140.68, 131.63, 130.59, 128.68, 126.62, 122.54, 121.86, 120.99, 120.81, 119.65, 117.58, 109.60, 99.95, 99.16, 65.90, 55.63, 44.10, 26.61, 21.35, 17.43, -1.66.



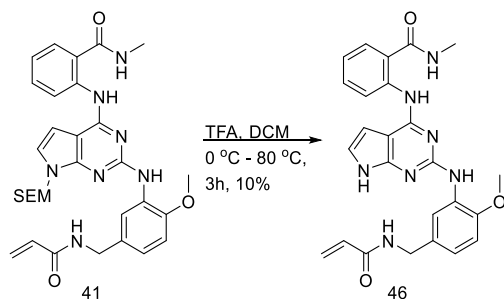
2-((2-((2-methoxy-5-(vinylsulfonamidomethyl)phenyl)amino)-7-((2-(trimethylsilyl)ethoxy)methyl)-7H-pyrrolo[2,3-d]pyrimidin-4-yl)amino)-N-methylbenzamide (**43**)

Compound **43** was synthesized using the protocol described for **28**. Yields a light yellow residue, 10 mg, 34%. HPLC: 7.534 min, Molecular Formula: C₃₀H₃₉N₇O₅SSi, Mass Calc: 637.25 ESI-MS-Found: 638 [M+1], purity: 85%. ¹HNMR (400 MHz, Chloroform-*d*) δ 8.37 (s, 1H), 8.04 (s, 1H), 7.50 (s, 1H), 6.89 (s, 3H), 6.50 (s, 1H), 6.22 (s, 1H), 5.91 (s, 1H), 5.57 (s, 2H), 4.23 (m, 2H), 3.95 (s, 3H), 3.61 (s, 2H), 3.37 (d, *J* = 16.6 Hz, 2H), 2.96 – 2.81 (m, 3H), 0.88 (d, *J* = 24.2 Hz, 2H), -0.07 (s, 9H). ¹³CNMR (176 MHz, cdcl₃) δ 169.98, 165.69, 155.06, 150.31, 147.80, 143.19, 135.08, 133.85, 131.70, 128.59, 122.86, 121.52, 120.55, 118.62, 117.86, 116.77, 115.07, 110.45, 103.85, 100.40, 74.30, 68.65, 55.73, 44.36, 25.17, 22.46, 17.58, -1.56.



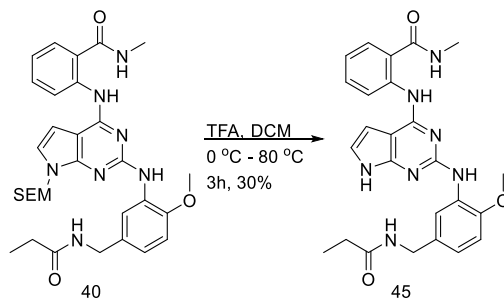
2-((2-((5-(but-2-ynamidomethyl)-2-methoxyphenyl)amino)-7-((2-(trimethylsilyl)ethoxy)methyl)-7H-pyrrolo[2,3-d]pyrimidin-4-yl)amino)-N-methylbenzamide (44)

Compound **44** was synthesized using the protocol described for **28**. Yields a light yellow residue, 10 mg, 36%. HPLC: 8.610 min, Molecular Formula: C₃₂H₃₉N₇O₄Si, Mass Calc: 613.28 ESI-MS-Found: 623, purity: 65%. ¹HNMR (500 MHz, Chloroform-*d*) δ 11.10 (s, 1H), 8.92 (d, *J* = 8.4 Hz, 1H), 8.65 (d, *J* = 8.3 Hz, 1H), 7.52 (d, *J* = 7.1 Hz, 1H), 7.49 (d, *J* = 8.2 Hz, 1H), 7.02 (t, *J* = 7.7 Hz, 1H), 6.95 (d, *J* = 3.6 Hz, 1H), 6.88 (d, *J* = 8.4 Hz, 1H), 6.83 (s, 1H), 6.72 (d, *J* = 8.2 Hz, 1H), 6.65 (d, *J* = 2.0 Hz, 1H), 6.63 (d, *J* = 2.3 Hz, 1H), 6.62 – 6.60 (m, 2H), 5.55 (d, *J* = 7.9 Hz, 2H), 4.32 (d, *J* = 5.7 Hz, 3H), 3.93 (s, 2H), 3.60 (t, *J* = 8.1 Hz, 2H), 3.03 (d, *J* = 4.7 Hz, 3H), 1.93 (s, 4H), 0.95 (t, *J* = 8.1 Hz, 2H), -0.06 (d, *J* = 4.0 Hz, 9H). ¹³CNMR (126 MHz, cdcl₃) δ 170.42, 155.90, 153.88, 153.48, 152.86, 148.01, 147.13, 141.38, 136.74, 132.34, 130.24, 129.42, 126.86, 122.79, 121.95, 121.19, 120.60, 120.30, 118.34, 118.09, 114.70, 110.58, 109.93, 100.33, 99.66, 83.71, 72.81, 66.38, 55.81, 43.86, 27.07, 17.92, 3.86, -1.21.



2-((2-((5-(acrylamidomethyl)-2-methoxyphenyl)amino)-7-((2-(trimethylsilyl)ethoxy)methyl)-7H-pyrrolo[2,3-d]pyrimidin-4-yl)amino)-N-methylbenzamide (**46**)

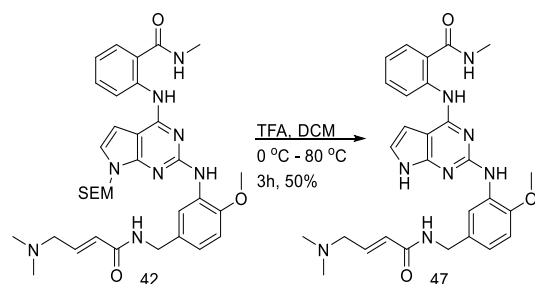
Compound **46** was synthesized using the protocol described for **34**. Yields a light yellow solid, 2 mg, 10%. HPLC: 5.114 min, Molecular Formula: C₂₅H₂₅N₇O₃, Mass Calc: 471.20 ESI-MS-Found: 471 [M], purity: 90%. ¹HNMR (700 MHz, DMSO-d₆) δ 11.70 (s, 1H), 8.80 (dd, J = 8.0, 3.3 Hz, 1H), 8.75 (t, J = 4.6 Hz, 1H), 8.57 (t, J = 6.0 Hz, 1H), 8.40 (d, J = 2.1 Hz, 1H), 7.76 (dd, J = 8.0, 1.5 Hz, 1H), 7.63 (d, J = 3.9 Hz, 1H), 7.52 – 7.49 (m, 1H), 7.16 (d, J = 3.5 Hz, 1H), 7.06 (t, J = 7.6 Hz, 1H), 6.99 (d, J = 4.5 Hz, 1H), 6.87 – 6.83 (m, 1H), 6.51 (t, J = 7.3 Hz, 1H), 6.40 (d, J = 3.6 Hz, 1H), 5.60 (ddd, J = 10.3, 4.3, 2.1 Hz, 1H), 4.31 (d, J = 6.0 Hz, 2H), 3.87 (d, J = 2.5 Hz, 3H), 2.82 (d, J = 4.5 Hz, 3H). ¹³CNMR (176 MHz, dmsO) δ 169.63, 167.25, 164.75, 155.43, 153.21, 147.32, 143.98, 134.27, 132.08, 131.91, 128.25, 125.52, 121.04, 120.71, 119.73, 118.62, 117.83, 116.41, 110.45, 99.58, 90.85, 56.10, 42.56, 26.55.



2-((2-((2-methoxy-5-(propionamidomethyl)phenyl)amino)-7-((2-(trimethylsilyl)ethoxy)methyl)-7H-pyrrolo[2,3-d]pyrimidin-4-yl)amino)-N-methylbenzamide (**45**)

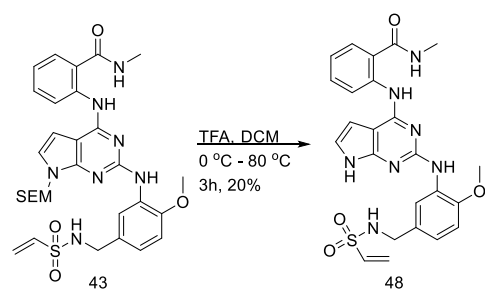
Compound **45** was synthesized using the protocol described for **34**. Yields a light yellow residue, 5 mg, 30%. HPLC: 4.99 min, Molecular Formula: C₂₅H₂₇N₇O₃, Mass Calc: 473.22 ESI-MS-Found: 474 [M+1], purity: 95% ¹HNMR (700 MHz, DMSO-d₆) δ 11.64 (s, 1H), 11.37 (s, 1H), 8.85 (d, J = 8.6 Hz, 1H), 8.74 (s, 1H), 8.26 – 8.19 (m, 2H), 8.11 – 8.04 (m, 2H), 7.75 (d, J = 8.1 Hz, 1H), 7.53 (s, 1H), 7.50 – 7.44 (m, 1H), 7.08 – 7.03 (m, 1H), 7.03 – 6.98 (m, 1H), 6.93 (s, 1H), 6.82 (d, J = 8.4 Hz, 1H), 4.24 (d, J = 6.6 Hz, 2H), 3.86 (d, J = 5.5 Hz, 3H), 2.83 (d, J = 4.6 Hz, 3H), 2.16 (q, J = 7.7 Hz, 2H), 1.05 (t, J = 7.6 Hz, 3H). ¹³CNMR(176 MHz, dmsO) δ 172.87, 169.81, 163.15, 161.80, 159.33, 155.89, 153.30, 152.61, 148.82,

145.71, 141.27, 137.80, 133.24, 132.28, 128.79, 128.34, 120.96, 119.90, 119.67, 119.40, 115.42, 113.37, 110.68, 99.47, 97.73, 55.73, 42.24, 28.85, 26.69, 10.39.



(E)-2-((2-((5-((4-(dimethylamino)but-2-enamido)methyl)-2-methoxyphenyl)amino)-7-((2-(trimethylsilyl)ethoxy)methyl)-7H-pyrrolo[2,3-d]pyrimidin-4-yl)amino)-*N*-methylbenzamide (**47**)

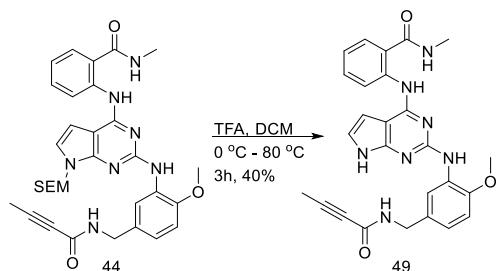
Compound **47** synthesized using the protocol described for **34**. Yields a bright yellow solid, 8 mg, 50%. HPLC: 5.485 min, Molecular Formula: C₂₈H₃₂N₈O₃, Mass Calc: 528.26 ESI-MS-Found: 562 [M+H+MeOH], purity: 95%. ¹HNMR (700 MHz, DMSO-d₆) δ 11.71 (s, 1H), 9.34 (t, J = 6.3 Hz, 1H), 8.80 (d, J = 8.4 Hz, 1H), 8.78 – 8.71 (m, 1H), 8.39 – 8.36 (m, 1H), 7.76 (dd, J = 7.9, 1.6 Hz, 1H), 7.64 (s, 1H), 7.53 – 7.48 (m, 1H), 7.16 (d, J = 3.5 Hz, 1H), 7.08 – 7.04 (m, 1H), 6.99 (d, J = 8.3 Hz, 1H), 6.86 (dd, J = 8.2, 2.2 Hz, 1H), 6.42 (t, J = 7.3 Hz, 1H), 6.40 (d, J = 3.6 Hz, 1H), 5.48 (d, J = 7.2 Hz, 2H), 4.29 (d, J = 6.3 Hz, 2H), 3.87 (s, 3H), 2.83 (d, J = 4.4 Hz, 3H), 1.26 (dd, J = 6.3, 3.7 Hz, 6H). ¹³CNMR (176 MHz, dmsO) δ 169.63, 160.56, 157.59, 155.46, 153.20, 147.55, 143.59, 140.93, 132.65, 132.09, 130.54, 128.22, 123.46, 121.00, 120.71, 119.67, 118.96, 118.06, 116.65, 114.47, 110.47, 99.57, 97.95, 66.48, 56.07, 42.76, 41.57, 26.54.



2-((2-((2-methoxy-5-(vinylsulfonamidomethyl)phenyl)amino)-7H-pyrrolo[2,3-d]pyrimidin-4-yl)amino)-*N*-methylbenzamide (**48**)

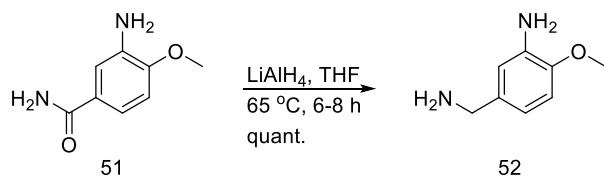
Compound **48** was synthesized using the protocol described for **34**. Yields a white residue, 2 mg, 20%. HPLC: 6.13 min, Molecular Formula: C₂₄H₂₅N₇O₄S, Mass Calc: 507.17 ESI-MS-Found: 508 [M+1], purity: 95%. ¹HNMR (700 MHz, Chloroform-d) δ 10.82 (s, 1H), 8.63 (s, 1H), 8.51 (s, 1H), 7.58 (s, 1H), 7.53 (s, 1H), 7.47 (s, 1H), 6.92 (s, 1H), 6.83 (s, 1H), 6.58 (s, 1H), 5.81 (s, 1H), 4.17 – 4.07 (m, 2H), 3.92 (s, 3H),

3.03 (s, 3H). ¹³CNMR (176 MHz, cdcl₃) δ 169.98, 165.69, 155.06, 150.31, 147.80, 143.19, 135.08, 133.85, 131.70, 128.59, 122.86, 121.52, 120.55, 118.62, 117.86, 116.77, 115.07, 110.45, 103.85, 100.40, 55.73, 44.36, 25.17.



2-((2-((5-(but-2-ynamidomethyl)-2-methoxyphenyl)amino)-7H-pyrrolo[2,3-d]pyrimidin-4-yl)amino)-N-methylbenzamide (49)

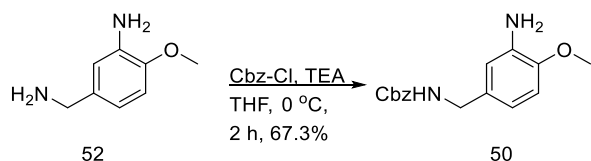
Compound **49** was synthesized using the protocol described for **34**. Yields a white residue, 4 mg, 40%. HPLC: 5.67 min, Molecular Formula: C₂₆H₂₅N₇O₃, Mass Calc: 483.20 ESI-MS-Found: 484 [M+1], 506 [M+Na], purity: 92% ¹H NMR (700 MHz, DMSO-d₆) δ 12.05 (s, 1H), 11.68 (s, 1H), 8.96 (s, 1H), 8.83 (s, 3H), 8.74 (s, 1H), 8.62 (d, J = 8.1 Hz, 1H), 8.28 (s, 1H), 7.75 (s, 1H), 7.61 (s, 1H), 7.51 (t, J = 3.4 Hz, 1H), 7.07 (s, 2H), 6.94 (s, 1H), 4.25 (d, J = 5.8 Hz, 2H), 3.86 (d, J = 3.4 Hz, 3H), 2.84 – 2.80 (m, 7H), 1.95 – 1.94 (m, 12H). ¹³CNMR (176 MHz, dmso) δ 162.92, 162.46, 161.19, 156.25, 152.67, 147.87, 145.77, 137.82, 134.02, 131.84, 131.51, 127.00, 122.23, 121.19, 121.07, 119.79, 119.58, 118.60, 116.58, 115.41, 113.24, 110.65, 55.73, 42.37, 26.70, 3.40.



5-(aminomethyl)-2-methoxyaniline (52)

A flame dried flask was charged with 995.4 mg of 3-amino-4-methoxybenzamide (**51**) (6 mmol, 1.0 equiv) and 30 mL of dry THF (0.1 molar). The solution was cooled to 0 °C and 6.1 mL of LAH (10 mmol, 2 equiv) were added dropwise over 5 min. The bright yellow solution was allowed to continue stirring at 0 °C for 30 min. After 30 min, the solution was warmed to 65 °C for 6-8 hours. Once complete, the reaction was cooled back to 0 °C and worked up with the Feiser Method: 0.457 mL water, followed by 0.457 mL of freshly prepared 15% NaOH, and 1.371 mL of water. The resultant brown solution was allowed to stir at rt

for 15 min. Then MgSO_4 was added and the solution was allowed to stir for additional 15 min. The MgSO_4 was filtered off and the solvent was removed to yield a yellow oil, 0.900 g, 100%. Molecular Formula: $\text{C}_8\text{H}_{12}\text{N}_2\text{O}$, Mass Calc: 152.09 ESI-MS-Found: 152 [M] HPLC: 0.96 min, purity: > 95% ^1H NMR (400 MHz, DMSO-d_6) δ 6.69 (d, $J = 8.1$ Hz, 1H), 6.59 (d, $J = 2.1$ Hz, 1H), 6.46 (dd, $J = 8.1, 2.1$ Hz, 1H), 4.59 (s, 2H), 3.72 (s, 3H), 3.52 (s, 2H), 1.63 (s, 2H).



benzyl (3-amino-4-methoxybenzyl)carbamate (50)

A flame dried flask was charged with 900.0 mg of **52** (5.91 mmol, 1.0 equiv) and 40 mL of dry THF (0.19 molar). The solution was cooled to 0 °C and 0.92 mL of TEA (6.6 mmol, 1.1 equiv), and 0.94 mL of Cbz-Cl (6.6 mmol, 1.1 equiv) were added in one portion, respectively. Once complete, the reaction was quenched with water and then extracted with EtOAc (3 x 50 mL). The combined organic layers were washed with brine (1 x 30 mL) and then dried over Na_2SO_4 . The crude oil was purified by column chromatography (0-100% EtOAc/Hex) to give a light yellow oil, 1.14 g, 67.3%. HPLC: 4.871 min, Molecular Formula: $\text{C}_{16}\text{H}_{18}\text{N}_2\text{O}_3$ Mass Calc: 286.13 ESI-MS-Found: 287, purity: 85% ^1H NMR (500 MHz, Chloroform- d) δ 7.34 (dd, $J = 21.0, 4.5$ Hz, 5H), 6.72 (d, $J = 8.1$ Hz, 1H), 6.65 (s, 1H), 6.62 (d, $J = 7.8$ Hz, 1H), 5.13 (s, 2H), 4.25 (d, $J = 5.9$ Hz, 2H), 3.83 (s, 3H), 3.79 (s, 2H).

2-chloro-N-methyl-7-((2-(trimethylsilyl)ethoxy)methyl)-7H-pyrrolo[2,3-d]pyrimidin-4-amine (53, RAR-5-75)

To a flask were added 249 mg of RAR-5-70 (SEM-protected dichloropyrrolopyrimidine) which was dissolved in 4 mL of MeOH. To this solution were added 0.1 mL of methylamine, and the solution was heated to 70 °C for 2 hours. Once complete, the solvent was removed under pressure to yield to desired product. Yields a white solid, 240 mg, 98%. ^1H NMR (500 MHz, Chloroform- d) δ 7.03 (t, $J = 3.8$ Hz, 1H), 6.41 (s, 1H), 5.52 (d, $J = 3.1$ Hz, 2H), 3.52 (t, $J = 8.2$ Hz, 2H), 0.90 (td, $J = 8.2, 3.2$ Hz, 2H), -0.06 (t, $J = 3.5$ Hz, 9H).

3-methoxy-4-nitrobenzoyl chloride (54, RAR-5-81)

To a dried flask were added 252.4 mg of 3-methoxy-4-nitrobenzoic acid, dissolved in 8 mL of dry THF. The solution was cooled to 0 °C and 0.02 mL of oxalyl chloride were added. The solution was allowed to stir at 0 °C for 1 hour or until complete. Once complete, the solvent was removed, and the acid chloride was rinsed with DCM (3 x 30 mL) before being used directly in the next step. HPLC: 6.43, 92%

(3-methoxy-4-nitrophenyl)(morpholino)methanone (55, RAR-5-82)

To a dried flask were added 273 mg of RAR-5-81, dissolved in 5 mL of THF. The solution was cooled to 0 °C and then 0.44 mL of DIPEA and 0.166 mL of morpholine were added respectively. The solution was allowed to stir at 0 °C for 1 h, and then the reaction was quenched with water and extracted with EtOAc (3 x 30 mL). The combined organic layers were then dried over Na₂SO₄ and the solvent was removed to yield a crude product. The crude yellow product was purified by column chromatography to give the desired product as a yellow oil, 306.7 mg, 91%. ¹H NMR (400 MHz, DMSO-d₆) δ 7.93 (d, J = 8.2 Hz, 1H), 7.37 (d, J = 1.5 Hz, 1H), 7.11 (dd, J = 8.2, 1.5 Hz, 1H), 3.94 (s, 3H), 3.75 – 3.39 (m, 8H).

(4-amino-3-methoxyphenyl)(morpholino)methanone (56, RAR-5-83)

To a flask were added 153 mg of RAR-5-82, dissolved in 3 mL of MeOH. The solution was degassed with 3 cycles of evacuation and backfill with nitrogen before Pd/C was added. The solution was then further degassed with an additional 3 cycles of evacuation and backfill with nitrogen, at which point hydrogen atmosphere was introduced. The reaction was allowed to run for 12-18 hours. Once complete, the hydrogen atmosphere was removed, and the solution was passed through a pad of celite. The solvent was removed to yield the desired product as a yellow solid, 57.2 mg, 43.0%. ¹H NMR (400 MHz, DMSO-d₆) δ 6.85 (d, J = 1.7 Hz, 1H), 6.80 (dd, J = 7.9, 1.8 Hz, 1H), 6.61 (d, J = 7.9 Hz, 1H), 5.15 (s, 1H), 3.77 (s, 3H), 3.61 – 3.55 (m, 4H), 3.50 (t, J = 4.6 Hz, 4H).

(3-methoxy-4-((4-(methylamino)-7-((2-(trimethylsilyl)ethoxy)methyl)-7H-pyrrolo[2,3-d]pyrimidin-2-yl)amino)phenyl)(morpholino)methanone (57, RAR-5-89)

To a three neck flask were added 57.2 mg of RAR-5-83, dissolved in 4.7 mL of dry and degassed nBuOH. To this solution were added 50 mg of RAR-5-75, 47.0 mg of K₂CO₃, XPhos, and Pd₂(dba)₃. The solution was degassed with 6 cycles of evacuation and backfill with nitrogen before a reflux condenser was fitted to the flask. The solution was then heated to 100 °C for 6-12 h. Once complete, the reaction was cooled to room temperature and then passed through a pad of celite. The filtrate was then purified by column chromatography to yield the desired product as a yellow oil, 49.8 mg, 60%. MS: 513, HPLC: 5.994, ¹H NMR (400 MHz, Chloroform-d) δ 8.79 (d, J = 8.1 Hz, 1H), 7.62 (s, 1H), 7.01 (d, J = 8.1 Hz, 1H), 6.94 (d, J = 1.8 Hz, 1H), 6.89 – 6.81 (m, 1H), 6.64 (d, J = 7.9 Hz, 1H), 5.51 (s, 1H), 3.94 (s, 3H), 3.86 (s, 3H), 3.72 – 3.61 (m, 8H), 3.17 (d, J = 5.0 Hz, 2H), 0.96 – 0.88 (m, 2H), -0.09 (s, 9H).

(3-methoxy-4-((4-(methylamino)-7H-pyrrolo[2,3-d]pyrimidin-2-yl)amino)phenyl)(morpholino)methanone (58, RAR-5-93, CCG-264018)

To a flask were added 49.8 mg of RAR-5-89, which was dissolved in 5 mL of DCM. To this solution were added 1.0 mL of TFA and the resultant bright orange solution was heated to 50 °C for 3 h. Once complete, the reaction was cooled to room temperature and then quenched with saturated NaHCO₃ and was extracted with EtOAc (3 x 30 mL). The combined organic layer was then washed with brine (1 x 30 mL) and dried

over Na₂SO₄. The crude material was purified by column chromatography to yield the final product, 30 mg, 80%. ¹H NMR (700 MHz, DMSO-d₆) δ 6.97 (d, J = 1.7 Hz, 1H), 6.92 (dd, J = 8.0, 1.7 Hz, 1H), 6.73 (d, J = 7.9 Hz, 1H), 5.27 (s, 2H), 3.90 (s, 3H), 3.70 (t, J = 4.7 Hz, 4H), 3.62 (t, J = 4.7 Hz, 4H). ¹³C NMR (176 MHz, dmsO) δ 169.80, 145.35, 139.75, 121.96, 121.15, 112.14, 110.31, 66.15, 55.30, 48.44, 28.96.

tert-butyl 4-(3-methoxy-4-nitrobenzoyl)piperazine-1-carboxylate (59, RAR-5-99)

This material was made using the same protocol described for the preparation of RAR-5-82. Yields the desired product as a dark brown oil, 785.1 mg, 80% ¹H NMR (400 MHz, Chloroform-d) δ 7.85 (d, J = 8.2 Hz, 1H), 7.13 (d, J = 1.5 Hz, 1H), 6.99 (dd, J = 8.2, 1.5 Hz, 1H), 3.97 (s, 3H), 3.52 (s, 4H), 3.38 (s, 4H), 1.46 (s, 9H). ¹³C NMR (100 MHz, cdCl₃) δ 168.34, 154.60, 153.39, 126.04, 118.46, 112.76, 80.79, 56.90, 28.51.

tert-butyl 4-(4-amino-3-methoxybenzoyl)piperazine-1-carboxylate (60, RAR-5-100)

This material was prepared using the same protocol described for the preparation of RAR-5-83. Yields a white residue, 100 mg, 50%. ¹H NMR (400 MHz, Chloroform-d) δ 6.94 (d, J = 1.7 Hz, 1H), 6.85 (dd, J = 7.9, 1.8 Hz, 1H), 6.65 (d, J = 7.9 Hz, 1H), 4.04 (s, 2H), 3.86 (s, 3H), 3.61 (t, J = 5.1 Hz, 4H), 3.45 (dd, J = 6.7, 3.9 Hz, 4H), 1.47 (s, 9H).

(3-methoxy-4-((4-(methylamino)-7H-pyrrolo[2,3-d]pyrimidin-2-yl)amino)phenyl)(piperazin-1-yl)methanone (61, RAR-6-4, CCG-264078)

This material was prepared using the same protocol described for the preparation of RAR-5-89. The final product is obtained as a white solid, 78.7 mg, 90%. LRMS: 401 [M+ H₂O], HPLC: 8.91. ¹H NMR (400 MHz, Chloroform-d) δ 11.54 (s, 1H), 8.80 (dd, J = 8.5, 1.1 Hz, 1H), 7.50 (ddd, J = 8.6, 7.4, 1.6 Hz, 1H), 7.39 (dd, J = 7.9, 1.5 Hz, 1H), 7.19 (d, J = 3.6 Hz, 1H), 6.92 (td, J = 7.6, 1.2 Hz, 1H), 6.71 (d, J = 3.6 Hz, 2H), 5.60 (s, 1H), 3.63 – 3.55 (m, 2H), 3.07 (d, J = 4.9 Hz, 3H), 1.01 – 0.93 (m, 1H). ¹³C NMR (100 MHz, cdCl₃) δ 170.22, 153.96, 151.76, 140.29, 132.33, 126.84, 125.41, 121.84, 121.34, 120.15, 104.16, 99.59, 72.97, 66.58, 26.96, 17.83.

N-(tert-butyl)-2-chloro-7-((2-(trimethylsilyl)ethoxy)methyl)-7H-pyrrolo[2,3-d]pyrimidin-4-amine (62, RAR-6-18)

This material was prepared using the same protocol to prepare RAR-5-75. The product is yielded as a yellow oil, 99.4 mg, 35%. ¹H NMR (400 MHz, Chloroform-d) δ 7.00 (dd, J = 3.7, 1.6 Hz, 1H), 6.29 (dd, J = 3.6, 1.4 Hz, 1H), 5.49 (d, J = 1.5 Hz, 2H), 4.93 (s, 1H), 3.55 – 3.47 (m, 2H), 1.55 (s, 9H), 0.94 – 0.87 (m, 2H).

(4-((4-(tert-butylamino)-7-((2-(trimethylsilyl)ethoxy)methyl)-7H-pyrrolo[2,3-d]pyrimidin-2-yl)amino)-3-methoxyphenyl)(morpholino)methanone (63, RAR-6-29)

This material was prepared using the same protocol described for the construction of RAR-5-89. Yields the desired product as a light yellow solid, 40.2 mg, 60%. HPLC: 8.14. ¹H NMR (500 MHz, Chloroform-d) δ

8.38 (s, 1H), 7.05 (d, J = 3.6 Hz, 1H), 6.98 (s, 1H), 6.87 (d, J = 3.6 Hz, 1H), 6.32 (d, J = 3.6 Hz, 1H), 5.56 (s, 2H), 4.79 (s, 1H), 4.34 (d, J = 7.6 Hz, 4H), 3.53 (t, J = 8.2 Hz, 4H), 1.58 (s, 9H), -0.05 (s, 9H).

4-((4-(tert-butylamino)-7H-pyrrolo[2,3-d]pyrimidin-2-yl)amino)-3-methoxyphenyl)(morpholino)methanone (64, RAR-6-37, CCG-264141)

This material was prepared using the same protocol described for the preparation of RAR-5-93. Yields the desired product as a dark yellow oil, 2 mg, 10%. HPLC: 5.9, MS: 425. ¹H NMR (700 MHz, DMSO-d₆) δ 11.06 (s, 1H), 7.94 (d, J = 8.2 Hz, 1H), 6.93 (d, J = 3.5 Hz, 2H), 6.82 (s, 1H), 4.23 (t, J = 6.7 Hz, 4H), 4.18 (t, J = 6.8 Hz, 4H), 3.95 (s, 3H), 1.49 (s, 9H).

2-chloro-N-cyclopropyl-7-((2-(trimethylsilyl)ethoxy)methyl)-7H-pyrrolo[2,3-d]pyrimidin-4-amine (65, RAR-6-24)

This material is prepared using the same protocol described for the preparation of RAR-5-75. Yields the desired product as a yellow oil, 67.1 mg, 25.1%. HPLC: 8.20, MS: 339. ¹H NMR (400 MHz, Chloroform-d) δ 7.06 (d, J = 3.7 Hz, 1H), 6.74 (s, 1H), 5.86 (s, 1H), 5.53 (s, 2H), 3.53 (dd, J = 9.1, 7.4 Hz, 2H), 3.01 – 2.93 (m, 1H), 0.98 – 0.87 (m, 4H), 0.76 – 0.67 (m, 2H), -0.06 (s, 9H).

4-((4-(cyclopropylamino)-7-((2-(trimethylsilyl)ethoxy)methyl)-7H-pyrrolo[2,3-d]pyrimidin-2-yl)amino)-3-methoxyphenyl)(morpholino)methanone (66, RAR-6-32)

This material was prepared using the protocol described for RAR-5-89. Isolated product could not be separated from oxidized XPhos, telescoped through after crude NMR indicated product was in sample. Yields the desired product as a yellow solid, 44.8 mg, 83%. MS: 539, HPLC: 7.991. ¹H NMR (500 MHz, Chloroform-d) δ 7.58 (q, J = 3.3, 2.8 Hz, 1H), 7.45 – 7.44 (m, 1H), 7.35 (d, J = 8.1 Hz, 1H), 7.31 (s, 1H), 7.03 (s, 1H), 5.55 (s, 2H), 4.36 (t, J = 6.6 Hz, 4H), 3.64 – 3.56 (m, 4H), 3.30 – 3.24 (m, 2H), 2.95 (q, J = 7.3 Hz, 1H), 0.98 – 0.94 (m, 4H), 0.74 (dd, J = 6.8, 4.1 Hz, 2H), 0.05 (s, 9H).

tert-butyl 4-((4-(cyclopropylamino)-7-((2-(trimethylsilyl)ethoxy)methyl)-7H-pyrrolo[2,3-d]pyrimidin-2-yl)amino)-3-methoxybenzoyl)piperazine-1-carboxylate (67, RAR-6-43)

This material was prepared using the protocol described for RAR-5-89 by using RAR-5-99. Yields the final product as a dark brown solid, 24.9 mg, 42%. HPLC: 7.17, MS: 638 [M+1]. ¹H NMR (700 MHz, Chloroform-d) δ 8.76 (d, J = 8.2 Hz, 1H), 7.66 (s, 1H), 7.01 (s, 2H), 6.97 (s, 1H), 6.89 (d, J = 3.6 Hz, 1H), 6.66 – 6.64 (m, 1H), 5.52 (s, 2H), 3.93 (s, 3H), 3.64 (t, J = 6.6 Hz, 4H), 3.58 (dd, J = 8.8, 7.5 Hz, 4H), 2.95 (d, J = 5.0 Hz, 1H), 1.47 (d, J = 4.6 Hz, 9H), 0.98 (t, J = 7.4 Hz, 2H), 0.87 (t, J = 7.0 Hz, 2H), -0.08 (d, J = 0.9 Hz, 9H). ¹³C NMR (176 MHz, cdcl₃) δ 171.02, 159.34, 154.63, 150.57, 147.24, 132.37, 127.05, 122.01, 116.28, 112.19, 109.47, 99.38, 84.16, 80.28, 66.25, 55.85, 50.52, 48.84, 28.37, 26.70, 8.79, -1.45.

4-((4-(cyclopropylamino)-7H-pyrrolo[2,3-d]pyrimidin-2-yl)amino)-3-methoxyphenyl)(piperazin-1-yl)methanone (68, RAR-6-46, CCG-264159)

This material was prepared using the protocol described for CCG-264078. Yields the final product as a yellow solid, 3 mg, 20%. HPLC: 3.93, MS: 406 [M-1] negative mode. ¹H NMR (500 MHz, DMSO-d₆) δ 8.87 (s, 1H), 7.60 (s, 1H), 7.39 (s, 1H), 7.00 (d, J = 4.4 Hz, 2H), 6.97 (d, J = 4.0 Hz, 2H), 3.93 (d, J = 3.9 Hz, 3H), 3.47 (s, 4H), 2.74 (s, 4H), 2.28 (t, J = 7.4 Hz, 1H), 0.81 (d, J = 5.4 Hz, 2H), 0.60 – 0.56 (m, 2H). *tert-butyl 4-(4-((4-(tert-butylamino)-7-((2-(trimethylsilyl)ethoxy)methyl)-7H-pyrrolo[2,3-d]pyrimidin-2-yl)amino)-3-methoxybenzoyl)piperazine-1-carboxylate* (69, RAR-6-41)

This material was prepared using the protocol described for RAR-6-43. Yields the desired product as dark yellow solid, 80 mg, 97%. HPLC: 7.90, MS: 658 [M+1]. ¹H NMR (700 MHz, Chloroform-d) δ 8.78 (d, J = 8.1 Hz, 1H), 7.53 (s, 1H), 7.27 (s, 1H), 7.02 (s, 2H), 6.97 (s, 1H), 6.84 (d, J = 3.6 Hz, 1H), 6.23 (d, J = 3.6 Hz, 1H), 5.50 (s, 2H), 3.95 (s, 3H), 3.63 (t, J = 6.6 Hz, 6H), 3.59 – 3.56 (m, 4H), 3.49 – 3.45 (s, 1H), 1.57 (s, 9H), 1.47 (s, 9H), -0.07 (s, 9H). ¹³C NMR (176 MHz, cdCl₃) δ 171.17, 156.36, 154.64, 151.53, 147.03, 132.79, 125.79, 123.48, 121.37, 116.18, 109.38, 103.67, 98.46, 80.27, 66.11, 62.62, 55.79, 52.04, 51.85, 29.44, 28.35, 24.03.

2-chloro-N-cyclobutyl-7-((2-(trimethylsilyl)ethoxy)methyl)-7H-pyrrolo[2,3-d]pyrimidin-4-amine (70, RAR-6-44)

This material was prepared using the protocol described for RAR-5-75. Yields the desired product as a yellow oil, 50 mg, 9.0%. HPLC: 8.79, MS (neg mode): 351. ¹H NMR (500 MHz, Chloroform-d) δ 7.03 (d, J = 3.6 Hz, 1H), 6.41 (s, 1H), 5.50 (s, 2H), 3.51 (t, J = 8.2 Hz, 2H), 2.52 – 2.44 (m, 2H), 2.01 – 1.90 (m, 3H), 1.78 (td, J = 10.4, 4.9 Hz, 2H), -0.05 (s, 9H). ¹³C NMR (126 MHz, cdCl₃) δ 156.50, 154.25, 151.92, 124.34, 103.16, 99.70, 72.96, 66.54, 31.97, 17.89, 15.21, -1.25.

(4-((4-(cyclobutylamino)-7-((2-(trimethylsilyl)ethoxy)methyl)-7H-pyrrolo[2,3-d]pyrimidin-2-yl)amino)-3-methoxyphenyl)(morpholino)methanone (71, RAR-6-49)

This material was prepared using the protocol described for RAR-5-89. Yields the desired product as a yellow solid, 32.2 mg, 82%. Note that some oxidized XPhos carried through with product. HPLC: 7.60, MS: 652. ¹H NMR (400 MHz, Chloroform-d) δ 8.79 (d, J = 8.5 Hz, 1H), 7.59 (s, 1H), 7.04 (dd, J = 6.6, 1.6 Hz, 2H), 7.00 – 6.93 (m, 1H), 6.87 (dd, J = 8.1, 5.0 Hz, 2H), 6.66 (d, J = 7.9 Hz, 1H), 6.33 (d, J = 3.6 Hz, 1H), 5.52 (s, 2H), 3.95 (s, 3H), 3.69 – 3.56 (m, 4H), 3.53 – 3.41 (m, 6H), 2.41 (p, J = 6.8 Hz, 1H), 2.05 – 1.95 (m, 3H), 1.89 – 1.79 (m, 3H), 0.98 – 0.90 (m, 2H), -0.07 (d, J = 1.2 Hz, 9H).

2-((2-chloro-5-methylpyrimidin-4-yl)amino)-N-methylbenzamide (72, RAR-9-8)

To a flask were added 0.22 mL of 2,4-dichloro-5-methylpyrimidine, and 304.5 mg of 2-amino-N-methylbenzamide, all of which were dissolved in 10 mL of dry DMF. The solution was cooled to 0 °C and then 2.6 mL of NaHMDS were added over five minutes. The solution was stirred at 0 °C for 4 h. Once complete, the reaction was quenched with brine and then extracted with EtOAc (4 x 30 mL). The combined organic layer was then washed with brine (1 x 30 mL) and dried over MgSO₄. The crude material was

purified by column chromatography to yield the desired product, 200 mg, 39%. HPLC: 5.952, LRMS: 277, ¹H NMR (500 MHz, Chloroform-d) δ 11.19 (s, 1H), 8.80 (dd, J = 8.5, 1.1 Hz, 1H), 8.03 (d, J = 1.0 Hz, 1H), 7.55 (ddd, J = 8.7, 7.4, 1.6 Hz, 1H), 7.49 (dd, J = 7.9, 1.5 Hz, 1H), 7.08 (td, J = 7.7, 1.2 Hz, 1H), 6.34 (s, 1H), 3.03 (d, J = 4.8 Hz, 3H), 2.27 (s, 3H). ¹³C NMR (126 MHz, cdcl₃) δ 170.21, 160.12, 156.26, 146.57, 140.25, 132.83, 126.78, 122.49, 121.87, 120.61, 115.33, 27.14, 13.86.

2-((2-((4-cyano-2-methoxyphenyl)amino)-5-methylpyrimidin-4-yl)amino)-N-methylbenzamide (73, RAR-9-13)

To a microwave flask were added 121.4 mg of RAR-9-8, 711.1 mg of Cs₂CO₃, 100.7 mg of nitrile amine, XantPhos (2 mol %), and Pd₂(dba)₃ (1-5 mol%). All materials were then dissolved in 3 mL of nBuOH. The solution was degassed with five cycles of evacuation and backfill with nitrogen before the flask was sealed. The reaction was heated to 160 °C for 15 mins. Once complete, the reaction was quenched with brine (1 x 25 mL) and extracted with EtOAc (3 x 25 mL). The crude material was purified by column chromatography to yield the desired product as a yellow solid, 33 mg, 12%. LRMS: 389, HPLC: 5.244. ¹H NMR (500 MHz, Chloroform-d) δ 10.65 (s, 1H), 8.65 (dd, J = 8.3, 5.9 Hz, 2H), 8.00 (s, 1H), 7.92 (dd, J = 7.8, 1.5 Hz, 1H), 7.72 (d, J = 6.4 Hz, 1H), 7.52 (dd, J = 8.9, 6.8 Hz, 2H), 7.13 – 7.08 (m, 1H), 7.06 (d, J = 1.8 Hz, 1H), 3.95 (s, 3H), 3.09 (s, 3H), 2.27 – 2.23 (m, 3H). ¹³C NMR (126 MHz, cdcl₃) δ 169.93, 167.41, 166.52, 159.02, 147.31, 144.14, 139.14, 132.65, 128.51, 126.63, 119.22, 118.03, 117.43, 103.30, 102.37, 55.96, 26.86, 13.59.

2-((2-((4-(aminomethyl)-2-methoxyphenyl)amino)-5-methylpyrimidin-4-yl)amino)-N-methylbenzamide (74, RAR-9-16)

To a flask were added 33 mg of RAR-9-13, dissolved in 5 mL of 7N NH₃ in MeOH. The solution was degassed with three cycles of evacuation and back fill with nitrogen before RaNi was added in one portion. The solution was then degassed with an additional 3 cycles of evacuation and backfill with nitrogen before the hydrogen atmosphere was introduced. Once complete, the atmosphere was removed, and the solution was passed through a pad of celite. The solvent was removed to yield the desired product as a light yellow solid, 30 mg, 90%. HPLC: 4.094, HRMS: 393.2027. ¹H NMR (500 MHz, Chloroform-d) δ 10.55 (s, 1H), 8.77 (d, J = 8.4 Hz, 1H), 8.38 (d, J = 8.1 Hz, 1H), 7.96 (s, 1H), 7.54 – 7.45 (m, 2H), 7.42 (s, 1H), 7.04 (t, J = 7.5 Hz, 1H), 6.85 (d, J = 10.7 Hz, 2H), 6.31 (s, 1H), 3.91 (s, 3H), 3.02 (d, J = 4.8 Hz, 3H), 2.22 (s, 3H). ¹³C NMR (126 MHz, cdcl₃) δ 170.03, 167.95, 166.11, 158.23, 155.77, 147.93, 140.67, 131.93, 131.28, 126.61, 120.69, 119.10, 118.66, 108.95, 107.35, 55.75, 48.03, 26.89, 13.63.

2-((2-((4-(but-2-ynamidomethyl)-2-methoxyphenyl)amino)-5-methylpyrimidin-4-yl)amino)-N-methylbenzamide (75, RAR-9-17, CCG-265507)

To a flask were added 13.9 mg of butynoic acid, 33.8 mg of HATU, 30 mg of RAR-9-16, and 0.05 mL of DIPEA. All materials were dissolved in 3 mL of DMF to yield a light yellow solution. This solution was

allowed to stir at room temperature for 5 hours. Once complete, the reaction was quenched with brine and extracted with EtOAc (3 x 30 mL). The combined organic layer was washed with brine (2 x 30 mL) and then dried over MgSO₄ before being purified by column chromatography. Yields a light yellow solid. LRMS: 459, HPLC: 4.943. ¹H NMR (700 MHz, Chloroform-d) δ 10.59 (s, 1H), 8.71 (d, J = 8.5 Hz, 1H), 8.36 (d, J = 8.1 Hz, 1H), 7.93 (s, 1H), 7.52 (s, 1H), 7.48 (d, J = 7.9 Hz, 2H), 7.04 (t, J = 7.5 Hz, 1H), 6.80 (d, J = 7.6 Hz, 1H), 6.36 (s, 1H), 4.41 (d, J = 5.7 Hz, 1H), 3.88 (s, 3H), 3.01 (d, J = 4.7 Hz, 3H), 1.93 (s, 2H). ¹³C NMR (176 MHz, cdCl₃) δ 170.02, 167.45, 166.15, 159.01, 155.47, 153.23, 146.36, 132.59, 131.80, 129.91, 126.59, 122.45, 121.46, 120.90, 118.80, 109.81, 104.44, 100.24, 80.64, 55.75, 43.98, 26.81, 13.56, 3.63.

2-((2-((4-(acrylamidomethyl)-2-methoxyphenyl)amino)-5-methylpyrimidin-4-yl)amino)-N-methylbenzamide (76, RAR-9-20, CCG-265508)

This material was prepared using the protocol described for CCG-265507. Yields the product as a light yellow solid, 2 mg, 9%. LRMS: 449, HPLC: 5.095. ¹H NMR (700 MHz, Chloroform-d) δ 8.64 (s, 1H), 8.32 (s, 1H), 8.30 – 8.25 (m, 1H), 7.90 (d, J = 7.6 Hz, 1H), 7.72 (d, J = 8.6 Hz, 1H), 7.62 (d, J = 8.3 Hz, 1H), 7.57 (s, 1H), 7.46 (d, J = 8.4 Hz, 1H), 6.84 (s, 1H), 6.64 (d, J = 8.1 Hz, 1H), 6.56 – 6.50 (m, 1H), 6.18 (d, J = 17.2 Hz, 1H), 3.64 (d, J = 3.1 Hz, 3H), 3.08 (d, J = 3.2 Hz, 3H), 2.64 (d, J = 3.1 Hz, 3H).

2-chloro-N-(pyridin-3-yl)-7-((2-(trimethylsilyl)ethoxy)methyl)-7H-pyrrolo[2,3-d]pyrimidin-4-amine (77, RAR-9-21)

To a three neck flask were added 500 mg of SEM-protected 2,4-dichloropyrrolopyrimidine, 208.2 mg of 3-aminopyridine, 469.0 mg of NaOtBu, XPhos (4 mol%) and Pd₂(dba)₃ (1 mol%). All materials were then dissolved in 8 mL of toluene, and then solution was degassed with 8 cycles of evacuation and backfill with nitrogen. The reaction was then heated to 90 °C for 2.5 h or until complete. Once complete, the reaction was cooled to rt and then passed through a pad of celite. The crude material was evaporated onto silica gel and then purified by column chromatography. Yields the desired product as a pale yellow solid, 195.4 mg, 32%. LRMS: 376, HPLC: 6.133. ¹H NMR (700 MHz, Chloroform-d) δ 8.72 (d, J = 2.9 Hz, 1H), 8.44 (s, 1H), 8.27 (d, J = 8.5 Hz, 1H), 7.40 – 7.36 (m, 1H), 7.14 (t, J = 3.2 Hz, 2H), 6.95 (s, 2H), 6.27 (s, 1H), 5.57 (d, J = 2.7 Hz, 2H), 3.57 – 3.53 (m, 2H), 2.21 (s, 3H), 0.01 (d, J = 2.7 Hz, 9H).

3-methoxy-4-((4-(pyridin-3-ylamino)-7-((2-(trimethylsilyl)ethoxy)methyl)-7H-pyrrolo[2,3-d]pyrimidin-2-yl)amino)benzotrile (78, RAR-9-24)

This material was prepared using the protocol described for RAR-9-13. Yields the desired product as a light brown solid, 75 mg, 58%. LRMS: 488, HPLC: 6.924. ¹H NMR (500 MHz, Chloroform-d) δ 8.92 (d, J = 2.6 Hz, 1H), 8.81 (d, J = 8.5 Hz, 1H), 8.43 (d, J = 5.0 Hz, 1H), 8.10 (d, J = 8.3 Hz, 1H), 7.78 (s, 1H), 7.36 (dd, J = 8.3, 4.6 Hz, 1H), 7.09 (d, J = 1.8 Hz, 1H), 7.02 (d, J = 3.7 Hz, 1H), 6.70 (s, 1H), 6.33 (d, J = 3.7 Hz, 1H), 5.57 (s, 2H), 3.98 (s, 3H), 3.62 – 3.58 (m, 2H), 0.99 – 0.92 (m, 2H), -0.06 (s, 9H).

N2-(4-(aminomethyl)-2-methoxyphenyl)-N4-(pyridin-3-yl)-7-((2-(trimethylsilyl)ethoxy)methyl)-7H-pyrrolo[2,3-d]pyrimidine-2,4-diamine (79, RAR-9-26)

This material was prepared using the protocol described for RAR-9-16. Yields the desired product as a light yellow solid, 15.6 mg, 51.6%. HPLC: 5.334, HRMS: 492.2535. ¹H NMR (500 MHz, Chloroform-d) δ 8.86 (s, 1H), 8.52 (d, J = 8.0 Hz, 1H), 8.36 (s, 1H), 8.15 (s, 1H), 7.47 (s, 1H), 7.31 (s, 3H), 6.95 (d, J = 3.3 Hz, 2H), 6.92 (d, J = 8.4 Hz, 1H), 6.69 (s, 1H), 6.30 (d, J = 3.4 Hz, 1H), 5.55 (s, 2H), 3.94 (s, 3H), 3.91 (s, 2H), 3.64 – 3.59 (m, 2H), 0.98 – 0.93 (m, 2H), -0.06 (s, 9H).

N-(3-methoxy-4-((4-(pyridin-3-ylamino)-7-((2-(trimethylsilyl)ethoxy)methyl)-7H-pyrrolo[2,3-d]pyrimidin-2-yl)amino)benzyl)acrylamide (80, RAR-9-29)

This material was prepared using the protocol described for CCG-265507. Yields the desired product as bright green solid, 10 mg, 45%. HRMS: 546.2641, HPLC: 6.287. Moved forwards without further characterization, is unstable in air.

N-(3-methoxy-4-((4-(pyridin-3-ylamino)-7H-pyrrolo[2,3-d]pyrimidin-2-yl)amino)benzyl)acrylamide (81, RAR-9-30, CCG-265595)

This material was prepared using the protocol described for CCG-265328. Yields a white residue, 2 mg, 20%. LRMS: 416, HPLC: 4.2700. ¹H NMR (700 MHz, Chloroform-d) δ 8.87 (d, J = 2.6 Hz, 1H), 8.45 (d, J = 8.2 Hz, 1H), 8.39 (d, J = 4.4 Hz, 1H), 8.29 (s, 1H), 8.15 (d, J = 8.5 Hz, 1H), 7.33 (dd, J = 8.1, 4.7 Hz, 1H), 6.90 (d, J = 5.8 Hz, 2H), 6.86 (s, 1H), 6.67 (s, 1H), 6.34 (d, J = 17.0 Hz, 1H), 6.29 (t, J = 2.8 Hz, 1H), 6.12 (dd, J = 17.0, 10.3 Hz, 1H), 5.84 (s, 1H), 5.68 (d, J = 11.4 Hz, 1H), 4.50 (d, J = 5.6 Hz, 2H), 3.92 (s, 3H).

N-(3-methoxy-4-((4-(pyridin-3-ylamino)-7-((2-(trimethylsilyl)ethoxy)methyl)-7H-pyrrolo[2,3-d]pyrimidin-2-yl)amino)benzyl)but-2-ynamide (82, RAR-9-33)

This material was prepared using the protocol described for CCG-265507. Yields the desired product as light yellow solid, 10 mg, 44%. LRMS: 558, HPLC: 6.2800. ¹H NMR (700 MHz, Chloroform-d) δ 8.88 (s, 1H), 8.56 (d, J = 8.2 Hz, 1H), 8.38 (d, J = 4.6 Hz, 1H), 8.15 (d, J = 8.1 Hz, 1H), 7.50 (s, 1H), 7.33 (dd, J = 8.3, 4.7 Hz, 1H), 6.96 (dd, J = 3.6, 0.9 Hz, 1H), 6.90 – 6.86 (m, 1H), 6.84 (s, 1H), 6.70 (s, 1H), 6.30 (dd, J = 3.6, 0.9 Hz, 1H), 6.05 (s, 1H), 5.57 – 5.54 (m, 2H), 4.44 (d, J = 5.7 Hz, 2H), 3.93 (d, J = 0.9 Hz, 3H), 3.63 – 3.58 (m, 2H), 1.95 (d, J = 0.9 Hz, 3H), 0.97 – 0.93 (m, 2H), -0.06 (d, J = 0.9 Hz, 9H).

N-(3-methoxy-4-((4-(pyridin-3-ylamino)-7H-pyrrolo[2,3-d]pyrimidin-2-yl)amino)benzyl)but-2-ynamide (83, RAR-9-11, CCG-265596)

This material was prepared using the protocol described for CCG-265328. Yields the desired product as a white solid, 2.0 mg, 26%. HRMS: 428.1824, HPLC: 4.223. ¹H NMR (700 MHz, Chloroform-d) δ 8.86 (s, 1H), 8.43 (s, 1H), 8.37 (d, J = 25.9 Hz, 2H), 8.14 (s, 1H), 7.41 (s, 1H), 7.33 (s, 1H), 6.88 (d, J = 13.6 Hz,

2H), 6.84 (s, 1H), 6.69 (s, 1H), 6.29 (s, 1H), 6.08 (s, 1H), 4.44 (s, 2H), 3.91 (d, J = 4.9 Hz, 3H), 1.95 (t, J = 3.8 Hz, 3H).

2-chloro-5-methylpyrimidin-4-amine (84, RAR-9-38)

To a pressure vessel were added 1.1 mL of 2,4-dichloro-5-methylpyrimidine dissolved in 2.2 mL of NH₃(aq). All materials were then further dissolved in 35 mL of EtOH, and the tube was sealed. The reaction was heated to 100 °C for 16 h, then cooled to room temperature. The desired product was filtered off as a white solid and washed with cold EtOH. Moved forward without further characterization. HRMS: 144.0321, HPLC: 2.100.

2-chloro-5-methyl-N-(pyridin-3-yl)pyrimidin-4-amine (85, RAR-9-43)

This material was prepared using the protocol described for RAR-9-21. Yields the desired product as a yellow solid, 38.3 mg, 50%. HRMS: 221.0584, HPLC: 3.909. ¹H NMR (401 MHz, Chloroform-d) δ 8.48 (d, J = 8.4 Hz, 1H), 8.30 (d, J = 4.9 Hz, 1H), 8.09 (s, 1H), 7.81 – 7.75 (m, 1H), 7.05 (dd, J = 7.3, 5.0 Hz, 1H), 2.23 (s, 3H).

3-methoxy-4-((5-methyl-4-(pyridin-3-ylamino)pyrimidin-2-yl)amino)benzonitrile (86, RAR-9-44)

This material was prepared using the protocol described in RAR-9-24. Yields the desired product as a dark red solid, 44.7 mg, 59%. HRMS: 333.1455, HPLC: 5.022. ¹H NMR (500 MHz, Chloroform-d) δ 7.76 (s, 1H), 7.73 (s, 1H), 7.62 (dd, J = 6.6, 2.9 Hz, 4H), 7.42 (dd, J = 5.0, 1.9 Hz, 7H), 7.13 (d, J = 1.7 Hz, 1H), 7.11 (d, J = 1.9 Hz, 2H), 7.08 (s, 1H), 6.96 (d, J = 1.7 Hz, 2H), 6.65 (d, J = 8.1 Hz, 2H), 4.29 (s, 2H), 3.87 (s, 3H).

N2-(4-(aminomethyl)-2-methoxyphenyl)-5-methyl-N4-(pyridin-3-yl)pyrimidine-2,4-diamine (87, RAR-9-46)

This material was prepared using the protocol described in RAR-9-16 and was moved forward without further characterization due to instability. Yields the desired product as dark yellow oil. HPLC: 3.520.

N-(3-methoxy-4-((5-methyl-4-(pyridin-3-ylamino)pyrimidin-2-yl)amino)benzyl)acrylamide (88, RAR-9-47, CCG-265647)

This material was prepared using the protocol described for CCG-265507. Yields the final product as a light yellow solid. MS: 359 [M-OMe], HPLC: 5.062. ¹H NMR (700 MHz, Chloroform-d) δ 7.94 (s, 1H), 7.79 (d, J = 7.6 Hz, 2H), 7.71 (dd, J = 5.7, 3.3 Hz, 3H), 7.54 (dd, J = 5.7, 3.3 Hz, 3H), 7.42 (s, 1H), 7.14 (d, J = 7.8 Hz, 2H), 7.12 (s, 1H), 6.42 (m, 1H), 6.12 (m, 1H), 5.86 (s, 2H), 3.88 (s, 3H), 2.21 (m, 3H).

N-(3-methoxy-4-((5-methyl-4-(pyridin-3-ylamino)pyrimidin-2-yl)amino)benzyl)but-2-ynamide (89, RAR-9-48, CCG-265648)

This material was prepared using the protocol described for CCG-265507. Yields the final product as a light yellow solid, 3.0 mg, 25%. MS: 420 [M+H₂O], HPLC: 4.539. ¹H NMR (700 MHz, Chloroform-d) δ

8.76 (s, 1H), 8.72 (s, 2H), 8.43 (s, 1H), 7.80 (s, 1H), 7.48 (d, J = 3.9 Hz, 1H), 7.42 (s, 1H), 7.14 (d, J = 8.1 Hz, 1H), 7.12 (s, 1H), 3.91 (s, 3H), 2.72 – 2.67 (m, 3H), 1.98 (s, 3H).

2-((2-chloro-5-methylpyrimidin-4-yl)amino)benzoic acid (90, RAR-10-24)

To a pressure vessel were added 0.360 mL of 2,4-dichloro-5-methylpyrimidine, 431.8 mg of 2-aminobenzoic acid and 10 mL of IPA. To this solution were added 2.7 mL of DIPEA, and the tube was sealed and heated to 80 °C for 36 h. Once complete, the reaction was cooled to rt and then the solvent was removed. The white solid was taken back up in EtOAc and then washed with 1N HCl, and saturated NaHCO₃ (1 x 30 mL, respectively). The combined organic layer was dried over MgSO₄ and then purified by column chromatography. Yields the desired product as a white solid, 310 mg, 38%. LRMS: 264, HPLC: 6.078 1H NMR (500 MHz, DMSO-d₆) δ 13.79 (s, 1H), 11.31 (s, 1H), 8.77 (d, J = 8.5 Hz, 1H), 8.21 (s, 1H), 8.06 (d, J = 7.9 Hz, 1H), 7.69 (t, J = 7.9 Hz, 1H), 7.17 (t, J = 7.6 Hz, 1H), 2.22 (s, 3H).

2-((2-chloro-5-methylpyrimidin-4-yl)amino)-N-(pyridin-3-ylmethyl)benzamide (91, RAR-10-25)

This material was prepared using the protocol described for CCG-265507. Yields a white solid, 17 mg, 13%. LRMS: 449 [M+Na, with DMF], HPLC: 6.378. 1H NMR (700 MHz, Chloroform-d) δ 11.09 (s, 1H), 8.89 – 8.71 (m, 1H), 8.59 (d, J = 45.0 Hz, 3H), 8.10 – 7.95 (m, 1H), 7.72 (d, J = 10.3 Hz, 1H), 7.61 – 7.43 (m, 2H), 7.14 – 6.98 (m, 1H), 6.87 (s, 1H), 4.75 – 4.56 (m, 2H), 2.26 (ddd, J = 15.1, 9.8, 5.1 Hz, 3H). 13C NMR (176 MHz, cdcl₃) δ 169.51, 156.23, 149.36, 149.26, 140.29, 135.66, 133.02, 126.70, 123.75, 122.28, 121.72, 119.80, 115.12, 41.53, 13.62.

2-((2-chloro-5-methylpyrimidin-4-yl)amino)-N-((3-(methoxymethyl)-1,2,4-oxadiazol-5-yl)methyl)benzamide (92, RAR-10-26)

This material is prepared using the protocol described for the creation of CCG-265507. Yields a white solid. LRMS: 389 [M+1], HPLC: 6.770. 1H NMR (700 MHz, Chloroform-d) δ 10.73 (s, 1H), 8.31 (t, J = 6.2 Hz, 1H), 7.81 (q, J = 6.7 Hz, 1H), 7.70 (d, J = 6.8 Hz, 1H), 7.42 (q, J = 5.9, 5.0 Hz, 2H), 4.96 – 4.92 (m, 2H), 4.60 (q, J = 2.9 Hz, 2H), 3.49 (q, J = 3.0 Hz, 2H), 2.23 (d, J = 4.4 Hz, 3H).

2-((2-((4-cyano-2-methoxyphenyl)amino)-5-methylpyrimidin-4-yl)amino)-N-(pyridin-3-ylmethyl)benzamide (93, RAR-10-27)

This material is prepared using the protocol described for RAR-9-13. Yields a pale yellow solid, 7 mg, 30%. HRMS: 466.1986, HPLC: 4.590. 1H NMR (700 MHz, Chloroform-d) δ 10.57 (s, 1H), 8.70 – 8.62 (m, 3H), 8.59 (s, 1H), 8.02 (d, J = 3.4 Hz, 1H), 7.76 – 7.70 (m, 2H), 7.55 (dd, J = 8.1, 3.3 Hz, 2H), 7.33 – 7.29 (m, 1H), 7.26 – 7.22 (m, 1H), 7.11 (d, J = 2.9 Hz, 1H), 7.08 – 7.04 (m, 1H), 6.56 (s, 1H), 4.69 (t, J = 4.7 Hz, 2H), 3.95 (d, J = 3.5 Hz, 3H), 2.25 (d, J = 3.4 Hz, 3H).

2-((2-((4-(aminomethyl)-2-methoxyphenyl)amino)-5-methylpyrimidin-4-yl)amino)-N-(pyridin-3-ylmethyl)benzamide (94, RAR-10-29)

This material was prepared using the protocol described for RAR-9-16. Moved forward without further characterization due to instability in air. Yields the product as a white residue, 6.3 mg, 90%. HPLC: 3.742, LRMS: 470 [M+1], 492 [M+Na].

3-((2-chloro-5-methylpyrimidin-4-yl)amino)benzoic acid (95, RAR-10-33)

This material was prepared using the protocol described in RAR-10-24. Yields a white solid, 310 mg, 20%. MS: 264, HPLC: 5.77. ¹H NMR (500 MHz, DMSO-d₆) δ 9.19 (d, J = 25.3 Hz, 1H), 8.75 (s, 1H), 8.22 (s, 0H), 8.07 (d, J = 9.3 Hz, 0H), 7.94 (s, 1H), 7.67 (d, J = 7.8 Hz, 0H), 7.43 (s, 1H).

3-((2-chloro-5-methylpyrimidin-4-yl)amino)-N-(pyridin-3-ylmethyl)benzamide (96, RAR-10-35)

This material was prepared using the protocol described for CCG-265507. Yields a yellow oil, 30 mg, 14%. MS: 360, HPLC: 2.84. ¹H NMR (500 MHz, Chloroform-d) δ 8.64 (s, 1H), 8.56 (d, J = 5.0 Hz, 1H), 8.02 (s, 3H), 7.88 (s, 1H), 7.75 (d, J = 8.0 Hz, 1H), 7.34 – 7.28 (m, 1H), 4.75 (d, J = 5.7 Hz, 2H), 2.81 (d, J = 1.3 Hz, 3H).

3-((2-((4-cyano-2-methoxyphenyl)amino)-5-methylpyrimidin-4-yl)amino)-N-(pyridin-3-ylmethyl)benzamide (97, RAR-10-37)

This material was prepared using the protocol described for RAR-9-21. Yields a light yellow solid, 10 mg, 25%. MS: 501 [M+Cl] from solvent, HPLC: 2.48 ¹H NMR (500 MHz, Chloroform-d) δ 8.65 (d, J = 11.0 Hz, 2H), 8.57 (s, 2H), 8.48 (d, J = 8.4 Hz, 1H), 7.89 (s, 1H), 7.85 (s, 1H), 7.74 (d, J = 7.8 Hz, 1H), 7.70 (d, J = 8.1 Hz, 2H), 7.31 (d, J = 6.2 Hz, 2H), 7.19 (d, J = 8.5 Hz, 1H), 4.75 (d, J = 5.7 Hz, 2H), 3.92 (s, 3H), 2.03 (s, 3H).

2-chloro-5-methyl-N-(pyridin-3-ylmethyl)pyrimidin-4-amine (98, RAR-10-44)

This material was prepared using the protocol described in CCG-265507. Yields a yellow solid, 100 mg, 30%. HPLC: 5.497. ¹H NMR (700 MHz, Chloroform-d) δ 8.69 (dt, J = 4.7, 1.6 Hz, 1H), 8.48 – 8.41 (m, 2H), 7.96 (s, 2H), 7.47 (ddd, J = 8.5, 4.5, 1.6 Hz, 1H), 2.52 – 2.46 (m, 3H). ¹³C NMR (176 MHz, cdCl₃) δ 167.62, 161.45, 157.54, 152.02, 140.51, 134.98, 129.79, 121.19, 115.35, 11.76.

3-methoxy-4-((5-methyl-4-((pyridin-3-ylmethyl)amino)pyrimidin-2-yl)amino)benzonitrile (99, RAR-10-48)

This material was prepared using the protocol described in RAR-9-21. Yields a light yellow solid, 14.4 mg, 43%. MS: 493.35 [3M + Na], HPLC: 6.546. ¹H NMR (500 MHz, Chloroform-d) δ 8.74 (d, J = 4.7 Hz, 1H), 8.58 (d, J = 8.4 Hz, 1H), 8.35 (s, 1H), 7.68 (s, 1H), 7.54 (dd, J = 8.0, 4.3 Hz, 1H), 7.12 (s, 1H), 3.83 (d, J = 4.2 Hz, 3H), 2.48 (s, 3H).

2-((2-chloro-5-methylpyrimidin-4-yl)amino)-6-fluorobenzoic acid (100, RAR-10-64)

This material was prepared using the protocol described in RAR-10-24. Yields an off-white solid, 430 mg, 50%. HPLC: 6.04. ¹H NMR (400 MHz, DMSO-d₆) δ 13.55 (s, 1H), 8.75 (q, J = 0.8 Hz, 2H), 8.37 – 8.31 (m, 1H), 8.06 (d, J = 1.0 Hz, 1H), 7.33 – 7.24 (m, 1H), 6.80 – 6.71 (m, 1H), 2.31 (d, J = 0.8 Hz, 3H).

2-((2-chloro-5-methylpyrimidin-4-yl)amino)-6-fluoro-N-(pyridin-2-ylmethyl)benzamide (RAR-10-81, 101)

This material was prepared using the protocol described in CCG-265507. Yields a white solid, 60 mg, 5%. MS: 372.0951, HPLC: 5.075. ¹H NMR (400 MHz, Chloroform-*d*) δ 11.46 (s, 1H), 8.68 (d, *J* = 8.6 Hz, 1H), 8.63 (dd, *J* = 11.1, 2.4 Hz, 1H), 8.54 (dd, *J* = 9.6, 4.6 Hz, 1H), 8.07 – 8.04 (m, 1H), 7.75 – 7.66 (m, 1H), 7.49 (td, *J* = 8.4, 4.1 Hz, 1H), 7.34 – 7.28 (m, 2H), 7.13 – 7.05 (m, 1H), 4.67 (dd, *J* = 19.4, 5.9 Hz, 2H), 2.24 (s, 3H).

2.8 References

- (1) Rowlands, R.; Cato, M. C.; Waldschmidt, H. V.; Bouley, R. A.; Chen, Q.; Avramova, L.; Larsen, S. D.; Tesmer, J. J. G.; White. Structure-Based Design of Selective, Covalent G Protein-Coupled Receptor Kinase 5 Inhibitors | ACS Medicinal Chemistry Letters <https://pubs.acs.org/doi/abs/10.1021/acsmchemlett.9b00365> (accessed Dec 23, 2019).
- (2) Penela, P.; Murga, C.; Ribas, C.; Tutor, A. S.; Peregrín, S.; Mayor, F. Mechanisms of Regulation of G Protein-Coupled Receptor Kinases (GRKs) and Cardiovascular Disease. *Cardiovasc. Res.* **2006**, *69* (1), 46–56. <https://doi.org/10.1016/j.cardiores.2005.09.011>.
- (3) Lymperopoulos, A.; Rengo, G.; Funakoshi, H.; Eckhart, A. D.; Koch, W. J. Adrenal GRK2 Upregulation Mediates Sympathetic Overdrive in Heart Failure. *Nat. Med.* **2007**, *13* (3), 315–323. <https://doi.org/10.1038/nm1553>.
- (4) Kemp, C. D.; Conte, J. V. The Pathophysiology of Heart Failure. *Cardiovasc. Pathol. Off. J. Soc. Cardiovasc. Pathol.* **2012**, *21* (5), 365–371. <https://doi.org/10.1016/j.carpath.2011.11.007>.
- (5) Traynham, C. J.; Hullmann, J.; Koch, W. J. “Canonical and Non-Canonical Actions of GRK5 in the Heart.” *J. Mol. Cell. Cardiol.* **2016**, *92* (Supplement C), 196–202. <https://doi.org/10.1016/j.yjmcc.2016.01.027>.
- (6) Hullmann, J. E.; Grisanti, L. A.; Makarewich, C. A.; Gao, E.; Gold, J. I.; Chuprun, J. K.; Tilley, D. G.; Houser, S. R.; Koch, W. J. GRK5-Mediated Exacerbation of Pathological Cardiac Hypertrophy Involves Facilitation of Nuclear NFAT Activity Novelty and Significance. *Circ. Res.* **2014**, *115* (12), 976–985. <https://doi.org/10.1161/CIRCRESAHA.116.304475>.
- (7) Raake, P. W.; Vinge, L. E.; Gao, E.; Boucher, M.; Rengo, G.; Chen, X.; DeGeorge, B. R.; Matkovich, S.; Houser, S. R.; Most, P.; et al. G Protein-Coupled Receptor Kinase 2 Ablation in Cardiac Myocytes before or after Myocardial Infarction Prevents Heart Failure. *Circ. Res.* **2008**, *103* (4), 413–422. <https://doi.org/10.1161/CIRCRESAHA.107.168336>.
- (8) Waldschmidt, H. V.; Homan, K. T.; Cruz-Rodríguez, O.; Cato, M. C.; Waninger-Saroni, J.; Larimore, K. M.; Cannavo, A.; Song, J.; Cheung, J. Y.; Kirchhoff, P. D.; et al. Structure-Based Design, Synthesis, and Biological Evaluation of Highly Selective and Potent G Protein-Coupled Receptor Kinase 2 Inhibitors. *J. Med. Chem.* **2016**, *59* (8), 3793–3807. <https://doi.org/10.1021/acs.jmedchem.5b02000>.
- (9) Waldschmidt, H. V.; Homan, K. T.; Cato, M. C.; Cruz-Rodríguez, O.; Cannavo, A.; Wilson, M. W.; Song, J.; Cheung, J. Y.; Koch, W. J.; Tesmer, J. J. G.; et al. Structure-Based Design of Highly Selective and Potent G Protein-Coupled Receptor Kinase 2 Inhibitors Based on Paroxetine. *J. Med. Chem.* **2017**, *60* (7), 3052–3069. <https://doi.org/10.1021/acs.jmedchem.7b00112>.
- (10) Yao, X.-Q.; Cato, M. C.; Labudde, E.; Beyett, T. S.; Tesmer, J. J. G.; Grant, B. J. Navigating the Conformational Landscape of G Protein-Coupled Receptor Kinases during Allosteric Activation. *J. Biol. Chem.* **2017**, *292* (39), 16032–16043. <https://doi.org/10.1074/jbc.M117.807461>.

- (11) Bouley, R.; Waldschmidt, H. V.; Cato, M. C.; Cannavo, A.; Song, J.; Cheung, J. Y.; Yao, X.-Q.; Koch, W. J.; Larsen, S. D.; Tesmer, J. J. G. Structural Determinants Influencing the Potency and Selectivity of Indazole-Paroxetine Hybrid G Protein-Coupled Receptor Kinase 2 Inhibitors. *Mol. Pharmacol.* **2017**, *92* (6), 707–717. <https://doi.org/10.1124/mol.117.110130>.
- (12) Cho, S. Y.; Lee, B. H.; Jung, H.; Yun, C. S.; Ha, J. D.; Kim, H. R.; Chae, C. H.; Lee, J. H.; Seo, H. W.; Oh, K.-S. Design and Synthesis of Novel 3-(Benzo[d]Oxazol-2-Yl)-5-(1-(Piperidin-4-Yl)-1H-Pyrazol-4-Yl)Pyridin-2-Amine Derivatives as Selective G-Protein-Coupled Receptor Kinase-2 and -5 Inhibitors. *Bioorg. Med. Chem. Lett.* **2013**, *23* (24), 6711–6716. <https://doi.org/10.1016/j.bmcl.2013.10.036>.
- (13) Ullrich, A.; Falcenberg, M.; Örfi, Z.; Kéri, G.; ÖRFI, L.; Horváth, Z.; SZOKOL, B.; DOBOS, J.; NEMES, Z. Indolinone Derivatives as Grk5 Modulators. WO2015022437 A1, February 19, 2015.
- (14) Boguth, C. A.; Singh, P.; Huang, C.; Tesmer, J. J. G. Molecular Basis for Activation of G Protein-coupled Receptor Kinases. *EMBO J.* **2010**, *29* (19), 3249–3259. <https://doi.org/10.1038/emboj.2010.206>.
- (15) Singh, J.; Petter, R. C.; Baillie, T. A.; Whitty, A. The Resurgence of Covalent Drugs. *Nat. Rev. Drug Discov.* **2011**, *10* (4), 307–317. <https://doi.org/10.1038/nrd3410>.
- (16) Leproult, E.; Barluenga, S.; Moras, D.; Wurtz, J.-M.; Winssinger, N. Cysteine Mapping in Conformationally Distinct Kinase Nucleotide Binding Sites: Application to the Design of Selective Covalent Inhibitors. *J. Med. Chem.* **2011**, *54* (5), 1347–1355. <https://doi.org/10.1021/jm101396q>.
- (17) Liu, Q.; Sabnis, Y.; Zhao, Z.; Zhang, T.; Buhrlage, S. J.; Jones, L. H.; Gray, N. S. Developing Irreversible Inhibitors of the Protein Kinase Cysteinome. *Chem. Biol.* **2013**, *20* (2), 146–159. <https://doi.org/10.1016/j.chembiol.2012.12.006>.
- (18) Zhang, T.; Inesta-Vaquera, F.; Niepel, M.; Zhang, J.; Ficarro, S. B.; Machleidt, T.; Xie, T.; Marto, J. A.; Kim, N.; Sim, T.; et al. Discovery of Potent and Selective Covalent Inhibitors of JNK. *Chem. Biol.* **2012**, *19* (1), 140–154. <https://doi.org/10.1016/j.chembiol.2011.11.010>.
- (19) Keating, G. M. Afatinib: A Review of Its Use in the Treatment of Advanced Non-Small Cell Lung Cancer. *Drugs* **2014**, *74* (2), 207–221. <https://doi.org/10.1007/s40265-013-0170-8>.
- (20) Homan, K. T.; Wu, E.; Cannavo, A.; Koch, W. J.; Tesmer, J. J. G. Identification and Characterization of Amlexanox as a G Protein-Coupled Receptor Kinase 5 Inhibitor. *Molecules* **2014**, *19* (10), 16937–16949. <https://doi.org/10.3390/molecules191016937>.

Chapter 3. Expanding the Arsenal: Virtual Screening & Validation of the Aminopyridine Scaffold

3.1 Preface

Ideas and conclusions from Chapter 3 are in preparation for publication and may appear verbatim in a future publication. I planned, executed and evaluated hits from the virtual screening efforts. I synthesized all compounds within this chapter. Pharmacological assays were performed by M. Claire Cato, Renee Bouley and me. GRK5 and GRK2 were provided by Renee Bouley.

3.2 Virtual Screening Mined New Scaffolds for GRK5 Inhibitors

In Chapter 2, Cys474 was established as a viable handle for selective inhibition of GRK5 through covalent modification.¹ However, the original pyrrolopyrimidine scaffold was unable to be improved upon despite our best efforts. While **CCG-265328** did show modest potency, the lack of tractable SAR meant another lead was urgently needed.

As the scaffold hop performed in Chapter 2 did not yield a more potent or selective analogue, the known scaffolds that target GRK5 were further dwindled. Of the known and confirmed lead options there were two: the indazole scaffold, exemplified by CCG-215022, and the paroxetine scaffold, exemplified by the pan-GRK2/GRK5 inhibitor, CCG-258748.^{2,3} However, both options present a similar barrier to development: the scaffolds are not amenable to modification to carry a covalent warhead. In our GRK5/GRK6 model neither CCG-215022 nor CCG-258748 have a position where a vector could be created to carry the covalent warhead. As non-covalent strategy has failed to produce a GRK5 selective inhibitor, these leads were deprioritized.

To generate a lead for this project, we chose to mine chemical space for an entirely new scaffold. Known chemical space is vast and searching for a lead with novel IP through traditional High-Throughput Screening (HTS) efforts can be expensive. Most novel leads are found through HTS, however, there are serious considerations such as reagent cost, instrumentation and assay development that can make HTS cost prohibitive. Additionally, HTS libraries are built of a discrete set of real compounds. Therefore, only those compounds available within a given collection may

be screened, thereby limiting the amount of novel chemical space that can be mined for a new lead.⁴⁻⁶ Fortunately, there has been rapid advancement in the field of virtual screening that has allowed medicinal chemists to mine novel chemical space using real, synthetically feasible lead compounds *in silico*.⁷ For these reasons, we chose to pursue virtual screening, utilizing a pharmacophore-based screening filter to mine new scaffolds for this project.

For our virtual screening effort a knowledge-based library was compiled, using compounds reported to have known GRK2, GRK5 and ROCK1 activity.^{8,9} This compiled library was then filtered using PipelinePilot to remove pan assay interfering compounds (PAINS).¹⁰ PAINS are compounds with apparent biochemical activity conveyed through interference with the assay readout or through an alternative mechanism. Common reasons a compound may be classified as a PAIN include: redox capability, chemical aggregation, chelation, sample impurities and non-selective interactions with proteins, to name a few.¹¹ By removing these compounds the risk of identifying leads with promiscuous activity is reduced. However, we were careful to leave compounds with the potential to covalently interact with our target protein, as we are searching for a lead compound to be developed into a covalent inhibitor.^{5,12}

A 3D pharmacophore screening method was pursued to further increase our chances of mining leads which would be active against our kinase target.^{8,13,14} For this particular screen, we chose to use the GRK5/GRK6 model that was developed in Chapter 2, as GRK5 is thought to be in a closed, active conformation in this structure.^{15,16}

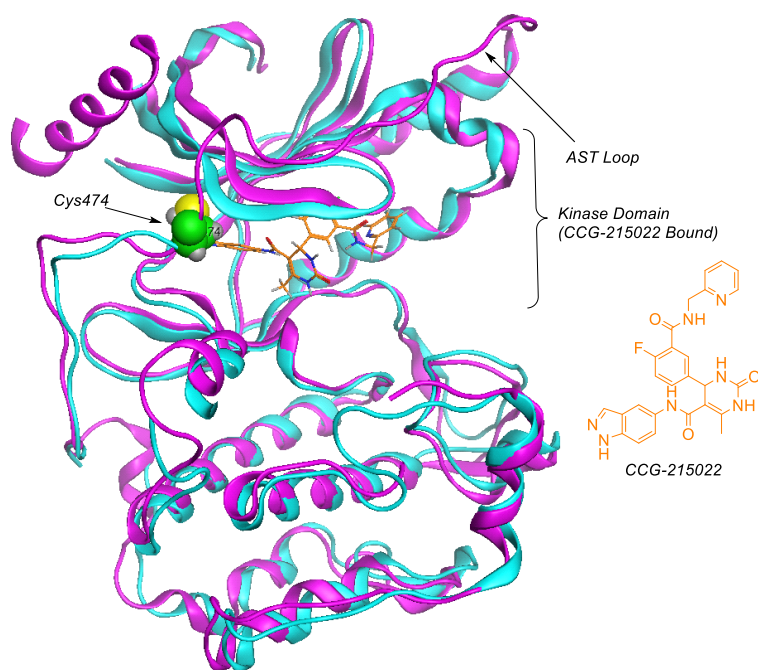


Figure 3.1 Overlay model of GRK5 (blue) and GRK6 (purple). Cys474, located on the AST loop is highlighted in green. CCG-215022 (orange) is bound to the hinge, within the kinase domain.

connecting the large and small lobes of the kinase. When the kinase interacts with a substrate, such as ATP, it adopts a closed-active conformation in which the AST-loop wraps over the front of the kinase domain (Figure 3.1). This flexibility allows the kinase to adopt different conformations, which is critical to the regulation of downstream signaling cascades. However, this flexibility often means that in crystal structures the AST-loop can adopt several conformations within one crystal. Thus, the exact position of the highly flexible loop is impossible to fully determine.^{17,18} This effect produces a crystallographic “blind spot” in which it is assumed that the AST-loop is present but cannot be modeled in space with any degree of reasonable certainty.

Resolving a crystallographic blind spot requires that a crystal structure of a highly related protein, in this case the GRK4-family member GRK6, has a partially or fully resolved AST-loop.

For the virtual screen, an appropriate model of the target protein was needed. In the GRK5 structure previously published by the Tesmer group, the desired covalent handle, Cys474, is missing from the assigned structure (PDB: 4WNK).¹⁵ This is due to the flexibility of piece of architecture where Cys474 is located. The active-site tether (AST)-loop is a highly flexible piece of architecture that runs along the face of the kinase,

In this overlay model, GRK6 (PDB: 3NYN) has a partially resolved AST-loop, which does display Cys474.¹⁶ As GRK5 and GRK6 are subfamily members that share sequence homology (72.6% overall) as well as a kinase domain which is conserved among all GRKs, our overlay model was constructed using these two proteins (GRK5-4WNK,

GRK6-3NYN).^{15,16,19-21} Having filled in the crystallographic blind spot, determining parameters for virtual screening was next determined.

In order to obtain a series of potential leads that are reasonable, and increase the attrition rate of our virtual screen, a training set and experimental set of compounds were created (Figure 3.2).⁸ The test-set, which is used to validate the model and screening parameters consisted of known GRK2 and GRK5 inhibitors as well as known FDA-approved kinase inhibitors, such as ROCK1 inhibitor Fasudil.²² The experimental set was consisted of compounds pulled from both

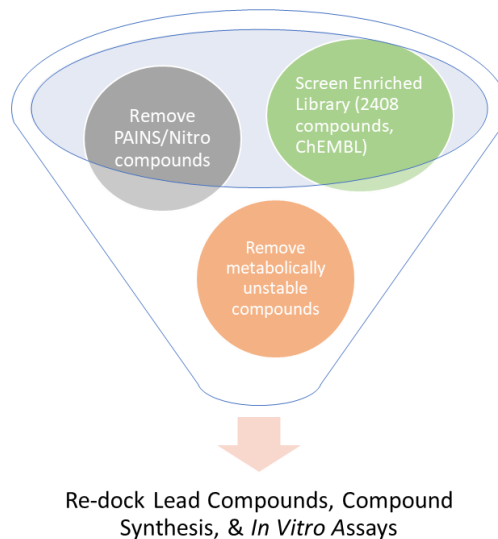


Figure 3.2 Screening funnel used for compilation, filtering and screening of *in silico* library of enriched compounds. Eventually, the “hit” compounds are redocked to validate through replication, and the individual “lead” is then either purchased or synthesized and tested for affinity data.

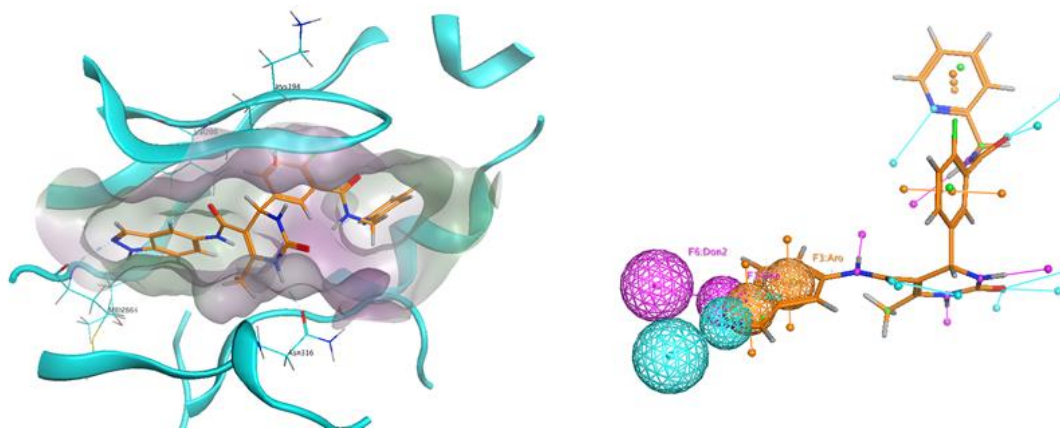


Figure 3.3 (a) binding mode for CCG-215022 as seen when crystallized with GRK5 (PDB: 4WNK). (b) pharmacophore generated from CCG-215022 to use in virtual screen. Hydrogen bond donors (magenta sphere), hydrogen bond acceptors (turquoise spheres) and aromatic rings (orange spheres) are selected as the pharmacophoric features required for virtual screening hits. Annotation points, automatically calculated by MOE, denote the potential location and type of interaction group on the molecule, as well as the projected positions of potential interactions.

the Maybridge chemical library and the ChEMBL compound library.^{23,24} These libraries were collated and filtered to include compounds that either had existing GRK5 or GRK2 activity data, or had a scaffold known to be privileged in kinase drug discovery.²⁵ Both sets of compounds were then subjected to an additional filtering system (Pipeline Pilot), which eliminated PAINS and other potentially reactive compounds.¹⁰ The final sets were then imported into Molecular Operating Environment (MOE 2018.01) in preparation for the virtual screen.²⁶

For the initial training set, the virtual screen had a number of parameters set to give potential leads that adopt an appropriate binding mode. In this instance, the key interaction for all compounds to contain was a hydrogen-bond acceptor that was congruent with the hinge hydrogen-bond donor on the hinge loop (Met266).^{27,28} Additionally, the pharmacophore was set to include a hydrogen bond-donor (blue) adjacent to the hydrogen-bond acceptor (purple) and at least one aromatic ring (orange) connecting the two hydrogen bond elements. This pharmacophore was based upon the binding pattern observed for CCG-215022, which was crystallized in GRK5 (PDB: 4WNK) (Figure 3.3). Once the pharmacophore had been set, the training set was run to validate the screening parameters. From this test, the screen returned a number of potential hits, including Fasudil, the known ROCK1 inhibitor, thereby validating that this method would produce potentially valid lead compounds.

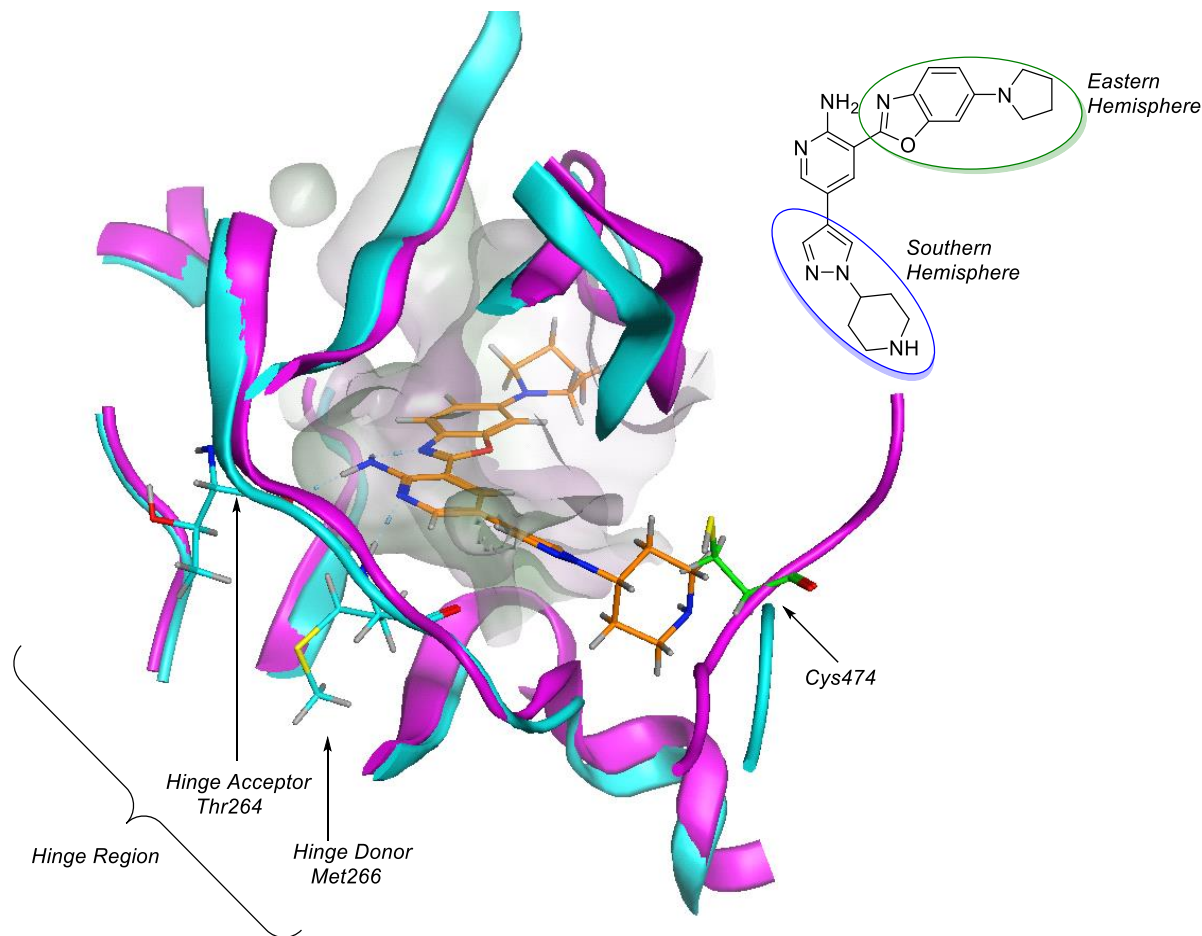


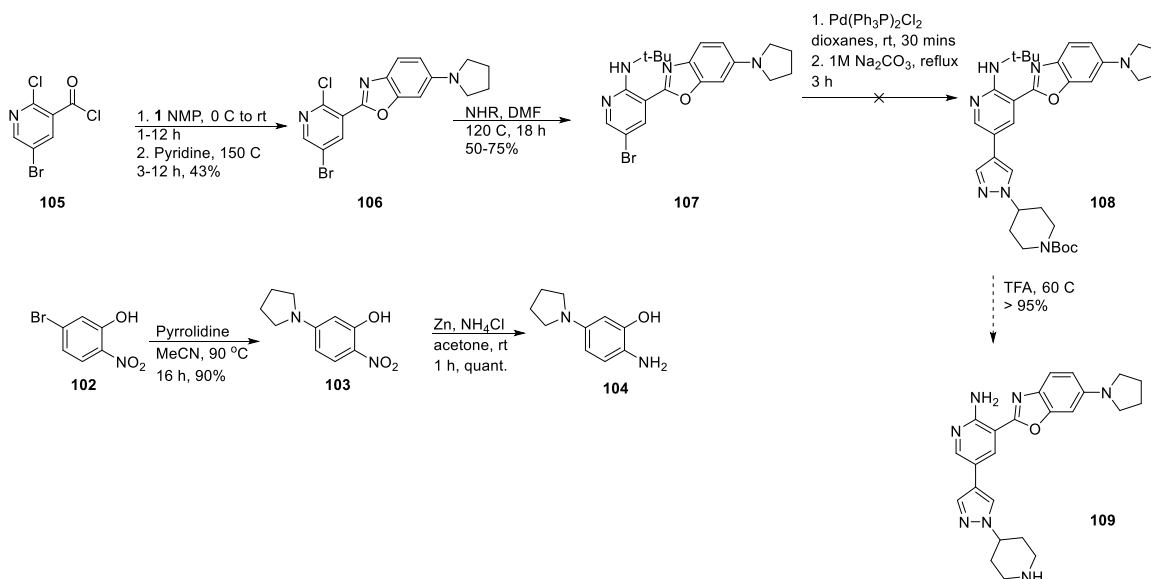
Figure 3.4 Lead compound Chembl-1607632 bound to GRK5 (blue)/GRK6 (purple) overlay model. Shows that the aminopyridine scaffold binds to the hinge region (Met266 and Thr264) with a two pronged hydrogen bonding pattern. Also shows that the southern piperidine ring could be removed and a warhead could be put there, and still maintain the correct vector for covalent engagement. Also, the eastern pyrrolidine ring has filled a deeper section of the hydrophobic back pocket, with a matched polar side chain.

Once validated, the same pharmacophore was used to screen the experimental set of compounds. In order to avoid an unmanageable amount of hit data, the number of poses generated for each compound was limited to five poses. Each hit from the virtual screen was evaluated by visual inspection, and top hits were then independently re-docked into the original model, forgoing the pharmacophore requirements for binding.²⁹ From this screen, four scaffolds were identified, the oxaindole scaffold, the thiopyrimidine scaffold, the pyrimidine scaffold and the aminopyridine scaffold. In total 11 compounds from the 3 former scaffolds were commercially available. Those compounds that were commercially available were purchased and evaluated. In total, none of the 11 compounds evaluated for biological activity were found to be active. Therefore, we chose to evaluate the aminopyridines, all of which seemed to bind the hinge region in the desired fashion

(Figure 3.4). Given its optimal binding mode, feasibility of modification to accommodate covalent warheads and excellent reported GRK5 activity data (GRK5 = 59 nM for lead compound Chembl-1607632), we chose to continue validating Chembl-1607632 as our lead compound for a new series of GRK5 inhibitors.³⁰

3.3 Independent Synthesis of Chembl-1607632 Required Route Optimization

An authentic standard of Chembl-1607632 was commercially unavailable, however in the literature that described its activity, there is also a brief synthetic scheme.³⁰ Thus, we set out to independently synthesis Chembl-1607632 for final validation of this lead compound and potential series of compounds. The original route for synthesis of this compound is described in Scheme 3.1.



Scheme 3.1 Original synthetic route proposed for Chembl-1607632A (**109**) and related compounds.

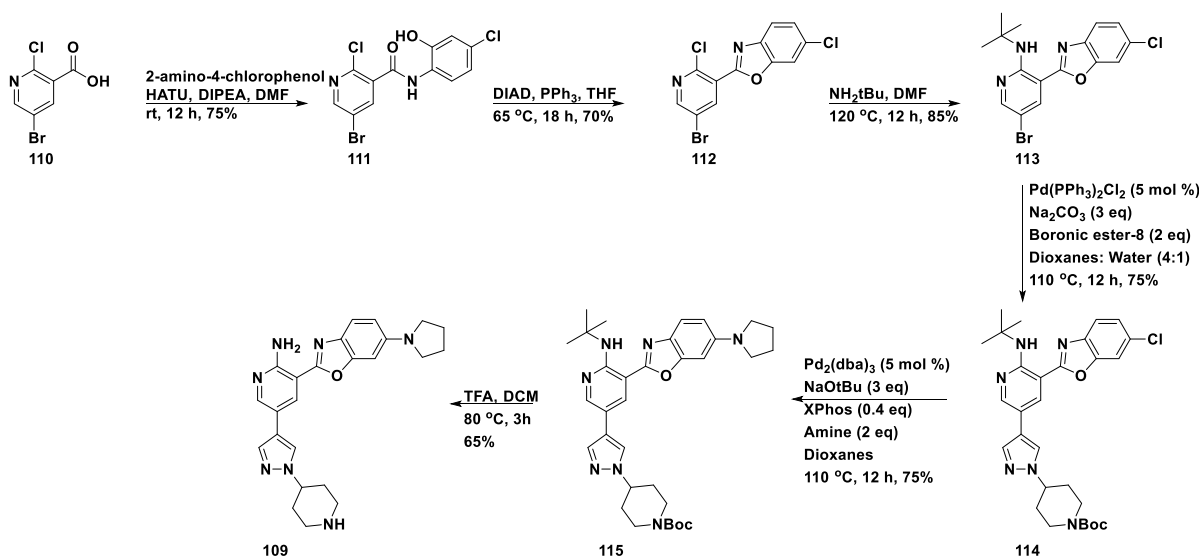
The original synthetic route to the lead compound begins with a SNAr of pyrrolidine with starting material **102** to yield intermediate **103**. The free aminophenol, **104** is revealed following a zinc catalyzed nitro-reduction, and it is immediately condensed with **105** to give the benzoxazole core seen in **106**.³¹ The yield for the production of **106** is severely limited for a few reasons. First, upon reduction of the nitro-group seen in **103**, a diamine, with a high level of resonance, is created (**104**). This diamine begins to immediately oxidize upon contact with air.³¹ As this reaction is run in the open atmosphere, these conditions yield an oxidized product and desired product (**104**) as an inseparable mixture. Only intermediate **104** is usable in the next step to create the benzoxazole ring, and therefore, the limited quantity of usable **104** limits the efficacy of the ring formation.

Also, the transformation from **104** to **106** occurs in one pot, starting with **105** undergoing an amide coupling. However, it is well known that the acid starting material of **105** is light sensitive and can undergo a UV-catalyzed decarboxylation. Therefore, special care was needed to form the intermediate **104** and use it in the ring formation of **106** (light protection and argon atmosphere). Given these challenges, we were never able to produce **106** in more than 30% yield.

Then the aminopyridine moiety was installed using a S_NAr with tert-butyl amine to give **107**. While the installation of the aminopyridine core through S_NAr proceeded smoothly, it also yielded inconsistent results with yields of 50-75%. This limited yield was due to steric hinderance from the tert-butyl amine in the 2-aminopyridine position. This exceptionally large group limited the rotational degrees of freedom for the compound and thus could only be produced in small batches. Additionally, there are multiple positions that can react with tert-butylamine to produce an undesired isomer of the desired product, **107**. Interestingly, we were unable to exchange this protecting group for a more conventional amine protecting group. The most common Boc-protecting group would have come off in our down-stream chemistry that features strongly acid conditions and metal catalyzed coupling reactions. Other allyl groups would have proved difficult to remove as well. This tert-butyl group is theorized to be removed by releasing a tert-butyl cation, other allyl groups would have to be removed by harsh boronic conditions. Therefore, we chose to keep this protecting group, despite its obvious limitations.

According to Cho. et al. attaching the southern hemisphere of the compound, constructed in a separate line of synthesis, could be achieved using a Suzuki-Miyara cross-coupling.³⁰ However, in our hands, we were never able to achieve this transformation. This failure to complete intermediate **108** may be due to the highly electron rich system of the starting material **107**. It is well known that highly electron rich, deactivated systems are rarely good participants in cross-coupling methods.³² Additionally, the bromine-leaving group of **107** is not the most ideal leaving group for these transformations, which typically prefer chlorines as leaving groups.^{33,34} Well it has been well established that bromine can be used in palladium catalyzed transformations, clearly, in this case, it is not an appropriate match under these conditions. As **108** could not be produced, we were unable to establish that the removal of the tert-butyl group by TFA was a legitimate way to produce the final product, **109**.

Given the amount of difficulty with this highly electron-rich and sensitive system, we chose to redesign the route to achieve the lead compound and derivatives. Ideally, the modified route avoids the unveiling of highly sensitive or reactive pendants, though certain precautions were taken to optimize the efficiency of each reaction. The actual route used to achieve **CCG-265649** is described in Scheme 3.2. Synthesis begins with an amide coupling between **110** and 2-amino-4-chlorophenol to yield the open intermediate, **111**. It was initially thought that an acid catalyzed ring closure would achieve **112**, however, we were only ever able to isolate 10-25% of the desired



Scheme 3.2 Optimized synthetic route to **CCG-265649**.

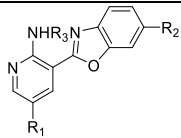
compound and the open intermediate **111** with those procedures.^{35–37} Through a Mitsunobu reaction with DEAD, **111** was successfully converted to the benzoxazole core, **112** in moderate yields (70%) allowing us to operate the next few difficult steps at a higher scale. The installation of the aminopyridine core is then accomplished through a S_NAr , yielding common intermediate **113**.³⁸ While we did attempt to optimize this S_NAr , we found that the conditions initially suggested by Cho et.al. proved to be the most effective, if erratic in yield (10-80%). Intermediate **113** is then submitted to the Suzuki-Miyara coupling conditions described by Thompson, thereby yielding the second common intermediate **114**.^{34,39,40} One advantage of this route is that it allowed us to rapidly generate a series of analogues using optimized Buchwald-Hartwig coupling conditions. One of the major issues with this is that Buchwald-Hartwig are often optimized case-by-case due to the sensitivity of the catalysts and the coupling partners.³² Despite these challenges we were able to

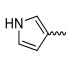
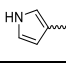
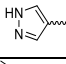
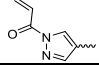
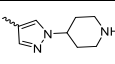
produce our own authentic sample of Chembl-1607632 (now known as CCG-265649) and an initial series of compounds produced while trying to validate our synthetic route.⁴¹

3.4 CCG-265649 Invalidates Chembl-1607632 Lead Compound in Radiometric Assays

With an authentic sample of Chembl-1607632 (CCG-265649) in hand, the next step was to validate the activity of the lead and by extension the series. We also chose to test a few compounds which were produced as part of the synthetic route validation process.

Table 3.1: IC₅₀ Values for Aminopyridine Route Development Compounds (μM ± SD)



Compound	R ₁	R ₂	R ₃	GRK5 (μM)	GRK2 (μM)
CCG† 264187	Br	H	tBu	>100	ND
CCG† 264222		H	tBu	>100	ND
CCG† 264240		Cl	H	>100	ND
CCG† 264485		H	H	>100	ND
CCG 265175		H	H	>100	>100
CCG 265176		H	H	>100	>100

Experimental values derived from this report were run in triplicate with n=3 experiments against GRK5.

ND = not determined. †Experimental values derived from this report were run in n=1 experiments against GRK5.

CCG-265649 was reported in the literature as having nanomolar potency against GRK5 (IC₅₀ = 59 nM), with relatively low-selectivity against GRK2 (IC₅₀ = 460 nM, 7-fold selective for GRK5). However, in our hands, this compound was found to have little to no activity against GRK5 with an IC₅₀ = >100 μM. Interestingly, compounds that were produced during route

optimization showed a similar level of inactivity. Unsurprisingly CCG-264187, and CCG-264222 do not show any level of appreciable activity, as the tert-butyl amine moiety blocks the ability of the amine to hydrogen bond with the hinge of GRK5. The inactivity of CCG-264240 and CCG-264485, is surprising as that moiety is not blocked from engaging with the hinge region of GRK5. As these compounds are smaller fragments, it is possible that an alternative binding mode, wherein the aminopyridine moiety doesn't bind to the hinge of GRK5 is possible, accounting for the lower

Table 3.2: IC₅₀ Values for Aminopyridine Compounds (μM ± SD)

The chemical structure shows a pyridine ring with an amino group (NHR₃) at the 2-position and a 5-membered heterocyclic ring (likely an imidazole or pyrrole derivative) at the 3-position. The pyridine ring has a substituent R₁ at the 4-position. The 5-membered ring has a substituent R₂ at the 5-position.

Compound	R ₁	R ₂	R ₃	GRK5 (μM)	GRK2 (μM)
CCG [†] 264262		Cl	H	>100	ND
CCG 265649			H	>100	>100
CCG 270957			H	>100	>100
CCG 270958			H	>100	>100
CCG 270962			H	>100	>100
CCG 270964			H	>100	>100

Experimental values derived from this report were run three times in duplicate against GRK5 and GRK2.

[†]Experimental values derived from this report were run once, in duplicate against GRK5. ND = not determined.

levels of activity observed. However, in a separate single dose experiment, conducted at 1 mM, CCG-265176 was found to strongly inhibit both GRK5 and GRK2 (data not shown). Given this discrepancy, it is clear that further investigation of key compounds, CCG-265175 and CCG-265176 is needed to better understand the relationship between GRK5 and this series.

Data from the initially developed compounds suggested that CCG-265649 may be an anomaly, as it shows no inhibitory activity with an IC₅₀ > 100 μM (Table 3.2) despite the reported literature data. To further investigate, compounds CCG-270957-CCG-270964 were created. CCG-270957 and CCG-270958 were designed to have some activity against GRK5 or GRK2, as the

pyridyl pendant is known to have activity against GRK2. However, their lack of activity suggests that otherwise, implying that these pyridyl pendants might not be positioned in the same hydrophobic pocket as the pyridyl pendant in the well known GRK2/GRK5 inhibitor, CCG-215022. Given the lack of activity from these compounds, further investigation is needed, and potentially a new scaffold may need to be pursued.

In an effort to expand our covalent arsenal of GRK5 inhibitors, we created CCG-265175 that features an acrylamide warhead. While this warhead demonstrated lower reactivity in our initial pyrrolopyrimidine series, we were able to observe covalent labeling. Given the knowledge that less potent compounds have a slower K_{on} which can then extend the timeframe needed to

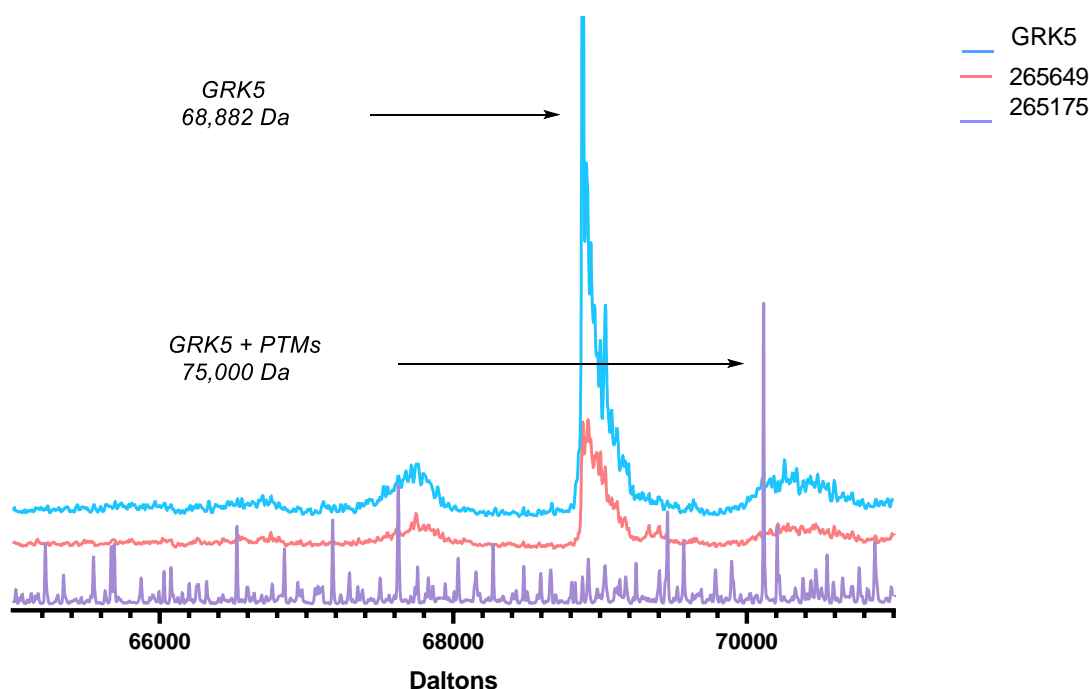


Figure 3.5 Intact protein mass spectrometry of CCG-265649 (coral), and CCG-265175 (lavender). All traces indicate that none of the compounds tested are capable of forming a covalent bond with GRK5. MS traces are an average of $n=1$ experiments.

observe a covalent engagement, we tested CCG-265175 in intact protein mass spectrometry with a 24 h incubation period (Figure 3.5). However, even with ample amount of time to form a covalent adduct CCG-265175 did not have any observable amount of labelled GRK5, instead only a GRK5 aggregate with a much higher weight than anticipated was observed, suggesting CCG-265175 may be causing the protein to aggregate and crash out of solution, rather than label GRK5 in the desired

fashion. Thus, we concluded that while the model suggested this scaffold would be amenable to carrying covalent modifiers, this is not the case.

Other rationally designed compounds, CCG-270957-270964, display a similar level of inactivity. Interestingly, we thought that the free pyrazole compound, CCG-270964, could adopt a different binding, one that is more similar to that seen in the crystal structure of GRK5 bound to CCG-215022 (Figure 3.6). In this model, we assumed that the free-pyrazole pendant could bind the hinge and the benzoxazole core could

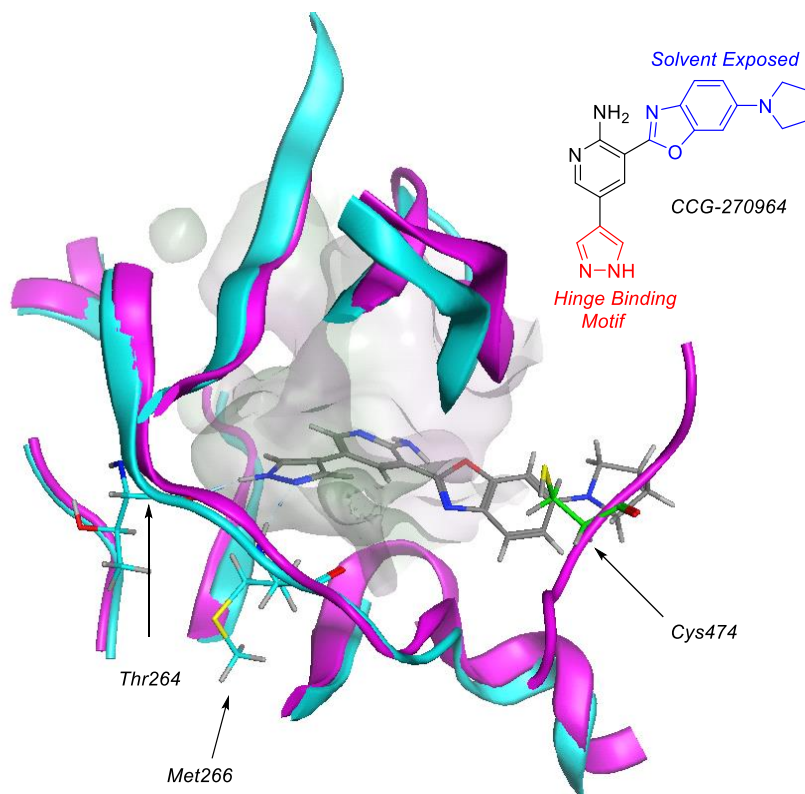


Figure 3.6 Alternate binding mode for CCG-270964 (gray) bound to the GRK5(blue)/GRK6 (purple) homology model. Changes in binding motif and solvent exposure are denoted in red and blue respectively. Key residues: Thr264, Met266 and Cys474 (green) indicated by arrows.

then fill the deeper hydrophobic pocket, similar to other known Type II kinase inhibitors. However, the inactivity of this compound suggests that this binding event does not occur.

3.5 Invalidation of CCG-265649 Means Abandoning the Series

While CCG-265649 originally seemed like an ideal candidate for a new series of covalent GRK5

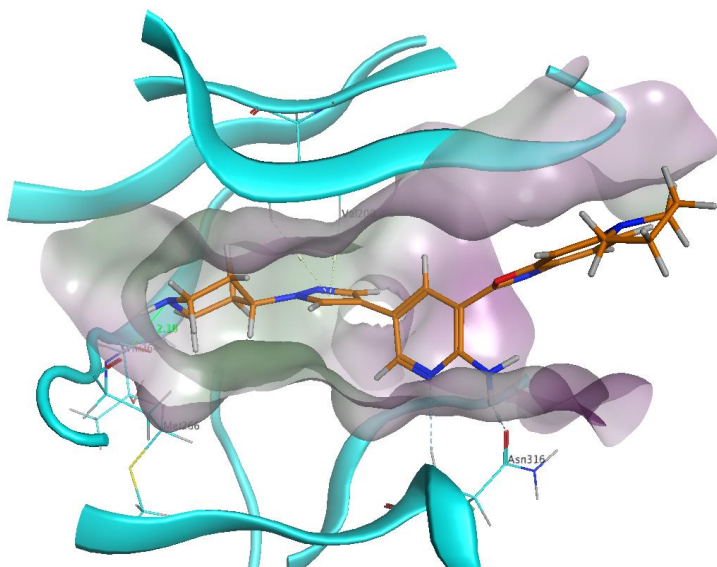


Figure 3.7 Alternate binding mode for CCG-265649 (orange) shown with the lipophilic pocket of GRK5 (blue). The more polar groups are seen to be situated ideally in this binding mode, and additional interactions with Asn316.

inhibitors, this is sadly not the case. We were unable to replicate the data set out in the literature, suggesting two possibilities. First, as Cho et. al. did not provide experimental data for Chembl-1607632, it is possible that CCG-265649, was not the active ingredient in their sample. Second, it is possible that a contaminant was present in their sample that conveyed activity

making it appear as if Chembl-1607632 was a potent compound.

None of the compounds made as part of the series yielded any appreciable level of activity. We can attribute this lack of activity to one of two reasons. Either these compounds do not bind as we predicted they would, or the aminopyridine scaffold does not have a sufficient amount of intrinsic potency to allow for binding. In independent docking experiments, we did observe that the original lead compound (and all other in the series with the southern piperidine pendant) could adopt a secondary binding mode. This secondary binding mode shows the piperidine ring forming a hydrogen bond with the hinge hydrogen bond-donor, but this is the only key interaction with the hinge in this binding mode (Figure 3.7). This alternate binding mode also indicates new types of interactions being made with Val200 and Asn316 which are not shown in the original binding mode posited by the virtual screening docking experiment. These new interactions are suggestive of overall better binding mode however, their presence is not enough to suggest strong binding, which is consistent with the data for CCG-265649.

As the aminopyridine scaffold is known in kinase drug-discovery to be a privileged scaffold (with appearances in known FDA-approved kinase inhibitors such as Crizotinib) it seems unlikely that the intrinsic potency of the aminopyridine scaffold wouldn't be enough to enable some low-activity level binding event.^{25,42} However, it is entirely possible that the electronics of

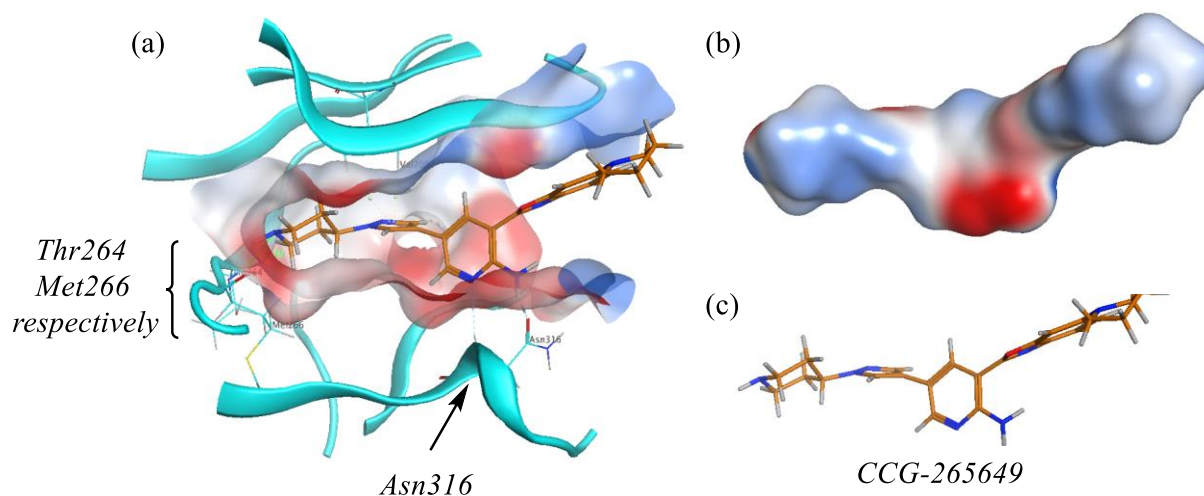


Figure 3.8 (a) Electrostatic map shown for alternate binding mode of CCG-265649 shown in blue and red. (b) Electronic density of CCG-265649, as shown in the alternate binding mode. (c) CCG-265649 (orange) in alternate binding mode indicates that additional hydrogen bonds can be achieved with Asn316 and the aminopyridine moiety. Hinge donor and acceptor are indicated in respective order (back to front) via bracket.

CCG-265649 and its series members make an inexact match with the binding pocket. Potentially these molecules are too electron-rich causing an electronic repulsion with residues within the binding site (Figure 3.8). Indeed, when looking at the electrostatic map of GRK5 (Figure 3.8a) against the electronic map of CCG-265649 (Figure 3.8b), we see that deeper in the hydrophobic pocket there is an inexact match occurring around the aminopyridine and pyrrolidine moiety. In fact, these two areas of CCG-265649 have almost the exact same properties of that seen in the GRK5 active site electrostatic map. This kind of mismatch is indicative of an electronic repulsion (in this case, blue shading matching with red shading indicates a strong electronic attraction). Therefore, this binding mode, while attractive when looking at just lipophilicity and hinge binding, is not ideal for high affinity compounds. This is consistent with the low affinity seen in this series, suggesting that potentially, this alternate binding mode is closer to what is actually occurring *in vivo*.

Despite this reasoning, we still have deep misgivings about this series due to the discrepancy between our data and the data reported in the literature. Given the large discrepancy

in data we have determined that unless the authentic third-party sample of ChEMBL-1607632 can be obtained and validated, this series is not worth pursuing further.

3.6 Materials, Methods and Synthetic Experimental Data

Computational Modeling General Information:

GRK5/GRK6 Overlay Model:

GRK5 (4WNK) and GRK6 (3NYN) were loaded into Molecular Operating Environment 2018.01 (Molecular Operating Environment (MOE), 2018.01; Chemical Computing Group ULC, 1010 Sherbrooke St. West, Suite #910, Montreal, QC, Canada, H3A 2R7, 2018) and proteins were prepared using QuickPrep function. Once preparation was complete, the sequences of both proteins were aligned. The alignment was used to create a super-position of the two proteins within 3D space. This super-position is herein referred to as the “GRK5/GRK6 overlay model” and serves as the basis for computational work described throughout this text.

Database Creation:

From ChEMBL database were downloaded compounds with activity for GRK2, GRK5 and ROCK1 (<https://www.ebi.ac.uk/chembl/>). These results were then collated with screening compounds from the Maybridge Chemical Library (https://www.maybridge.com/portal/alias_Rainbow/lang_en/tabID_177/DesktopDefault.aspx).

Compounds with known GRK2, GRK5 and ROCK1 activity were added to test if the virtual screening could find these compounds as hits. The collated library of compounds were then sorted using Pipeline Pilot to remove compounds that contain: nitro groups, Michael acceptors and other chemically reactive moieties, and may have redox potential (PAINS). The refined list of compounds were imported into MOE, washed and converted from 2D to 3D space. The resultant MDB file, with 2408 compounds, was saved and used in the virtual screening efforts described below.

Building a Pharmacophore Model:

For the virtual screen, a pharmacophore was built around the known GRK5 ligand, CCG-215022, as shown in the GRK5 crystal structure (4WNK). The pharmacophore query included the two aromatic rings that form the indazole core of the CCG-215022 scaffold, and the hydrogen bond donor and acceptor from the indazole core. This query was saved and used to determine potential hits within the virtual screening efforts described below. For additional details, see Figure 3.3

Running the Virtual Screen:

With the screening database and pharmacophore model in hand, the virtual screen was conducted. In the MOE docking protocol, the following parameters were used: Amber10:EHT as the force field, the above-mentioned pharmacophore as the placement, rigid receptor refinement, and London dG, GBVI/WSA dG as the scoring method. All results from the screen were then refined by visual inspection, and compounds with desired binding modes were duplicated for later examination and identification of commercially available sources. As validation of our method, our screen drew Fasudil, a known ROCK1 inhibitor, as a hit. Further visual inspection produced four novel scaffolds, the oxaindoles, the thiopyrimidines, the pyrimidines and the aminopyridines. To evaluate hits, 11 commercially available compounds were purchased, see list below, and evaluated by radiometric assay (described below). Of the compounds tested, none were found to be active (data not shown).

Virtual Screening Compounds Purchased:

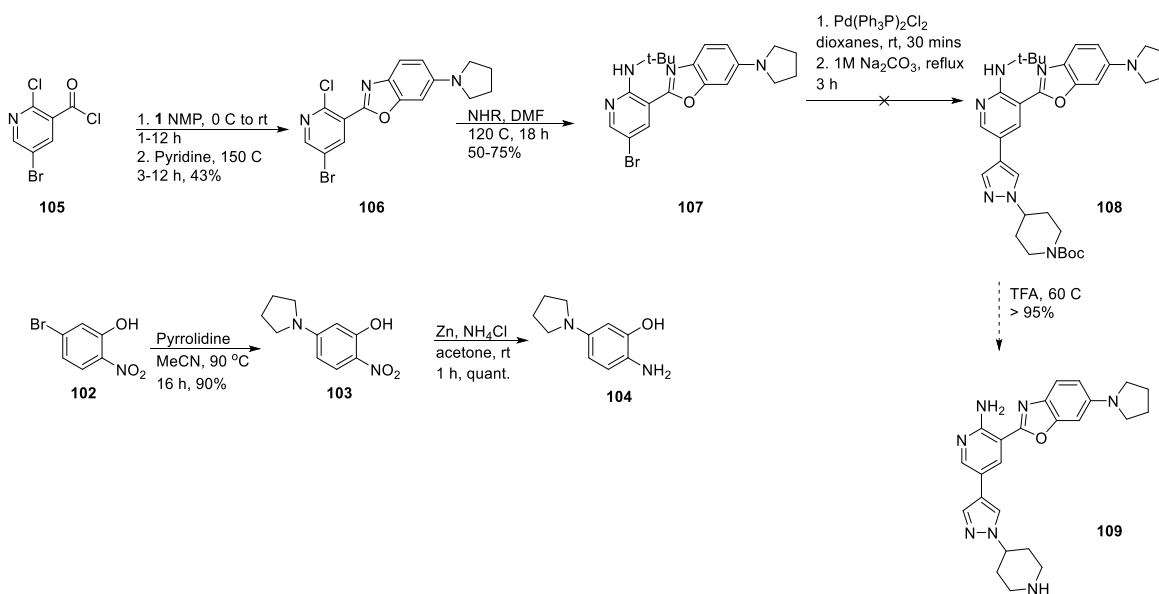
- Oxaindoles, sourced from Sigma Aldrich and used without further purification
Z1213677549, Z1119386706, 477862-37-6

- Thiopyrimidines, sourced from Enamine Building Blocks and used without further purification
Z5676559, Z1699857079, Z11263716020, Z1575308464
- Pyrimidines, sourced from Sigma Aldrich and used without further purification
B0241956, B0241957, B0241958, B02410012

Chemistry General Information: All reagents from commercial sources were used without further purification unless otherwise noted. ¹HNMR spectra were taken in DMSO-d₆, MeOD or CDCl₃ at room temperature on Varian MR 400 MHz, Varian Vnmrs 500 MHz and Varian Vnmrs 700 MHz instruments. Reported chemical shifts for the ¹HNMR spectra were recorded in parts per million (ppm) on the δ scale from an internal tetramethylsilane (TMS) standard (0.0 ppm). Small molecule mass spectrometry data was measured using a Waters Corporation Micromass LCT or Agilent6230 Q-TOF instrument. HPLC was used to determine purity of biologically tested compounds on an Agilent 1100 series with an Agilent Zorbax Eclipse Plus-C18 column. A gradient of 10-90% acetonitrile/water over 6 minutes followed by 90% acetonitrile/water for 7 minutes was used with detection at 254 nm.

Intact Protein MS Information: Intact Protein mass spectrometry was acquired with a Phenomenex C4 column paired with an Agilent 6545 Q-TOF LC/MS. For intact MS all samples were prepared with 20 μ M GRK in assay buffer (see below), 1 mM compound, and incubated at 4 °C for 3-24 hours before being quenched with 1.0 μ L of formic acid.

Biology General Information: IC₅₀s for human GRK5, bovine GRK2, bovine GRK6, and bovine GRK5-C474S were determined using a radiometric assay as follows. 50 nM GRK was incubated with 500 nM porcine brain tubulin (Cytoskeleton) and 1 nM–1 mM inhibitor in Reaction Buffer (20 mM HEPES pH 7.5, 10 mM NaCl, 10 mM MgCl₂, 2 mM DTT) for 4 h at room temperature prior to initiation with the addition of 5 μ M ATP supplemented with radioactive [γ -³²P]-ATP (PerkinElmer Life Sciences). Reactions were quenched at 8 min by transferring 10 μ L reaction into 5 μ L 4X SDS gel loading dye. 10 μ L samples were separated on a 4-15% Criterion TGX precast gel (Bio-Rad), and gels were dried, exposed to a storage phosphor screen overnight, and scanned using a Typhoon scanner. Bands corresponding to phosphorylated tubulin were quantified using ImageQuant, plotted as a function of log[inhibitor], and fit to the three-parameter log(inhibitor) vs. response model in GraphPad Prism 7.03 to determine IC₅₀s. Experiments were performed with an $n = 3$, and mean and standard deviation values were calculated using the column statistics function of GraphPad Prism 7.03.



Scheme 3.3. Original synthetic route to CCG-265649.

2-nitro-5-(pyrrolidin-1-yl)phenol (103, RAR-5-7)

To a sealed tube were added 2.0012 g of 5-bromo-2-nitrophenol, dissolved in 45 mL of MeCN. To this solution were added 4 mL of pyrrolidine, and the tube was sealed and heated to 80 °C for 12-18 h. Once complete, the reaction was cooled to rt and the solvent was removed under pressure. The crude material was purified by column chromatography (80% DCM/Hex) to yield the desired product. ¹H NMR (500 MHz, Chloroform-d) δ 10.61 (s, 2H), 7.97 (dt, J = 9.3, 2.6 Hz, 2H), 7.96 – 7.91 (m, 1H), 7.37 (q, J = 2.9, 2.4 Hz, 2H), 7.14 (dt, J = 8.6, 1.9 Hz, 2H), 6.20 – 6.13 (m, 1H), 6.01 (d, J = 2.9 Hz, 1H), 3.41 (d, J = 5.9 Hz, 4H), 2.07 (td, J = 5.9, 3.3 Hz, 4H). ¹³C NMR (126 MHz, cdcl₃) δ 128.01, 126.57, 124.40, 123.52, 109.85, 106.92, 97.89, 48.57, 25.84.

2-amino-5-(pyrrolidin-1-yl)phenol (104, RAR-5-18)

To a flask were added 50 mg of 2-nitro-5-(pyrrolidin-2-yl)phenol, dissolved in 3 mL of 1:1 MeOH/EtOAc. The solution was degassed with three rounds of evacuation and back fill with nitrogen before Pd/C catalyst was introduced. The solution was then degassed with an additional 3 cycles of evacuation and back fill with nitrogen. The atmosphere was replaced with hydrogen gas, and the resultant solution was allowed to stir at rt until complete (about 12 h). Once complete, the hydrogen atmosphere was removed, and the solution was passed through a pad of celite. The solvent was removed under pressure and the crude material was taken forward without further characterization due to instability in open atmosphere.

5-bromo-2-chloronicotinoyl chloride (105, RAR-5-17)

To a dried flask were added 50.1 mg of 5-bromo-2-chloronicotinic acid. All materials were then dissolved in 3 mL of dry DCM, and the flask was wrapped in foil (to prevent light catalyzed decarboxylation). The solution was cooled to 0 °C and 0.1 mL of DMF as well as 0.02 mL of

Oxalyl chloride were added sequentially. The solution was allowed to gently warm to rt and run for 2 h. Once complete, the solvent was removed under pressure and the crude material was further rinsed with DCM (3 x 15 mL). Due to instability in air, this product was moved forward without further characterization.

2-(5-bromo-2-chloropyridin-3-yl)-6-(pyrrolidin-1-yl)benzo[d]oxazole (106, RAR-4-100)

To a flask were 50 mg of freshly prepared 5-bromo-2-chloronicotinoyl chloride, and 30 mg of 2-amino-5-(pyrrolidine-1-yl)phenol, dissolved in 3 mL of NMP. The solution was cooled to 0 °C and 0.1 mL of pyridine were added in one portion before being stirred for 20 mins. The solution was then slowly warmed to 120 °C for 4 hours. Once complete, the reaction was quenched with brine and the aqueous layer was extracted with EtOAc (4 x 30 mL). The combined organic layer was then washed with brine (1 x 30 mL) and then dried over Na₂SO₄. The crude material was then purified by column chromatography to yield the desired product as a light yellow solid, 46.6 mg, 60%. ¹H NMR (400 MHz, DMSO-d₆) δ 9.74 (s, 1H), 9.34 (s, 1H), 8.65 (d, J = 2.5 Hz, 1H), 8.32 (d, J = 2.5 Hz, 1H), 7.44 (d, J = 8.6 Hz, 1H), 6.08 (d, J = 2.6 Hz, 1H), 6.04 (dd, J = 8.7, 2.5 Hz, 1H), 3.17 (d, J = 6.4 Hz, 4H), 2.01 – 1.86 (m, 4H).

5-bromo-N-(tert-butyl)-3-(6-(pyrrolidin-1-yl)benzo[d]oxazol-2-yl)pyridin-2-amine (107, RAR-5-2)

To a sealed tube were added 220 mg of (106) dissolved in 5 mL of dry DMF. To this solution were added 0.06 mL of tert-butylamine and the tube was sealed. The solution was then heated to 120 °C for 18 h. Once complete, the reaction was cooled to rt and diluted with 50% EtOAc/Hex. The organic layer was washed with water (1 x 30 mL) and brine (1 x 30 mL) before being dried over Na₂SO₄. The solvent was removed under pressure, evaporating the product onto silica gel. The crude material was purified by column chromatography to yield the product as a white solid, 100 mg, 50%. ¹H NMR (500 MHz, Chloroform-d) δ 8.31 (d, J = 2.4 Hz, 1H), 8.23 (d, J = 2.5 Hz, 1H), 8.15 (d, J = 2.4 Hz, 1H), 7.78 (dd, J = 5.9, 3.3 Hz, 1H), 7.58 (dt, J = 7.3, 3.7 Hz, 1H), 7.47 (dd, J = 9.0, 2.4 Hz, 1H), 7.39 – 7.36 (m, 2H), 6.25 (d, J = 9.0 Hz, 1H), 3.45 – 3.37 (m, 4H), 2.97 (d, J = 1.1 Hz, 7H), 2.04 – 1.97 (m, 4H). ¹³C NMR (126 MHz, cdcl₃) δ 150.45, 142.66, 125.53, 124.95, 120.36, 77.50, 77.25, 76.99, 47.06, 41.48, 25.79, 0.24.

2-(5-bromo-2-chloropyridin-3-yl)benzo[d]oxazole (116, RAR-8-3)

To a flask were added 1.5 g of 5-bromo-2-chloronicotinoyl chloride, dissolved in 30 mL of toluene. To this solution were added 694.0 mg of aminophenol and 1.7 mL of triethylamine. The solution was then stirred at rt for 2 h. After 2 h, 1.6 g of PPTS were added to the solution in one portion, and the reaction was heated to 170 °C for 24-48 h. Once complete, the reaction was cooled to rt and the solvent was removed under pressure. The material was then diluted with EtOAc and washed with water (1 x 50 mL) and brine (2 x 50 mL). The organic layer was dried over Na₂SO₄ and the solvent was removed. The crude product was purified using a silica plug, eluting with 5% EtOAc/Hexanes. The solvent was removed to give the desired product as a yellow solid, 420 mg, 21% LRMS: 310 [M+1], HPLC: 8.053. ¹H NMR (700 MHz, Chloroform-d) δ 8.75 – 8.54 (m, 2H), 7.87 (s, 1H), 7.65 (s, 1H), 7.45 (s, 3H).

3-(benzo[d]oxazol-2-yl)-5-bromo-N-(tert-butyl)pyridin-2-amine (117, RAR-8-4)

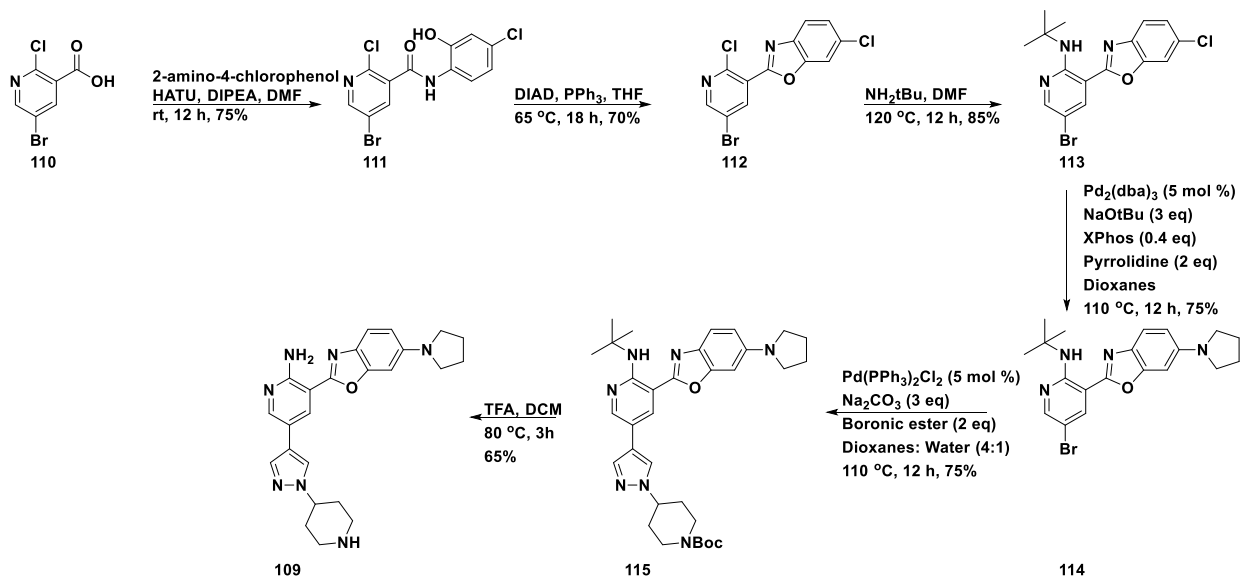
To a sealed tube were added 202.4 mg of RAR-8-3 which was dissolved in 6 mL of DMF. To this solution were added 1.0 mL of tert-butylamine and then the tube was sealed. The reaction was heated to 120 °C for 20 h. Once complete, the reaction was cooled to rt and then the reaction was quenched with brine. The aqueous layer was extracted with EtOAc/Hex (50%, 3 x 30 mL). The combined organic layer was then washed with brine (2 x 25 mL), and then dried over Na₂SO₄. The solvent was removed under pressure, and the crude material was purified by column chromatography yielding 186.9 mg, 80%. MS: 348, HPLC: 8.215. ¹H NMR (500 MHz, Chloroform-d) δ 8.77 (s, 1H), 8.30 (dd, J = 40.5, 21.9 Hz, 3H), 7.73 (d, J = 6.1 Hz, 1H), 7.62 – 7.53 (m, 2H), 7.37 (d, J = 8.0 Hz, 4H), 3.06 – 2.92 (m, 3H), 1.59 (s, 9H).

tert-butyl 4-(4-(5-(benzo[d]oxazol-2-yl)-6-(tert-butylamino)pyridin-3-yl)-1H-pyrazol-1-yl)piperidine-1-carboxylate (118, RAR-8-7)

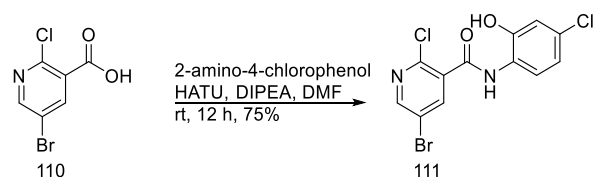
This material was prepared using the protocol described for RAR-9-45. LRMS: 517 [M+1], HPLC: 9.060. ¹H NMR (700 MHz, Chloroform-d) δ 8.75 (s, 1H), 8.45 (d, J = 2.4 Hz, 1H), 8.36 – 8.32 (m, 1H), 7.79 (s, 1H), 7.74 (dd, J = 5.9, 3.2 Hz, 1H), 7.67 (s, 1H), 7.58 (dd, J = 5.9, 3.3 Hz, 1H), 7.53 – 7.51 (m, 2H), 7.42 (d, J = 2.3 Hz, 2H), 7.37 – 7.35 (m, 2H), 6.27 (t, J = 2.2 Hz, 2H), 3.71 (s, 1H), 3.31 (ddd, J = 13.6, 8.1, 3.7 Hz, 1H), 2.22 – 2.17 (m, 2H), 2.02 – 1.95 (m, 4H), 1.86 – 1.79 (m, 2H), 1.62 (s, 10H), 1.50 (s, 9H). ¹³C NMR (176 MHz, cdcl₃) δ 161.90, 155.00, 154.58, 149.49, 148.33, 141.45, 138.93, 135.89, 133.56, 126.39, 125.03, 124.46, 122.65, 119.89, 119.57, 115.83, 110.18, 105.26, 103.94, 79.86, 77.18, 59.48, 59.15, 51.82, 38.85, 32.44, 29.27, 28.41.

3-(benzo[d]oxazol-2-yl)-5-(1-(piperidin-4-yl)-1H-pyrazol-4-yl)pyridin-2-amine (119, CCG-265176, RAR-8-15)

To a flask were added 8.1 mg of tert-butyl 4-(4-(5-(benzo[d]oxazol-2-yl)-6-(tert-butylamino)pyridin-3-yl)-1H-pyrazol-1-yl)piperidine-1-carboxylate (0.019 mmol) and 2 mL of xylenes. To this solution were added 0.2 mL of TFA (1.9 mmol) and the solution was heated to 70 °C for 3-12 h. Once complete, the solution was cooled to room temperature and then quenched with saturated Na₂CO₃ and then extracted with EtOAc (3 x 10 mL). The combined organic layer was then dried over Na₂SO₄ and the crude product was purified by column chromatography. Product is a yellow solid, 1.0 mg, 14%. MS: 549 [M+Toluene], HPLC: 5.997. ¹H NMR (700 MHz, Chloroform-d) δ 8.75 (s, 1H), 8.45 (d, J = 2.5 Hz, 1H), 8.35 (d, J = 2.4 Hz, 1H), 7.79 (s, 1H), 7.74 (dd, J = 5.9, 3.2 Hz, 1H), 7.69 (s, 1H), 7.59 (dd, J = 5.8, 3.3 Hz, 1H), 7.36 (dt, J = 6.0, 3.4 Hz, 2H), 4.35 – 4.29 (m, 1H), 3.34 (d, J = 12.9 Hz, 2H), 2.86 (t, J = 12.2 Hz, 2H), 2.27 (d, J = 13.3 Hz, 2H), 2.03 (dd, J = 12.4, 3.5 Hz, 2H). ¹³C NMR (176 MHz, cdcl₃) δ 161.93, 155.00, 149.51, 141.47, 141.11, 137.86, 135.77, 133.58, 129.02, 128.21, 125.02, 124.46, 122.59, 119.84, 110.20, 106.37, 62.66, 45.22, 29.70.

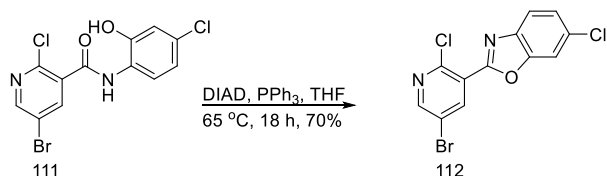


Scheme 3.4 Synthetic route to lead compound **109**. Modification to the route for derivation are described in generalized fashion.



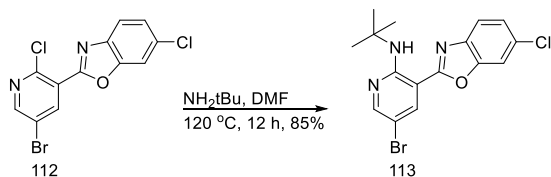
5-bromo-2-chloro-N-(4-chloro-2-hydroxyphenyl)nicotinamide (111, RAR-9-88)

To a dried flask were added 1.009 g of 5-bromo-2-chloronicotinic acid (1 eq), 1.9997 g of HATU (2 eq), 802.0 mg of 2-amino-4-chlorophenol (1 eq). All materials were dissolved in 30 mL of DMF, and 2.2 mL of DIPEA were added. Bright red solution was protected under foil and allowed to stir at room temperature (rt) for 12 hours. Once complete, reaction was quenched with brine (200 mL) and then extracted with EtOAc (3 x 150 mL). The combined organic layers were washed with brine (2 x 100 mL) and then dried over MgSO₄. The material was then purified by column chromatography (20-100% EtOAc/Hex) and the major product was collected as the final product. Result: bright red solid, 1 g, 75%. HRMS: 362.9121, HPLC: 6.880, purity: 85%. ¹H NMR (700 MHz, Chloroform-d) δ 9.06 (s, 1H), 8.83 (s, 1H), 8.66 (d, J = 9.6 Hz, 1H), 8.56 – 8.50 (m, 3H), 7.97 (s, 2H), 7.93 (d, J = 8.6 Hz, 1H), 7.36 (d, J = 8.9 Hz, 1H), 6.88 (d, J = 8.5 Hz, 1H). ¹³C NMR (176 MHz, cdcl₃) δ 163.11, 152.50, 151.15, 145.92, 143.50, 135.20, 132.21, 124.47, 123.45, 122.07, 116.93.



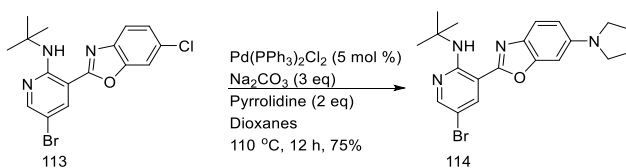
2-(5-bromo-2-chloropyridin-3-yl)-6-chlorobenzo[d]oxazole (112, RAR-9-94)

To a dried flask were added 2.0044 g of **111**, dissolved in 30 mL of THF. To this solution were added 2.5 mL of DIAD, and 5.0 g of triphenylphosphine. The bright red mixture was allowed to stir at 65 °C for 18 hours. Once complete, reaction was cooled to rt and solvent was removed under pressure. Resultant pink solid was then titrated in absolute EtOH and a light pink solid was filtered off as the final product. Result: light pink solid, 1.300 g, 70%. HRMS: 343.99, HPLC: 8.597, Purity: 95% ¹H NMR (700 MHz, Chloroform-d) δ 8.63 (d, J = 2.5 Hz, 1H), 8.61 (d, J = 2.6 Hz, 1H), 7.77 (dd, J = 8.4, 2.3 Hz, 1H), 7.67 (d, J = 2.1 Hz, 1H), 7.41 (dd, J = 8.6, 2.0 Hz, 1H). ¹³C NMR (176 MHz, cdcl₃) δ 158.50, 152.22, 150.93, 148.00, 142.25, 140.19, 132.35, 128.51, 126.13, 124.15, 121.43, 119.02, 111.68.



5-bromo-N-(tert-butyl)-3-(6-chlorobenzo[d]oxazol-2-yl)pyridin-2-amine (113, RAR-9-99)

To a pressure vessel were added 86.0 mg (1 eq) of **112**, 0.32 mL of tert-butylamine (12 eq) with all materials dissolved in 3 mL of DMF. The tube was sealed and heated to 120 °C for 18 hours. Once complete, the solution was cooled to rt, quenched with brine and extracted with EtOAc:Hex (1:1, 3 x 50 mL). The combined organic layers were then washed with brine (1 x 30 mL) and then dried over MgSO₄. The bright orange residue was purified by column chromatography (0-50% EtOAc/Hex) and the product was collected to give a pale yellow solid. Result: pale yellow solid, 34.7 mg, 36%. HRMS: 384.00, HPLC: 8.990, Purity: > 95%. ¹H NMR (700 MHz, Chloroform-d) δ 8.62 (s, 1H), 8.29 – 8.25 (m, 2H), 7.67 (d, J = 8.6 Hz, 1H), 7.61 (d, J = 8.4 Hz, 1H), 7.36 – 7.31 (m, 2H), 1.57 (s, 9H). ¹³C NMR (176 MHz, cdcl₃) δ 161.38, 157.76, 151.72, 140.01, 128.45, 125.32, 120.54, 120.08, 110.97, 105.00, 52.08, 29.03.



5-bromo-N-(tert-butyl)-3-(6-(pyrrolidin-1-yl)benzo[d]oxazol-2-yl)pyridin-2-amine (114, RAR-9-25)

To a three neck flask were added 150 mg of **113**, 0.05 mL of pyrrolidine (2 equiv), 126.4 mg of NaOtBu (3 equiv), XPhos (2 mol%) and Pd₂(dba)₃ (1 mol%). All materials were dissolved in 3 mL of Dioxanes and the solution was degassed with 8 cycles of evacuation and back fill with nitrogen. The reaction was then heated to 110 °C for 18 h. Once complete, the reaction was cooled to rt and then passed through a pad of celite. The filtrate was then purified by column chromatography to yield the desired product as a bright yellow residue. MS: (des tBu) 371, HPLC: 8.273. ¹H NMR

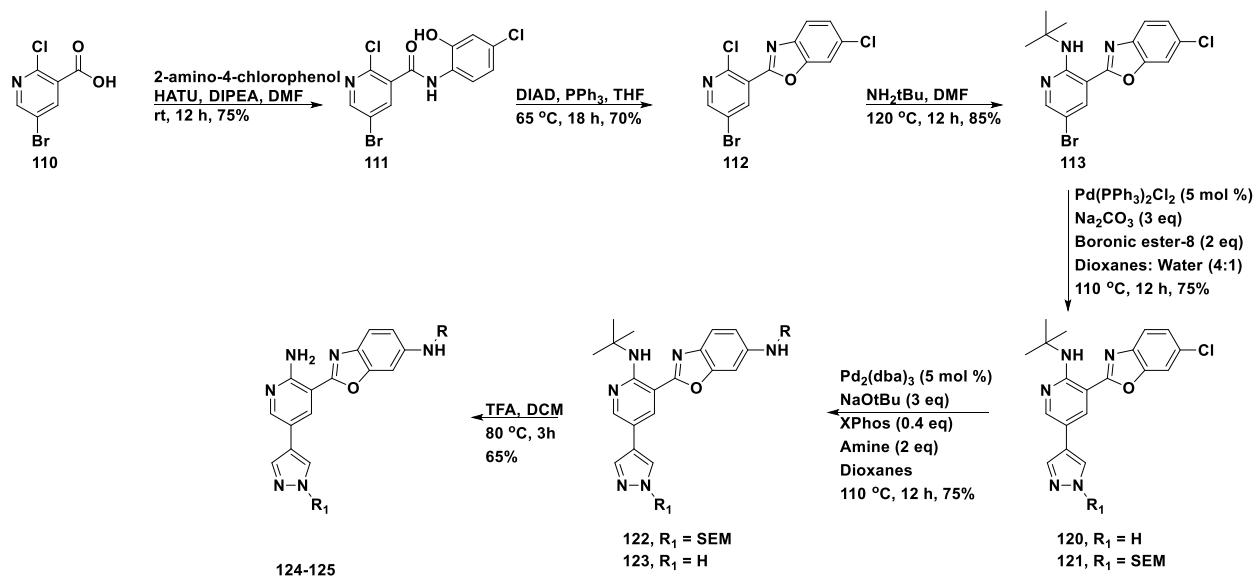
(500 MHz, Chloroform-d) δ 8.64 (s, 1H), 8.29 (s, 1H), 8.24 (d, J = 7.9 Hz, 1H), 7.63 (d, J = 8.4 Hz, 2H), 7.57 (t, J = 2.8 Hz, 2H), 6.62 (dd, J = 7.8, 4.8 Hz, 1H), 3.32 (s, 4H), 2.06 (s, 4H), 1.60 (s, 9H).

tert-butyl 4-(4-(6-(tert-butylamino)-5-(6-(pyrrolidin-1-yl)benzo[d]oxazol-2-yl)pyridin-3-yl)-1H-pyrazol-1-yl)piperidine-1-carboxylate (115, RAR-9-45)

To a three neck flask were added 50 mg of 114, 44.7 mg of *tert-butyl 4-(4-(4,4,5,5-tetramethyl-1,3,2-dioxaborolan-2-yl)-1H-pyrazol-1-yl)piperidine-1-carboxylate* (RAR-9-36), Pd(PPh₃)₂Cl₂ (1 mol%). All materials were then dissolved in 3 mL of dry dioxanes. The bright yellow solution was then degassed (3 cycles of evac./back fill). After 10 mins, 0.5 mL of Na₂CO₃ (1M) were added. The solution was then further degassed (3 cycles of evac./backfill) and heated to 110 °C (reflux) for 3-6 h. Once complete, the reaction was cooled to rt and then passed through a pad of celite. The filtrate was then purified by column chromatography to yield the desired product and the starting material as an inseparable mixture. MS: 586 (with Cl starting material still present at 551), HPLC: 5.376. ¹H NMR (700 MHz, Chloroform-d) δ 8.63 (s, 1H), 8.46 (d, J = 2.4 Hz, 1H), 8.30 (d, J = 2.5 Hz, 1H), 8.08 (s, 1H), 7.79 (d, J = 9.0 Hz, 2H), 7.67 (d, J = 7.7 Hz, 2H), 7.64 (d, J = 8.5 Hz, 1H), 7.59 (d, J = 1.9 Hz, 1H), 7.53 (d, J = 1.8 Hz, 3H), 7.48 (d, J = 7.6 Hz, 2H), 7.43 (d, J = 2.3 Hz, 3H), 7.39 – 7.33 (m, 3H), 6.27 (d, J = 2.2 Hz, 3H), 4.30 (tdt, J = 11.6, 8.0, 4.1 Hz, 12H), 2.90 (s, 12H), 2.19 (d, J = 5.5 Hz, 5H), 2.13 (d, J = 12.2 Hz, 8H), 1.96 – 1.88 (m, 9H), 1.61 (s, 9H). ¹³C NMR (176 MHz, cdcl₃) δ 162.75, 159.51, 155.10, 154.74, 149.85, 148.90, 140.43, 139.11, 136.64, 136.06, 133.74, 132.74, 130.72, 129.02, 126.57, 125.63, 125.33, 123.68, 122.85, 120.15, 119.90, 116.12, 111.05, 105.44, 103.57, 80.04, 59.68, 59.63, 59.33, 52.08, 43.40, 42.65, 32.63, 29.42, 28.59.

5-(1-(piperidin-4-yl)-1H-pyrazol-4-yl)-3-(6-(pyrrolidin-1-yl)benzo[d]oxazol-2-yl)pyridin-2-amine (109, CCG-265649 RAR-9-49, RAR-13-44)

To a flask were added 20 mg of **115**, and 1.2 mL of TFA. The neat solution was heated to 80 °C for 3 hours. Once complete, the solvent was removed, and the orange residue was purified by preparatory TLC plate (5% DCM/MeOH). Result: dark orange residue, 2 mg, 9%. HRMS: 430.2343, HPLC: 5.029. ¹H NMR (700 MHz, DMSO-d₆) δ 8.63 (s, 1H), 8.54 (s, 1H), 8.23 (t, J = 3.1 Hz, 1H), 7.90 – 7.82 (m, 1H), 7.69 (s, 1H), 7.43 (s, 1H), 6.22 (s, 1H), 3.76 (s, 1H), 3.38 (d, J = 13.5 Hz, 4H), 3.06 (s, 2H), 2.93 (t, J = 10.4 Hz, 2H), 2.15 (d, J = 9.5 Hz, 4H), 2.10 (d, J = 2.4 Hz, 2H), 1.86 (q, J = 12.3, 7.4 Hz, 4H).



Scheme 3.5. Synthesis of other final compounds using the optimized route.

N-(*tert*-butyl)-3-(6-chlorobenzo[*d*]oxazol-2-yl)-5-(1-((2-(trimethylsilyl)ethoxy)methyl)-1*H*-pyrazol-4-yl)pyridin-2-amine (RAR-10-41, 121)

To a dried flask were added 1.7 g of compound **120**, dissolved in 26 mL of dry THF. The solution was cooled to 0 °C and 220.4 mg of NaH were added in one portion. The solution was allowed to stir at 0 °C for 30 mins, before 0.90 mL of SEM-Cl were added. The yellow solution was then allowed to warm to rt for 2.5 hours. Once complete, the reaction was quenched with water, and then extracted with EtOAc (3 x 30 mL). The combined organic layers were then washed with brine (1 x 30 mL) and dried over MgSO₄. The resultant material was purified by column chromatography to yield a light yellow solid, 700 mg, 50%. HPLC: 8.280, HRMS: 498.1980, Purity: 90%. ¹H NMR (500 MHz, Chloroform-*d*) δ 8.65 (s, 1H), 8.48 (d, *J* = 2.4 Hz, 1H), 8.33 (d, *J* = 2.5 Hz, 1H), 7.82 (d, *J* = 4.8 Hz, 2H), 7.64 (d, *J* = 8.7 Hz, 1H), 7.60 – 7.57 (m, 1H), 7.37 – 7.32 (m, 1H), 5.49 (s, 2H), 3.65 – 3.61 (m, 2H), 1.62 (s, 9H), 0.95 (t, *J* = 8.2 Hz, 9H).

N-(*tert*-butyl)-3-(6-(pyrrolidin-1-yl)benzo[*d*]oxazol-2-yl)-5-(1-((2-(trimethylsilyl)ethoxy)methyl)-1*H*-pyrazol-4-yl)pyridin-2-amine (RAR-10-43, 122)

This material was prepared using the protocol described in RAR-9-25. Yields the desired product as a fluorescent yellow solid, 32 mg, 60%. HRMS: 533.3050, HPLC: 9.870. ¹H NMR (700 MHz, Chloroform-*d*) δ 8.74 (d, *J* = 5.2 Hz, 1H), 8.41 (dd, *J* = 5.4, 2.5 Hz, 1H), 8.30 (dd, *J* = 5.4, 2.5 Hz, 1H), 7.82 (dd, *J* = 17.1, 5.5 Hz, 2H), 7.54 (dd, *J* = 8.9, 5.4 Hz, 1H), 6.70 (dd, *J* = 5.4, 2.3 Hz, 1H), 6.61 (dt, *J* = 8.4, 3.7 Hz, 1H), 5.48 (d, *J* = 5.5 Hz, 2H), 3.67 – 3.59 (m, 2H), 3.37 (q, *J* = 6.3 Hz, 4H), 2.11 – 2.05 (m, 4H), 1.62 (s, 9H). ¹³C NMR (176 MHz, cdcl₃) δ 146.77, 136.72, 132.50, 124.89, 119.32, 115.12, 109.53, 92.00, 80.23, 66.59, 51.48, 47.98, 29.08, 25.36, 17.65, -1.61.

N-(tert-butyl)-5-(1H-pyrazol-4-yl)-3-(6-(pyrrolidin-1-yl)benzo[d]oxazol-2-yl)pyridin-2-amine (RAR-11-6, 123)

To a flask were added 97.0 mg of RAR-10-43, dissolved in 2 mL of MeOH. To this yellow solution were added 3 mL of 4 N HCl (in dioxanes/water). The resulting orange solution was allowed to stir at rt for 12 hours. Once complete, the solvent was removed and the residue was purified by column chromatography (0-10% DCM/MeOH) to give an orange residue, 70 mg, quant. HPLC: 7.591, HRMS: 403.2233, purity: 90%. ¹H NMR (700 MHz, Methanol-d₄) δ 8.75 (t, J = 20.0 Hz, 1H), 8.25 (s, 1H), 8.12 (s, 2H), 7.69 – 7.63 (m, 1H), 7.58 (d, J = 8.6 Hz, 2H), 6.85 (s, 1H), 6.77 (d, J = 9.0 Hz, 1H), 3.40 (s, 4H), 2.11 (s, 4H), 1.69 (s, 9H).

3-(benzo[d]oxazol-2-yl)-5-bromo-N-(tert-butyl)pyridin-2-amine (CCG-264187, RAR-6-56)

To a sealed tube were added 160 mg of 2-(5-bromo-2-chloropyridin-3-yl)benzo[d]oxazole (0.517 mmol), and 0.28 mL of tert-butylamine (2.58 mmol). All materials were then dissolved in 3 mL of dry DMF, and the solution was heated to 120 °C for 12-18 h. Once complete, the reaction was cooled to room temperature and quenched with brine (30 mL). The aqueous layer was extracted with EtOAc:Hexanes (1:1) (3 x 30 mL). The combined organic layer was then dried over Na₂SO₄ and solvent was removed to give the desired product. Yields a fluffy yellow solid, 179 mg, 80%. HPLC: 8.010, LRMS: 288. ¹H NMR (500 MHz, Chloroform-d) δ 8.36 (d, J = 2.6 Hz, 1H), 8.28 (d, J = 2.3 Hz, 1H), 7.88 (d, J = 7.8 Hz, 1H), 7.73 (dd, J = 7.0, 2.6 Hz, 2H), 7.38 – 7.35 (m, 2H), 1.59 (s, 9H). ¹³C NMR (126 MHz, cdcl₃) δ 163.02, 160.90, 151.62, 151.19, 141.50, 138.48, 124.87, 123.02, 119.94, 110.58, 104.62, 59.10, 29.30, 0.25.

5-bromo-2-(tert-butylamino)-N-(4-chloro-2-hydroxyphenyl)nicotinamide (CCG-264221, RAR-6-59)

To a sealed tube were added 274.1 mg of 5-bromo-2-chloro-N-(5-chloro-2-hydroxyphenyl)nicotinamide (0.76 mmol), and 0.400 mL of tert-butylamine (3.8 mmol). All materials were then dissolved in 5 mL of dry DMF, and the solution was heated to 120 °C for 12-18 h. Once complete, the solution was cooled to room temperature, and quenched with brine (30 mL). The aqueous layer was then extracted with EtOAc (3 x 30 mL). The combined organic layer was washed with brine (1 x 30 mL) and then dried over Na₂SO₄. The solvent was then removed under pressure to give the crude product, which was purified by column chromatography (0-100% EtOAc/Hexanes). Yields an orange solid, 90.0 mg, 30%. HPLC: 6.800, LRMS: 412 [M+MeOH]. ¹H NMR (500 MHz, Chloroform-d) δ 8.54 (d, J = 2.9 Hz, 1H), 8.46 (d, J = 2.5 Hz, 1H), 8.30 (d, J = 12.2 Hz, 1H), 7.68 (s, 1H), 7.08 (s, 1H), 6.96 (d, J = 8.2 Hz, 1H), 1.35 (s, 9H).

3-(benzo[d]oxazol-2-yl)-N-(tert-butyl)-5-(1H-pyrrol-3-yl)pyridin-2-amine (CCG-264222, RAR-7-5)

To a three neck flask were added 100 mg of Cs₂CO₃ (0.289 mmol), 43.7 mg of tert-butyl 4-(4,4,5,5-tetramethyl-1,3,2-dioxaborolan-2-yl)-1H-pyrazole-1-carboxylate (0.14 mmol), and tetrakis(triphenylphosphine)palladium(0) (0.014 mmol). The materials were degassed with 3 cycles of evacuation and back fill with nitrogen. To the flask were added 56.0 mg of 3-(benzo[d]oxazol-2-yl)-5-bromo-N-(tert-butyl)pyridin-2-amine (0.144 mmol) and dissolved in 4

mL of 3:1 Dioxanes:Water. The solution was then degassed with an additional 6 cycles of evacuation and backfill with nitrogen. The three neck flask was fitted with a reflux condenser, and the solution was heated to 100 °C for 12-24 h. Once complete, the solution was cooled to room temperature, and then passed through a pad of celite. The mother liquor was then diluted with water and extracted with EtOAc (2 x 25 mL). The combined organic layer was washed with brine (1 x 15 mL) and then dried over Na₂SO₄ and the product was evaporated onto silica gel. The crude material was purified by column chromatography to yield the final product. Product is a bright yellow solid, 7.5 mg, 30%. MS: 333 [M+1], HPLC: 6.900. ¹H NMR (700 MHz, Chloroform-d) δ 8.79 (s, 1H), 8.49 (s, 1H), 8.39 (s, 1H), 7.87 (s, 2H), 7.74 (s, 1H), 7.59 (s, 1H), 7.37 (s, 2H), 1.64 (d, J = 4.6 Hz, 9H).

N-(tert-butyl)-3-(6-chlorobenzo[d]oxazol-2-yl)-5-(1H-pyrrol-3-yl)pyridin-2-amine (CCG-264223, RAR-6-67)

To a three neck flask were added 90.2 mg of Cs₂CO₃ (0.236 mmol), 46.0 mg of (1-(triisopropylsilyl)-1H-pyrrol-3-yl)boronic acid (0.177 mmol), 45.0 mg of 5-bromo-N-(tert-butyl)-3-(6-chlorobenzo[d]oxazol-2-yl)pyridin-2-amine (0.118 mmol) and tetrakis(triphenylphosphine)palladium(0) (0.014 mmol). All materials dissolved in 4 mL of 3:1 Dioxanes:Water. The solution was then degassed with 8 cycles of evacuation and backfill with nitrogen. The three neck flask was fitted with a reflux condenser, and then the solution was heated to 100 °C for 12 h. Once complete, the solution was cooled to room temperature and passed through a pad of celite. The mother liquor was then diluted with water and extracted with EtOAc (3 x 30 mL). The combined organic layer was then dried over Na₂SO₄ and the crude material was purified by column chromatography. Yields a white solid, 11.5 mg, 26.5%. HPLC: 6.8, LRMS: 371. ¹H NMR (500 MHz, Chloroform-d) δ 8.54 (t, J = 3.3 Hz, 1H), 8.46 (t, J = 2.3 Hz, 1H), 7.43 (d, J = 9.2 Hz, 1H), 7.32 (d, J = 8.6 Hz, 1H), 7.23 – 7.20 (m, 2H), 7.07 – 7.03 (m, 1H), 6.98 (d, J = 8.4 Hz, 1H), 1.60 (s, 9H).

2-amino-N-(4-chloro-2-hydroxyphenyl)-5-(1H-pyrrol-3-yl)nicotinamide (CCG-264240, RAR-6-72)

To a flask were added 11 mg of 2-(tert-butylamino)-N-(5-chloro-2-hydroxyphenyl)-5-(1H-pyrrol-3-yl)nicotinamide (0.029 mmol) and 0.46 mL of TFA (5.7 mmol) dissolved in 2 mL of toluene. The solution was heated to 70 °C for 3 h. Once complete, the reaction was quenched with saturated Na₂CO₃ and extracted with DCM (3 x 30 mL). The combined organic layer was dried over Na₂SO₄ and purified by column chromatography. Product is a yellow solid, 3 mg, 30%. HPLC: 7.199. ¹H NMR (500 MHz, DMSO-d₆) δ 10.94 (s, 1H), 10.86 (s, 1H), 8.65 (dt, J = 11.3, 3.4 Hz, 1H), 8.38 (dd, J = 5.1, 2.6 Hz, 1H), 7.47 (t, J = 3.3 Hz, 1H), 7.39 – 7.33 (m, 2H), 7.23 – 7.16 (m, 3H).

2-amino-5-bromo-N-(4-(dimethylamino)-2-hydroxyphenyl)nicotinamide (CCG-264241, RAR-6-74-p1)

To a three neck flask were added 218.3 mg of Cs₂CO₃ (0.5 mmol), 80 mg of tert-butyl 4-(4,4,5,5-tetramethyl-1,3,2-dioxaborolan-2-yl)-1H-pyrazole-1-carboxylate (0.3mmol), tetrakis(triphenylphosphine)palladium(0) (0.014 mmol) and 100 mg of 5-bromo-N-(tert-butyl)-3-(6-chlorobenzo[d]oxazol-2-yl)pyridin-2-amine (0.3 mmol). All materials were dissolved in 4 mL

of 3:1 Dioxanes:Water, and the solution was degassed with 7 cycles of evacuation and backfill with nitrogen. The solution was heated to 100 °C for 12 h. Once complete, the solution was cooled to room temperature, and passed through a pad of celite. The mother liquor was diluted with water and extracted with EtOAc (3 x 30 mL). The combined organic layer was dried over Na₂SO₄ and the crude product was purified by column chromatography. Light orange solid, 79.2 mg, 79%. HPLC: 7.199, LRMS: 371. 1H NMR (500 MHz, Chloroform-d) δ 11.47 (s, 1H), 9.36 (s, 1H), 8.53 (dt, J = 14.5, 2.3 Hz, 2H), 7.08 (d, J = 2.2 Hz, 1H), 7.00 – 6.97 (m, 1H), 6.90 (dd, J = 8.5, 2.2 Hz, 1H), 2.92 (d, J = 1.8 Hz, 6H).

2-amino-N-(4-chloro-2-hydroxyphenyl)-5-(1-(piperidin-4-yl)-1H-pyrazol-4-yl)nicotinamide (CCG-264262, RAR-6-75)

To a flask were added 21.5 mg of tert-butyl 4-(4-(6-(tert-butylamino)-5-((5-chloro-2-hydroxyphenyl)carbamoyl)pyridin-3-yl)-1H-pyrazol-1-yl)piperidine-1-carboxylate (0.0378 mmol) and 2 mL of toluene. To this dark red solution were added 0.46 mL of TFA (7.56 mmol) and the solution was heated to 70 °C for 3 h. Once complete, the solution was cooled to room temperature and quenched with saturated Na₂CO₃ and then extracted with EtOAc (3 x 30 mL). The combined organic layer was dried over Na₂SO₄ and purified by column chromatography. Product is a yellow solid⁴⁴, 1 mg, 6%. MS: 413 [M+1], HPLC: 6.800. 1H NMR (700 MHz, DMSO-d₆) δ 8.25 (s, 1H), 8.11 (d, J = 5.8 Hz, 1H), 7.85 – 7.80 (m, 1H), 7.77 (s, 1H), 7.72 (s, 1H), 7.44 – 7.38 (m, 2H), 6.90 (s, 1H), 6.21 (d, J = 6.6 Hz, 2H), 5.02 (s, 2H), 2.11 – 2.03 (m, 2H), 1.96 (s, 3H), 1.93 – 1.86 (m, 5H), 1.76 – 1.69 (m, 6H).

3-(benzo[d]oxazol-2-yl)-5-(1H-pyrazol-4-yl)pyridin-2-amine (CCG-264485, RAR-7-9)

To a flask were added 35.5 mg of 3-(benzo[d]oxazol-2-yl)-N-(tert-butyl)-5-(1H-pyrazol-4-yl)pyridin-2-amine (0.106 mmol), and 1.5 mL of toluene. To this light blue solution were added 0.16 mL of TFA (2.13 mmol), and the solution was heated to 70 °C for 3 h. Once complete, the solution was cooled to room temperature and quenched with saturated Na₂CO₃ and then extracted with EtOAc (3 x 10 mL). The combined organic layer was then dried over Na₂SO₄ and the crude product was purified by column chromatography. Product is a bright yellow solid, 2.5 mg, 8.5%. MS: 278 [M+1], HPLC: 4.77. 1H NMR (700 MHz, DMSO-d₆) δ 8.55 (d, J = 2.3 Hz, 1H), 8.49 (d, J = 2.1 Hz, 1H), 8.12 (s, 2H), 7.85 (d, J = 7.7 Hz, 1H), 7.81 (d, J = 7.5 Hz, 1H), 7.49 – 7.41 (m, 3H).

3-(benzo[d]oxazol-2-yl)-N-(tert-butyl)-5-(1H-pyrazol-4-yl)pyridin-2-amine (RAR-8-6)

To a flask were added 84.2 mg of RAR-8-4, 65.3 mg of tert-butyl 4-(4,4,5,5-tetramethyl-1,3,2-dioxaborolan-2-yl)-1H-pyrazole-1-carboxylate, 156.7 mg of Cs₂CO₃ and cat. Palladium tetrakis. All materials were then dissolved in 3 mL of dioxanes, and the solution was degassed with six cycles of evacuation and backfill with nitrogen. Once degassed, the reaction was heated to 110 °C for 18-24 h. Once complete, the solution was cooled to rt and passed through a pad of celite. The filtrate was then washed with brine (1 x 30 mL) and then dried over Na₂SO₄. The crude material was purified by column chromatography to yields a yellow solid, 24.5 mg, 30%. 1H NMR (500 MHz, Chloroform-d) δ 8.78 (s, 1H), 8.52 – 8.47 (m, 1H), 8.39 (dd, J = 5.1, 2.5 Hz, 1H), 7.87 (s,

2H), 7.76 – 7.72 (m, 2H), 7.65 – 7.61 (m, 3H), 7.39 – 7.34 (m, 4H), 6.37 (s, 1H), 1.63 (d, J = 1.7 Hz, 9H).

1-(4-(5-(benzo[d]oxazol-2-yl)-6-(tert-butylamino)pyridin-3-yl)-1H-pyrazol-1-yl)prop-2-en-1-one (RAR-8-9)

To a dried flask were added 0.05 mL of acrylic acid, dissolved in 2 mL of DCM. The solution was cooled to 0 °C where upon 0.01 mL of DMF and 0.05 mL of oxalyl chloride were added consecutively. The solution was then warmed to rt for 1 h. Once complete, the solvent was removed, and the crude material was moved forward without characterization. This acid chloride was then dissolved in DCM (3 mL) and the solution was cooled to 0 °C and 24.5 mg of RAR-8-6 were added in one portion. Then 0.04 mL of DIPEA were added to the solution and then reaction was run for 2 h. Once complete, the reaction was quenched with water and extracted with EtOAc (3 x 30 mL). The combined organic layer was washed with brine (1 x 25 mL) and then dried over Na₂SO₄. The crude material was then purified by column chromatography to yield the product as a yellow solid, 15 mg, 52%. LRMS: 388, HPLC: 10.48. ¹H NMR (700 MHz, Chloroform-d) δ 8.90 (s, 1H), 8.56 (s, 1H), 8.54 (d, J = 2.5 Hz, 1H), 8.44 (d, J = 2.5 Hz, 1H), 8.08 (s, 1H), 7.76 – 7.73 (m, 1H), 7.64 – 7.58 (m, 2H), 7.39 – 7.37 (m, 2H), 6.79 (dd, J = 17.3, 1.4 Hz, 1H), 6.13 (dd, J = 10.5, 1.5 Hz, 1H), 1.63 (s, 9H). ¹³C NMR (176 MHz, cdcl₃) δ 162.91, 161.51, 155.50, 149.51, 148.59, 141.78, 141.33, 133.91, 133.42, 126.18, 125.25, 124.58, 124.19, 122.94, 119.64, 113.64, 110.31, 106.61, 104.21, 52.05, 29.20.

1-(4-(6-amino-5-(benzo[d]oxazol-2-yl)pyridin-3-yl)-1H-pyrazol-1-yl)prop-2-en-1-one (CCG-265175, RAR-8-12)

To a flask were added 10 mg of 1-(4-(5-(benzo[d]oxazol-2-yl)-6-(tert-butylamino)pyridin-3-yl)-1H-pyrazol-1-yl)prop-2-en-1-one (0.026 mmol) and 2 mL of xylenes. To this solution were added 0.200 mL of TFA (2.6 mmol) and the solution was heated to 70 °C overnight. Once complete, the solution was cooled to room temperature and then quenched with saturated Na₂CO₃ and then extracted with EtOAc (3 x 10 mL). The combined organic layer was then dried over Na₂SO₄ and the crude product was purified by column chromatography. Product is a yellow solid, 1.0 mg, 12%. MS: 334 [M+1], HPLC: 4.40. ¹H NMR (700 MHz, Chloroform-d) δ 8.45 (s, 1H), 8.39 (s, 1H), 7.89 (s, 2H), 7.79 – 7.73 (m, 1H), 7.64 – 7.58 (m, 1H), 7.41 – 7.38 (m, 2H), 6.46 – 6.39 (m, 1H), 6.12 (ddd, J = 17.3, 14.2, 10.5 Hz, 1H), 5.86 – 5.81 (m, 1H).

3-(6-(4-ethylpiperazin-1-yl)benzo[d]oxazol-2-yl)-5-(1-(piperidin-4-yl)-1H-pyrazol-4-yl)pyridin-2-amine (CCG-270962, RAR-10-46)

To a flask were added 42.0 mg of tert-butyl 4-(4-(6-(tert-butylamino)-5-(6-(4-ethylpiperazin-1-yl)benzo[d]oxazol-2-yl)pyridin-3-yl)-1H-pyrazol-1-yl)piperidine-1-carboxylate (0.067 mmol) and 2 mL of toluene. To this solution were added 0.3 mL of TFA (3 mmol) and the solution was heated to 70 °C for 3 h. Once complete, the reaction was cooled to room temperature and the toluene was removed by azeotrope with MeOH to give the product as a TFA salt. The crude product was then purified by preparatory plate. MS: 633, ¹H NMR (700 MHz, Chloroform-d) δ 8.56 (s, 1H), 8.50 (s, 1H), 7.99 (d, J = 13.0 Hz, 1H), 7.36 (s, 1H), 6.72 (s, 1H), 3.66 (d, J = 2.9 Hz,

1H), 3.36 (d, J = 2.9 Hz, 8H), 3.03 – 3.00 (m, 2H), 2.75 (td, J = 8.0, 7.6, 3.0 Hz, 2H), 2.35 (d, J = 13.4 Hz, 2H), 2.05 (d, J = 3.2 Hz, 2H), 1.77 (s, 2H), 1.12 – 1.10 (m, 3H).

5-(1H-pyrazol-4-yl)-3-(6-(pyrrolidin-1-yl)benzo[d]oxazol-2-yl)pyridin-2-amine (CCG-270964, RAR-10-58)

To a flask were added 82 mg of N-(tert-butyl)-3-(6-(pyrrolidin-1-yl)benzo[d]oxazol-2-yl)-5-(1-((2-(trimethylsilyl)ethoxy)methyl)-1H-pyrazol-4-yl)pyridin-2-amine (0.15 mmol), 0.4 mL of TFA (5.3 mmol) all of which are dissolved in 5 mL of DMF. The bright orange solution was allowed to stir overnight or until complete. Once complete, the solvent was removed under pressure and the crude material was purified by column chromatography (5% EtOAc/MeOH). The final product was collected, and the solvent was removed to give the product as a bright yellow solid. MS: 347.1717 [M+1], HPLC: 5.229. ¹H NMR (500 MHz, DMSO-d₆) δ 8.54 (m, 1H), 8.44 (m, 1H), 8.35 (m, 2H), 7.95 (m, 2H), 7.55 (m, 1H), 7.02 (s, 1H), 6.61 (s, 1H), 3.50 (m, 4H), 2.11-2.05 (m, 4H).

2-(2-amino-5-(1-(piperidin-4-yl)-1H-pyrazol-4-yl)pyridin-3-yl)-N-(pyridin-4-ylmethyl)benzo[d]oxazol-6-amine (CCG-270957, RAR-10-11)

To a flask were added 20 mg of tert-butyl 4-(4-(6-(tert-butylamino)-5-(6-((pyridin-4-ylmethyl)amino)benzo[d]oxazol-2-yl)pyridin-3-yl)-1H-pyrazol-1-yl)piperidine-1-carboxylate (0.032 mmol) and 0.05 mL of TFA (0.39 mmol) all of which were dissolved in 2 mL of toluene. The solution was heated to 70 °C for 3 hours or until complete. Once complete, the solution was cooled to room temperature and then the toluene was removed under pressure. The crude oil was then purified by preparatory TLC plate (5% EtOAc/MeOH) to give the final product as a yellow solid. HPLC: 5.006 MS: 467.2297 [free base] and 695.2556 [M+2TFA] ¹H NMR (500 MHz, Chloroform-d) δ 8.84 (d, J = 13.5 Hz, 2H), 8.74 (d, J = 5.5 Hz, 1H), 8.06 (d, J = 5.1 Hz, 1H), 7.97 (d, J = 5.2 Hz, 1H), 7.81 (d, J = 5.4 Hz, 1H), 7.62 – 7.58 (m, 1H), 7.48 (s, 1H), 6.09 (s, 1H), 4.71 (d, J = 6.3 Hz, 1H), 3.65 (d, J = 20.8 Hz, 1H), 3.27 (s, 1H), 3.06 (s, 1H), 2.64 (s, 1H), 2.05 (s, 2H), 1.89 (s, 2H).

2-(2-amino-5-(1-(piperidin-4-yl)-1H-pyrazol-4-yl)pyridin-3-yl)-N-(pyridin-3-ylmethyl)benzo[d]oxazol-6-amine (CCG-270958, RAR-10-21)

To a flask were added 32 mg of tert-butyl 4-(4-(6-(tert-butylamino)-5-(6-((pyridin-3-ylmethyl)amino)benzo[d]oxazol-2-yl)pyridin-3-yl)-1H-pyrazol-1-yl)piperidine-1-carboxylate (0.032 mmol), dissolved in 2 mL of toluene. To this solution were added 0.05 mL of TFA (0.39 mmol) and the solution was heated to 70 °C until complete. Once complete, the reaction was cooled to room temperature and the solvent was removed under pressure. The crude oil was then purified by preparatory TLC plate, to give the product as yellow solid. HPLC: 4.072 MS: 468.1769, ¹H NMR (500 MHz, Chloroform-d) δ 8.64 (s, 1H), 8.57 (s, 1H), 8.49 (s, 1H), 8.34 (s, 1H), 7.94 (m, 2H), 7.86 (s, 1H), 7.47 (m, 2H), 7.05 (m, 2H), 4.53 (s, 2H), 3.74 (s, 1H), 3.15 (m, 2H), 3.02 (m, 2H), 2.06 (m, 2H), 1.83 (m, 2H).

tert-butyl 4-(4-(6-(tert-butylamino)-5-(6-chlorobenzo[d]oxazol-2-yl)pyridin-3-yl)-1H-pyrazol-1-yl)piperidine-1-carboxylate (RAR-10-2, RAR-13-31)

To a three neck flask were added 149.1 mg of RAR-9-99 (0.525 mmol), 234 mg of RAR-9-54 (1.05 mmol), 192.0 mg of Na₂CO₃ (1.58 mmol), and Pd(PPh₃)₂Cl₂ (0.0014 mmol). All materials were then dissolved in 7.5 mL of Dioxanes:Water (3:1). The solution was then degassed with 9 cycles of evacuation and backfill with nitrogen. The solution was then heated to 112 °C for 3-12 h. Once complete, the solution was cooled to room temperature and then passed through a pad of celite before being purified by column chromatography. Yields a fluorescent yellow residue, 76.1 mg, 25%. HRMS: 551.2528, HPLC: 8.34. ¹H NMR (500 MHz, Chloroform-d) δ 8.62 (s, 1H), 8.27 (dd, J = 4.8, 2.0 Hz, 1H), 8.22 (dd, J = 7.8, 2.0 Hz, 1H), 7.72 (ddt, J = 13.3, 6.9, 1.4 Hz, 3H), 7.55 (d, J = 2.0 Hz, 1H), 7.32 (d, J = 2.0 Hz, 1H), 7.31 (t, J = 1.7 Hz, 1H), 3.88 (s, 1H), 3.71 – 3.65 (m, 2H), 3.31 (ddd, J = 13.6, 7.7, 3.6 Hz, 2H), 2.31 (dd, J = 9.2, 5.9 Hz, 2H), 1.97 – 1.90 (m, 2H), 1.46 (s, 9H). ¹³C NMR (126 MHz, cdcl₃) δ 151.64, 136.94, 132.55, 131.78, 128.79, 125.29, 120.13, 111.11, 110.84, 62.35, 52.07, 49.75, 29.95, 29.45, 28.66.

tert-butyl 4-(4-(6-(tert-butylamino)-5-(6-((pyridin-4-ylmethyl)amino)benzo[d]oxazol-2-yl)pyridin-3-yl)-1H-pyrazol-1-yl)piperidine-1-carboxylate (RAR-10-10)

To a microwave vessel were added 25.4 mg of RAR-10-2 (0.045 mmol), Pd₂(dba)₃ (0.0014 mmol), XPhos (0.007 mmol), 15.6 mg of NaOtBu (0.14 mmol) and 0.01 mL of 4-picolyamine (0.064 mmol). The materials were dissolved in 3 mL of toluene, and the solution was degassed with 5 cycles of evacuation and back fill with nitrogen. The solution was heated to 160 °C for 30-40 mins. Once complete, the solution was rinsed through a pad of celite and the filtrate was purified by column chromatography to yield the desired product. Yields a fluorescent yellow solid, 10 mg, 35%. HRMS: 623.3444, HPLC: 6.809. ¹H NMR (500 MHz, Chloroform-d) δ 8.64 (s, 1H), 8.59 (s, 8H), 8.56 (s, 7H), 8.39 (s, 1H), 8.22 (s, 1H), 7.50 (d, J = 8.5 Hz, 1H), 7.34 (s, 2H), 6.67 (s, 2H), 4.47 (s, 2H), 4.30 (s, 1H), 3.93 (s, 2H), 3.36 (s, 1H), 2.13 (s, 2H), 1.95 (s, 2H), 1.62 – 1.59 (m, 9H), 1.50 (d, J = 1.7 Hz, 9H).

tert-butyl 4-(4-(6-(tert-butylamino)-5-(6-((pyridin-3-ylmethyl)amino)benzo[d]oxazol-2-yl)pyridin-3-yl)-1H-pyrazol-1-yl)piperidine-1-carboxylate (RAR-10-16)

To a microwave vessel were added 48 mg of RAR-10-2 (0.087 mmol), Pd₂(dba)₃ (0.0014 mmol), XPhos (0.007 mmol), 39.2 mg of NaOtBu (0.35 mmol) and 0.05 mL of 3-picolyamine (0.12 mmol). The materials were then dissolved in 3 mL of toluene, and then degassed with 5 cycles of evacuation and backfill with nitrogen. The solution was then heated to 160 °C for 30-45 mins. Once complete, the reaction was cooled to room temperature, and then passed through a pad of celite. The filtrate was then purified by column chromatography to give the desired product. Yields a light yellow fluorescent solid, 19 mg, 35%. HRMS: 623.34, HPLC: 6.513. ¹H NMR (700 MHz, Chloroform-d) δ 8.57 (s, 2H), 8.39 (d, J = 2.4 Hz, 1H), 8.18 (d, J = 8.0 Hz, 1H), 7.98 – 7.95 (m, 2H), 7.83 – 7.79 (m, 1H), 7.49 (s, 1H), 7.36 (d, J = 7.2 Hz, 2H), 6.68 (dd, J = 8.6, 2.2 Hz, 2H), 5.14 (s, 1H), 4.33 (s, 2H), 3.74 (m, 1H), 3.60-3.56 (m, 1H), 3.46 – 3.44 (m, 2H), 2.22 (m, 2H), 1.97 (m, 2H), 1.61 (s, 9H), 1.50 (s, 9H).

N-(tert-butyl)-3-(6-chlorobenzo[d]oxazol-2-yl)-5-(1H-pyrazol-4-yl)pyridin-2-amine (RAR-10-18)

To a flask were added 250 mg of RAR-10-2 (0.657 mmol), 420.6 mg of tert-butyl 4-(4,4,5,5-tetramethyl-1,3,2-dioxaborolan-2-yl)-1H-pyrazole-1-carboxylate (1.31 mmol), Pd(PPh₃)₂Cl₂

(0.065 mmol) and 246.3 mg of Na₂CO₃ (2 mmol). All materials were then dissolved in 7 mL of Dioxanes:Water (3:1). The solution was then degassed with 8 cycles of evacuation and back fill with nitrogen before being heated to 110 °C for 12 h. once complete, the solution was cooled to room temperature, and then passed through a pad of celite. The filtrate was then purified by column chromatography to give the desired product. Yields a fluorescent yellow solid, 161 mg, 67%. HRMS: 368.1268, HPLC: 8.517. ¹H NMR (500 MHz, Chloroform-d) δ 8.65 (s, 1H), 8.50 (s, 1H), 8.35 (s, 1H), 7.87 (d, J = 4.1 Hz, 2H), 7.53 (d, J = 7.5 Hz, 1H), 7.35 (d, J = 8.5 Hz, 1H), 7.25 (s, 1H), 1.62 (s, 9H). ¹³C NMR (126 MHz, cdcl₃) δ 162.75, 159.16, 154.61, 140.42, 139.84, 135.45, 133.85, 128.87, 126.63, 125.78, 121.83, 119.98, 110.91, 104.62, 59.09, 29.25.

tert-butyl 4-(6-(tert-butylamino)-5-(6-chlorobenzo[d]oxazol-2-yl)pyridin-3-yl)-1H-pyrazole-1-carboxylate (RAR-10-20)

To a flask were added 161 mg of RAR-10-18 (0.435 mmol), cat. DMAP and 0.12 mL of Boc₂O (0.478 mmol). All materials were dissolved in 20 mL of THF and allowed to stir at room temperature for 1 h. Once complete, the solvent was removed under pressure, and the crude product was brought back up in EtOAc. The organic layer was rinsed with water (1 x 30 mL) and brine (1 x 50 mL) before drying the organic layer over Na₂SO₄. The solvent was removed under pressure to give the desired product. *Product was moved forward without further characterization.* Yields a yellow solid, 171.1 mg, 84%. HRMS: 468.17, HPLC: 7.385

tert-butyl 4-(4-(6-(tert-butylamino)-5-(6-(4-ethylpiperazin-1-yl)benzo[d]oxazol-2-yl)pyridin-3-yl)-1H-pyrazol-1-yl)piperidine-1-carboxylate (RAR-10-40)

To a three necked flask were added 61 mg of RAR-10-2 (0.09 mmol), 37.8 mg of NaOtBu (0.27 mmol), 0.04 mL of ethylpiperazine (0.13 mmol), XPhos (2 umol) and Pd₂(dba)₃ (1 umol). All materials were dissolved in 4 mL of dioxanes and then the solution was degassed with 8 cycles of evacuation and backfill with nitrogen. The solution was then heated to 110 °C for 18 h. Once complete, the reaction was cooled to room temperature, and then passed through a pad of celite. The filtrate was then purified by column chromatography to give the desired product. Yields a light yellow solid, 42.0 mg, 66%. HRMS: 629.3915, HPLC: 6.700. ¹H NMR (700 MHz, Chloroform-d) δ 8.67 (s, 1H), 8.40 (d, J = 2.4 Hz, 1H), 8.27 (d, J = 2.5 Hz, 1H), 7.77 (s, 1H), 7.64 (s, 1H), 7.57 (d, J = 8.7 Hz, 1H), 7.10 (d, J = 2.2 Hz, 1H), 7.00 (dd, J = 8.7, 2.2 Hz, 1H), 4.31 (tt, J = 11.6, 4.1 Hz, 2H), 3.31 (t, J = 5.0 Hz, 4H), 2.72 (t, J = 5.0 Hz, 4H), 2.55 (q, J = 7.2 Hz, 2H), 2.21 – 2.16 (m, 2H), 1.97 (tt, J = 11.7, 6.2 Hz, 2H), 1.61 (s, 9H), 1.17 (t, J = 7.2 Hz, 3H). ¹³C NMR (176 MHz, cdcl₃) δ 160.85, 154.74, 150.97, 150.24, 147.71, 136.03, 134.89, 133.15, 122.76, 120.19, 119.56, 115.89, 114.73, 104.64, 97.74, 80.07, 59.61, 52.67, 52.33, 51.89, 49.88, 29.44, 28.60, 11.79.

3.7 References

- (1) Rowlands, R.; Cato, M. C.; Waldschmidt, H. V.; Bouley, R. A.; Chen, Q.; Avramova, L.; Larsen, S. D.; Tesmer, J. J. G.; White. Structure-Based Design of Selective, Covalent G Protein-Coupled Receptor Kinase 5 Inhibitors | ACS Medicinal Chemistry Letters <https://pubs.acs.org/doi/abs/10.1021/acsmchemlett.9b00365> (accessed Dec 23, 2019).

- (2) Waldschmidt, H. V.; Homan, K. T.; Cruz-Rodríguez, O.; Cato, M. C.; Waninger-Saroni, J.; Larimore, K. M.; Cannavo, A.; Song, J.; Cheung, J. Y.; Kirchhoff, P. D.; et al. Structure-Based Design, Synthesis, and Biological Evaluation of Highly Selective and Potent G Protein-Coupled Receptor Kinase 2 Inhibitors. *J. Med. Chem.* **2016**, *59* (8), 3793–3807. <https://doi.org/10.1021/acs.jmedchem.5b02000>.
- (3) Waldschmidt, H. V.; Homan, K. T.; Cato, M. C.; Cruz-Rodríguez, O.; Cannavo, A.; Wilson, M. W.; Song, J.; Cheung, J. Y.; Koch, W. J.; Tesmer, J. J. G.; et al. Structure-Based Design of Highly Selective and Potent G Protein-Coupled Receptor Kinase 2 Inhibitors Based on Paroxetine. *J. Med. Chem.* **2017**, *60* (7), 3052–3069. <https://doi.org/10.1021/acs.jmedchem.7b00112>.
- (4) McInnes, C. Virtual Screening Strategies in Drug Discovery. *Curr. Opin. Chem. Biol.* **2007**, *11* (5), 494–502. <https://doi.org/10.1016/j.cbpa.2007.08.033>.
- (5) Oprea, T. I.; Matter, H. Integrating Virtual Screening in Lead Discovery. *Curr. Opin. Chem. Biol.* **2004**, *8* (4), 349–358. <https://doi.org/10.1016/j.cbpa.2004.06.008>.
- (6) Hughes, J.; Rees, S.; Kalindjian, S.; Philpott, K. Principles of Early Drug Discovery. *Br. J. Pharmacol.* **2011**, *162* (6), 1239–1249. <https://doi.org/10.1111/j.1476-5381.2010.01127.x>.
- (7) Hoffmann, T.; Gastreich, M. The next Level in Chemical Space Navigation: Going Far beyond Enumerable Compound Libraries. *Drug Discov. Today* **2019**, *24* (5), 1148–1156. <https://doi.org/10.1016/j.drudis.2019.02.013>.
- (8) Muegge, I.; Enyedy, I. J. Virtual Screening for Kinase Targets. *Curr. Med. Chem. Schiph.* **2004**, *11* (6), 693–707. <http://dx.doi.org/10.2174/0929867043455684>.
- (9) van Linden, O. P. J.; Kooistra, A. J.; Leurs, R.; de Esch, I. J. P.; de Graaf, C. KLIFS: A Knowledge-Based Structural Database To Navigate Kinase–Ligand Interaction Space. *J. Med. Chem.* **2014**, *57* (2), 249–277. <https://doi.org/10.1021/jm400378w>.
- (10) Pipeline Pilot Scientific Application Overview | Dassault Systèmes BIOVIA <https://www.3dsbiovia.com/products/collaborative-science/biovia-pipeline-pilot/> (accessed Jan 2, 2020).
- (11) Dahlin, J. L.; Nissink, J. W. M.; Strasser, J. M.; Francis, S.; Higgins, L.; Zhou, H.; Zhang, Z.; Walters, M. A. PAINS in the Assay: Chemical Mechanisms of Assay Interference and Promiscuous Enzymatic Inhibition Observed during a Sulfhydryl-Scavenging HTS. *J. Med. Chem.* **2015**, *58* (5), 2091–2113. <https://doi.org/10.1021/jm5019093>.
- (12) Ekins, S.; Mestres, J.; Testa, B. In Silico Pharmacology for Drug Discovery: Methods for Virtual Ligand Screening and Profiling. *Br. J. Pharmacol.* **2007**, *152* (1), 9–20. <https://doi.org/10.1038/sj.bjp.0707305>.
- (13) Foloppe, N.; Fisher, L. M.; Howes, R.; Potter, A.; Robertson, A. G. S.; Surgenor, A. E. Identification of Chemically Diverse Chk1 Inhibitors by Receptor-Based Virtual Screening. *Bioorg. Med. Chem.* **2006**, *14* (14), 4792–4802. <https://doi.org/10.1016/j.bmc.2006.03.021>.
- (14) Lyne, P. D. Structure-Based Virtual Screening: An Overview. *Drug Discov. Today* **2002**, *7* (20), 1047–1055. [https://doi.org/10.1016/S1359-6446\(02\)02483-2](https://doi.org/10.1016/S1359-6446(02)02483-2).
- (15) Homan, K. T.; Waldschmidt, H. V.; Glukhova, A.; Cannavo, A.; Song, J.; Cheung, J. Y.; Koch, W. J.; Larsen, S. D.; Tesmer, J. J. G. Crystal Structure of G Protein-Coupled Receptor Kinase 5 in Complex with a Rationally Designed Inhibitor. *J. Biol. Chem.* **2015**, *290* (34), 20649–20659. <https://doi.org/10.1074/jbc.M115.647370>.

- (16) Boguth, C. A.; Singh, P.; Huang, C.; Tesmer, J. J. G. Molecular Basis for Activation of G Protein-coupled Receptor Kinases. *EMBO J.* **2010**, *29* (19), 3249–3259. <https://doi.org/10.1038/emboj.2010.206>.
- (17) Call, M. E.; Chou, J. J. A View into the Blind Spot: Solution NMR Provides New Insights into Signal Transduction Across the Lipid Bilayer. *Struct. Lond. Engl. 1993* **2010**, *18* (12), 1559–1569. <https://doi.org/10.1016/j.str.2010.11.002>.
- (18) Hinsen, K. Structural Flexibility in Proteins: Impact of the Crystal Environment. *Bioinformatics* **2008**, *24* (4), 521–528. <https://doi.org/10.1093/bioinformatics/btm625>.
- (19) Premont, R. T.; Macrae, A. D.; Aparicio, S. A. J. R.; Kendall, H. E.; Welch, J. E.; Lefkowitz, R. J. The GRK4 Subfamily of G Protein-Coupled Receptor Kinases ALTERNATIVE SPLICING, GENE ORGANIZATION, AND SEQUENCE CONSERVATION. *J. Biol. Chem.* **1999**, *274* (41), 29381–29389. <https://doi.org/10.1074/jbc.274.41.29381>.
- (20) Mushegian, A.; Gurevich, V. V.; Gurevich, E. V. The Origin and Evolution of G Protein-Coupled Receptor Kinases. *PLOS ONE* **2012**, *7* (3), e33806. <https://doi.org/10.1371/journal.pone.0033806>.
- (21) GRK5 - G protein-coupled receptor kinase 5 - Homo sapiens (Human) - GRK5 gene & protein https://www.uniprot.org/uniprot/P34947#family_and_domains (accessed Jan 3, 2020).
- (22) Huang, Y.; Wu, J.; Su, T.; Zhang, S.; Lin, X. Fasudil, a Rho-Kinase Inhibitor, Exerts Cardioprotective Function in Animal Models of Myocardial Ischemia/Reperfusion Injury: A Meta-Analysis and Review of Preclinical Evidence and Possible Mechanisms. *Front. Pharmacol.* **2018**, *9*. <https://doi.org/10.3389/fphar.2018.01083>.
- (23) Maybridge.com https://www.maybridge.com/portal/alias__Rainbow/lang__en/tabID__146/DesktopDefault.aspx (accessed Jan 2, 2020).
- (24) ChEMBL Database <https://www.ebi.ac.uk/chembl/> (accessed Jan 2, 2020).
- (25) Welsch, M. E.; Snyder, S. A.; Stockwell, B. R. Privileged Scaffolds for Library Design and Drug Discovery. *Curr. Opin. Chem. Biol.* **2010**, *14* (3), 347–361. <https://doi.org/10.1016/j.cbpa.2010.02.018>.
- (26) Molecular Operating Environment (MOE) | MOEsaic | PSILO <https://www.chemcomp.com/Products.htm> (accessed Jan 2, 2020).
- (27) Cowan-Jacob, S. W.; Möbitz, H.; Fabbro, D. Structural Biology Contributions to Tyrosine Kinase Drug Discovery. *Curr. Opin. Cell Biol.* **2009**, *21* (2), 280–287. <https://doi.org/10.1016/j.ceb.2009.01.012>.
- (28) Ghose, A. K.; Herbertz, T.; Pippin, D. A.; Salvino, J. M.; Mallamo, J. P. Knowledge Based Prediction of Ligand Binding Modes and Rational Inhibitor Design for Kinase Drug Discovery. *J. Med. Chem.* **2008**, *51* (17), 5149–5171. <https://doi.org/10.1021/jm800475y>.
- (29) Kitchen, D. B.; Decornez, H.; Furr, J. R.; Bajorath, J. Docking and Scoring in Virtual Screening for Drug Discovery: Methods and Applications. *Nat. Rev. Drug Discov.* **2004**, *3* (11), 935–949. <https://doi.org/10.1038/nrd1549>.
- (30) Cho, S. Y.; Lee, B. H.; Jung, H.; Yun, C. S.; Ha, J. D.; Kim, H. R.; Chae, C. H.; Lee, J. H.; Seo, H. W.; Oh, K.-S. Design and Synthesis of Novel 3-(Benzo[d]Oxazol-2-Yl)-5-(1-(Piperidin-4-Yl)-1H-Pyrazol-4-Yl)Pyridin-2-Amine Derivatives as Selective G-Protein-Coupled Receptor Kinase-2 and -5 Inhibitors. *Bioorg. Med. Chem. Lett.* **2013**, *23* (24), 6711–6716. <https://doi.org/10.1016/j.bmcl.2013.10.036>.

- (31) Larsen, M. A.; Hartwig, J. F. Iridium-Catalyzed C–H Borylation of Heteroarenes: Scope, Regioselectivity, Application to Late-Stage Functionalization, and Mechanism. *J. Am. Chem. Soc.* **2014**, *136* (11), 4287–4299. <https://doi.org/10.1021/ja412563e>.
- (32) Applications of Palladium-Catalyzed C–N Cross-Coupling Reactions | Chemical Reviews <https://pubs.acs.org/doi/10.1021/acs.chemrev.6b00512> (accessed Jan 2, 2020).
- (33) Martin, R.; Buchwald, S. L. Palladium-Catalyzed Suzuki–Miyaura Cross-Coupling Reactions Employing Dialkylbiaryl Phosphine Ligands. *Acc. Chem. Res.* **2008**, *41* (11), 1461–1473. <https://doi.org/10.1021/ar800036s>.
- (34) Billingsley, K.; Buchwald, S. L. Highly Efficient Monophosphine-Based Catalyst for the Palladium-Catalyzed Suzuki–Miyaura Reaction of Heteroaryl Halides and Heteroaryl Boronic Acids and Esters. *J. Am. Chem. Soc.* **2007**, *129* (11), 3358–3366. <https://doi.org/10.1021/ja068577p>.
- (35) Piatnitski Chekler, E. L.; Elokda, H. M.; Butera, J. Efficient One-Pot Synthesis of Substituted 2-Amino-1,3,4-Oxadiazoles. *Tetrahedron Lett.* **2008**, *49* (47), 6709–6711. <https://doi.org/10.1016/j.tetlet.2008.09.057>.
- (36) Perry, R. J.; Wilson, B. D.; Miller, R. J. Synthesis of 2-Arylbenzoxazoles via the Palladium-Catalyzed Carbonylation and Condensation of Aromatic Halides and o-Aminophenols. *J. Org. Chem.* **1992**, *57* (10), 2883–2887. <https://doi.org/10.1021/jo00036a025>.
- (37) Haugwitz, R. D.; Angel, R. G.; Jacobs, G. A.; Maurer, B. V.; Narayanan, V. L.; Cruthers, L. R.; Szanto, J. Antiparasitic Agents. 5. Synthesis and Anthelmintic Activities of Novel 2-Heteroaromatic-Substituted Isothiocyanatobenzoxazoles and -Benzothiazoles. *J. Med. Chem.* **1982**, *25* (8), 969–974. <https://doi.org/10.1021/jm00350a017>.
- (38) Wrobel, Z.; Kwast, A. Nucleophilic Substitution of Halogens with Amines in 2- and 4-Nitrophenols. *ChemInform* **2007**, *38* (19). <https://doi.org/10.1002/chin.200719072>.
- (39) Thompson, A. E.; Hughes, G.; Batsanov, A. S.; Bryce, M. R.; Parry, P. R.; Tarbit, B. Palladium-Catalyzed Cross-Coupling Reactions of Pyridylboronic Acids with Heteroaryl Halides Bearing a Primary Amine Group: Synthesis of Highly Substituted Bipyridines and Pyrazinopyridines. *J. Org. Chem.* **2005**, *70* (1), 388–390. <https://doi.org/10.1021/jo0402226>.
- (40) Barlaam, B.; Cosulich, S.; Delouvrié, B.; Ellston, R.; Fitzek, M.; Germain, H.; Green, S.; Hancox, U.; Harris, C. S.; Hudson, K.; et al. Discovery of 1-(4-(5-(5-Amino-6-(5-Tert-Butyl-1,3,4-Oxadiazol-2-Yl)Pyrazin-2-Yl)-1-Ethyl-1,2,4-Triazol-3-Yl)Piperidin-1-Yl)-3-Hydroxypropan-1-One (AZD8835): A Potent and Selective Inhibitor of PI3K α and PI3K δ for the Treatment of Cancers. *Bioorg. Med. Chem. Lett.* **2015**, *25* (22), 5155–5162. <https://doi.org/10.1016/j.bmcl.2015.10.002>.
- (41) Lee, J.; Han, S.-Y.; Jung, H.; Yang, J.; Choi, J.-W.; Chae, C. H.; Park, C. H.; Choi, S. U.; Lee, K.; Ha, J. D.; et al. Synthesis and Structure–Activity Relationship of Aminopyridines with Substituted Benzoxazoles as c-Met Kinase Inhibitors. *Bioorg. Med. Chem. Lett.* **2012**, *22* (12), 4044–4048. <https://doi.org/10.1016/j.bmcl.2012.04.083>.
- (42) FDA-approved small-molecule kinase inhibitors: Trends in Pharmacological Sciences [https://www.cell.com/trends/pharmacological-sciences/comments/S0165-6147\(15\)00077-2](https://www.cell.com/trends/pharmacological-sciences/comments/S0165-6147(15)00077-2) (accessed Sep 28, 2019).
- (43) Barlaam, B. C.; Bower, J. F.; Delouvrié, B.; Fairley, G.; Harris, C. S.; Lambert, C.; Ouvry, G.; Winter, J. J. G. Pyridine and Pyrazine Derivatives Useful in the Treatment of Cell Proliferative Disorders. WO2009053737A2, April 30, 2009.

Chapter 4. Indolinone-Based Covalent, Selective Inhibitors of GRK5

4.1 Preface

Ideas and conclusions from Chapter 4 are in preparation for publication and may appear verbatim in a future publication or patent. Design and synthesis for compounds presented in Chapter 4, as well as intact protein and tandem mass spectrometry experiments, I performed. Pharmacological evaluation of compounds was performed by Renee Bouley (CCG-271421, CCG-271423, CCG-271424), Qiuyan Chen and Larisa Avramova (all remaining compounds). Any additional efforts towards modeling and docking experiments, I performed.

4.2 Validation of Indolinone-Ullrich 57 Provides a New Scaffold for GRK5 Inhibitor Development

There is still a need for an ultra-selective GRK5 inhibitor as the pyrrolopyrimidine scaffold developed in Chapter 2 could not be further improved upon. Considering the inability to validate the reported ChEMBL-1607632 lead, there remains a need to develop new scaffolds for GRK5 inhibition. There exists a limited set of known GRK inhibitors, only one of which is reported to be GRK5 selective. Balanol and Takeda 103 are known GRK2 inhibitors, are were not initially developed in the previous GRK2 inhibitor campaign within the Tesmer group. Given the difficulties that were faced in building in GRK5 activity through canonical means, any new scaffold must be amenable to modification to carry a covalent warhead. Balanol, a natural product, is complex and would require a serious undertaking to identify and develop the chemistry needed to create a covalent analogue; thus, it will not serve as an appropriate scaffold. Takeda 103 is a known pharmaceutical agent that has optimized pharmacokinetic properties. However, the scaffold itself is not amenable to modification to carry a covalent warhead. Thus, these two known inhibitors are deprioritized choices for new scaffolds.

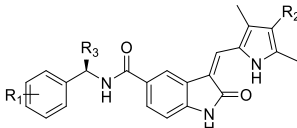
The last of the known scaffolds was initially developed as a GRK5 modifiers for use in diabetes.^{1,2} However, there is limited specific data available for this new scaffold. The lead compound Ullrich-57, which features an indolinone scaffold, was reported as having $IC_{50} < 0.1 \mu M$ activity against GRK5. Unfortunately, the originally reported data did not give a definitive IC_{50} for any compound but rather gave ranges of activity against GRK5. In terms of selectivity, little is known about this series as there was no reported data for GRK2 or other related kinases.

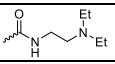
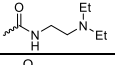
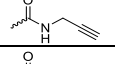
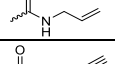
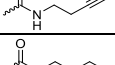
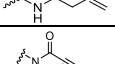
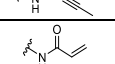
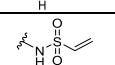
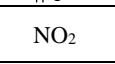
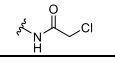
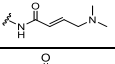
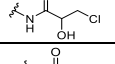
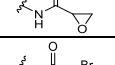
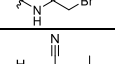
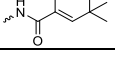
This indolinone scaffold is originally derived from the FDA approved receptor tyrosine kinase inhibitor (RTKI) Sunitinib.³ Sunitinib was originally approved for use in various cancers and features an optimized scaffold. Additionally, Sunitinib and the originally designed analogues from Ullrich and co-workers are easily amenable to modification to carry a covalent warhead.

However, the indolinone scaffold is not without its own problems. The indolinone scaffold is known to undergo a liquid state photoisomerization. This isomerization produces an active (Z-conformer) and an inactive (E-conformer) configuration.⁴ Restriction of the molecular conformation can limit this isomerization but cannot completely eliminate the reaction. Additionally, Sunitinib has been known to induce cardiotoxicity in large doses.^{3,5} It was hypothesized that if a ultra-potent compound could be produced this issue could be overcome. Sunitinib is also approved as a pan-RKTI.³ Thus, special care must be taken to examine the extent of kinome-wide selectivity. As the covalent strategy developed in Chapter 2 will be applied to this new scaffold, we expected these new compounds to be subfamily selective. However, if an ultra-selective compound could be produced through this method, then kinome-wide selectivity could be less of a liability. Despite these known issues, this scaffold presents the best option to continue developing a second generation of covalent, selective GRK5 inhibitors.

The original lead, CCG-271421 (previously Ullrich-57), was shown in our assays to have exceptional potency against GRK5 ($IC_{50} = 15$ nM) with a minimal intrinsic amount of selectivity for GRK2 ($IC_{50} = 1100$ nM), about 74-fold selective (Table 4.1). This data was indicative of the fact that this series can definitely serve as lead for the second generation of our GRK5 covalent inhibitors. We predicted that if these compounds could be modified to carry a covalent warhead, the selectivity could be improved by 100-fold or greater while potency could also potentially be in the picomolar range.

4.3 Haloketones Produce a Rapid Covalent Interaction with Cys474

Table 4.1: IC₅₀ Values for Indolinones With Various Warheads (μM ± SD)


Compound	R ₁	R ₂	R ₃	GRK5	GRK2	GRK2/ GRK5 [§]	PKA
Sunitinib	NA		N/A	0.83 ± 0.7 (3)	130 ± 200 (3)	150	ND
CCG 271421	H		CH ₃	0.015 ± 0.02 (7)	1.1 ± 0.7 (4)	74	>250 (2)
CCG 271423	H		CH ₃	0.021 ± 0.01 (7)	44 ± 40* (6)	2100	ND
CCG 271424	H		CH ₃	0.048 ± 0.008 (3)	22 ± 10 (3)	460	>250 (2)
CCG 271441	H		CH ₃	0.091 ± 0.04 (3)	130 ± 50 (3)	1400	>250 (2)
CCG 271442	H		CH ₃	1.9 ± 0.4 (2)	630 ± 200 (2)	330	ND
CCG 273180	H		CH ₃	2.5 ± 0.8 (3)	150 ± 30 (3)	61	ND
CCG 273181	H		CH ₃	0.81 ± 0.7 (4)	87 ± 30 (3)	110	ND
CCG 273182	H		CH ₃	0.74 ± 0.6 (5)	280 ± 110 (3)	370	ND
CCG 273183	H	NO ₂	CH ₃	0.73 ± 0.5 (3)	7.2 ± 3 (3)	10.	ND
CCG 273220	H		CH ₃	0.22 ± 0.04 (3)	350 ± 100 (2)	1500	>250 (2)
CCG 273221	H		CH ₃	0.36 ± 0.2 (3)	17 ± 10 (2)	47	ND
CCG 273464	H		CH ₃	0.08 ± 0.03 (3)	6.7 ± 5 (3)	83	>250 (2)
CCG 273462	H		CH ₃	0.74 ± 0.2 (3)	>250 (5)	>340	ND
CCG 273463	H		CH ₃	0.0086 ± 0.003 (7)	12 ± 20 (3)	1400	>250 (2)
CCG 273240	H		CH ₃	0.28 ± 0.1 (3)	120 ± 80 (2)	430	>250 (2)
CCG 215022				0.28 ± 0.1 (6)	ND		>250 (2)
paroxetine				ND	0.78 ± 0.3 (3)		850 ± 400 (4)

All data were fit to a log([Inhibitor]) versus response model with variable slope and automatic outlier rejection in GraphPad Prism. Curves that had R squared values less than 0.8 after fitting were omitted. ND, not determined. Numbers in parentheses indicate the number of independent experimental curves.

First and foremost, the focus for this series was establishing the appropriate warhead for covalent engagement with Cys474. Initially, the linkage for the warhead was maintained and simple alkynyl-amine and alkenyl-amines were appended to the pyrrole ring through the free carboxylic acid.⁶ These compounds, CCG-271423-CCG-271442, demonstrated reasonable but lower potency than the initial lead, CCG-271421. Interestingly, CCG-271423, which features a propargyl group, has the highest level of selectivity among the compounds made, with a 2100-fold selectivity

against GRK2. Such an increase activity indicates that there is a clear interaction between the propargyl group and the GRK5 P-loop that is not present in GRK2. Indeed, it is known that the GRK2 P-loop extends farther down over the face of the active site, and therefore may cause a steric clash with the propargyl group of CCG-271423.⁷ However, we were able to rule out the idea that this warhead engages C474 covalently through intact protein mass spectrometry (MS).

Additionally, compounds with longer linker length, CCG-271441 and CCG-271442 respectively, were shown to have variable potency from 0.91 μM to 1.9 μM . Interestingly, the selectivity trends between the alkyne and alkene warheads remained consistent in these two analogues, suggesting that linker flexibility does not allow the propargyl group to avoid a steric clash with the GRK2 P-loop. These data suggest that linker lengths for our warhead cannot be extended beyond one methylene unit without causing a steric clash with either the GRK2 or GRK5 P-loop. Thus, the key to maintaining potency may be to maintain the initial linker length of CCG-271421, but selectivity necessitates a different covalent modifier be present.

Given that the initial warheads developed in Chapter 2 were inaccessible via the initial route, a new strategy was used. The pyrrole-amide was reversed so that the warheads used in

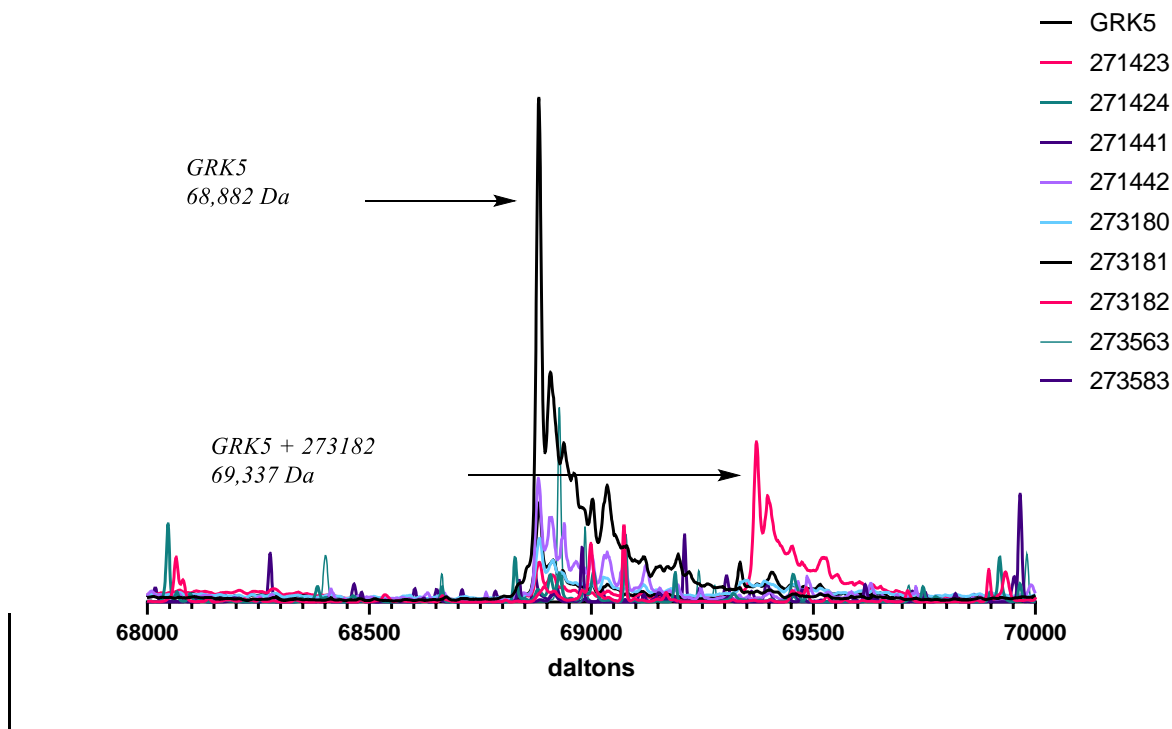


Figure 4.1 Intact protein MS for original warheads. Only the vinyl sulfone in CCG-273182 makes a covalent interaction with GRK5.

developing CCG-265328 could be tested within this scaffold. Immediately, the most desired compound was CCG-273221, which features the N,N-dimethylethylenediamine warhead that has a basic terminal amine.^{8,9} Since the original lead, CCG-271421, also features a terminal amine we anticipated that this warhead would be highly effective. However, CCG-273221 has modest potency against GRK5 ($IC_{50} = 0.36 \mu\text{M}$) with only 47-fold selectivity over GRK2. This level of selectivity indicates that CCG-273221 may not be covalent, which indeed was found to be the case in intact protein mass spectrometry experiments. A drop in potency, as compared to CCG-271421, indicates that the terminal amine on the warhead may be making an interaction with the P-loop, as was observed in CCG-264629 in Chapter 2.

Interestingly, CCG-273180, which features the 2-methylbutyne warhead from CCG-265328, has very limited potency against GRK5 ($IC_{50} = 2.5 \mu\text{M}$), but still retains selectivity against GRK2 (61-fold selective). Therefore, we concluded that while this warhead was initially useful in the pyrrolopyrimidine series, there must be a type of steric repulsion happening between the 2-methyl portion of this warhead and the GRK5 P-loop. This data also indicates that the steric clash originally observed in CCG-271423 is still prevalent despite having a reversed linker orientation. Thus, our previously most reactive warhead is no longer useful in this scaffold, suggesting that SAR for covalent warheads is case-specific, and must be optimized with each new scaffold.

Other traditional Michael acceptor warheads such as acrylamides and vinyl sulfones, featured in CCG-273181 ($IC_{50} = 0.81 \mu\text{M}$) and CCG-273182 ($IC_{50} = 0.74 \mu\text{M}$), show lower levels of activity to that seen in CCG-273221. Interestingly, of the original warheads tested, only the vinyl sulfone in CCG-273182 was able to form a covalent interaction (Figure 4.1). In intact protein MS, CCG-273182 took three hours to form a covalent interaction with GRK5, which was consistent with the development of the CCG-265328.¹⁰ However, this delay in covalent engagement does suggest that there is a slower K_{on} for CCG-273182 than other compounds in this series. This slower K_{on} rate may be due to a potential steric clash between the GRK5 P-loop and the vinylsulfone, before C474 is engaged, which ultimately realigns the spent warhead into a more

favorable position. Additionally, the vinyl sulfone is one of the more polar warheads tested within the series, potentially causing a slower K_{on} rate, as our model suggests that the warhead is positioned directly beneath the P-loop in a more highly lipophilic area while the acrylate piece of the warhead is solvent exposed.

The most reactive warhead, the chloroketone featured in CCG-273220, did demonstrate covalent interaction with GRK5 within 30 minutes, has a reasonable potency ($IC_{50} = 0.22 \mu M$) and excellent selectivity against GRK2 ($IC_{50} = 350 \mu M$, 1500-fold selective for GRK5) (Figure 4.2). Unsurprisingly given the covalent engagement, CCG-273220 has a 1500-fold selectivity for GRK5 over GRK2. Similarly, the bromoketone seen in CCG-273463, is shown to have better potency

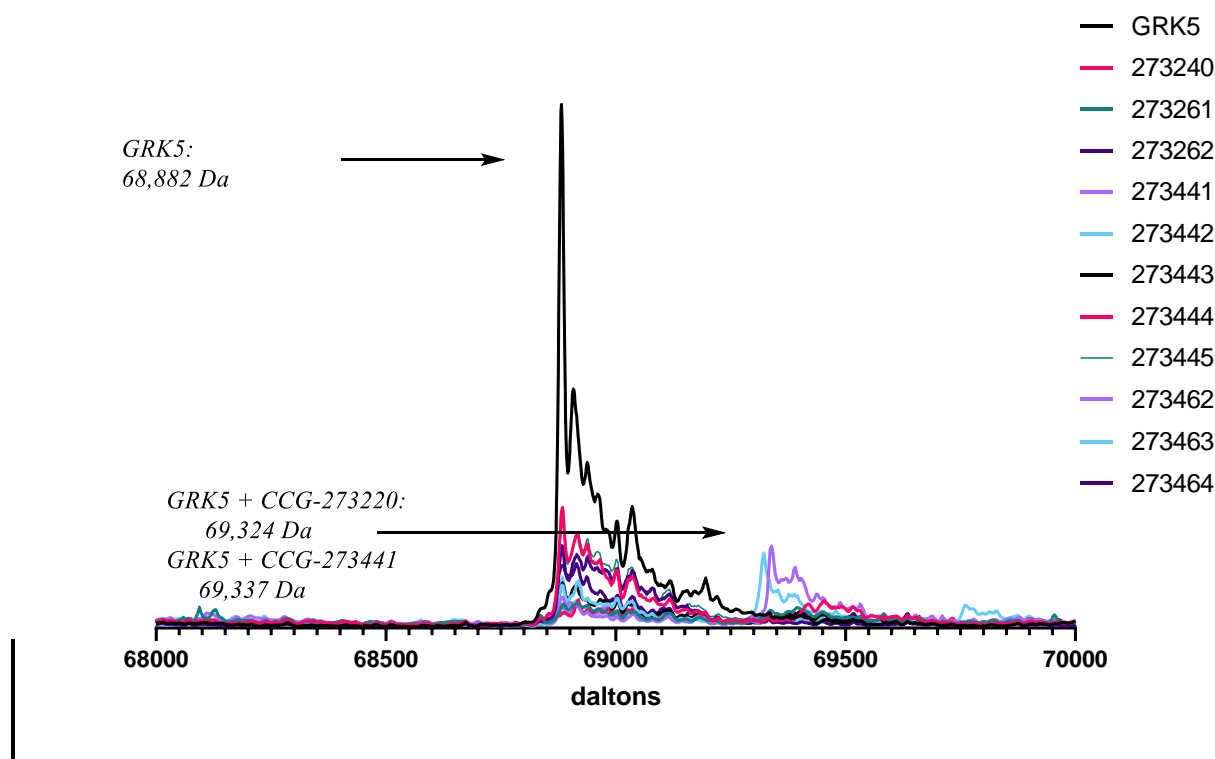


Figure 4.2 Intact protein MS for haloketones. CCG-273220 (purple) shows labelling in 30 mins. CCG-273441 (light blue) also shows labelling at 30 mins, but the other analogues show no labeling at that time point. As labeling events are controlled by kinetics, this data suggests that other analogues have a slower K_{on} rate.

than its chloroketone counterpart, but with 50% labelling of GRK5 within 30 minutes. However, the bromoketone CCG-273463 is one of the most potent and selective compounds from the series. Indeed, with 8.6 nM potency and 1400-fold selectivity for GRK5, CCG-273463 is unique. Such data indicates that two main factors may be at play. Firstly, the bromoketone may be fulfilling some

kind of lipophilic pocket fill within the area where the warhead of these compounds is modeled to sit. Additionally, the bromine of the warhead is known to be a softer electrophile than its chlorine counterpart.^{11,12} In hard-soft acid-base (HSAB) theory, soft electrophiles are most effective when paired with equally soft nucleophiles.¹³ As cysteine (in this case, C474 specifically) is a particularly soft nucleophile, it is possible that the bromoketone is a HSAB match for C474, making this compound exceptionally potent and selective. However, the bromoketone warhead is more labile than its chlorine based counterpart, making it less ideal in the further development of this series.

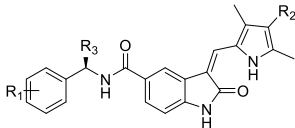
In keeping with what was learned from CCG-271441 and CCG-271442, the homologated chloroketone seen in CCG-273464 had a two-fold reduced potency and was unable to make a covalent engagement with GRK5. The epoxide warhead, seen in CCG-273462 was similarly unable to make a covalent engagement with GRK5, though it has a moderate level of potency ($IC_{50} = 0.74 \mu M$). Interestingly, this result is consistent with what other groups have observed when testing epoxides for labeling in proteomic experiments.^{6,14} As CCG-273462 does not form a covalent interaction in intact MS and has less than 100-fold selectivity for GRK5 over GRK2, it can safely be assumed that this analogue is not making the desired interaction with Cys474. Thus, we were able to determine, that while the intrinsic potency of the scaffold is good (between 10-500 nM), only the haloketone and vinyl sulfone warheads were able to form a covalent interactions and improve both potency and selectivity.

4.4 Filling Lipophilicity Pockets Increases Potency, But Electronics Also Plays a Critical Role

Having determined the best warhead for covalent interaction for this scaffold, the next focus was on improving solubility and intrinsic potency of this scaffold. Initial changes focused on the most amenable sites for removing or adding pendants. The phenyl ring pendant was the easiest to modify and served as the primary point for SAR expansion.

Interestingly, GRK5 has a strong preference for *para* substitutions on the phenyl ring. As seen in CCG-273441, CCG-273442 and CCG-273583, possessing a *para* pendant gains a small boost in potency. CCG-273445, which features the 4-methyl pendant, has the worst activity of any of the compounds from this series (Table 4.2). This drop in potency could be a function of electronic mismatches between the compound and the deeper hydrophobic pocket of GRK5 or a clash between the 4-methyl pendant and the floor of the GRK5 active site. Interestingly, the 3-methyl analogue, CCG-273261 shows low nanomolar activity, suggesting that either there are less steric clashes with the GRK5 pocket. Similarly, CCG-273442 demonstrates that even the position

Table 4.2: Expanded SAR for Indolinone Series ($\mu\text{M} \pm \text{SD}$)



Compound	R ₁	R ₂	R ₃	GRK5	GRK2	GRK2/ GRK5 [§]	PKA
Sunitinib	NA		N/A	0.83 ± 0.7 (3)	130 ± 200 (3)	150	ND
CCG 273261	3-Me		CH ₃	0.029 ± 0.03 (5)	11 ± 6 (3)	360	>250 (6)
CCG † 273262	H		CH ₃	1.30 ± 0.1 (3)	44 ± 18 (3)	32	ND
CCG 273441	4-F		CH ₃	0.0038 ± 0.001 (7)	4.8 ± 3 (3)	1300	>250 (6)
CCG 273442	4-Py		CH ₃	0.13 ± 0.05 (3)	4.8 ± 3 (3)	13	ND
CCG 273443	2-Py		CH ₃	0.45 ± 0.1 (3)	9.6 ± 5 (3)	21	ND
CCG 273444	3-Cl		CH ₃	0.14 ± 0.04 (3)	19 ± 10 (3)	140	>250 (6)
CCG 273445	4-Me		CH ₃	0.78 ± 0.3 (3)	2.1 ± 2 (5)	3	ND
CCG 273561	H		-	0.13 ± 0.09 (4)	13 ± 3 (3)	99	>250 (6)
CCG 273562	H			12 ± 5 (3)	190 ± 70 (2)	15	ND
CCG 273583	4-Cl		CH ₃	0.11 ± 0.05 (3)	0.70 ± .2 (3)	7	ND
CCG 273564	H			0.087 ± 0.02 (3)	23 ± 20 (4)	260	>250 (6)
CCG 273563	H			0.095 ± 0.03 (3)	15 ± 7 (3)	160	69 ± 10 (6)

All data were fit to a log([Inhibitor]) versus response model with variable slope and automatic outlier rejection in GraphPad Prism. Curves that had R squared values less than 0.8 after fitting were omitted. ND, not determined. Numbers in parenthesis indicate the number of independent experimental curves. † CCG-273262 is the (S) enantiomer of CCG-271421.

of a heteroatom within a ring matters in terms of potency. CCG-273442, which features a 4-pyridyl pendant, has improved potency over its 2-pyridyl counterpart, CCG-273443, by 2-fold. Looking

at the model, it is clear that GRK5 can accommodate a more polar pendant within this deeper hydrophobic pocket (Figure 4.3). What is less clear at first glance, is that CCG-273442 may be fulfilling an electronic deficit which is not filled by CCG-273443. Comparison of the electrostatic map of the GRK5 binding site with the electrostatic map of CCG-273442, it is clear that CCG-

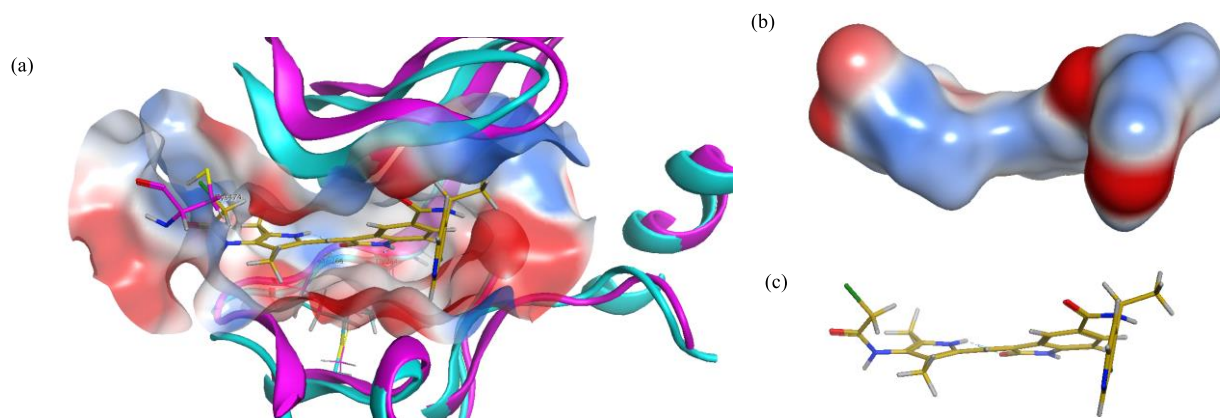


Figure 4.3 Electrostatic map comparison between GRK5 (Blue) and CCG-273442 (Gold carbons). (a) GRK5/GRK6 with CCG-273442 in the active site, an electrostatic map for the GRK5 active site is shown in blue/red shading, (b) electrostatic map of CCG-273442 shown in blue/red shading, (c) CCG-273442 represented in 3D (gold carbons).

273442 has an appropriate match with the electrostatics of the binding site. Meanwhile, CCG-273443 does not have an electrostatic match. Indeed, this electrostatic effect also seems to come into play with CCG-273441. CCG-273441, which is one of the most potent, but not the most selective GRK5 inhibitor of the series, does have an exact electrostatic match within the deeper hydrophobic pocket of the active site. Thus, the subtle electrostatics that control the deeper hydrophobic pocket when combined with a softer electrophile yield the best results from this series. This principle is reinforced by CCG-359090, featuring a 4-fluoro pendant and a bromoketone warhead, which has exceptional potency against GRK5 ($IC_{50} = 20$ nM) but lower selectivity over GRK2 than CCG-273441 (CCG-359090 has 233-fold subfamily selectivity). As these two functionalities afforded the highest levels of potency and selectivity seen in the series, it was assumed that the combination would have a synergistic effect producing a potentially sub-nanomolar analogue. However, the need to balance the subtle electrostatic effects of the ligand and the GRK5 binding pocket combined with a less reactive haloketone warhead resulted in an analogue that sees an additive effect of these efficacious pendants.

Table 4.3 Thermodynamic Solubility of Indolinone Series Analogues

Compound ID	Solubility	μM	$\mu\text{g/mL}$	Dose Concentration (mg/mL)	pH After Assay
CCG-273220	water	75.1	35.7	5.6	5
CCG-273221	water	125.3	64	3	5
CCG-273441	water	90.7	44.8	4	3
CCG-273443	water	261.7	124.9	7.6	4
CCG-273445	water	252.1	123.6	7.6	2.5
CCG-273583	water	205.4	104.8	6	4

Experimental data collected by Analiza Inc. Experimental data represents an average of n=1 experiments.

Pleasingly, we were able to demonstrate that classic medicinal chemistry strategy can improve the solubility of these compounds. Indeed, CCG-273443 is the most soluble of the limited set tested, with an aqueous solubility of 261.7 μM (Table 4.3). While this level of aqueous solubility is not optimal, it is certainly still more advantageous than that of CCG-273220 (Aq. Sol.: 75.1 μM). Interestingly, there was an increase in solubility with every change to the base scaffold of CCG-273220. The addition of either a 4-fluoro or a 4-methyl pendant resulted in highly levels of aqueous solubility (90.7 μM and 252.1 μM , respectively). However, there was a drop in the pH of each sample following thermodynamic solubility testing, indicating that potentially the chloroketone warhead is hydrolyzing during testing conditions. If true, the corresponding alpha-hydroxy ketone would most certainly be more water soluble than its counterpart. Interestingly, the addition of a terminal amine, as in CCG-273221, improves aqueous solubility by 1.6-fold, compared to CCG-273220. This improvement in solubility implies that by building in a terminal amine to our warhead or linker, solubility could be increased in an atom economic fashion. We were able to increase the aqueous solubility of these compounds and also found that in some cases, CCG-273443 being a prime example, this does not help to optimize potency. Indeed, there seems to be a sensitive electronic balance underlying the intrinsic reactivity of each analogue. Therefore, compounds which are more soluble can also be less potent, potentially due to loss of the electrophilic warhead due to higher reactivity of the modifier which is supported by the more highly electron-rich scaffold.

4.5 The Stereocenter Cannot Be Replaced or Activity Will Be Lost

One of the biggest challenges we faced was the stereocenter that is prominently featured in the original lead CCG-271421. While some stereocenters cannot be removed from lead compounds, it is generally advisable to attempt to uncover whether or not a stereocenter can be removed or racemized. Large scale or preparative synthesis of lead compounds is known to be cheaper, and less complex without the inclusion of such structural elements, making their removal ideal.

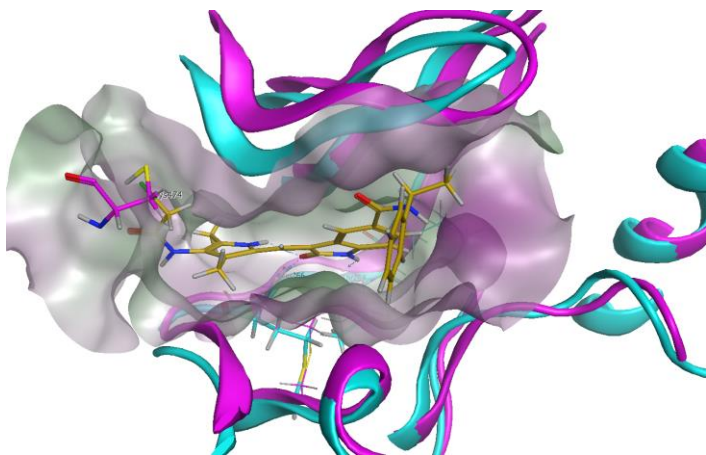


Figure 4.4 CCG-273220 (gold carbons) docked into the GRK5 (blue)/GRK6 (purple) model. The (R)-methyl group is positioned in a more spacious pocket, instead of directly underneath the P-loop/roof of the kinase.

From our model, it is clear that the (R) configuration has the effect of positioning the phenyl pendant into a lipophilic pocket beyond the gatekeeper (Figure 4.4). When the (S) enantiomer is featured, however, potency is drastically limited, as seen in CCG-273262 which has an $IC_{50} = 1.3 \mu M$ (43-fold less potent than CCG-271421). Removal of the stereocenter entirely in CCG-273561 demonstrated 130 nM level of potency, which is still highly potent, but about 10-fold less potent than our best compounds. While expanding the pendant from an (R)-methyl to an (R)-isopropyl group, demonstrated in CCG-273564 causes a steric repulsion deeper in the hydrophobic pocket, leading to a subsequent loss of potency. Replacing the stereocenter with a geminal di-methyl group, shown in CCG-273562, has moderate potency and was generally well tolerated. The same proved to be true of using an oxetane ring at the benzyl position (CCG-273563). This effect suggests that the positioning of the methyl pendant in the (R)-configuration provides a great boost in potency and can even negate the effects of simultaneously positioning a secondary pendant in the (S)-configuration. Thus, we have been able to show that the key to selectivity and potency for GRK5 lies in not only a covalent interaction with Cys474 but also in placement of pendants deep in the hydrophobic pocket in the correct orientation. Thus, we determined that while we cannot remove the stereocenter completely without a loss in potency, some changes to the benzylic position are well tolerated. As the oxetane ring and the geminal dimethyl groups were meant to protect against metabolic instability, it is encouraging that these changes were moderately tolerated by GRK5.

4.6 Tandem Mass Spectrometry Confirms Cys474 Engagement

Similar to what was seen in Chapter 2, we chose to further explore the exact location of covalent engagement by both CCG-273182 and CCG-273220. As demonstrated by initial intact protein mass spectrometry experiments, these compounds were found to have covalent interactions, but the exact location of engagement cannot be determined by those methods. Thus, tandem mass spectrometry was used to definitively determine sites of covalent engagement.

In the case of CCG-273182, when incubated for three hours with GRK5, the predominantly labelled residue was Cys474 (Figure 4.5). However, even at 100 μ M concentrations, some concentration dependent labelling events were observed.^{15,16} Cys145 and Cys520 were also

Checked	Confidence	Annotated Sequence	Modifications	# PSMs	Master Protein Accessions	Positions in Master Proteins
FALSE	High	[E].AGMLDPPFVDPRAVYCKDVLIDIE.[Q]	1xOxidation [M3]; 1xCCG273182_Smith [C17]	1	P34947	P34947 [458-481]
FALSE	High	[E].LFSACAQSVHE.[Y]	1xCCG273182_Smith [C5]	1	P34947	P34947 [141-151]
FALSE	High	[E].TECFKE.[L]	1xCCG273182_Smith [C3]	1	P34947; GRK_C474S	P34947 [518-523]; GRK_C474S [518-523]
FALSE	High	[E].AGMLDPPFVDPRAVYCKDVLIDIE.[Q]	1xCCG273182_Smith [C17]	1	P34947	P34947 [458-481]
FALSE	High	[E].AGMLDPPFVDPRAVYCKD.[V]	1xCCG273182_Smith [C17]	1	P34947	P34947 [458-476]

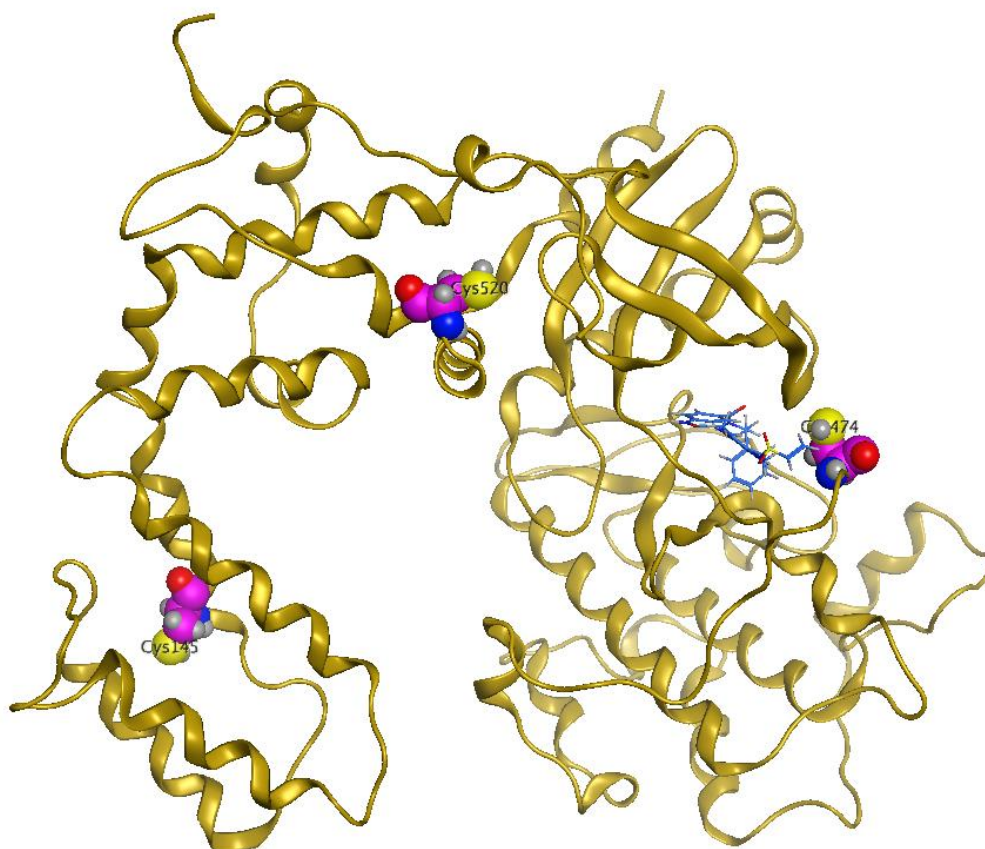


Figure 4.5 Tandem MS data shown in the table above indicates that Cys474 is the most predominantly labeled cysteine. Sites of labeling are shown in magenta in the GRK5 model (gold). Shown in the active site is CCG-273182 (blue carbons).

labelled in this sample, but they constitute some of the most solvent exposed cysteine residues in GRK5. Due to the level of solvent exposure, these extra labelling events are not considered to be biologically relevant. Pleasingly, this data confirms that our initially targeted residue, Cys474, is the site of covalent engagement for this new series.

Given that CCG-273220 served as a lead for the covalent warheads in the indolinone series, it was also tested with tandem MS. After a three hour incubation with GRK5, tandem MS of this sample was not able to detect a covalent label from CCG-273220 on any GRK5 cysteine. As it is known that GRK5 is labelled by the less reactive CCG-273182 at Cys474, this data seemed incongruent. However, the chloroketone of CCG-273220 is more labile than the vinyl sulfone of CCG-273182 and could have undergone hydrolysis within the three hour incubation, causing a lack of covalent engagement. Further examination of the peptide fragments from the CCG-273220-GRK5 sample also appear to be cut into fragments at the upper weight limit for tandem mass spectrometry detection. With the addition of the covalent label, it is possible that fragments would be above the upper limit for tandem MS detection. If this proves true, then covalent labels on Cys474 exist it simply cannot be detected in these tandem MS conditions.

Given the ambiguous results of the tandem MS for CCG-273220, we chose to return to intact protein MS utilizing a mutant GRK5-C474S strain. This replacement of the nucleophile to a less reactive serine should prevent covalent engagement. Indeed, this effect is observed in the CCG-273220-GRK5-C474S sample. Pleasingly, this data further confirms our suspicions that

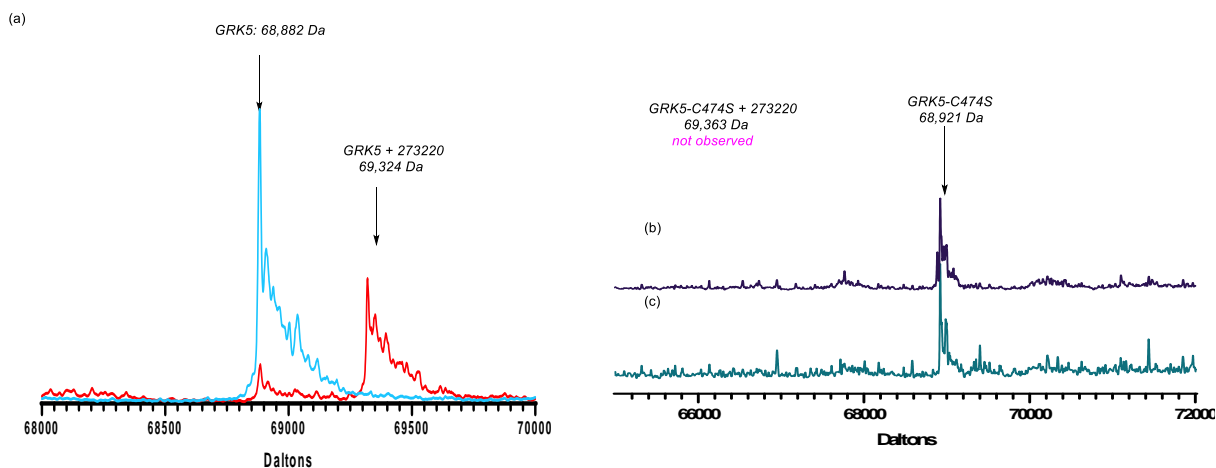


Figure 4.6 Intact MS of GRK5 and GRK5-C474S with CCG-273220. (a) GRK5 incubated with CG-273220, shows covalent engagement, (b) GRK5-C474S shows unlabeled peak at 68,921 Da, (c) GRK5-C474S incubated with CCG-273220 shows an unlabeled peak at 68,921 Da, indicating that covalent engagement is lost if the C474 nucleophile is replaced.

CCG-273220 and all other covalent analogues from this series are engaging Cys474, as designed (Figure 4.6).

4.7 Screening of CCG-273463 and CCG-271423 against a Kinase Panel Indicates High Selectivity for This Series

Given the high potency and subfamily selectivity of this series their limitation may prove to be kinome-wide selectivity. The indolinone series was originally derived from a RTKI (Sunitinib) therefore it is possible that multiple side target liabilities remain.^{3,4,17} The introduction of the covalent warhead is intended to remove these liabilities, as Cys474 is not conserved among all kinases rather it is only found in GRK5 and GRK6.

The use of a covalent warhead may prove to be a sufficient deterrent to activity against multiple targets, however, the haloketone warhead is known to be one of the most reactive warheads used in covalent drug discovery.¹¹ For this reason, the currently developed indolinone series could have activity against multiple targets, not just those kinases within the AGC kinase family. Therefore, to determine the exact utility of this series, a kinome-wide selectivity screen was pursued.

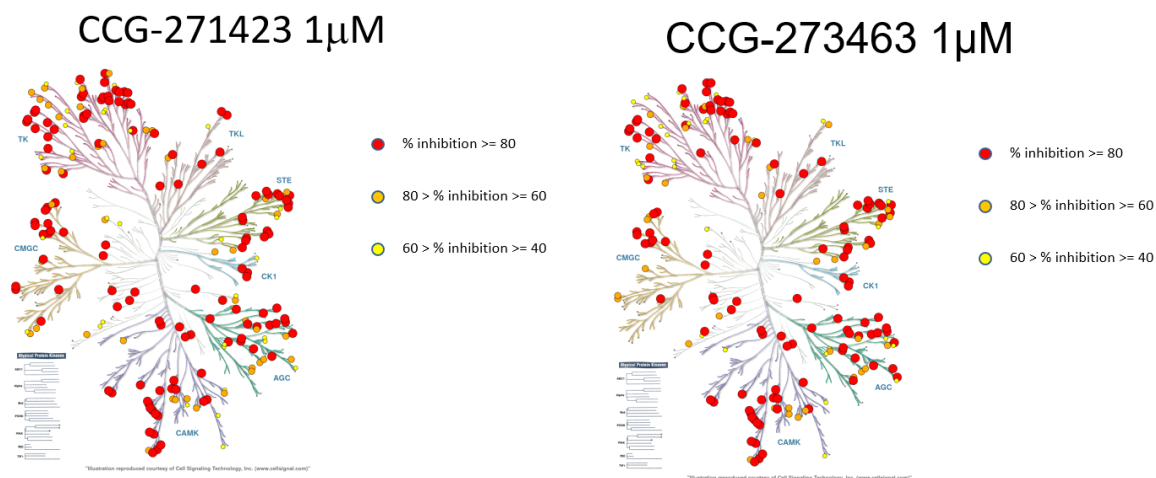


Figure 4.7 Kinase selectivity panel for **CCG-271423** and **CCG-273463**. Inhibition values are an average of n=2 experiment. Levels of inhibition are indicated by gradient color, with higher levels of protein inhibition labeled as red. (A) Kinome selectivity map for **CCG-271423** indicates subfamily selectivity levels are not maintained across the kinome.. (B) Kinome selectivity map for **CCG-273463** indicates that subfamily selectivity levels are not maintained across the kinome.

As the most developed compounds in the series feature a haloketone, the most active and subfamily selective compound, CCG-273463, was selected for testing. Additionally, as CCG-271423 was the most selective non-covalent compound developed in this series, this compound was also submitted for selectivity screening. Thus, the samples that were screened for kinome

selectivity represent the two most selective and potent covalent and non-covalent inhibitors developed, respectively.

Against a panel of 300 kinases, CCG-273463 was found to be promiscuous, hitting kinases across all families within the panel (Figure 4.7). Indeed, while CCG-273463 does show incredible subfamily selectivity this level of selectivity is not extended to the entire kinome. As the original scaffold was derived from a promiscuous RTKI, this lack of selectivity is not altogether surprising. Especially since known targets of Sunitinib, platelet-derived growth factor receptor (PDGFR) and vascular endothelial growth factor receptor (VEGFR), are also major off-targets for CCG-273463. However, it is possible that the highly reactive warhead has contributed to this lack of selectivity across the kinome. Should that prove to be true, a lower concentration of CCG-273463 tested against this kinase panel would yield more selectivity.

Against the same panel of 300 kinases, CCG-271423 was found to be equally as promiscuous as CCG-273463. As CCG-271423 is non-covalent, it is not predicted to suffer promiscuity within this screening panel. These data indicate that the base scaffold is sufficiently potent against multiple kinases across several families to produce a non-selective inhibitor. Again, as the original scaffold is derived from a pan-RTKI these data are not surprising. Thus, we have demonstrated that changes to our scaffold are sufficient to produce subfamily selectivity but not kinome selectivity, suggesting further changes are needed for a truly ultra-selective GRK5 inhibitor.

From this screening data it is clear that the haloketone warhead does bestow ultra-selectivity for GRK4 subfamily members but does not convey that same level of selectivity against all kinases. Given the lack of kinome-wide selectivity, a new utility for these compounds has arisen. The covalent GRK5 inhibitors may be used to investigate the role of GRK5 within various cancers, where the activity against multiple targets, including classic cancer targets such as PDGFR and VEGFR might prove advantageous.

4.8 Indolinones Do Not Increase Cardiomyocyte Contractility, But They Do Alter Ca²⁺ Flow

With ultra-selectivity against GRK4 subfamily members, and reasonable selectivity across the kinome, this indolinone series was used to investigate the role of GRK5 in cardiomyocyte contractility. Originally, it was thought that selective GRK5 inhibitors would act similarly to

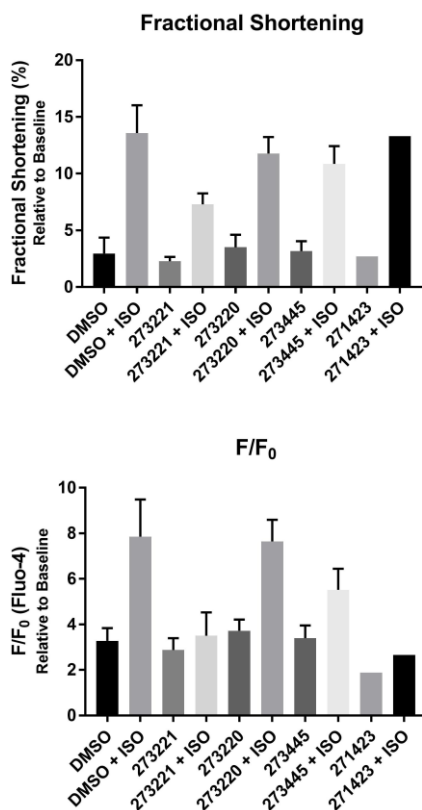


Figure 4.8 (top) Fractional shortening of cardiomyocytes, both without and with an isoproterenol challenge. Data shown are an average of n 1-3 experiments. (bottom) Measurements of the calcium transience in cardiomyocytes without and with an isoproterenol challenge. Data shown are an average of n 1-3 experiments.

GRK2 inhibitors in that they would increase cardiomyocyte contractility, as demonstrated by Waldschmidt et. al.^{18,19}

A survey of a representative sample of covalent, and non-covalent selective, potent GRK5 inhibitors in cardiomyocytes indicated that these inhibitors do not act in the same manner as described for GRK2 inhibitors. Rather, these compounds do not alter cardiomyocyte contractility significantly, when compared to a negative control (DMSO). Even the non-covalent CCG-271423 did not show a significant increase in cardiomyocyte contractility when compared with the DMSO negative control (Figure 4.8). Similarly, CCG-273220, a forerunner to CCG-273463, does not increase cardiomyocyte contractility when compared to the negative control. This data suggests

that the mechanism of action, regardless of covalency, for these compounds does not directly impact cardiomyocyte contractility in the same fashion as GRK2 inhibitors such as CCG-215022.

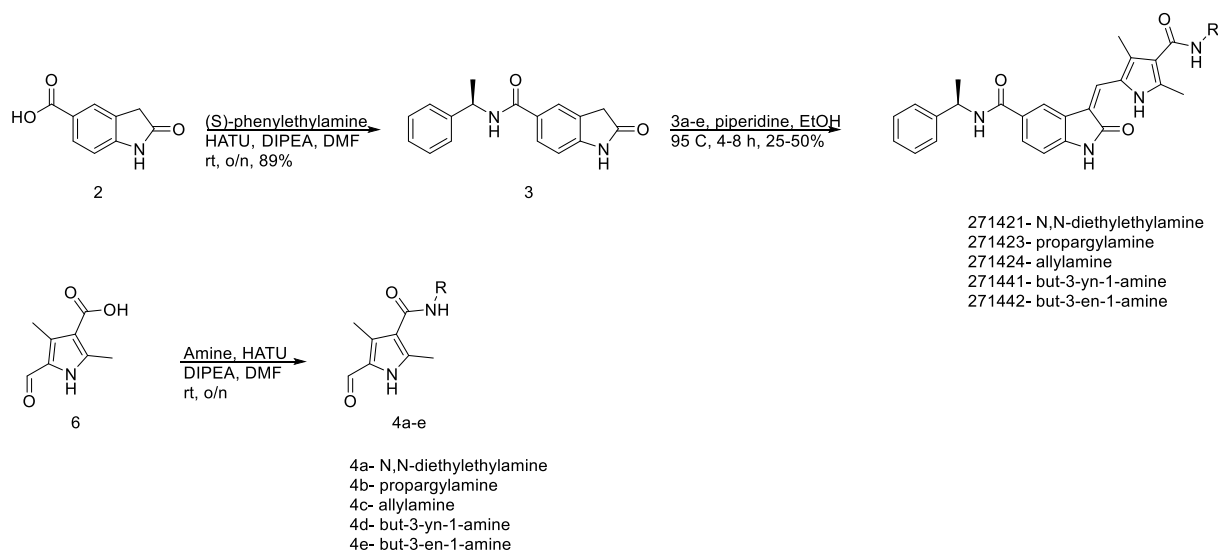
Interestingly, these indolinone samples were found to affect Ca^{2+} transience in negative fashion. This is an intriguing discovery, as GRK5 is not known to affect Ca^{2+} transience in cardiomyocytes. However, this study does shed some light on why the indolinone series does not affect cardiomyocyte contractility. Ca^{2+} transience is known to be linked in a positive feedback loop with cardiomyocyte contractility.²⁰⁻²² With inhibitors such as CCG-271423 and CCG-273220 showing a decrease in Ca^{2+} transience when compared with the negative control (DMSO) it is not surprising that these compounds do not increase contractility. Additionally, the remaining compounds in the tested set also show a drastic decrease in Ca^{2+} transience when compared to the negative control, indicating that they too may not increase cardiomyocyte contractility. Indeed, this proves to be the case, as CCG-273221 and CCG-273445 do not increase cardiomyocyte contractility in the same manner that CCG-273220 and CCG-271423 do not increase contractility. While it remains unclear how GRK5 affects cardiomyocyte contractility, it is clear that the effect of GRK5 is different than GRK2 in the cardiovascular system.

4.9 Concluding Thoughts on the Indolinone Series

With the development of this new series, there now exists a suitable selective GRK5 inhibitor. In this series I have shown how a scaffold with a high affinity can be made ultra-subfamily selective using the same covalent strategy applied in Chapter 2. Given the high levels of selectivity and potency for key compounds, CCG-271423, CCG-273441 and CCG-359090, these new probes will serve as excellent tools to further study the role of GRK5 in various disease states.

4.10 Synthesis of Compounds

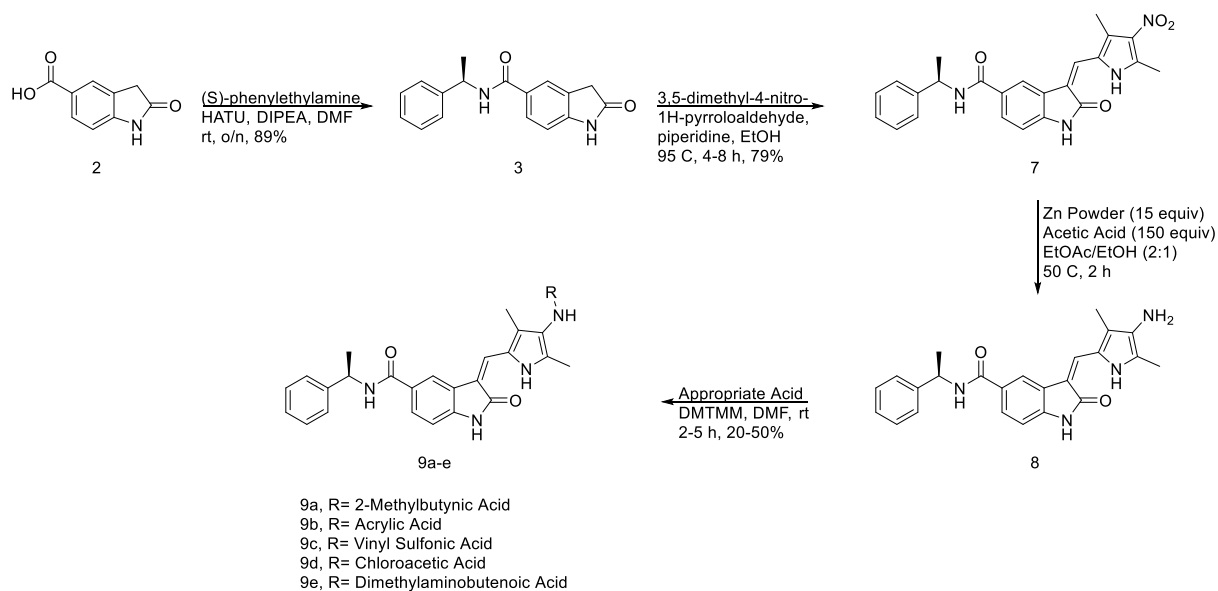
Synthesis of the original compound CCG-273421 and its analogues begins with a divergent route.² In the first line of synthesis, the free indolinone carboxylic acid, **2**, undergoes an amide coupling with (R)-phenylethylamine to give the intermediate, **3**. In the second line of synthesis, the pyrrole



Scheme 4.1 Synthetic route to **CCG-27421-271442**.

carbaldehyde starting material **6** undergoes an amide coupling with an amine of choice to give the intermediate **4a-e**. Intermediate **3** is then condensed with **4a-e** using standard Knoevenagel conditions to yield the desired products **271421-271442** (Scheme 4.1).

In a similar route, the final analogues of **273180-273583** can be achieved. Starting from the common intermediate **3**, a Knoevenagel condensation with 3,5-dimethyl-4-nitro-



Scheme 4.2 Synthetic route to **273180-359090**.

pyrrolocarbaldehyde gives the common intermediate **7** (Scheme 4.2). Compound **7** can then undergo a zinc catalyzed nitro group reduction to give the free amine, **8**. Free amine **8** can then be immediately used in an amide coupling with a chosen acid to give the final compounds. For almost all compounds, the final step involved the inclusion of the chloroacetic acid warhead. For those final compounds that include a different warhead, DMTMM was used to couple the free warhead acid with the free amine **8**. For variations in the phenyl ring substituent or in the benzylic position, all modifications start back at the amide coupling with **2**, and use the appropriate amine to yield the intermediate **3a-h**. From **3a-h** the rest of the route remains unchanged yielding the final compounds **273441-359090**.

4.11 Materials, Methods and Synthetic Experimental Data

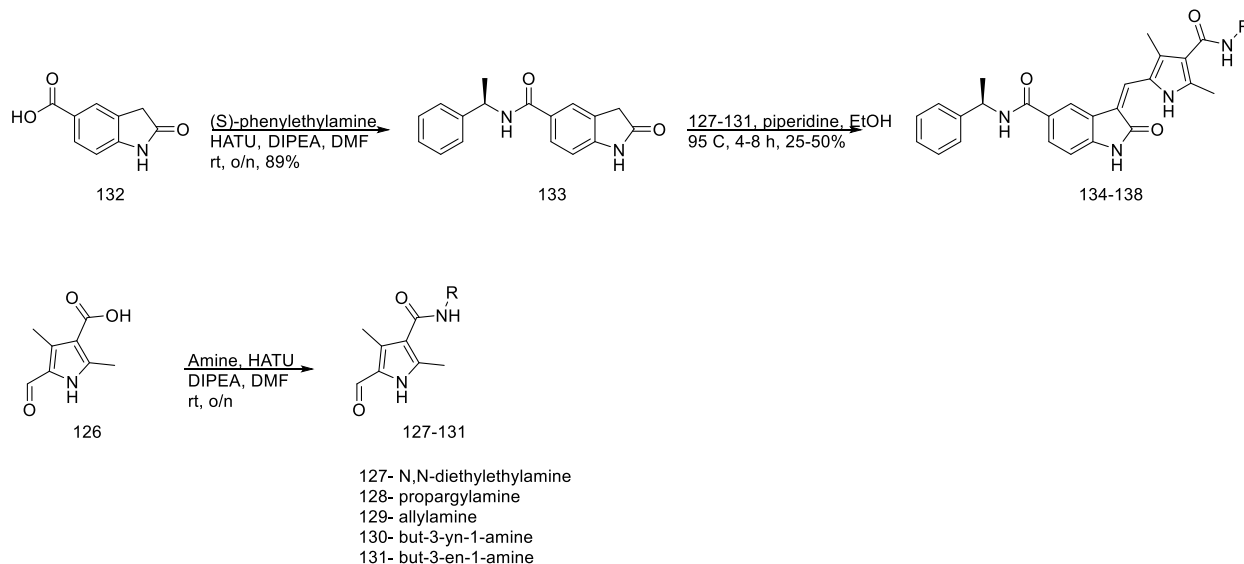
General Chemistry: All reagents from commercial sources were used without further purification unless otherwise noted. ¹H-NMR spectra were taken in DMSO-d₆, MeOD or CDCl₃ at room temperature on Varian MR 400 MHz; Varian Vnmrs 500 MHz; and Varian Vnmrs 700 MHz instruments. The reported chemical shifts for the ¹HNMR spectra were recorded in parts per million (ppm) on the δ scale from an internal tetramethylsilane (TMS) standard (0.0 ppm). Small molecule mass spectrometry data was measured using a Waters Corporation Micromass LCT or Agilent6230 Q-TOF instrument. HPLC was used to determine purity of compounds on an Agilent 1100 series with an Agilent Zorbax Eclipse Plus-C18 column. A gradient of 10-90% acetonitrile/water over 6 min followed by 90% acetonitrile/water for 7 min was used with detection at 254 nm.

Intact Protein MS and Tandem MS/MS: Intact protein MS was acquired with a Phenomenex C4 column paired with an Agilent 6545 Q-TOF LC/MS. For intact MS and Tandem MS, all samples were prepared with 20 μM GRK in assay buffer (see below), 1 mM compound, and incubated at 4 °C for 3 hr before being quenched with 1.0 μL of formic acid. In Tandem MS/MS, we chose Glu-C as the restricting enzyme to avoid small fragments with mass-to-charge ratios below the limit of detection of our instrument. All samples were digested with Glu-C sequencing enzyme, procured from Sigma Aldrich (Roche Life Sciences subsidiary) and used without further purification. MS/MS experiments were run on a nano-LC (Dionex RSLC-nano) with an Orbitrap Fusion Tribrid ETD mass spectrometer. This work was conducted by the Proteomics Resource Facility at the University of Michigan.

Inhibition Assays: For compounds CCG-271421-359090, IC₅₀ values for human GRK5, bovine GRK2, and bovine GRK1 were determined using a radiometric assay as follows. 50 nM GRK was incubated with 500 nM porcine brain tubulin (Cytoskeleton) and 0 - 333 μM inhibitor in 20 mM HEPES pH 7.0, 2 mM MgCl₂, 0.025% dodecylmaltoside (DDM), 3% DMSO for 20-30 min for GRK1 and 2 and 0-1 hr for GRK5, as denoted in Table 1, on ice, prior to initiation with the addition of 5 μM ATP supplemented with radioactive [γ -³²P]-ATP (PerkinElmer Life Sciences). Reactions were quenched at 5 min by addition of 6 μL of 4X SDS gel loading dye to the 6 μL reactions. 8 μL samples were separated on a 4-15% Criterion TGX precast gel (Bio-Rad). Experiments were performed with an n = 3 in duplicate.

Gels were dried, exposed to a storage phosphor screen overnight, and scanned using a Typhoon scanner. Bands corresponding to phosphorylated tubulin were quantified using ImageQuant, plotted as a function of log[inhibitor], and fit to the three-parameter log(inhibitor) vs. response model in GraphPad Prism 7.03 to determine the IC₅₀, and mean and standard deviation values were calculated using the column statistics function of GraphPad Prism 7.03.

Standard control compounds are run during each assay to assess consistency across time, experimenters, and subtle changes in assay conditions that are sometimes required to keep some of the compounds soluble and disperse (such as through addition of DDM or 3% DMSO). CCG215022 was used as controls for CCG-271421-359090.



Scheme 4.3. Synthetic route to indolone materials.

(R)-2-oxo-N-(1-phenylethyl)indoline-5-carboxamide (**132**, RAR-11-87)

To a round bottom flask were added 297.7 mg (1.69 mmol) of 2-oxoindoline-5-carboxylic acid, dissolved in 7 mL of dry DMF. To this dark red solution were added 0.244 mL (1.88 mmol) of (S)-1-phenylethan-1-amine, 0.300 mL (1.69 mmol) of DIPEA and 746.1 mg (1.95 mmol) of HATU. The resultant dark red solution was allowed to stir at rt for 12 h, and then added 200 mL of sat. Na₂CO₃ and extracted with EtOAc (3 x 100 mL). The combined organic layer was washed with brine (2 x 50 mL) and then dried over MgSO₄. Purified by column chromatography (0-15% DCM/MeOH) to give the desired product as a strawberry pink solid. Yield: 401.9 mg, 84% Molecular Formula: C₁₇H₁₆N₂O₂ ESI-MS calc: 280.12 ESI-MS found: 281.1283 [M+1] HPLC: 5.198 1H NMR (400 MHz, DMSO-d₆) δ 10.62 (s, 1H), 8.63 (d, J = 8.0 Hz, 1H), 7.78 (d, J = 7.0 Hz, 2H), 7.39 – 7.35 (m, 2H), 7.31 (dd, J = 8.4, 6.8 Hz, 2H), 7.23 – 7.18 (m, 1H), 6.88 – 6.83 (m, 1H), 5.15 (p, J = 7.2 Hz, 1H), 3.53 (s, 2H), 1.46 (d, J = 7.1 Hz, 3H). 13C NMR (100 MHz, dms0) δ 177.17, 165.76, 146.85, 145.65, 129.29, 128.67, 126.52, 126.06, 108.90, 48.85, 36.09, 22.84.

N-(2-(diethylamino)ethyl)-5-formyl-2,4-dimethyl-1H-pyrrole-3-carboxamide (**127**, RAR-11-93)

To a round bottom flask were added 200.9 mg (1.20 mmol) of 5-formyl-2,4-dimethyl-1H-pyrrole-3-carboxylic acid, 365.8 mg (1.79 mmol) of EDCI, 277.7 mg (1.79 mmol) of HOBT, 7 mL of dry DMF, 0.200 mL (1.44 mmol) of N₁,N₁-diethylethane-1,2-diamine and 0.34 mL (2.39 mmol) of TEA. The dark red solution was allowed to stir at rt for 12 h before being quenched with water and extracted with DCM (3 x 30 mL). The combined organic layer was washed with brine (2 x 20 mL) and then washed with 10% Citric acid (3 x 50 mL), *drawing the desired product into the water layer*.²³ The organic layer was discarded. The aqueous layer was basified with Na₂CO₃, bringing the pH up to 10, and then extracted with DCM (4 x 50 mL). The combined organic layers were dried over MgSO₄ and then evaporated onto silica gel and purified by column chromatography (5-15% MeOH/DCM). The solvent was removed under pressure to give a yellow solid. Result: light yellow solid, 90 mg, 27% Molecular Formula: C₁₄H₂₃N₃O₂, ESI-MS Calc: 265.18 ESI-MS found: 266.1749 HPLC: 2.681 1H NMR (400 MHz, DMSO-d₆) δ 11.85 (s, 1H), 9.54 (s, 1H), 7.95 (s, 2H), 2.34 (d, J = 20.8 Hz, 7H), 0.99 (s, 6H).

5-formyl-2,4-dimethyl-*N*-(prop-2-yn-1-yl)-1H-pyrrole-3-carboxamide (**128**, RAR-11-97)

To a round bottom flask were added 199.4 mg (1.20 mmol) of 5-formyl-2,4-dimethyl-1H-pyrrole-3-carboxylic acid, 688.0 mg (1.79 mmol) of HATU, 6 mL of dry DMF, 0.100 mL (1.44 mmol) of propargylamine and 0.34 mL (2.39 mmol) of TEA. The dark red solution was allowed to stir at rt for 12 h before being quenched with water and extracted with DCM (3 x 30 mL). Took the combined organic layers and washed with brine (2 x 20 mL) and then washed with 10% Citric acid (3 x 50 mL), *taking the desired product into the aqueous layer*. Discarded the organic layer. The aqueous layer was basified with Na₂CO₃, bringing the pH up to 10, and then extracted with DCM (4 x 50 mL). The combined organic layer was dried over over MgSO₄ and then removed solvent to give the final product as a light orange oil. Result: light orange oil, 61 mg, 25% Molecular Formula: C₁₁H₁₂N₂O₂ ESI-MS calc: 204.09 ESI-MS found: 205.0873 [M+1], 242.1167 [M+K] HPLC: 3.625 1H NMR (700 MHz, DMSO-d₆) δ 11.87 (s, 1H), 9.55 (s, 1H), 7.95 (s, 16H), 3.97 (ddd, J = 12.7, 5.7, 2.5 Hz, 3H), 3.08 (t, J = 2.4 Hz, 1H), 2.36 (s, 3H), 2.31 (s, 3H). 13C NMR (176 MHz, dms0) δ 177.82, 164.77, 139.11, 138.51, 128.26, 119.20, 89.92, 82.16, 72.95, 55.38, 40.24, 38.71, 28.42, 12.90, 10.00.

N-allyl-5-formyl-2,4-dimethyl-1H-pyrrole-3-carboxamide (**129**, RAR-11-99)

To a round bottom flask were added 204.4 mg (1.20 mmol) of 5-formyl-2,4-dimethyl-1H-pyrrole-3-carboxylic acid, 350.3 mg of EDCI (1.79 mmol), 275.3 mg (1.79 mmol) of HOBt, 6 mL of dry DMF, 0.110 mL (1.44 mmol) of allylamine and 0.34 mL (2.39 mmol) of TEA. The dark red solution was allowed to stir at rt for 12 h before being quenched with water and extracted with DCM (3 x 30 mL). Took combined organic layers and washed with LiCl 3 x 20 mL) and then washed with 10% Citric acid (3 x 50 mL), *drawing the desired product into the aqueous layer*. Discarded the organic layer. The aqueous layer was basified with Na₂CO₃, bringing the pH up to 8, and then extracted with DCM (4 x 50 mL) The combined organic layer was dried over MgSO₄ and then removed solvent to give a yellow solid. Result: light yellow solid, 64 mg, 25% Molecular Formula: C₁₁H₁₄N₂O₂ ESI-MS calc: 206.11 ESI-MS: 246.1621 [M+ MeCN] HPLC: 3.885 ¹H NMR (500 MHz, DMSO-*d*₆) δ 11.38 (s, 1H), 9.54 (s, 1H), 8.17 (s, 1H), 6.01 (tt, *J* = 10.8, 5.4 Hz, 1H), 5.87 (ddt, *J* = 16.4, 10.6, 5.3 Hz, 2H), 5.18 (t, *J* = 15.7 Hz, 3H), 5.08 (dd, *J* = 16.5, 10.2 Hz, 3H), 4.14 (d, *J* = 5.5 Hz, 2H), 3.82 (t, *J* = 5.7 Hz, 3H), 2.31 (s, 5H), 2.23 (s, 3H). ¹³C NMR (126 MHz, dms) δ 161.78, 150.29, 135.45, 135.21, 115.01, 114.35, 114.20, 40.54, 40.50, 39.50, 39.33, 39.17, 39.00, 38.83, 38.67, 38.50, 35.26, 30.25, 11.95, 9.27.

N-(but-3-yn-1-yl)-5-formyl-2,4-dimethyl-1H-pyrrole-3-carboxamide (**130**, RAR-12-2)

To a round bottom flask were added 199.6 mg (1.20 mmol) of 5-formyl-2,4-dimethyl-1H-pyrrole-3-carboxylic acid, 684.3 mg (1.79 mmol) of HATU, 6 mL of dry DMF, 0.100 mL (1.44 mmol) of 1-amino-3-butyne and 0.30 mL (2.39 mmol) of DIPEA. The dark red solution was allowed to stir at rt for 12 h before being quenched with water and extracted with DCM (3 x 30 mL). The combined organic layers were washed with LiCl (2 x 20 mL) and then washed with 10% Citric acid (3 x 50 mL), *drawing the desired product into the water layer*. Discarded the organic layer. The aqueous layer was basified with Na₂CO₃, bringing the pH up to 10, and then extracted with DCM (4 x 50 mL). The combined organic layer was dried over MgSO₄ and then removed solvent under pressure to give the final product as a yellow solid. Result: light yellow solid, 99.6 mg, 38.1% Molecular Formula: C₁₂H₁₄N₂O₂ ESI-MS calc: 218.11 ESI-MS found: 219.1129 HPLC: 3.997 ¹H NMR (700 MHz, DMSO-*d*₆) δ 11.83 (s, 1H), 2.83 (s, 1H), 2.69 (d, *J* = 1.0 Hz, 1H), 2.60 (d, *J* = 2.4 Hz, 3H), 2.37 (s, 4H), 2.32 (s, 3H). ¹³C NMR (176 MHz, dms) δ 178.94, 164.54, 160.23, 152.56, 147.04, 146.58, 126.55, 115.31, 88.48, 82.43, 72.02, 55.77, 37.85, 18.85, 13.97, 10.55.

N-(but-3-en-1-yl)-5-formyl-2,4-dimethyl-1H-pyrrole-3-carboxamide (**131**, RAR-12-3)

To a round bottom flask were added 197.8 mg (1.20 mmol) of 5-formyl-2,4-dimethyl-1H-pyrrole-3-carboxylic acid, 685.8 mg (1.79 mmol) of HATU, 6 mL of dry DMF, 107.1 mg (1.44 mmol) of but-3-en-1-amine and 0.45 mL (2.40 mmol) of DIPEA. The dark red solution was allowed to stir at rt for 12 h before being quenched with water and extracted with DCM (3 x 30 mL). The combined organic layers were washed with brine (2 x 20 mL) and then washed with 10% Citric acid (3 x 50 mL), *drawing the desired material in to the aqueous layer*. Discarded the organic layer. The aqueous layer was basified with Na₂CO₃, bringing the pH up to 10, and then extracted with DCM (4 x 50 mL). The combined organic layer was dried over MgSO₄ and then removed

solvent. Result: light orange oil, 106.1 mg, 37.2% Molecular Formula: C₁₂H₁₆N₂O₂ ESI-MS calc: 220.12 MS: 221.1304 HPLC: 5.554 1H NMR (500 MHz, DMSO-d₆) δ 9.77 (s, 1H), 8.84 (d, J = 4.5 Hz, 1H), 8.73 (d, J = 8.4 Hz, 1H), 7.95 (s, 4H), 7.66 (dd, J = 8.7, 4.6 Hz, 1H), 5.12 – 4.99 (m, 1H), 2.59 (s, 7H). 13C NMR (126 MHz, dms) δ 179.37, 165.02, 162.73, 152.99, 146.27, 140.66, 134.88, 130.23, 122.09, 36.21, 31.20, 14.39, 10.98.

(R,Z)-3-((4-((2-(diethylamino)ethyl)carbamoyl)-3,5-dimethyl-1H-pyrrol-2-yl)methylene)-2-oxo-N-(1-phenylethyl)indoline-5-carboxamide (**134**, RAR-11-96)

To a dried sealed tube were added 97.9 mg (0.371 mmol) of (**133**), 107.0 mg (0.357 mmol) of (**127**) all of which were dissolved in abs. EtOH (3.5 mL). To this solution were added 2 drops of piperidine and heated to reflux (95 °C) for 4 h. Once complete, cooled to room temperature and then filtered off the product as an orange solid. Yield: orange solid, 38.3 mg, 22% Molecular Formula: C₃₁H₃₇N₅O₃ ESI-MS calc: 527.29 ESI-MS found: 528.2955 HPLC: 5.621 1HNMR (500 MHz, DMSO-d₆) δ 13.59 (s, 1H), 11.13 (s, 1H), 8.59 (d, J = 8.1 Hz, 1H), 8.25 (s, 1H), 7.71 (d, J = 6.8 Hz, 2H), 7.44 (d, J = 6.0 Hz, 1H), 7.41 (d, J = 7.9 Hz, 2H), 7.33 (t, J = 7.7 Hz, 2H), 7.22 (t, J = 7.7 Hz, 1H), 6.93 (d, J = 8.3 Hz, 1H), 5.19 (t, J = 7.5 Hz, 1H), 3.28 (d, J = 7.0 Hz, 2H), 2.44 (d, J = 6.7 Hz, 6H), 1.51 (d, J = 7.1 Hz, 3H), 0.97 (t, J = 7.1 Hz, 7H). 13CNMR (176 MHz, dms) δ 169.90, 165.95, 164.71, 145.11, 140.64, 136.48, 129.93, 128.30, 127.78, 126.64, 126.37, 126.18, 125.86, 125.28, 124.09, 120.76, 117.69, 114.37, 108.94, 51.72, 48.55, 46.59, 45.44, 39.86, 39.74, 39.62, 39.50, 39.38, 39.26, 39.14, 37.06, 22.35, 13.40, 11.92, 10.79.

(R,Z)-3-((3,5-dimethyl-4-(prop-2-yn-1-yl)carbamoyl)-1H-pyrrol-2-yl)methylene)-2-oxo-N-(1-phenylethyl)indoline-5-carboxamide (**135**, RAR-11-98)

To a dried sealed tube were added 75.1 mg (0.27 mmol) of (**133**), 50 mg (0.28 mmol) of (**128**) all of which were dissolved in abs. EtOH (1.8 mL). To this solution were added 0.05 mL of piperidine and heated to reflux (95 °C) for 4 h. Once complete, cooled to room temperature and filtered off an orange solid. The solid was rinsed with cold EtOH to give the final product. Yield: bright orange solid, 58.6 mg, 46% Molecular Formula: C₂₈H₂₆N₄O₃ ESI-MS calc: 466.20 ESI-MS found: 467.2037 HPLC: 6.360 1H NMR (700 MHz, DMSO-d₆) δ 13.61 (s, 1H), 11.15 (s, 1H), 8.61 (d, J = 8.0 Hz, 1H), 8.26 (s, 1H), 8.06 (t, J = 5.5 Hz, 1H), 7.71 (d, J = 9.0 Hz, 2H), 7.41 (d, J = 7.8 Hz, 2H), 7.33 (q, J = 5.8, 3.9 Hz, 2H), 7.23 (t, J = 7.2 Hz, 1H), 6.94 (d, J = 8.2 Hz, 1H), 5.20 (t, J = 7.7 Hz, 1H), 4.02 (d, J = 5.5 Hz, 2H), 3.14 – 3.08 (m, 1H), 2.44 (d, J = 9.2 Hz, 7H), 1.51 (d, J = 7.1 Hz, 3H). 13C NMR (176 MHz, dms) δ 170.30, 166.26, 145.52, 141.06, 136.92, 130.46, 128.67, 128.29, 127.00, 126.82, 126.58, 126.28, 124.49, 120.45, 118.23, 115.03, 109.28, 82.17, 73.04, 48.87, 28.49, 22.77, 13.76, 11.13.

(R,Z)-3-((4-(allyl)carbamoyl)-3,5-dimethyl-1H-pyrrol-2-yl)methylene)-2-oxo-N-(1-phenylethyl)indoline-5-carboxamide (**136**, RAR-11-100)

To a dried sealed tube were added 53.6 mg (0.27 mmol) of (**133**), 50 mg (0.28 mmol) of (**129**) all of which were dissolved in abs. EtOH (3 mL). To this solution were added 2 drops (0.05 mL) of piperidine and heated to reflux (95 °C) for 4 h. Once complete, the reaction was cooled to room temperature and then an orange solid was filtered off. The solid was washed with cold EtOH to give the final product. Result: orange solid, 79.5 mg, 63% Molecular Formula: C₂₈H₂₈N₄O₃ ESI-

MS calc: 468.22 ESI-MS found: 469.2224 HPLC: 6.450 1H NMR (700 MHz, DMSO-d₆) δ 13.60 (s, 1H), 11.14 (s, 1H), 8.60 (d, J = 8.0 Hz, 1H), 8.25 (d, J = 1.6 Hz, 1H), 7.83 (t, J = 5.8 Hz, 1H), 7.73 – 7.68 (m, 2H), 7.41 (d, J = 7.6 Hz, 2H), 7.33 (t, J = 7.6 Hz, 2H), 7.22 (t, J = 7.3 Hz, 1H), 6.94 (d, J = 8.1 Hz, 1H), 5.90 (ddt, J = 15.7, 10.3, 5.2 Hz, 1H), 5.22 – 5.18 (m, 2H), 5.10 (dd, J = 10.3, 1.8 Hz, 1H), 3.87 (t, J = 5.6 Hz, 2H), 2.44 (d, J = 7.8 Hz, 6H), 1.51 (d, J = 7.1 Hz, 3H). 13C NMR (176 MHz, dms) δ 170.50, 145.29, 135.97, 130.84, 129.65, 128.44, 128.02, 126.34, 115.20, 108.42, 103.80, 91.16, 59.93, 22.53, 13.55, 10.93.

(R,Z)-3-((4-(but-3-yn-1-ylcarbonyl)-3,5-dimethyl-1H-pyrrol-2-yl)methylene)-2-oxo-N-(1-phenylethyl)indoline-5-carboxamide (**137**, RAR-12-4)

To a dried sealed tube were added 99.9 mg (0.357 mmol) of (**133**), 82 mg of RAR-12-2 (**130**) all of which were dissolved in abs. EtOH (3.5 mL). To this solution were added 2 drops (0.05 mL) of piperidine and heated to reflux (95 °C) for 4 h. Once complete, the solution was cooled to room temperature and then an orange solid was filtered off. The solid was washed with cold EtOH to give the final product. Yield: orange solid, 19 mg, 10% Molecular Formula: C₂₉H₂₈N₄O₃ ESI-MS calc: 480.22 ESI-MS found: 481.2226 HPLC: 6.444 1H NMR (700 MHz, DMSO-d₆) δ 13.60 (s, 1H), 11.15 (s, 1H), 8.62 (d, J = 8.0 Hz, 1H), 8.25 (s, 1H), 7.79 (t, J = 5.8 Hz, 1H), 7.71 (d, J = 6.3 Hz, 2H), 7.41 (d, J = 7.6 Hz, 2H), 7.33 (t, J = 7.6 Hz, 2H), 7.23 (t, J = 7.3 Hz, 1H), 6.94 (d, J = 8.2 Hz, 1H), 5.19 (p, J = 7.3 Hz, 1H), 2.86 (t, J = 2.5 Hz, 1H), 2.45 (d, J = 12.0 Hz, 6H), 2.42 (td, J = 7.1, 2.4 Hz, 2H), 1.51 (d, J = 7.0 Hz, 3H). 13C NMR (176 MHz, dms) δ 169.83, 165.81, 164.71, 145.08, 140.56, 136.34, 130.00, 128.23, 127.80, 126.55, 126.12, 125.79, 125.18, 124.08, 120.61, 117.76, 82.50, 72.12, 48.42, 37.95, 22.33, 13.33, 10.70.

(R,Z)-3-((4-(but-3-en-1-ylcarbonyl)-3,5-dimethyl-1H-pyrrol-2-yl)methylene)-2-oxo-N-(1-phenylethyl)indoline-5-carboxamide (**138**, RAR-12-5)

To a dried sealed tube were added 94.8 mg (0.27 mmol) of (**133**), 87.2 mg (0.28 mmol) of RAR-12-3 (**131**) all of which were dissolved in abs. EtOH (2.2 mL). To this solution were added 2 drops (0.07 mL) of piperidine and heated to reflux (95 °C) for 4 h. Once complete, solution was cooled to room temperature and then purified by column chromatography. Fractions were collected and solvent was removed under pressure to give the desired product, as an orange solid. Yield: orange solid, 103 mg, 59% Molecular Formula: C₂₉H₃₀N₄O₃ ESI-MS calc: 482.23 ESI-MS found: 483.2382 [M+1] HPLC: 6.720 1H NMR (700 MHz, DMSO-d₆) δ 13.54 (s, 1H), 11.13 (s, 1H), 8.61 (d, J = 8.2 Hz, 2H), 8.27 – 8.18 (m, 2H), 7.73 – 7.71 (m, 1H), 7.68 (s, 1H), 7.42 (d, J = 8.3 Hz, 3H), 7.35 – 7.31 (m, 4H), 7.25 – 7.21 (m, 2H), 6.94 (d, J = 8.1 Hz, 1H), 5.21 (p, J = 7.3 Hz, 2H), 2.43 (d, J = 9.0 Hz, 2H), 2.29 (d, J = 11.4 Hz, 7H), 1.63 – 1.59 (m, 3H), 1.51 (d, J = 7.1 Hz, 6H). 13C NMR (176 MHz, dms) δ 169.79, 165.81, 165.04, 145.07, 140.57, 133.90, 128.74, 128.19, 127.78, 126.52, 126.11, 125.22, 123.96, 120.71, 117.70, 116.21, 114.09, 108.74, 48.41, 35.77, 33.74, 22.26, 12.40, 10.15.

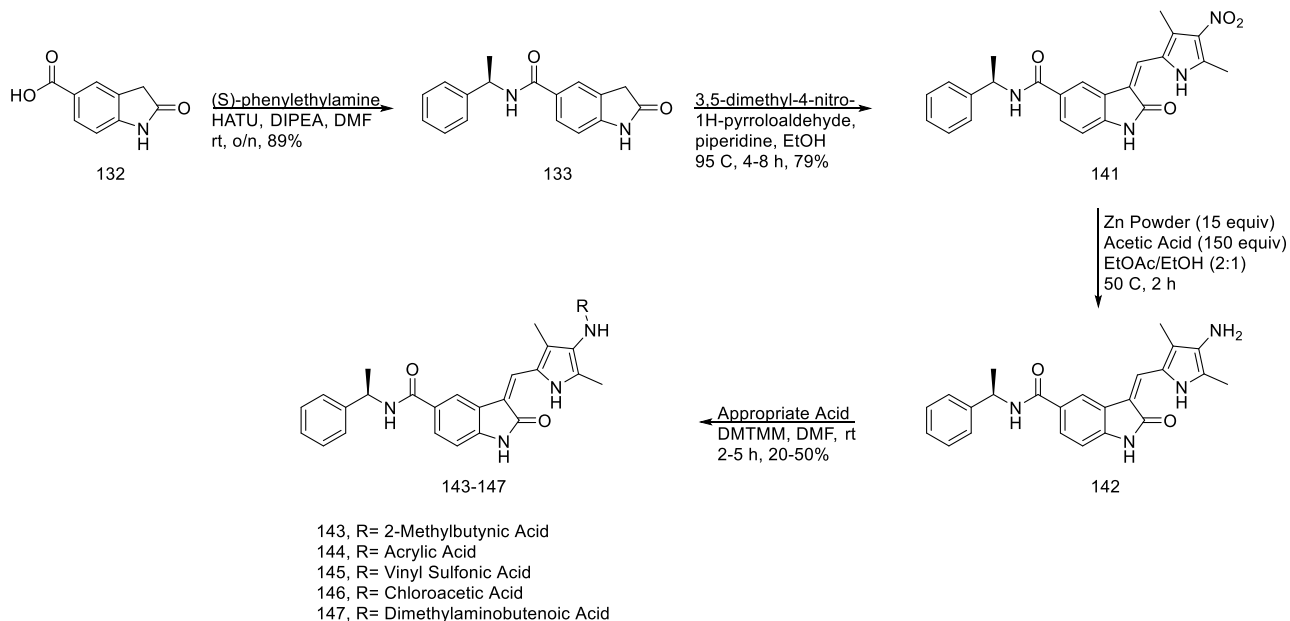
(S)-2-oxo-N-(1-phenylethyl)indoline-5-carboxamide (**139**)

To a round bottom flask were added 201.8 mg (1.13 mmol) of 2-oxoindoline-5-carboxylic acid, dissolved in 7 mL of dry DMF. To this dark red solution were added 0.160 mL (1.24 mmol) of (S)-1-phenylethan-1-amine, 0.200 mL (1.13 mmol) of DIPEA and 492.4 mg (1.30 mmol) of HATU. The resultant dark red solution was allowed to stir at rt for 12 h, and then added 200 mL

of sat. Na₂CO₃ and extracted with EtOAc (3 x 100 mL). The combined organic layer was washed with brine (2 x 50 mL) and then dried over MgSO₄. Purified by column chromatography (0-15% DCM/MeOH) to give the desired product as a strawberry pink solid. Yield: 280 mg, 84%
Molecular Formula: C₁₇H₁₆N₂O₂ ESI-MS calc: 280.12 ESI-MS found: 281.0903 [M+1] HPLC: 5.249 1H NMR (500 MHz, DMSO-d₆) δ 10.67 (s, 1H), 8.66 (d, J = 8.0 Hz, 1H), 7.78 (d, J = 7.2 Hz, 2H), 7.38 (d, J = 8.4 Hz, 2H), 7.31 (t, J = 7.6 Hz, 2H), 7.20 (t, J = 7.3 Hz, 1H), 6.86 (d, J = 8.2 Hz, 1H), 5.15 (p, J = 7.2 Hz, 1H), 3.53 (s, 2H), 1.46 (d, J = 7.1 Hz, 3H). 13C NMR (176 MHz, dms) δ 176.83, 165.50, 146.49, 145.22, 128.27, 127.77, 127.54, 126.60, 126.14, 125.64, 123.69, 108.62, 48.52, 39.86, 39.74, 39.62, 39.50, 39.38, 39.26, 39.14, 35.70, 22.40.

(S,Z)-3-((4-((2-(diethylamino)ethyl)carbonyl)-3,5-dimethyl-1H-pyrrol-2-yl)methylene)-2-oxo-N-(1-phenylethyl)indoline-5-carboxamide (**140**)

To a dried sealed tube were added 91.2 mg (0.325 mmol) of (**139**), 79.9 mg (0.299 mmol) of (**127**) all of which were dissolved in abs. EtOH (2.5 mL). To this solution were added 2 drops of piperidine and heated to reflux (95 °C) for 4 h. Once complete, cooled to room temperature and then filtered off the product as an orange solid. Yield: orange solid, 38.3 mg, 22% Molecular Formula: C₃₁H₃₇N₅O₃ ESI-MS calc: 527.29 ESI MS found: 528.2043 HPLC: 5.753 1H NMR (500 MHz, DMSO-d₆) δ 13.59 (s, 1H), 11.16 (s, 1H), 8.67 (s, 1H), 8.32 (d, J = 5.5 Hz, 1H), 7.75 – 7.68 (m, 2H), 7.48 (s, 1H), 7.42 (d, J = 7.7 Hz, 3H), 7.32 (t, J = 7.6 Hz, 3H), 7.22 (t, J = 7.3 Hz, 1H), 6.94 (d, J = 8.1 Hz, 1H), 5.19 (p, J = 7.2 Hz, 1H), 2.45 (d, J = 3.4 Hz, 8H), 2.37 (s, 1H), 2.32 (s, 1H), 2.08 (s, 1H), 1.51 (d, J = 7.1 Hz, 4H), 0.99 (t, J = 7.5 Hz, 8H). 13C NMR (126 MHz, dms) δ 170.28, 147.82, 141.01, 130.32, 128.66, 127.23, 126.98, 126.61, 126.26, 125.66, 124.60, 118.30, 106.84, 102.36, 48.92, 47.02, 22.80, 17.46, 13.83, 11.24, 9.18.



Scheme 4.4. Synthesis of compounds 143-147

(R,Z)-3-((3,5-dimethyl-4-nitro-1H-pyrrol-2-yl)methylene)-2-oxo-N-(1-phenylethyl)indoline-5-carboxamide (**141**, RAR-12-6)

To a dried sealed tube were added 91.2 mg (0.892 mmol) of (**133**), 79.9 mg (1.39 mmol) of 3,5-dimethyl-4-nitro-1H-pyrrole-2-carbaldehyde, all of which were dissolved in abs. EtOH (2.5 mL). To this solution were added 2 drops (0.05 mL) of piperidine and heated to reflux (95 °C) for 4 h. Once complete, the reaction was cooled to room temperature and an orange solid was filtered off. The solid was washed with cold EtOH to give the desired product. Result: orange solid, 269.3 mg, 69% Molecular Formula: C₂₄H₂₂N₄O₄ ESI-MS calc: 430.16 ESI-MS found: 431.1715 HPLC: 7.400 1H NMR (700 MHz, DMSO-d₆) δ 8.63 (d, J = 8.0 Hz, 1H), 8.36 (d, J = 1.6 Hz, 1H), 7.83 (s, 1H), 7.76 (dd, J = 8.1, 1.7 Hz, 1H), 7.41 (d, J = 7.5 Hz, 2H), 7.33 (t, J = 7.6 Hz, 2H), 7.22 (t, J = 7.3 Hz, 1H), 6.97 (d, J = 8.1 Hz, 1H), 5.19 (p, J = 7.2 Hz, 1H), 2.08 (d, J = 1.0 Hz, 1H), 1.50 (d, J = 7.1 Hz, 3H). 13C NMR (176 MHz, dmsO) δ 169.90, 165.69, 144.98, 142.47, 136.80, 132.12, 130.48, 129.11, 128.20, 127.74, 126.10, 125.56, 123.33, 121.76, 115.38, 53.66, 22.28, 18.23, 10.50.

(R,Z)-3-((4-amino-3,5-dimethyl-1H-pyrrol-2-yl)methylene)-2-oxo-N-(1-phenylethyl)indoline-5-carboxamide (**142**, RAR-12-7)

To a flask were added 90.7 mg of (**141**), dissolved in 5 mL of 2:1 EtOH/EtOAc. To this slurry were added 226.8 mg (14 equiv) of Zn powder and 2 mL (150 equiv) of AcOH. The turbid orange solution was allowed to stir at 50 C for 2 h. Once complete, the reaction was cooled to rt and then add EtOAc before basifying with sat. Na₂CO₃. The basified aqueous layer was extracted with EtOAc (3 x 30 mL) and then washed with water and brine (1 x 30 mL), respectively. The organic layer was dried over MgSO₄ and then solvent was removed under pressure to give the desired product as a red solid.²⁴ *Note: the free amine is very reactive, so it was moved forward without further characterization* Result: orange solid, 66.7 mg, 79.0% Molecular Formula: C₂₄H₂₄N₄O₂ ESI-MS calc: 400.19 ESI-MS found: 401.1955 HPLC: 5.177 1H NMR (700 MHz, DMSO-d₆) δ 13.45 (s, 1H), 10.88 (s, 1H), 8.56 (d, J = 8.0 Hz, 1H), 8.12 (d, J = 1.6 Hz, 1H), 7.62 (dd, J = 8.1, 1.6 Hz, 1H), 7.46 (s, 1H), 7.41 (d, J = 7.6 Hz, 3H), 7.33 (t, J = 7.6 Hz, 3H), 7.22 (t, J = 7.3 Hz, 1H), 6.89 (d, J = 8.1 Hz, 1H), 5.20 (q, J = 7.4 Hz, 1H), 4.02 (d, J = 14.5 Hz, 2H), 2.26 (s, 3H), 2.17 (s, 3H), 1.51 (d, J = 7.1 Hz, 3H).

(R,Z)-3-((4-(but-2-ynamido)-3,5-dimethyl-1H-pyrrol-2-yl)methylene)-2-oxo-N-(1-phenylethyl)indoline-5-carboxamide (**143**, RAR-12-17)

To a flask were added 22.3 mg (0.37 mmol) of butynoic acid, 157.5 mg (0.37 mmol) of HATU, cat. DMAP and 50 mg (0.19 mmol) of RAR-12-15 dissolved in 1 mL of DMF. To this bright red solution were added 0.25 mL (1.3 mmol) of DIPEA, and the solution was allowed to stir at rt for 2 h. Once complete, the reaction mixture was diluted with EtOAc and washed with sat. LiCl and then dried over MgSO₄. The crude material was purified by preparatory TLC with 50% Acetone/Hexanes. The desired band was collected, and the material was rinsed off the silica gel with acetone and then solvent was removed under pressure to give the desired product. Result: yellow solid, 17.5 mg, 20% Molecular Formula: C₂₈H₂₆N₄O₃ ESI-MS calc: 466.20 ESI-MS found 467.2071 HPLC: 6.336 1H NMR (700 MHz, DMSO-d₆) δ 13.53 (s, 1H), 11.07 (s, 1H), 9.78 (s, 1H), 8.86 (d, J = 4.5 Hz, 2H), 8.68 (d, J = 8.8 Hz, 2H), 8.60 (d, J = 7.7 Hz, 2H), 8.21 (s, 1H), 7.69 (d, J = 8.9 Hz, 2H), 7.65 – 7.62 (m, 3H), 7.41 (d, J = 7.9 Hz, 5H), 7.33 (t, J = 7.3 Hz, 7H), 7.23 (d, J = 7.0 Hz, 3H), 6.93 (d, J = 8.1 Hz, 1H), 6.59 (s, 3H), 5.21 – 5.17 (m, 1H), 2.19 (s, 4H), 2.17 (s, 4H), 2.03 (s, 3H), 1.52 (s, 2H). 13C NMR (176 MHz, dmsO) δ 170.28, 167.22, 165.79, 149.50, 148.74, 145.19, 139.73, 135.08, 130.24, 128.98, 128.19, 127.41, 126.55, 125.97, 125.02, 122.58, 120.62, 117.41, 112.97, 55.89, 22.67, 12.09, 9.59, 3.60.

(R,Z)-3-((4-acrylamido-3,5-dimethyl-1H-pyrrol-2-yl)methylene)-2-oxo-N-(1-phenylethyl)indoline-5-carboxamide (**144**, RAR-12-32)

To a round bottom flask that contained RAR-12-31 (50 mg, 0.12 mmol) were added 0.01 mL (0.12 mmol) of acrylic acid, 58.8 mg (0.12 mmol) of HATU, cat. DMAP and 0.50 mL (0.87 mmol) of TEA. All materials were dissolved in 2 mL of DMF and sonicated to give a homogenous solution. The solution was allowed to stir at 56 °C for two hours. Once complete, quenched with sat. LiCl and then extracted with EtOAc (3 x 30 mL). The combined organic layers were then dried over MgSO₄ and the material was purified by preparatory TLC (50% Acetone/Hexanes) collecting the baseline product, which was washed off the silica gel with acetone. The solvent was removed to give the final product as an orange solid, 13.9 mg, 24%. Molecular Formula: C₂₇H₂₆N₄O₃ ESI-MS calc: 454.20 ESI-MS found: 455.1632 [M+1] HPLC: 6.147 ¹H NMR (700 MHz, DMSO-*d*₆) δ 13.53 (s, 1H), 11.07 (s, 1H), 9.41 (s, 1H), 8.60 (d, *J* = 8.1 Hz, 2H), 8.21 (d, *J* = 9.5 Hz, 1H), 7.69 (d, *J* = 8.3 Hz, 2H), 7.66 (s, 1H), 7.41 (d, *J* = 7.8 Hz, 5H), 7.33 (t, *J* = 7.5 Hz, 5H), 7.22 (t, *J* = 7.4 Hz, 3H), 6.93 (dd, *J* = 8.1, 3.6 Hz, 1H), 6.45 (dd, *J* = 17.1, 10.3 Hz, 1H), 6.23 – 6.19 (m, 1H), 5.72 (dd, *J* = 10.7, 1.9 Hz, 1H), 5.19 (t, *J* = 7.3 Hz, 2H), 2.21 (s, 3H), 2.20 (s, 3H), 1.50 (d, *J* = 7.1 Hz, 3H). ¹³C NMR (176 MHz, dms) δ 180.81, 169.69, 169.00, 167.87, 165.86, 153.99, 145.07, 141.22, 140.27, 136.23, 131.78, 129.29, 128.18, 127.56, 126.86, 126.49, 126.09, 124.16, 120.41, 109.40, 108.64, 53.84, 22.28.

(R,Z)-3-((3,5-dimethyl-4-(vinylsulfonamido)-1H-pyrrol-2-yl)methylene)-2-oxo-N-(1-phenylethyl)indoline-5-carboxamide (**145**, RAR-12-34)

Step 1: To a dried flask were added 0.03 mL (0.12 mmol) of vinyl sulfonic acid, 2 drops of DMF and 2 mL of DCM. The solution was cooled to 0 °C and then 0.02 mL (0.14 mmol) of oxalyl chloride were added in one portion. The solution was warmed to rt and allowed to stir until complete (1 hour). Once complete, then solvent was removed, and the resultant clear oil was rinsed with DCM (3 x 15 mL) and dried under high pressure until ready for second step

Step 2: To the flask holding the acid chloride were added RAR-12-33 (50 mg, 0.12 mmol) dissolved in 3 mL of THF. To this murky orange solution were added 0.50 mL (7 equiv) of TEA, and the solution was allowed to stir at rt for 5 hours. Once complete, removed solvent under pressure and brought yellow residue back up in EtOAc. The organic layer was washed with sat. Na₂CO₃ and then brine (1 x 30 mL) respectively. Purified by preparatory TLC plate (40% Acetone/Hexanes), collecting secondary spot (*R*_f = 0.2-0.3). The material was rinsed off silica with acetone and the solvent was removed to give a dark orange solid as the desired product. Result: orange solid, 16 mg, 27% Molecular Formula: C₂₆H₂₆N₄O₄S ESI-MS calc: 490.17 ESI-MS found: 491.1249 HPLC: 6.43 ¹H NMR (400 MHz, DMSO-*d*₆) δ 13.50 (s, 1H), 11.38 (s, 1H), 11.09 (s, 1H), 8.98 (s, 1H), 8.64 – 8.57 (m, 2H), 8.36 (s, 1H), 8.20 (s, 1H), 7.84 (s, 1H), 7.77 (d, *J* = 8.3 Hz, 1H), 7.70 (d, *J* = 8.2 Hz, 1H), 7.63 (s, 1H), 7.41 (d, *J* = 7.8 Hz, 5H), 7.33 (t, *J* = 7.6 Hz, 5H), 7.21 (d, *J* = 7.3 Hz, 2H), 6.98 (s, 1H), 6.93 (d, *J* = 8.1 Hz, 1H), 6.84 (dd, *J* = 16.5, 9.8 Hz, 1H), 5.93 (d, *J* = 8.0 Hz, 1H), 5.19 (t, *J* = 7.4 Hz, 2H), 2.29 (s, 4H), 2.26 (s, 3H), 1.50 (d, *J* = 7.1 Hz, 6H). ¹³C NMR (176 MHz, dms) δ 169.90, 165.56, 145.07, 141.33, 136.84, 133.74, 128.32, 128.19, 127.65, 126.53, 126.15, 125.20, 124.79, 124.46, 123.83, 119.49, 119.12, 109.21, 48.52, 45.44, 39.88, 39.76, 39.64, 39.52, 39.40, 39.28, 39.16, 22.33, 14.83, 11.29, 8.63.

(R,Z)-3-((4-(2-chloroacetamido)-3,5-dimethyl-1H-pyrrol-2-yl)methylene)-2-oxo-N-(1-phenylethyl)indoline-5-carboxamide (**146**, RAR-12-52)

To a dried round bottom flask were added RAR-12-51 (60 mg, 0.15 mmol) dissolved in 3 mL of THF. The yellow solution was cooled to 0 °C and 0.01 mL (0.18 mmol) of chloroacetylchloride was added dropwise. The solution was allowed to stir at 0 °C for 30 mins. Once complete by TLC, quenched with water and extracted with EtOAc. The solvent was removed, and the crude material was purified by prep plate (50% Acetone/Hexanes) collecting the major product. The desired product was rinsed off of silica gel and then the solvent was removed to give a bright yellow solid. The yellow solid was washed with DCM and sonicated to give a red solid. The red solid was then pulped in water:acetone (30:1) to give the final product. Result: red solid, 25.1 mg, 35% Molecular Formula: C₂₆H₂₅ClN₄O₃ ESI-MS calc: 476.16 ESI-MS found: 477.0999 HPLC: 6.388 ¹H NMR (700 MHz, DMSO-*d*₆) δ 11.08 (s, 1H), 9.53 (s, 1H), 8.60 (d, *J* = 8.0 Hz, 1H), 8.22 (s, 1H), 7.69 (d, *J* = 8.2 Hz, 1H), 7.65 (s, 1H), 7.41 (d, *J* = 7.8 Hz, 2H), 7.33 (t, *J* = 7.5 Hz, 2H), 7.22 (t, *J* = 7.4 Hz, 1H), 6.93 (d, *J* = 8.0 Hz, 1H), 5.19 (t, *J* = 7.5 Hz, -1H), 2.20 (d, *J* = 12.1 Hz, 7H), 2.08 (s, 3H), 1.50 (d, *J* = 7.1 Hz, 3H). ¹³C NMR (176 MHz, dms) δ 169.67, 168.51, 156.78, 145.12, 140.30, 131.64, 129.98, 128.13, 127.50, 126.89, 126.44, 126.11, 124.45, 122.62, 121.01, 117.42, 116.93, 112.94, 48.39, 42.71, 22.29, 11.67, 9.24.

(Z)-3-((4-((*E*)-4-(dimethylamino)but-2-enamido)-3,5-dimethyl-1H-pyrrol-2-yl)methylene)-2-oxo-N-((*R*)-1-phenylethyl)indoline-5-carboxamide (**147**, RAR-12-54)

To a round bottom flask were added RAR-12-53 (50 mg, 0.12 mmol), 20.2 mg (0.12 mmol) of N,N-dimethylaminobutenoic acid and 36 mg (0.12 mmol) of DMTMM and 0.20 mL (0.24 mmol) of TEA. All materials were brought up in 2 mL of DMF, and the resulting solution was allowed to stir at rt for 12 h. Once complete, the reaction was quenched with Sat. NaCl, and extracting with EtOAc (3 x 50 mL). The organic layer was washed with sat. Na₂CO₃ and brine (1 x 50 mL) respectively and then dried over MgSO₄. The solvent was removed under pressure, evaporating the material onto silica gel. Purified by column chromatography 5-100% Acetone/Hexanes. Flushed the column with 7N NH₃ in MeOH to yield the final product as a bright yellow oil. Result: yellow oil, 13 mg, 20% Molecular Formula: C₃₀H₃₃N₅O₃ ESI-MS calc: 511.26 ESI-MS found: 512.2110 [M+1], 534.1905 [M+Na] HPLC: 5.424 ¹H NMR (700 MHz, DMSO-*d*₆) δ 13.56 (s, 1H), 11.06 (s, 2H), 9.29 (s, 2H), 8.59 (d, *J* = 7.9 Hz, 2H), 8.21 (d, *J* = 1.5 Hz, 2H), 7.68 (d, *J* = 8.1 Hz, 2H), 7.65 (s, 2H), 7.41 (d, *J* = 7.6 Hz, 4H), 7.33 (t, *J* = 7.6 Hz, 4H), 7.22 (t, *J* = 7.5 Hz, 2H), 6.93 (d, *J* = 8.1 Hz, 2H), 6.71 – 6.64 (m, 1H), 6.27 (d, *J* = 15.5 Hz, 1H), 5.21 – 5.17 (m, 1H), 3.05 (d, *J* = 5.6 Hz, 2H), 2.21 (s, 6H), 2.19 (s, 3H), 2.18 (s, 3H), 1.50 (d, *J* = 7.1 Hz, 3H). ¹³C NMR (176 MHz, dms) δ 170.09, 166.24, 163.98, 145.47, 141.00, 140.66, 132.25, 128.68, 128.55, 127.91, 127.30, 126.87, 126.48, 126.08, 125.81, 125.74, 125.61, 124.86, 124.52, 122.19, 117.61, 112.99, 109.03, 62.41, 48.96, 25.82, 22.64, 14.44, 12.32, 9.77.

(R)-2-oxo-N-(1-(*m*-tolyl)ethyl)indoline-5-carboxamide (**148** RAR-12-63)

To a round bottom flask were added 236.1 mg (1.33 mmol) of 2-oxoindoline-5-carboxylic acid, dissolved in 7 mL of dry DMF. To this dark red solution were added 0.200 mL (1.47 mmol) of (*R*)-1-(*m*-tolyl)ethan-1-amine, 0.300 mL (1.73 mmol) of DIPEA and 510.2 mg (1.33 mmol) of

HATU. The resultant dark red solution was allowed to stir at rt for 12 h, and then added 200 mL of sat. Na₂CO₃ and extracted with EtOAc (3 x 100 mL). The combined organic layer was washed with brine (2 x 50 mL) and then dried over MgSO₄. Purified by column chromatography (0-15% DCM/MeOH) to give the desired product as a strawberry pink solid. Yield: 125.6 mg, 31% Molecular Formula: C₁₈H₁₈N₂O₂ ESI-MS calc: 294.14 ESI-MS found: 295.0167 [M+1] HPLC: 5.395 1H NMR (700 MHz, DMSO-d₆) δ 10.61 (s, 1H), 8.58 (d, J = 8.1 Hz, 1H), 7.77 (d, J = 8.1 Hz, 2H), 7.18 (p, J = 7.6 Hz, 4H), 7.02 (d, J = 7.3 Hz, 1H), 6.85 (d, J = 7.9 Hz, 1H), 5.11 (p, J = 7.3 Hz, 1H), 2.28 (s, 3H), 1.44 (d, J = 7.0 Hz, 3H). 13C NMR (176 MHz, dmsO) δ 176.62, 165.16, 146.32, 145.07, 137.11, 128.06, 127.65, 127.48, 127.10, 126.66, 125.53, 123.51, 123.09, 108.36, 48.29, 39.86, 39.74, 39.62, 39.50, 39.38, 39.26, 39.14, 38.22, 35.57, 22.34, 21.11.

(R)-N-(1-(4-fluorophenyl)ethyl)-2-oxoindoline-5-carboxamide (149 RAR-12-74)

To a round bottom flask were added 246.6 mg (1.41 mmol) of 2-oxoindoline-5-carboxylic acid, dissolved in 7 mL of dry DMF. To this dark red solution were added 0.200 mL (1.55 mmol) of (R)-1-(4-fluorophenyl)ethan-1-amine, 0.25 mL (1.41 mmol) of DIPEA and 667.1 mg (1.61 mmol) of HATU. The resultant dark red solution was allowed to stir at rt for 12 h, and then added 200 mL of sat. Na₂CO₃ and extracted with EtOAc (3 x 100 mL). The combined organic layer was washed with brine (2 x 50 mL) and then dried over MgSO₄. Purified by column chromatography (0-15% DCM/MeOH) to give the desired product as a strawberry pink solid. Yield: 315 mg, 71% Molecular Formula: C₁₇H₁₅FN₂O₂ ESI-MS calc: 298.11 ESI-MS found: 299.1216 [M+1] HPLC: 5.414 1H NMR (500 MHz, DMSO-d₆) δ 10.61 (s, 1H), 8.62 (d, J = 8.0 Hz, 1H), 7.76 (d, J = 7.5 Hz, 2H), 7.43 – 7.38 (m, 2H), 7.16 – 7.08 (m, 2H), 6.87 – 6.82 (m, 1H), 5.14 (p, J = 7.2 Hz, 1H), 3.53 (s, 2H), 1.45 (d, J = 7.1 Hz, 3H). 13C NMR (176 MHz, dmsO) δ 176.84, 165.47, 160.34, 146.46, 141.34, 128.06, 128.01, 127.77, 127.49, 125.69, 123.63, 114.99, 114.87, 108.55, 47.90, 39.86, 39.74, 39.62, 39.50, 39.38, 39.26, 39.14, 38.33, 35.67, 22.35.

(R)-2-oxo-N-(1-(pyridin-4-yl)ethyl)indoline-5-carboxamide (150 RAR-12-75)

To a round bottom flask were added 248.1 mg (1.41 mmol) of 2-oxoindoline-5-carboxylic acid, dissolved in 7 mL of dry DMF. To this dark red solution were added 0.200 mL (1.55 mmol) of (R)-1-(pyridin-4-yl)ethan-1-amine, 0.25 mL (1.41 mmol) of DIPEA and 652.4 mg (1.61 mmol) of HATU. The resultant dark red solution was allowed to stir at rt for 12 h, and then added 200 mL of sat. Na₂CO₃ and extracted with EtOAc (3 x 100 mL). The combined organic layer was washed with brine (2 x 50 mL) and then dried over MgSO₄. Purified by column chromatography (0-15% DCM/MeOH) to give the desired product as a strawberry pink solid. Yield: 200 mg, 48% Molecular Formula: C₁₆H₁₅N₃O₂ ESI-MS calc: 281.12 ESI-MS found: 282.1236 [M+1] HPLC: 2.378 1H NMR (700 MHz, DMSO-d₆) δ 10.64 (s, 1H), 8.74 (dd, J = 7.6, 2.1 Hz, 1H), 8.55 – 8.52 (m, 2H), 7.79 (dd, J = 7.5, 2.2 Hz, 2H), 7.45 – 7.42 (m, 2H), 7.08 (d, J = 2.3 Hz, 1H), 7.01 (s, 1H), 6.89 – 6.85 (m, 1H), 5.14 (td, J = 7.3, 2.2 Hz, 1H), 3.55 (s, 2H), 3.46 – 3.41 (m, 3H), 1.47 (dd, J = 7.2, 2.3 Hz, 3H), 1.07 – 1.03 (m, 3H). 13C NMR (176 MHz, dmsO) δ 176.63, 165.65, 155.16, 148.63, 146.56, 127.76, 127.03, 125.62, 123.57, 121.58, 108.43, 56.00, 47.92, 39.86, 39.74, 39.62, 39.50, 39.38, 39.26, 39.14, 35.56, 21.45, 18.54.

(R)-2-oxo-N-(1-(pyridin-2-yl)ethyl)indoline-5-carboxamide (151 RAR-12-78)

To a round bottom flask were added 251.1 mg (1.41 mmol) of 2-oxoindoline-5-carboxylic acid, dissolved in 7 mL of dry DMF. To this dark red solution were added 0.200 mL (1.55 mmol) of (R)-1-(pyridin-2-yl)ethan-1-amine, 0.25 mL (1.41 mmol) of DIPEA and 625.1 mg (1.62 mmol) of

HATU. The resultant dark red solution was allowed to stir at rt for 12 h, and then added 200 mL of sat. Na₂CO₃ and extracted with EtOAc (3 x 100 mL). The combined organic layer was washed with brine (2 x 50 mL) and then dried over MgSO₄. Purified by column chromatography (0-15% DCM/MeOH) to give the desired product as a strawberry pink solid. Yield: 165 mg, 39%
Molecular Formula: C₁₆H₁₅N₃O₂ ESI-MS calc: 281.12 ESI-MS found: 282.1236 [M+1] HPLC: 2.111 1H NMR (700 MHz, DMSO-d₆) δ 10.62 (d, J = 5.2 Hz, 1H), 8.63 (t, J = 6.6 Hz, 1H), 8.51 (t, J = 5.3 Hz, 1H), 7.80 (d, J = 5.6 Hz, 2H), 7.74 (q, J = 7.0 Hz, 1H), 7.38 (t, J = 6.8 Hz, 1H), 7.24 (q, J = 6.0 Hz, 1H), 6.86 (t, J = 6.7 Hz, 1H), 5.17 (p, J = 7.2 Hz, 1H), 3.54 (d, J = 5.2 Hz, 3H), 1.49 (t, J = 6.4 Hz, 3H). 13C NMR (176 MHz, dmsO) δ 177.27, 166.16, 163.50, 149.12, 137.26, 128.18, 127.79, 126.11, 124.08, 122.46, 120.59, 108.98, 50.76, 40.22, 40.10, 39.98, 39.86, 39.74, 39.62, 39.50, 36.07, 21.45.

(R)-N-(1-(3-chlorophenyl)ethyl)-2-oxoindoline-5-carboxamide (152 RAR-12-86)

To a round bottom flask were added 251.1 mg (1.41 mmol) of 2-oxoindoline-5-carboxylic acid, dissolved in 7 mL of dry DMF. To this dark red solution were added 0.200 mL (1.55 mmol) of (R)-1-(3-chlorophenyl)ethan-1-amine, 0.25 mL (1.41 mmol) of DIPEA and 717.7 mg (1.91 mmol) of HATU. The resultant dark red solution was allowed to stir at rt for 12 h, and then added 200 mL of sat. Na₂CO₃ and extracted with EtOAc (3 x 100 mL). The combined organic layer was washed with brine (2 x 50 mL) and then dried over MgSO₄. Purified by column chromatography (0-15% DCM/MeOH) to give the desired product as a strawberry pink solid. Yield: 423.3 mg, 91%
Molecular Formula: C₁₇H₁₅ClN₂O₂ ESI-MS calc: 314.08 ESI-MS found: 315.0438 [M+1] HPLC: 5.730 1H NMR (700 MHz, DMSO-d₆) δ 10.64 – 10.57 (m, 1H), 8.65 (dd, J = 7.5, 2.2 Hz, 1H), 7.78 – 7.74 (m, 2H), 7.41 (t, J = 2.1 Hz, 1H), 7.33 (dt, J = 6.7, 1.8 Hz, 2H), 7.26 (dp, J = 6.4, 2.2 Hz, 1H), 6.85 (dd, J = 8.1, 2.5 Hz, 1H), 5.15 – 5.06 (m, 1H), 3.53 (s, 2H), 1.45 – 1.42 (m, 3H). 13C NMR (176 MHz, dmsO) δ 176.91, 165.61, 148.09, 146.73, 133.15, 130.39, 127.97, 126.74, 126.14, 125.88, 125.13, 123.78, 108.70, 56.27, 48.40, 40.12, 40.00, 39.88, 39.76, 39.64, 39.52, 39.40, 35.83, 22.43, 18.80.

(R)-2-oxo-N-(1-(p-tolyl)ethyl)indoline-5-carboxamide (153 RAR-12-90)

To a round bottom flask were added 244.2 mg (1.41 mmol) of 2-oxoindoline-5-carboxylic acid, dissolved in 7 mL of dry DMF. To this dark red solution were added 0.220 mL (1.55 mmol) of (R)-1-(3-chlorophenyl)ethan-1-amine, 0.25 mL (1.41 mmol) of DIPEA and 622.1 mg (1.62 mmol) of HATU. The resultant dark red solution was allowed to stir at rt for 12 h, and then added 200 mL of sat. Na₂CO₃ and extracted with EtOAc (3 x 100 mL). The combined organic layer was washed with brine (2 x 50 mL) and then dried over MgSO₄. Purified by column chromatography (0-15% DCM/MeOH) to give the desired product as a strawberry pink solid. Yield: 300.8 mg, 69%
Molecular Formula: C₁₈H₁₈N₂O₂ ESI-MS calc: 294.14 ESI-MS found: 317 [M+Na] HPLC: 5.556 1H NMR (700 MHz, DMSO-d₆) δ 10.61 (s, 1H), 8.57 (d, J = 8.1 Hz, 1H), 7.77 (d, J = 8.1 Hz, 2H), 7.26 (d, J = 7.8 Hz, 2H), 7.11 (d, J = 7.8 Hz, 2H), 6.85 (d, J = 8.0 Hz, 1H), 5.12 (p, J = 7.3 Hz, 1H), 3.53 (s, 2H), 2.26 (s, 3H), 1.44 (d, J = 7.0 Hz, 3H). 13C NMR (176 MHz, dmsO) δ 176.63, 165.17, 146.30, 142.10, 135.44, 128.66, 127.64, 127.54, 125.93, 125.51, 123.51, 108.36, 48.03, 39.86, 39.74, 39.62, 39.50, 39.38, 39.26, 39.14, 35.57, 22.29, 20.59.

N-benzyl-2-oxoindoline-5-carboxamide (154, RAR-12-100)

Prepared with protocol described in making **133**. Yields a strawberry pink solid, 174.5 mg, 56%
Molecular Formula: C₁₆H₁₄N₂O₂ ESI-MS calc: 266.11 ESI-MS found: 267.2180 [M+1] HPLC:

4.822 1H NMR (700 MHz, DMSO-d₆) δ 10.61 (s, 1H), 8.87 (t, J = 6.1 Hz, 1H), 7.79 – 7.75 (m, 2H), 7.34 – 7.28 (m, 5H), 7.23 (dt, J = 7.2, 4.3 Hz, 2H), 6.86 (d, J = 8.0 Hz, 1H), 4.46 (d, J = 5.9 Hz, 2H), 3.53 (s, 2H). 13C NMR (176 MHz, dmsO) δ 176.60, 165.95, 146.42, 139.88, 128.65, 128.19, 128.12, 127.70, 127.59, 127.47, 127.29, 127.11, 126.61, 125.66, 123.45, 108.44, 47.80, 45.00, 42.52, 39.86, 39.74, 39.62, 39.50, 39.38, 39.26, 39.14, 38.22, 35.57.

(R)-N-(2-methyl-1-phenylpropyl)-2-oxoindoline-5-carboxamide (155, RAR-13-4)

Synthesized using protocol described in **133**. Yields a strawberry pink solid, 389.9 mg, quantitative yield. Molecular Formula: C₁₉H₂₀N₂O₂ ESI-MS calc: 308.15 ESI-MS found: 309.2172 HPLC: 5.793 1H NMR (700 MHz, DMSO-d₆) δ 10.44 (s, 1H), 8.37 (d, J = 8.9 Hz, 1H), 7.58 (dd, J = 10.7, 2.9 Hz, 2H), 7.22 (d, J = 7.6 Hz, 2H), 7.12 (t, J = 7.5 Hz, 2H), 7.03 (t, J = 7.3 Hz, 1H), 6.68 (d, J = 8.0 Hz, 1H), 4.48 (t, J = 9.2 Hz, 1H), 3.36 (s, 2H), 1.06 (d, J = 6.4 Hz, 2H), 0.83 (d, J = 6.5 Hz, 3H), 0.53 (d, J = 6.7 Hz, 3H). 13C NMR (176 MHz, dmsO) δ 176.69, 165.65, 164.62, 162.32, 146.32, 143.33, 128.02, 127.75, 127.70, 127.41, 126.61, 125.54, 123.53, 108.43, 59.92, 56.08, 41.67, 39.86, 39.74, 39.62, 39.50, 39.38, 39.26, 39.14, 38.23, 35.78, 35.62, 32.55, 30.77, 20.09, 19.90, 18.56.

2-oxo-N-(3-phenyloxetan-3-yl)indoline-5-carboxamide (156, RAR-13-8)

Synthesized using protocol described in **133**. Yield a strawberry pink solid, 62.1 mg, 31% Molecular Formula: C₁₈H₁₆N₂O₃ ESI-MS calc: 308.12 ESI-MS found: 309.1235 HPLC: 4.601 1H NMR (700 MHz, DMSO-d₆) δ 10.49 (d, J = 4.6 Hz, 1H), 9.16 (d, J = 4.6 Hz, 1H), 7.65 – 7.60 (m, 2H), 7.38 – 7.34 (m, 2H), 7.22 – 7.18 (m, 2H), 7.10 (tdd, J = 7.3, 4.9, 2.2 Hz, 1H), 6.74 – 6.70 (m, 1H), 4.82 (dd, J = 6.7, 4.8 Hz, 2H), 4.59 (dd, J = 6.7, 4.8 Hz, 2H), 3.38 (d, J = 4.7 Hz, 2H). 13C NMR (176 MHz, dmsO) δ 176.66, 165.18, 146.78, 143.10, 129.97, 128.28, 128.17, 127.72, 126.91, 126.72, 126.06, 125.80, 125.41, 124.81, 123.53, 120.11, 108.72, 108.56, 81.89, 58.27, 53.49, 39.86, 39.74, 39.62, 39.50, 39.38, 39.26, 39.14, 38.23, 35.58, 35.52, 30.66, 14.07.

2-oxo-N-(2-phenylpropan-2-yl)indoline-5-carboxamide (157, RAR-13-12)

Synthesized using protocol described in **133**. Yields a strawberry pink solid, 210.8 mg, 48%. Molecular Formula: C₁₈H₁₈N₂O₂ ESI-MS calc: 294.14 ESI-MS found: 295.1456 [M+1], 317.1275 [M+Na] HPLC: 5.199 1H NMR (700 MHz, DMSO-d₆) δ 10.60 (s, 1H), 8.23 (s, 1H), 7.74 (s, 1H), 7.74 – 7.71 (m, 1H), 7.35 (d, J = 7.8 Hz, 2H), 7.26 (t, J = 7.7 Hz, 2H), 7.15 (t, J = 7.2 Hz, 1H), 6.84 (d, J = 8.1 Hz, 1H), 3.53 (s, 2H), 1.65 (s, 6H). 13C NMR (176 MHz, dmsO) δ 176.64, 165.50, 148.19, 146.15, 128.51, 128.35, 127.82, 127.67, 125.59, 125.37, 124.81, 124.61, 123.65, 108.26, 55.22, 39.86, 39.74, 39.62, 39.50, 39.38, 39.26, 39.14, 35.59, 29.66.

(R)-N-(1-(4-chlorophenyl)ethyl)-2-oxoindoline-5-carboxamide (158, RAR-13-16)

Synthesized using protocol described in **133**. Yields a strawberry pink solid, 471.0 mg, quantitative yield. Molecular Formula: C₁₇H₁₅ClN₂O₂ ESI-MS calc: 314.08 ESI-MS found: 337.0717 [M+Na] HPLC: 5.682 1H NMR (500 MHz, DMSO-d₆) δ 10.61 (s, 1H), 8.64 (d, J = 7.9 Hz, 1H), 7.76 (d, J = 7.9 Hz, 2H), 7.42 – 7.34 (m, 4H), 6.85 (d, J = 8.1 Hz, 1H), 5.13 (p, J = 7.2 Hz, 1H), 3.53 (s, 2H), 1.45 (d, J = 7.0 Hz, 3H). 13C NMR (126 MHz, dmsO) δ 176.61, 165.29, 146.40, 144.17, 130.98, 128.09, 127.92, 127.67, 127.28, 125.55, 123.49, 108.37, 47.87, 40.00, 39.83, 39.67, 39.50, 39.33, 39.17, 39.00, 35.55, 22.09.

(R,Z)-3-((3,5-dimethyl-4-nitro-1H-pyrrol-2-yl)methylene)-2-oxo-N-(1-(*m*-tolyl)ethyl)indoline-5-carboxamide (**159** RAR-12-65)

To a dried sealed tube were added 200 mg (0.679 mmol) of (**148**), 139.6 mg (0.815 mmol) of 3,5-dimethyl-4-nitro-1H-pyrrole-2-carbaldehyde, all of which were dissolved in abs. EtOH (6.0 mL). To this solution were added 0.05 ml of piperidine and heated to reflux (95 °C) for 4 h. Once complete, cooled to room temperature and then filtered off the product as a lemon yellow solid. Yield: lemon yellow solid, 100 mg, 29.8 % Molecular Formula: C₂₅H₂₄N₄O₄ ESI-MS calc: 444.18 ESI-MS found: 445.1862 [M+1] HPLC: 7.732 1H NMR (700 MHz, DMSO-d₆) δ 11.34 (s, 1H), 8.58 (d, J = 8.0 Hz, 1H), 8.33 (d, J = 1.6 Hz, 1H), 7.78 (s, 1H), 7.76 (dd, J = 8.2, 1.6 Hz, 1H), 7.23 – 7.18 (m, 3H), 7.03 (d, J = 6.1 Hz, 1H), 6.94 (d, J = 8.1 Hz, 1H), 5.16 (p, J = 7.2 Hz, 1H), 2.62 (s, 3H), 2.57 (s, 3H), 2.30 (s, 3H), 1.49 (d, J = 7.0 Hz, 3H). 13C NMR (176 MHz, dmsO) δ 169.83, 165.49, 144.90, 141.26, 137.14, 136.75, 133.66, 128.34, 128.09, 127.51, 127.15, 126.74, 125.07, 124.71, 124.39, 123.59, 123.17, 119.39, 118.96, 109.09, 48.36, 39.86, 39.74, 39.62, 39.50, 39.38, 39.26, 39.14, 22.26, 21.11, 14.76, 11.21.

(R,Z)-3-((3,5-dimethyl-4-nitro-1H-pyrrol-2-yl)methylene)-N-(1-(4-fluorophenyl)ethyl)-2-oxoindoline-5-carboxamide (**160**, RAR-12-76)

To a dried sealed tube were added 128 mg (0.429 mmol) of (**149**), 101.3 mg (0.60 mmol) of 3,5-dimethyl-4-nitro-1H-pyrrole-2-carbaldehyde, all of which were dissolved in abs. EtOH (3.0 mL). To this solution were added 0.05 ml of piperidine and heated to reflux (95 °C) for 4 h. Once complete, cooled to room temperature and then filtered off the product as an orange solid. Yield: orange solid, 96.3 mg, 50 % Molecular Formula: C₂₄H₂₁FN₄O₄ ESI-MS calc: 448.15 ESI-MS found: 449.1619 [M+1] HPLC: 7.422 1H NMR (700 MHz, DMSO-d₆) δ 11.37 (s, 1H), 8.64 (d, J = 7.8 Hz, 1H), 8.35 (d, J = 1.7 Hz, 1H), 7.83 (s, 1H), 7.76 (dd, J = 8.1, 1.7 Hz, 1H), 7.47 – 7.44 (m, 2H), 7.18 – 7.14 (m, 2H), 6.97 (d, J = 8.1 Hz, 1H), 5.19 (p, J = 7.2 Hz, 1H), 2.65 (s, 3H), 2.60 (s, 3H), 1.51 (d, J = 7.0 Hz, 3H). 13C NMR (176 MHz, dmsO) δ 169.85, 165.62, 136.79, 133.69, 128.31, 128.02, 127.97, 124.71, 123.71, 119.03, 114.88, 114.76, 50.22, 47.86, 39.86, 39.74, 39.62, 39.50, 39.38, 39.26, 39.14, 22.26, 14.78, 11.22.

(R,Z)-3-((3,5-dimethyl-4-nitro-1H-pyrrol-2-yl)methylene)-2-oxo-N-(1-(pyridin-4-yl)ethyl)indoline-5-carboxamide (**161**, RAR-12-77)

To a dried sealed tube were added 100 mg (0.455 mmol) of (**150**), 77.1 mg (0.459 mmol) of 3,5-dimethyl-4-nitro-1H-pyrrole-2-carbaldehyde, all of which were dissolved in abs. EtOH (3.0 mL). To this solution were added 0.05 ml of piperidine and heated to reflux (95 °C) for 4 h. Once complete, cooled to room temperature and then filtered off the product as a yellow solid. Yield: yellow solid, 48.0 mg, 31.3 % Molecular Formula: C₂₃H₂₁N₅O₄ ESI-MS calc: 431.16 ESI-MS found: 432.1656 [M+1] HPLC: 5.496 1H NMR (700 MHz, DMSO-d₆) δ 11.36 (s, 1H), 8.73 (d, J = 7.6 Hz, 1H), 8.52 – 8.50 (m, 2H), 8.36 (d, J = 1.6 Hz, 1H), 7.82 (s, 1H), 7.77 (dd, J = 8.1, 1.6 Hz, 1H), 7.40 (d, J = 5.2 Hz, 2H), 6.97 (d, J = 8.0 Hz, 1H), 5.15 (p, J = 7.3 Hz, 1H), 2.64 (s, 3H), 2.59 (s, 3H), 1.51 (d, J = 7.1 Hz, 3H). 13C NMR (176 MHz, dmsO) δ 170.11, 166.24, 153.97, 149.80, 137.07, 135.63, 128.31, 127.80, 125.45, 124.98, 124.02, 121.55, 119.37, 109.42, 48.18, 40.12, 40.00, 39.88, 39.76, 39.64, 39.52, 39.40, 21.78, 15.04, 11.48.

(R,Z)-3-((3,5-dimethyl-4-nitro-1H-pyrrol-2-yl)methylene)-2-oxo-N-(1-(pyridin-2-yl)ethyl)indoline-5-carboxamide (**162**, RAR-12-83)

To a dried sealed tube were added 165 mg (0.587 mmol) of (**151**), 122.8 mg (0.762 mmol) of 3,5-dimethyl-4-nitro-1H-pyrrole-2-carbaldehyde, all of which were dissolved in abs. EtOH (3.0 mL). To this solution were added 0.05 ml of piperidine and heated to reflux (95 °C) for 4 h. Once complete, cooled to room temperature and then filtered off the product as a yellow solid. Yield: yellow solid, 116 mg, 34 % Molecular Formula: C₂₃H₂₁N₅O₄ ESI-MS calc: 431.16 ESI-MS found: 432.0558 [M+1] HPLC: 5.49 1H NMR (700 MHz, DMSO-d₆) δ 11.36 (d, J = 7.2 Hz, 1H), 8.65 – 8.58 (m, 1H), 8.55 – 8.47 (m, 1H), 8.39 (t, J = 7.7 Hz, 1H), 7.78 (ddd, J = 33.0, 15.8, 7.2 Hz, 3H), 7.42 (q, J = 10.5, 9.0 Hz, 1H), 7.25 (dd, J = 12.7, 6.8 Hz, 1H), 6.95 (d, J = 7.0 Hz, 1H), 5.22 (q, J = 8.8, 8.0 Hz, 1H), 2.66 – 2.60 (m, 3H), 2.59 (s, 3H), 1.56 – 1.49 (m, 3H). 13C NMR (176 MHz, dmsO) δ 169.21, 165.90, 148.79, 136.83, 128.23, 124.86, 123.81, 120.44, 119.09, 109.32, 58.91, 50.44, 40.00, 39.88, 39.76, 39.74, 39.64, 39.62, 39.52, 39.40, 39.28, 21.09, 11.38.

(R,Z)-N-(1-(3-chlorophenyl)ethyl)-3-((3,5-dimethyl-4-nitro-1H-pyrrol-2-yl)methylene)-2-oxoindoline-5-carboxamide (**163**, RAR-12-87)

To a dried sealed tube were added 242.2 mg (0.769 mmol) of (**152**), 150.1 mg (0.892 mmol) of 3,5-dimethyl-4-nitro-1H-pyrrole-2-carbaldehyde, all of which were dissolved in abs. EtOH (6.0 mL). To this solution were added 0.05 ml of piperidine and heated to reflux (95 °C) for 4 h. Once complete, cooled to room temperature and then filtered off the product as an orange solid. Yield: orange solid, 46 mg, 16% Molecular Formula: C₂₄H₂₁ClN₄O₄ ESI-MS calc: 464.13 ESI-MS found: 465.1318 HPLC: 7.699 1H NMR (700 MHz, DMSO-d₆) δ 11.38 (s, 1H), 8.68 (d, J = 7.8 Hz, 1H), 8.36 (d, J = 1.6 Hz, 1H), 7.84 (s, 1H), 7.76 (dd, J = 8.2, 1.7 Hz, 1H), 7.46 (d, J = 2.1 Hz, 1H), 7.37 (d, J = 6.6 Hz, 2H), 7.29 (dt, J = 6.7, 2.3 Hz, 1H), 6.97 (d, J = 8.1 Hz, 1H), 5.17 (p, J = 7.2 Hz, 1H), 2.65 (s, 3H), 2.60 (s, 3H), 1.50 (d, J = 7.1 Hz, 3H). 13C NMR (176 MHz, dmsO) δ 165.88, 147.85, 144.31, 138.20, 130.27, 126.64, 126.10, 125.34, 125.04, 123.98, 119.28, 109.31, 102.54, 48.41, 40.00, 39.88, 39.76, 39.64, 39.52, 39.40, 39.28, 22.27, 14.93.

(R,Z)-3-((3,5-dimethyl-4-nitro-1H-pyrrol-2-yl)methylene)-2-oxo-N-(1-(p-tolyl)ethyl)indoline-5-carboxamide (**164**, RAR-12-91)

To a dried sealed tube were added 253.9 mg (0.862 mmol) of (**153**), 140.9 mg (0.837 mmol) of 3,5-dimethyl-4-nitro-1H-pyrrole-2-carbaldehyde, all of which were dissolved in abs. EtOH (3.0 mL). To this solution were added 0.05 ml of piperidine and heated to reflux (95 °C) for 4 h. Once complete, cooled to room temperature and then filtered off the product as an orange solid. Yield: orange solid, 76.1 mg, 25% Molecular Formula: C₂₅H₂₄N₄O₄ ESI-MS calc: 444.18 ESI-MS found: 445.1864 [M+1] HPLC: 7.662 1H NMR (700 MHz, DMSO-d₆) δ 9.73 (s, 1H), 8.57 (d, J = 8.2 Hz, 2H), 8.35 (d, J = 1.7 Hz, 1H), 7.83 (s, 1H), 7.76 (dd, J = 8.1, 1.7 Hz, 2H), 7.30 (d, J = 7.8 Hz, 3H), 7.14 (d, J = 7.9 Hz, 3H), 6.96 (d, J = 8.0 Hz, 2H), 5.17 (p, J = 7.2 Hz, 1H), 2.55 (d, J = 8.7 Hz, 6H), 2.28 (s, 5H). 13C NMR (176 MHz, dmsO) δ 170.11, 165.77, 155.70, 142.17, 141.51, 137.04, 135.76, 135.76, 128.94, 126.27, 125.36, 119.23, 109.39, 52.91, 40.12, 40.00, 39.88, 39.76, 39.64, 39.52, 39.40, 22.49, 20.86, 15.04, 11.49, 10.19.

(Z)-N-benzyl-3-((3,5-dimethyl-4-nitro-1H-pyrrol-2-yl)methylene)-2-oxoindoline-5-carboxamide (**165**, RAR-13-1)

Yield: orange solid, 150 mg, 55% Molecular Formula: C₂₃H₂₀N₄O₄ ESI-MS calc: 416.15 ESI-MS found: 417.2934, HPLC: 7.158, ¹H NMR (700 MHz, DMSO-d₆) δ 11.44 – 11.06 (m, 1H), 8.84 (t, J = 6.1 Hz, 1H), 8.34 (s, 1H), 7.76 (d, J = 8.3 Hz, 1H), 7.69 (s, 1H), 7.34 (d, J = 5.6 Hz, 4H), 7.25 (d, J = 6.6 Hz, 1H), 6.92 (d, J = 8.2 Hz, 1H), 4.52 (d, J = 5.7 Hz, 2H). ¹³C NMR (176 MHz, dmsO) δ 169.75, 166.10, 141.33, 139.82, 136.69, 133.57, 128.23, 127.89, 127.37, 127.18, 126.67, 124.95, 124.69, 124.44, 123.25, 119.29, 118.57, 109.16, 42.62, 39.86, 39.74, 39.62, 39.50, 39.38, 39.26, 39.14, 14.73, 11.11.

(R,Z)-3-((3,5-dimethyl-4-nitro-1H-pyrrol-2-yl)methylene)-N-(2-methyl-1-phenylpropyl)-2-oxoindoline-5-carboxamide (**166**, RAR-13-5)

Synthesized using protocol described in **164**. Yields an orange solid, 144.6 mg, 64.8% Molecular Formula: C₂₆H₂₆N₄O₄ ESI-MS calc: 458.20 ESI-MS found: 459.2109 HPLC: 7.896 ¹H NMR (700 MHz, DMSO-d₆) δ 11.32 (s, 1H), 8.56 (p, J = 9.3, 8.3 Hz, 1H), 8.29 (dq, J = 13.4, 7.5 Hz, 1H), 7.88 – 7.63 (m, 2H), 7.48 – 7.28 (m, 4H), 7.22 (qd, J = 14.5, 9.4, 7.5 Hz, 1H), 6.94 (tt, J = 14.2, 7.5 Hz, 1H), 4.79 – 4.64 (m, 1H), 2.64 – 2.58 (m, 3H), 2.58 (s, 3H), 1.05 (tt, J = 13.4, 8.0 Hz, 3H), 0.75 (dp, J = 25.8, 6.7 Hz, 3H). ¹³C NMR (176 MHz, dmsO) δ 169.69, 165.86, 143.12, 141.05, 127.89, 127.29, 127.17, 126.47, 125.00, 124.61, 124.32, 123.62, 119.24, 119.05, 108.85, 59.80, 39.74, 39.62, 39.50, 39.38, 39.26, 39.15, 39.03, 32.40, 19.97, 19.82, 14.64, 11.05.

(Z)-3-((3,5-dimethyl-4-nitro-1H-pyrrol-2-yl)methylene)-2-oxo-N-(3-phenyloxetan-3-yl)indoline-5-carboxamide (**167**, RAR-13-9)

Synthesized using protocol described in **164**. Yields an orange solid, 47 mg, 42%. Molecular Formula: C₂₅H₂₂N₄O₅ ESI-MS calc: 458.16 ESI-MS found: 459.1656 HPLC: 6.923, ¹H NMR (700 MHz, DMSO-d₆) δ 11.39 (s, 1H), 9.36 (s, 1H), 8.40 (d, J = 2.0 Hz, 1H), 7.83 (d, J = 2.2 Hz, 1H), 7.81 – 7.77 (m, 1H), 7.59 – 7.55 (m, 2H), 7.40 (t, J = 7.8 Hz, 2H), 7.29 (t, J = 7.4 Hz, 1H), 6.99 (dd, J = 8.4, 2.0 Hz, 1H), 5.04 (d, J = 6.7 Hz, 2H), 4.81 (d, J = 6.7 Hz, 2H), 2.63 (d, J = 2.0 Hz, 3H), 2.58 (d, J = 2.1 Hz, 3H). ¹³C NMR (176 MHz, dmsO) δ 169.85, 165.50, 142.99, 141.58, 136.84, 133.69, 127.65, 127.44, 126.92, 125.26, 124.89, 124.72, 124.58, 123.78, 119.24, 109.26, 81.88, 58.33, 14.77, 11.15.

(Z)-3-((3,5-dimethyl-4-nitro-1H-pyrrol-2-yl)methylene)-2-oxo-N-(2-phenylpropan-2-yl)indoline-5-carboxamide (**158**, RAR-13-13)

Synthesized using protocol described in **164**. Yields an orange solid, 76.1 mg, 32.1%. Molecular Formula: C₂₅H₂₄N₄O₄ ESI-MS calc: 444.18 ESI-MS found: 445.2680 [M+1] HPLC: 7.713 ¹H NMR (700 MHz, DMSO-d₆) δ 11.32 (s, 1H), 8.31 (d, J = 1.7 Hz, 1H), 8.25 (s, 1H), 7.80 (s, 1H), 7.72 (dd, J = 8.0, 1.7 Hz, 1H), 7.42 – 7.39 (m, 2H), 7.28 (t, J = 7.8 Hz, 2H), 7.17 (t, J = 7.3 Hz, 1H), 6.92 (d, J = 8.1 Hz, 1H), 2.61 (s, 3H), 2.57 (s, 3H), 1.70 (s, 6H). ¹³C NMR (176 MHz, dmsO) δ 169.84, 165.70, 148.16, 141.11, 136.71, 133.63, 129.19, 127.83, 127.58, 125.62, 125.05, 124.73, 124.69, 124.29, 123.61, 119.44, 119.02, 108.96, 55.31, 39.86, 39.74, 39.62, 39.50, 39.38, 39.26, 39.14, 29.65, 14.76, 11.21.

(R,Z)-N-(1-(4-chlorophenyl)ethyl)-3-((3,5-dimethyl-4-nitro-1H-pyrrol-2-yl)methylene)-2-oxoindoline-5-carboxamide (**159**, RAR-13-17)

Synthesized using protocol described in **164**. Yields an orange solid, 213.3 mg, 96%. Molecular Formula: C₂₄H₂₁N₄O₄ ESI-MS calc: 464.13 ESI-MS found: 465.1318 [M+1] HPLC: 7.795 1H NMR (500 MHz, DMSO-d₆) δ 11.34 (s, 1H), 8.65 (d, J = 7.8 Hz, 1H), 8.35 – 8.30 (m, 1H), 7.79 (s, 1H), 7.75 (dd, J = 8.1, 1.7 Hz, 1H), 7.43 (d, J = 8.3 Hz, 2H), 7.39 (d, J = 8.5 Hz, 3H), 6.94 (d, J = 8.1 Hz, 1H), 5.17 (p, J = 7.2 Hz, 1H), 2.62 (s, 3H), 2.57 (s, 3H), 1.49 (d, J = 7.1 Hz, 3H). 13C NMR (126 MHz, dmsO) δ 169.83, 165.67, 144.05, 141.32, 136.76, 133.66, 131.02, 128.18, 128.10, 128.00, 127.49, 125.11, 124.70, 124.41, 123.63, 119.35, 118.98, 109.10, 48.00, 40.00, 39.83, 39.67, 39.50, 39.34, 39.17, 39.00, 22.07, 14.76, 11.21.

(R,Z)-3-((4-amino-3,5-dimethyl-1H-pyrrol-2-yl)methylene)-2-oxo-N-(1-(*m*-tolyl)ethyl)indoline-5-carboxamide (**168**, RAR-12-68)

To a flask were added 86.4 mg of (**159**), dissolved in 5 mL of 2:1 EtOH/EtOAc. To this slurry were added 210.9 mg (14 equiv) of Zn powder and 2 mL (150 equiv) of AcOH. The turbid orange solution was allowed to stir at 50 C for 2 h. Once complete, the reaction was cooled to rt and then add EtOAc before basifying with sat. Na₂CO₃. The basified aqueous layer was extracted with EtOAc (3 x 30 mL) and then washed with water and brine (1 x 30 mL), respectively. The organic layer was dried over MgSO₄ and then solvent was removed under pressure to give the desired product as a red solid. *Note: the free amine is very reactive, so it was moved forward without further characterization* Result: red solid, 86.6 mg, 94% Molecular Formula: C₂₅H₂₆N₄O₂ ESI-MS calc: 414.21 ESI-MS found: 415.2120 [M+1] HPLC: 5.627

(R,Z)-3-((4-amino-3,5-dimethyl-1H-pyrrol-2-yl)methylene)-N-(1-(4-fluorophenyl)ethyl)-2-oxoindoline-5-carboxamide (**169**, RAR-12-79)

To a flask were added 96.3 mg of (**160**), dissolved in 5 mL of 2:1 EtOH/EtOAc. To this slurry were added 295 mg (14 equiv) of Zn powder and 2 mL (150 equiv) of AcOH. The turbid orange solution was allowed to stir at 50 C for 2 h. Once complete, the reaction was cooled to rt and then add EtOAc before basifying with sat. Na₂CO₃. The basified aqueous layer was extracted with EtOAc (3 x 30 mL) and then washed with water and brine (1 x 30 mL), respectively. The organic layer was dried over MgSO₄ and then solvent was removed under pressure to give the desired product as a red solid. *Note: the free amine is very reactive, so it was moved forward without further characterization* Result: red solid, 96 mg, 100% Molecular Formula: C₂₄H₂₃FN₄O₂ ESI-MS calc: 418.18 ESI-MS found: 419.1938 [M+1] HPLC: 5.713

(R,Z)-3-((4-amino-3,5-dimethyl-1H-pyrrol-2-yl)methylene)-2-oxo-N-(1-(pyridin-4-yl)ethyl)indoline-5-carboxamide (**170** RAR-12-80)

To a flask were added 48.0 mg of (**161**), dissolved in 5 mL of 2:1 EtOH/EtOAc. To this slurry were added 208 mg (14 equiv) of Zn powder and 2 mL (150 equiv) of AcOH. The turbid orange solution was allowed to stir at 50 C for 2 h. Once complete, the reaction was cooled to rt and then add EtOAc before basifying with sat. Na₂CO₃. The basified aqueous layer was extracted with EtOAc (3 x 30 mL) and then washed with water and brine (1 x 30 mL), respectively. The organic layer was dried over MgSO₄ and then solvent was removed under pressure to give the desired product as a red solid. *Note: the free amine is very reactive, so it was moved forward without further characterization* Result: red solid, 41.5 mg, 89% Molecular Formula: C₂₃H₂₃N₅O₂ ESI-MS calc: 401.19 ESI-MS found: 402.1920 [M+1] HPLC: 3.928

(R,Z)-3-((4-amino-3,5-dimethyl-1H-pyrrol-2-yl)methylene)-2-oxo-N-(1-(pyridin-2-yl)ethyl)indoline-5-carboxamide (**171**, RAR-12-84)

To a flask were added 73.9 mg of (**162**), dissolved in 5 mL of 2:1 EtOH/EtOAc. To this slurry were added 289 mg (14 equiv) of Zn powder and 2 mL (150 equiv) of AcOH. The turbid orange solution was allowed to stir at 50 C for 2 h. Once complete, the reaction was cooled to rt and then add EtOAc before basifying with sat. Na₂CO₃. The basified aqueous layer was extracted with EtOAc (3 x 30 mL) and then washed with water and brine (1 x 30 mL), respectively. The organic layer was dried over MgSO₄ and then solvent was removed under pressure to give the desired product as a red solid. *Note: the free amine is very reactive, so it was moved forward without further characterization* Result: red solid, 73.8 mg, 100% Molecular Formula: C₂₃H₂₃N₅O₂ ESI-MS calc: 401.19 ESI-MS found: 402.1450 [M+1] HPLC: 3.920

(R,Z)-3-((4-amino-3,5-dimethyl-1H-pyrrol-2-yl)methylene)-N-(1-(3-chlorophenyl)ethyl)-2-oxoindoline-5-carboxamide (**173**, RAR-12-88)

To a flask were added 46.0 mg of (**163**), dissolved in 5 mL of 2:1 EtOH/EtOAc. To this slurry were added 170.1 mg (14 equiv) of Zn powder and 1.4 mL (150 equiv) of AcOH. The turbid orange solution was allowed to stir at 50 C for 2 h. Once complete, the reaction was cooled to rt and then add EtOAc before basifying with sat. Na₂CO₃. The basified aqueous layer was extracted with EtOAc (3 x 30 mL) and then washed with water and brine (1 x 30 mL), respectively. The organic layer was dried over MgSO₄ and then solvent was removed under pressure to give the desired product as a red solid. *Note: the free amine is very reactive, so it was moved forward without further characterization* Result: red solid, 40 mg, 95% Molecular Formula: C₂₄H₂₃ClN₄O₂ ESI-MS calc: 434.15 ESI-MS found: 435.1569 [M+1] HPLC: 5.556

(R,Z)-3-((4-amino-3,5-dimethyl-1H-pyrrol-2-yl)methylene)-2-oxo-N-(1-(p-tolyl)ethyl)indoline-5-carboxamide (**174** RAR-12-92)

To a flask were added 76.1 mg of (**164**), dissolved in 5 mL of 2:1 EtOH/EtOAc. To this slurry were added 314.4 mg (14 equiv) of Zn powder and 2.0 mL (150 equiv) of AcOH. The turbid orange solution was allowed to stir at 50 C for 2 h. Once complete, the reaction was cooled to rt and then add EtOAc before basifying with sat. Na₂CO₃. The basified aqueous layer was extracted with EtOAc (3 x 30 mL) and then washed with water and brine (1 x 30 mL), respectively. The organic layer was dried over MgSO₄ and then solvent was removed under pressure to give the desired product as a red solid. *Note: the free amine is very reactive, so it was moved forward without further characterization* Result: red solid, 220 mg, 100% Molecular Formula: C₂₅H₂₆N₄O₂ ESI-MS calc: 414.21 ESI-MS found: 415.2119 [M+1] HPLC: 5.573

(Z)-3-((4-amino-3,5-dimethyl-1H-pyrrol-2-yl)methylene)-N-benzyl-2-oxoindoline-5-carboxamide (**175**, RAR-13-2)

Synthesized using protocol described in **168**. Yields a red solid, 210 mg, quantitative yield. Molecular Formula: C₂₃H₂₂N₄O₂ ESI-MS calc: 386.17 ESI-MS found: 387.1810 HPLC: 5.129.

(R,Z)-3-((4-amino-3,5-dimethyl-1H-pyrrol-2-yl)methylene)-N-(2-methyl-1-phenylpropyl)-2-oxoindoline-5-carboxamide (**176**, RAR-13-6)

Synthesized using protocol described in **168**. Yields a red solid, 220 mg, quantitative yield. Molecular Formula: C₂₆H₂₈N₄O₂ ESI-MS calc: 428.22 ESI-MS found: 429.2201 HPLC: 5.497

(Z)-3-((4-amino-3,5-dimethyl-1*H*-pyrrol-2-yl)methylene)-2-oxo-*N*-(3-phenyloxetan-3-yl)indoline-5-carboxamide (**177**, RAR-13-10)

Synthesized using protocol described in **168**. Yields a red solid, 20.6 mg, 47%. Molecular Formula: C₂₅H₂₄N₄O₃ ESI-MS calc: 428.18 ESI-MS found: 429.1494 HPLC: 4.710

(Z)-3-((4-amino-3,5-dimethyl-1*H*-pyrrol-2-yl)methylene)-2-oxo-*N*-(2-phenylpropan-2-yl)indoline-5-carboxamide (**178**, RAR-13-14)

Synthesized using protocol described in **168**. Yields a red solid, 307 mg, quantitative yield. Molecular Formula: C₂₅H₂₆N₄O₂ ESI-MS calc: 414.21 ESI-MS found: 415.2119 [M+1] HPLC: 5.245

(R,Z)-3-((4-amino-3,5-dimethyl-1*H*-pyrrol-2-yl)methylene)-*N*-(1-(4-chlorophenyl)ethyl)-2-oxoindoline-5-carboxamide (**179**, RAR-13-18)

Synthesized using protocol described in **168**. Yields a red solid, 36.1 mg, 48%. Molecular Formula: C₂₄H₂₃ClN₄O₂ ESI-MS calc: 434.15 ESI-MS found: 435.15612 HPLC: 5.398

(R,Z)-3-((4-(2-cyanoacetamido)-3,5-dimethyl-1*H*-pyrrol-2-yl)methylene)-2-oxo-*N*-(1-phenylethyl)indoline-5-carboxamide (**180**, RAR-12-67)

To a round bottom flask were added 20.2 mg of **141** (0.05 mmol), 6.7 mg (0.075 mmol) of cyanoacetic acid and 24.6 mg (0.1 mmol) of DMTMM. All materials were brought up in 2 mL of DMF, and the resulting solution was allowed to stir at rt for 12 h. Once complete, the reaction was quenched with Sat. NaCl, and extracting with EtOAc (3 x 50 mL). The organic layer was washed with sat. Na₂CO₃ and brine (1 x 50 mL) respectively and then dried over MgSO₄. The solvent was removed under pressure, evaporating the material onto silica gel. Purified by column chromatography 5-100% Acetone/Hexanes. Flushed the column with 7*N* NH₃ in MeOH to yield the final product as a bright orange solid. Result: orange solid, 10 mg, 43% Molecular Formula: C₂₇H₂₅N₅O₃ ESI-MS calc: 467.20 ESI-MS found: 468.1297 HPLC: 6.100. ¹H NMR (700 MHz, DMSO-*d*₆) δ 13.51 (s, 1H), 11.08 (s, 1H), 9.52 (s, 1H), 8.60 (d, *J* = 8.2 Hz, 1H), 8.21 (d, *J* = 1.7 Hz, 1H), 7.69 (dd, *J* = 8.1, 1.7 Hz, 1H), 7.65 (s, 1H), 7.41 (d, *J* = 7.7 Hz, 2H), 7.33 (t, *J* = 7.6 Hz, 3H), 7.22 (t, *J* = 7.3 Hz, 1H), 6.93 (d, *J* = 8.1 Hz, 1H), 5.19 (p, *J* = 7.2 Hz, 1H), 3.88 (s, 2H), 2.20 (dd, *J* = 12.9, 10.8 Hz, 6H), 1.50 (d, *J* = 7.1 Hz, H). ¹³C NMR (499 MHz, DMSO-*d*₆) δ 170.92, 130.6, 129.23, 128.8, 127.2, 126.2, 125.48, 123.25, 122.22, 118.36, 109.03, 50.20, 25.49, 22.99, 12.52, 9.63 (derived from HSQC, so quaternary carbons are missing: 168.2, 167.5, 154.1, 120.1, 144.8, 141.5)

(R,Z)-3-((4-(2-chloroacetamido)-3,5-dimethyl-1*H*-pyrrol-2-yl)methylene)-2-oxo-*N*-(1-(*m*-tolyl)ethyl)indoline-5-carboxamide (**181** RAR-12-69)

To a dried round bottom flask were added 86.6 mg of **168**, (0.209 mmol) dissolved in 3 mL of THF. The yellow solution was cooled to 0 °C and 0.04 mL (0.30 mmol) of chloroacetylchloride was added dropwise. The solution was allowed to stir at 0 °C for 30 mins. Once complete by TLC, quenched with water and extracted with EtOAc. The solvent was removed, and the crude material was purified by prep plate (50% Acetone/Hexanes) collecting the major product. The desired product was rinsed off of silica gel and then the solvent was removed to give a bright yellow solid. The yellow solid was washed with DCM and sonicated to give a red solid. The red solid was then pulped in water:acetone (30:1) to give the final product. Result: red solid, 57.2 mg, 55% Molecular

Formula: C₂₇H₂₇ClN₄O₃ ESI-MS calc: 490.18 ESI-MS found: 491.1133 HPLC: 6.68 1H NMR (500 MHz, DMSO-d₆) δ 13.52 (s, 1H), 11.07 (s, 1H), 9.53 (s, 1H), 8.56 (d, J = 8.1 Hz, 1H), 8.21 (s, 1H), 7.74 – 7.62 (m, 2H), 7.24 – 7.15 (m, 4H), 7.03 (s, 1H), 6.93 (d, J = 8.0 Hz, 1H), 5.15 (s, 1H), 4.26 (s, 2H), 2.30 (s, 3H), 2.20 (d, J = 8.9 Hz, 6H), 1.49 (d, J = 7.0 Hz, 3H). 13C NMR (126 MHz, dmsO) δ 170.18, 169.06, 166.24, 165.84, 145.51, 140.80, 137.63, 132.18, 128.59, 128.10, 127.62, 127.24, 126.26, 125.83, 124.93, 123.68, 121.47, 117.93, 113.45, 109.13, 48.80, 43.22, 22.79, 21.62, 12.15, 9.70.

(R,Z)-3-((4-(2-chloroacetamido)-3,5-dimethyl-1H-pyrrol-2-yl)methylene)-N-(1-(4-fluorophenyl)ethyl)-2-oxoindoline-5-carboxamide (**182**, RAR-12-81)

To a dried round bottom flask were added 96.0 mg of **169**, (0.23 mmol) dissolved in 4 mL of THF. The yellow solution was cooled to 0 °C and 0.02 mL (0.25 mmol) of chloroacetylchloride was added dropwise. The solution was allowed to stir at 0 °C for 30 mins. Once complete by TLC, quenched with water and extracted with EtOAc. The solvent was removed, and the crude material was purified by prep plate (50% Acetone/Hexanes) collecting the major product. The desired product was rinsed off of silica gel and then the solvent was removed to give a bright yellow solid. The yellow solid was washed with DCM and sonicated to give a red solid. The red solid was then pulped in water:acetone (30:1) to give the final product. Result: red solid, 46.5 mg, 41% Molecular Formula: C₂₆H₂₄FCIN₄O₃ ESI-MS calc: 494.15 ESI-MS found: 495.0480 [M+1] HPLC: 6.439 1H NMR (700 MHz, DMSO-d₆) δ 13.52 (s, 1H), 11.08 (s, 1H), 9.54 (s, 1H), 8.63 (d, J = 7.9 Hz, 1H), 8.23 (d, J = 1.7 Hz, 1H), 7.68 (dd, J = 8.1, 1.8 Hz, 1H), 7.66 (s, 1H), 7.46 – 7.43 (m, 2H), 7.15 (tt, J = 9.9, 3.2 Hz, 3H), 6.93 (d, J = 8.2 Hz, 1H), 5.19 (p, J = 7.2 Hz, 1H), 4.28 – 4.26 (m, 4H), 2.20 (d, J = 10.1 Hz, 6H), 1.50 (d, J = 6.9 Hz, 4H). 13C NMR (176 MHz, dmsO) δ 170.20, 169.07, 166.36, 165.86, 162.12, 160.75, 141.78, 141.76, 140.85, 132.22, 128.54, 128.49, 128.41, 128.02, 127.42, 126.27, 125.87, 124.96, 124.70, 121.50, 117.90, 115.38, 115.26, 113.44, 109.15, 48.33, 43.23, 41.97, 40.37, 40.25, 40.13, 40.01, 39.89, 39.77, 39.65, 36.07, 29.51, 22.78, 12.16, 9.72.

(R,Z)-3-((4-(2-chloroacetamido)-3,5-dimethyl-1H-pyrrol-2-yl)methylene)-2-oxo-N-(1-(pyridin-4-yl)ethyl)indoline-5-carboxamide (**183**, RAR-12-82)

To a dried round bottom flask were added 41.5 mg of **170**, (0.103 mmol) dissolved in 2 mL of THF. The yellow solution was cooled to 0 °C and 0.01 mL (0.103 mmol) of chloroacetylchloride was added dropwise. The solution was allowed to stir at 0 °C for 30 mins. Once complete by TLC, quenched with water and extracted with EtOAc. The solvent was removed, and the crude material was purified by prep plate (50% Acetone/Hexanes) collecting the major product as the desired product. Result: red solid, 6.3 mg, 13% Molecular Formula: C₂₅H₂₄ClN₅O₃ ESI-MS calc: 477.16 ESI-MS found: 478.1734 [M+H] HPLC: 4.363 1H NMR (700 MHz, DMSO-d₆) δ 13.51 (s, 1H), 11.15 (s, 1H), 10.56 (s, 1H), 9.86 (s, 1H), 8.73 (s, 1H), 8.48 (s, 2H), 7.75 (s, 1H), 7.72 (d, J = 7.9 Hz, 1H), 7.34 (d, J = 7.6 Hz, 2H), 7.27 (s, 1H), 6.96 (d, J = 7.9 Hz, 1H), 5.33 (t, J = 7.0 Hz, 1H), 4.27 (s, 2H), 2.21 (s, 6H), 1.50 (d, J = 7.8 Hz, 3H). 13C NMR (176 MHz, dmsO) δ 168.53, 166.49, 165.34, 154.01, 141.60, 140.65, 130.38, 129.30, 129.05, 127.97, 124.37, 123.04, 122.68, 121.09, 119.53, 118.36, 108.73, 54.90, 42.72, 21.66, 10.38, 8.77.

(R,Z)-3-((4-(2-chloroacetamido)-3,5-dimethyl-1H-pyrrol-2-yl)methylene)-2-oxo-N-(1-(pyridin-2-yl)ethyl)indoline-5-carboxamide (**184**, RAR-12-85)

To a dried round bottom flask were added 73.8 mg of **171**, (0.18 mmol) dissolved in 4 mL of THF. The yellow solution was cooled to 0 °C and 0.04 mL (0.50 mmol) of chloroacetylchloride was added dropwise. The solution was allowed to stir at 0 °C for 30 mins. Once complete by TLC, removed solvent under pressure and then added DCM to the dark red residue. The DCM solution was sonicated to give a dark red precipitate. The solid was filtered off and rinsed with THF and DCM to give the desired product as a dark red solid. Result: red solid, 37.1 mg, 42% Molecular Formula: C₂₅H₂₄ClN₅O₃ ESI-MS calc: 477.16 ESI-MS found: 478.1547 [M+1] HPLC: 4.743 1H NMR (700 MHz, DMSO-d₆) δ 13.28 (t, J = 13.6 Hz, 1H), 11.02 (q, J = 7.5, 5.9 Hz, 1H), 9.86 (s, 1H), 8.98 (d, J = 52.4 Hz, 1H), 8.57 (d, J = 9.4 Hz, 1H), 8.42 (d, J = 9.4 Hz, 1H), 8.26 (q, J = 9.9, 9.4 Hz, 2H), 7.86 (d, J = 11.1 Hz, 1H), 7.64 (s, 2H), 7.58 (d, J = 9.2 Hz, 1H), 7.50 (dt, J = 27.4, 8.6 Hz, 1H), 6.72 (p, J = 8.1 Hz, 1H), 5.23 – 5.16 (m, 1H), 4.03 (t, J = 8.6 Hz, 1H), 2.92 (d, J = 16.9 Hz, 14H), 2.26 (d, J = 10.2 Hz, 7H), 2.17 (dt, J = 18.1, 8.8 Hz, 4H), 1.97 (q, J = 8.9 Hz, 2H), 1.48 – 1.40 (m, 3H). 13C NMR (176 MHz, dmso) δ 169.75, 166.56, 165.36, 159.41, 145.67, 142.08, 141.13, 140.72, 131.91, 128.62, 127.17, 126.78, 126.44, 125.11, 124.85, 124.26, 123.99, 121.10, 118.54, 52.68, 42.73, 20.48, 11.23, 8.81.

(R,Z)-3-((4-(2-chloroacetamido)-3,5-dimethyl-1H-pyrrol-2-yl)methylene)-N-(1-(3-chlorophenyl)ethyl)-2-oxoindoline-5-carboxamide (185, RAR-12-89)

To a dried round bottom flask were added 40 mg of **172**, (0.16 mmol) dissolved in 4 mL of THF. The yellow solution was cooled to 0 °C and 0.01 mL (0.18 mmol) of chloroacetylchloride was added dropwise. The solution was allowed to stir at 0 °C for 30 mins. Once complete by TLC, removed solvent under pressure and then added DCM to the dark red residue. The DCM solution was sonicated to give a dark red precipitate. The solid was filtered off and rinsed with THF and DCM to give the desired product as a dark red solid. Result: red solid, 23.4 mg, 28% Molecular Formula: C₂₆H₂₄Cl₂N₄O₃ ESI-MS calc: 510.12 ESI-MS found: 511.1579 [M+1] HPLC: 6.742 1H NMR (500 MHz, DMSO-d₆) δ 13.52 (s, 1H), 11.09 (s, 1H), 9.53 (s, 1H), 8.66 (d, J = 7.9 Hz, 1H), 8.21 (d, J = 1.7 Hz, 1H), 7.68 (dd, J = 8.2, 1.7 Hz, 1H), 7.66 (s, 1H), 7.47 – 7.45 (m, 1H), 7.38 – 7.36 (m, 2H), 7.29 (dq, J = 6.2, 2.2 Hz, 1H), 6.94 (d, J = 8.1 Hz, 1H), 5.17 (p, J = 7.2 Hz, 1H), 4.26 (s, 2H), 2.20 (d, J = 8.6 Hz, 6H), 1.50 (d, J = 7.1 Hz, 4H). 13C NMR (126 MHz, dmso) δ 169.51, 165.17, 147.64, 140.23, 132.71, 131.57, 129.96, 127.20, 126.77, 126.30, 125.79, 125.55, 125.23, 124.73, 124.28, 120.82, 117.27, 112.71, 48.03, 42.55, 39.83, 39.67, 39.50, 39.33, 39.17, 39.00, 38.83, 21.96, 11.48, 9.02.

(R,Z)-3-((4-(2-chloroacetamido)-3,5-dimethyl-1H-pyrrol-2-yl)methylene)-2-oxo-N-(1-(p-tolyl)ethyl)indoline-5-carboxamide (186, RAR-12-93)

To a dried round bottom flask were added 93 mg of **173**, (0.19 mmol) dissolved in 5 mL of THF. The yellow solution was cooled to 0 °C and 0.1 mL (1.3 mmol) of chloroacetylchloride was added dropwise. The solution was allowed to stir at 0 °C for 30 mins. Once complete by TLC, removed solvent under pressure and then added DCM to the dark red residue. The DCM solution was sonicated to give a dark red precipitate. The solid was filtered off and rinsed with THF and DCM to give the desired product as a dark red solid. Result: red solid, 73.6 mg, 77% Molecular Formula: C₂₇H₂₇ClN₄O₃ ESI-MS calc: 490.18 ESI-MS found 473.05 [M-Cl] HPLC: 6.625 1H NMR (500 MHz, DMSO-d₆) δ 13.51 (s, 1H), 11.06 (s, 1H), 9.52 (s, 1H), 8.53 (d, J = 8.0 Hz, 1H), 8.20 (s,

1H), 7.71 – 7.65 (m, 1H), 7.64 (s, 1H), 7.27 (t, J = 10.7 Hz, 4H), 7.12 (d, J = 7.8 Hz, 6H), 6.92 (d, J = 8.1 Hz, 1H), 5.18 – 5.12 (m, 2H), 2.26 (d, J = 3.9 Hz, 8H), 1.48 (d, J = 7.1 Hz, 5H).

(Z)-3-((4-(3-chloro-2-hydroxypropanamido)-3,5-dimethyl-1H-pyrrol-2-yl)methylene)-2-oxo-N-((*R*)-1-phenylethyl)indoline-5-carboxamide (**187** RAR-12-95)

To a round bottom flask were added 80 mg of **168** (0.20 mmol), 31.1 mg (0.26 mmol) of 3-chloro-2-hydroxypropionic acid and 81.8 mg (0.32 mmol) of DMTMM. All materials were brought up in 2 mL of DMF, and the resulting solution was allowed to stir at rt for 12 h. Once complete, the reaction was quenched with Sat. NaCl, and extracting with EtOAc (3 x 50 mL). The organic layer was washed with sat. Na₂CO₃ and brine (1 x 50 mL) respectively and then dried over MgSO₄. The solvent was removed under pressure, evaporating the material onto silica gel. Purified by column chromatography 5-100% Acetone/Hexanes. Result: orange solid, 72.8 mg, 58% Molecular Formula: C₂₇H₂₇ClN₄O₄ ESI-MS calc: 506.17 ESI-MS found: 507.1809 [M+1], 540.2377 [M+H+MeOH] HPLC: 6.043 1H NMR (700 MHz, DMSO-d₆) δ 13.58 – 13.42 (m, 1H), 11.07 (d, J = 4.9 Hz, 1H), 8.60 (d, J = 8.1 Hz, 1H), 8.23 – 8.19 (m, 1H), 7.95 (s, 1H), 7.69 – 7.67 (m, 1H), 7.64 (d, J = 5.9 Hz, 1H), 7.41 (d, J = 7.2 Hz, 2H), 7.33 (t, J = 7.1 Hz, 3H), 7.22 (t, J = 7.2 Hz, 1H), 6.93 (dt, J = 8.2, 2.1 Hz, 1H), 5.19 (p, J = 7.3 Hz, 1H), 3.96 (d, J = 7.9 Hz, 1H), 3.74 (s, 1H), 2.21 – 2.18 (m, 4H), 2.16 (s, 2H), 1.50 (d, J = 7.0 Hz, 3H). 13C NMR (176 MHz, dmsO) δ 172.44, 166.31, 162.74, 145.53, 128.63, 127.95, 126.94, 126.54, 125.88, 124.64, 121.80, 117.71, 115.92, 109.07, 107.36, 55.41, 48.82, 22.73, 21.51, 9.74.

(Z)-3-((3,5-dimethyl-4-(oxirane-2-carboxamido)-1H-pyrrol-2-yl)methylene)-2-oxo-N-((*R*)-1-phenylethyl)indoline-5-carboxamide (**188** RAR-12-96)

To a flask were added 36.4 mg of RAR-12-95, and 47.2 mg of K₂CO₃. All materials were brought up in 3.0 mL of Acetone and then refluxed (60 C) for 30 mins. Cooled to rt and then checked by TLC, not complete, so run for another 60 mins. HPLC confirms still not done. MS looks like mostly the starting material. Heated up to 70 C for another 1 h, TLC shows it's not complete. So added cat. KI and heated back up to 70 C for 45 mins. Cooled to rt and check again by TLC/HPLC. Not complete (even after o/n run --> 76% complete) Added 2 more equiv of KI and 1 mL of MeCN (to solubilize) and then heated back to 70 C, after 1 h, if not complete, work up and try to isolate. Quenched with water (1 x 30 mL) and then extracted with EtOAc (2 x 25 mL). Dried over Na₂SO₄ and then purified by column chromatography 25-100% Acetone/Hexanes Collected F19-23 as the potential product and F24-31 as the starting material. Double check by MS before NMR Result: yellow residue, 3.0 mg, 6% Molecular Formula: C₂₇H₂₆ClN₄O₄ ESI-MS calc: 470.20 ESI-MS found: 471.2158 [M+1] HPLC: 6.591 1H NMR (700 MHz, Acetone-d₆) δ 13.62 (s, 1H), 10.01 (s, 1H), 8.24 – 8.22 (m, 2H), 7.83 (d, J = 8.3 Hz, 1H), 7.75 (dt, J = 8.1, 2.2 Hz, 1H), 7.69 (s, 1H), 7.46 (d, J = 8.0 Hz, 3H), 7.33 (t, J = 7.7 Hz, 3H), 7.23 (t, J = 7.3 Hz, 1H), 6.99 (dd, J = 8.3, 5.5 Hz, 1H), 5.33 (q, J = 7.3 Hz, 2H), 3.91 (s, 2H), 3.79 (s, 2H), 2.30 (s, 2H), 2.25 (d, J = 2.7 Hz, 3H), 2.19 (d, J = 5.5 Hz, 2H), 2.14 (d, J = 5.1 Hz, 3H), 1.56 (dd, J = 7.1, 1.3 Hz, 3H). 13C NMR (126 MHz, dmsO) δ 171.84, 169.70, 167.77, 152.56, 145.07, 140.26, 132.32, 128.18, 127.58, 127.45, 126.50, 126.09, 124.43, 121.76, 120.08, 118.18, 108.61, 54.27, 54.08, 48.37, 22.28, 11.87, 9.44.

(R,Z)-3-((4-(2-bromoacetamido)-3,5-dimethyl-1H-pyrrol-2-yl)methylene)-2-oxo-N-(1-phenylethyl)indoline-5-carboxamide (**189** RAR-12-98)

To a round bottom flask were added 83.7 mg of **142** (0.21 mmol), 60.1 mg (0.41 mmol) of bromoacetic acid and 100 mg (0.25 mmol) of DMTMM. All materials were brought up in 2 mL of DMF, and the resulting solution was allowed to stir at rt for 1.5 h. Once complete, the reaction was quenched with brine and then extracted with EtOAc (3 x 20 mL). The combined organic layer was dried over Na₂SO₄ and then solvent was removed under pressure to give a dark orange solid. The solid was then dissolved in DCM, and the resultant solution was sonicated to give a dark red precipitate. The solid was filtered off and rinsed with excess cold DCM to give the final product. Result: red solid, 42.9 mg, 39%. Molecular Formula: C₂₆H₂₅BrN₄O₃ ESI-MS calc: 520.11 ESI-MS found: 523.1164 HPLC: 6.397 1H NMR (700 MHz, DMSO-d₆) δ 13.52 (s, 1H), 11.08 (s, 1H), 9.60 (s, 1H), 8.60 (d, J = 7.9 Hz, 1H), 8.21 (d, J = 1.6 Hz, 1H), 7.69 (dd, J = 8.1, 1.7 Hz, 1H), 7.65 (s, 1H), 7.41 (d, J = 7.7 Hz, 2H), 7.33 (t, J = 7.6 Hz, 2H), 7.22 (t, J = 7.3 Hz, 1H), 6.93 (d, J = 8.1 Hz, 1H), 5.20 (p, J = 7.2 Hz, 1H), 4.03 (s, 2H), 2.20 (d, J = 10.4 Hz, 6H), 1.51 (d, J = 7.0 Hz, 3H). 13C NMR (176 MHz, dms) δ 169.68, 165.82, 165.54, 145.05, 140.30, 131.64, 128.15, 127.59, 126.78, 126.47, 126.07, 125.76, 125.33, 124.44, 124.13, 121.01, 117.35, 112.95, 108.62, 48.34, 29.33, 22.26, 11.61, 9.14.

(Z)-N-benzyl-3-((4-(2-chloroacetamido)-3,5-dimethyl-1H-pyrrol-2-yl)methylene)-2-oxoindoline-5-carboxamide (RAR-13-3, 273561, **190**)

Synthesized using protocol described in **143**. Yields an orange solid, 18.2 mg, 21%. Molecular Formula: C₂₅H₂₃ClN₄O₃ ESI-MS calc: 462.15 ESI-MS found: 463.1529 [M+1] HPLC: 6.177. 1H NMR (700 MHz, DMSO-d₆) δ 13.49 (s, 1H), 11.08 (s, 1H), 9.52 (s, 1H), 8.85 (dt, J = 12.4, 6.1 Hz, 1H), 8.26 (d, J = 1.7 Hz, 1H), 7.78 (d, J = 9.4 Hz, 1H), 7.71 (dd, J = 8.2, 1.7 Hz, 1H), 7.64 (s, 1H), 7.35 – 7.32 (m, 4H), 7.24 (tt, J = 6.2, 3.0 Hz, 2H), 6.94 (d, J = 8.1 Hz, 1H), 4.51 (d, J = 6.0 Hz, 2H), 4.26 (s, 2H), 2.21 (s, 3H), 2.18 (s, 3H). 13C NMR (176 MHz, dms) δ 170.18, 166.91, 165.85, 140.89, 140.42, 132.22, 128.74, 128.72, 128.70, 127.98, 127.78, 127.68, 127.67, 127.62, 127.38, 127.15, 126.21, 125.93, 124.95, 124.54, 123.95, 121.48, 117.63, 113.41, 109.28, 68.98, 56.32, 43.22, 43.09, 43.03, 40.37, 40.25, 40.13, 40.01, 39.89, 39.77, 39.65, 36.08, 32.59, 30.08, 12.14, 11.67, 9.92, 9.65.

(R,Z)-3-((4-(2-chloroacetamido)-3,5-dimethyl-1H-pyrrol-2-yl)methylene)-N-(2-methyl-1-phenylpropyl)-2-oxoindoline-5-carboxamide (RAR-13-7, 273562, **191**)

Synthesized using protocol described in **143**. Yields an orange solid, 5.5 mg, 5.8%. Molecular Formula: C₂₈H₂₉ClN₄O₃ ESI-MS calc: 504.19 ESI-MS found: 505.1997 HPLC: 6.803 1H NMR (700 MHz, DMSO-d₆) δ 13.52 (s, 1H), 11.06 (s, 1H), 9.52 (s, 1H), 8.53 (d, J = 8.9 Hz, 1H), 8.14 (d, J = 1.6 Hz, 1H), 7.67 – 7.62 (m, 2H), 7.43 – 7.40 (m, 2H), 7.32 (t, J = 7.6 Hz, 2H), 7.22 (t, J = 7.3 Hz, 1H), 6.92 (d, J = 8.1 Hz, 1H), 4.69 (t, J = 9.2 Hz, 1H), 4.26 (s, 2H), 2.20 (d, J = 10.3 Hz, 6H), 1.04 (d, J = 6.6 Hz, 4H), 0.73 (d, J = 6.7 Hz, 4H). 13C NMR (126 MHz, dms) δ 170.14, 166.69, 165.80, 151.43, 143.78, 140.68, 132.14, 128.47, 128.45, 127.89, 127.78, 127.38, 127.05, 125.84, 124.90, 124.74, 121.43, 118.01, 108.97, 60.35, 43.19, 32.97, 20.45, 12.12, 9.62.

(Z)-3-((4-(2-chloroacetamido)-3,5-dimethyl-1H-pyrrol-2-yl)methylene)-2-oxo-N-(3-phenyloxetan-3-yl)indoline-5-carboxamide (RAR-13-11, 273563, **192**)

Synthesized using the protocol described in **143** Yields a red solid, 5.0 mg, 21%. Molecular Formula: C₂₇H₂₅ClN₄O₄ ESI-MS calc: 504.16 ESI-MS found: 505.1619 HPLC: 5.332 1H NMR (700 MHz, DMSO-d₆) δ 13.52 (s, 1H), 11.28 (s, 1H), 9.54 (d, J = 13.2 Hz, 1H), 8.43 (s, 1H), 7.84 (s, 2H), 7.77 (d, J = 13.4 Hz, 2H), 7.52 (t, J = 9.1 Hz, 4H), 7.39 (dt, J = 14.7, 7.8 Hz, 5H), 7.31 (dd, J = 16.7, 7.7 Hz, 3H), 7.19 (s, 1H), 7.11 (s, 1H), 7.04 (s, 2H), 4.85 (d, J = 9.0 Hz, 2H), 4.45 (t, J = 9.9 Hz, 2H), 4.27 (d, J = 3.1 Hz, 2H), 2.22 (d, J = 4.8 Hz, 6H). 13C NMR (126 MHz, dms) δ 170.16, 167.57, 165.90, 154.45, 143.80, 130.21, 129.17, 129.09, 129.04, 128.64, 126.55, 126.07, 125.78, 125.47, 125.31, 122.08, 121.39, 120.35, 115.60, 110.34, 78.59, 72.40, 43.21, 11.78, 9.23.

(Z)-3-((4-(2-chloroacetamido)-3,5-dimethyl-1H-pyrrol-2-yl)methylene)-2-oxo-N-(2-phenylpropan-2-yl)indoline-5-carboxamide (RAR-13-15, 273564, **193**)

Synthesized using the protocol described in **143**. Yields a brown solid, 14.2 mg, 15%. Molecular Formula: C₂₇H₂₇ClN₄O₃ ESI-MS calc: 490.18 ESI-MS found: 491.1832 [M+1], 513.1656 [M+Na] HPLC: 6.63. 1H NMR (500 MHz, DMSO-d₆) δ 13.52 (s, 1H), 11.06 (s, 1H), 9.53 (s, 1H), 8.24 (s, 1H), 8.19 (d, J = 1.8 Hz, 1H), 7.68 (s, 1H), 7.64 (dd, J = 8.1, 1.7 Hz, 1H), 7.40 (dd, J = 7.9, 1.8 Hz, 3H), 7.28 (t, J = 7.8 Hz, 2H), 7.16 (dd, J = 8.3, 6.3 Hz, 1H), 6.91 (d, J = 8.1 Hz, 1H), 4.26 (s, 2H), 2.20 (d, J = 8.2 Hz, 6H), 1.69 (s, 6H). 13C NMR (126 MHz, dms) δ 170.12, 166.37, 165.75, 148.67, 143.56, 140.59, 132.03, 128.86, 128.24, 127.26, 126.00, 125.65, 125.11, 124.86, 124.66, 121.37, 117.90, 108.94, 55.69, 43.14, 30.13, 12.07, 9.61.

(R,Z)-3-((4-(2-chloroacetamido)-3,5-dimethyl-1H-pyrrol-2-yl)methylene)-N-(1-(4-chlorophenyl)ethyl)-2-oxoindoline-5-carboxamide (RAR-13-19, 273583, **194**)

Synthesized using the protocol described in **143**. Yields a brown solid, 43.5 mg, 100%. Molecular Formula: C₂₆H₂₄Cl₂N₄O₃ ESI-MS calc: 510.12 ESI-MS found: 511.12917 [M+1] HPLC: 6.723. 1H NMR (499 MHz, DMSO-d₆) δ 13.52 (s, 1H), 11.08 (d, J = 7.8 Hz, 1H), 9.53 (s, 1H), 8.64 (dd, J = 7.9, 5.3 Hz, 2H), 8.20 (d, J = 1.5 Hz, 1H), 7.67 (dt, J = 8.0, 2.1 Hz, 2H), 7.65 (s, 1H), 7.44 – 7.40 (m, 4H), 7.40 – 7.37 (m, 5H), 6.93 (d, J = 8.1 Hz, 1H), 5.16 (dq, J = 13.7, 7.0 Hz, 1H), 4.26 (d, J = 2.8 Hz, 2H), 2.20 (d, J = 8.4 Hz, 6H), 1.49 (d, J = 7.1 Hz, 3H). 13C NMR (126 MHz, dms) δ 170.31, 169.68, 165.92, 165.35, 144.15, 140.36, 131.73, 130.99, 128.11, 128.01, 127.44, 126.92, 126.09, 125.76, 125.35, 124.44, 123.36, 122.09, 121.43, 120.99, 120.43, 117.37, 108.64, 55.81, 42.72, 22.10, 11.65, 9.21.

(R,Z)-3-((4-(2-bromoacetamido)-3,5-dimethyl-1H-pyrrol-2-yl)methylene)-N-(1-(4-fluorophenyl)ethyl)-2-oxoindoline-5-carboxamide (195, RAR-13-26, **CCG-359090**)

This material was prepared using the protocol described for 143. Yields a bright orange solid, 13.7 mg, 23%. HRMS: 541.1106 [M+1, Br⁸¹], HPLC: 6.449. 1H NMR (700 MHz, DMSO-d₆) δ 13.52 (s, 1H), 11.08 (s, 1H), 9.60 (s, 1H), 8.61 (d, J = 8.1 Hz, 1H), 8.20 (s, 1H), 7.68 (d, J = 8.4 Hz, 1H), 7.65 (s, 1H), 7.44 (t, J = 4.8 Hz, 2H), 7.17 – 7.13 (m, 2H), 6.93 (dd, J = 8.2, 2.5 Hz, 1H), 5.19 (q, J = 7.4 Hz, 1H), 4.26 (d, J = 2.4 Hz, 1H), 4.03 (d, J = 2.4 Hz, 1H), 2.22 – 2.18 (m, 6H), 1.51 – 1.48 (m, 3H). 13C NMR (176 MHz, dms) δ 170.07, 167.64, 166.24, 162.00, 155.00, 144.70, 140.72,

132.05, 129.71, 128.41, 127.92, 124.56, 122.76, 121.42, 117.77, 115.96, 115.26, 109.01, 48.19, 29.73, 22.66, 12.01, 9.54.

4.12 References

- (1) Falckenberg, M.; Ullrich, A. Kinases as Targets for Anti-Diabetic Therapy. US20150079108 A1, March 19, 2015.
- (2) Ullrich, A.; Falckenberg, M.; Örfi, Z.; Kéri, G.; ÖRFI, L.; Horváth, Z.; SZOKOL, B.; DOBOS, J.; NEMES, Z. Indolinone Derivatives as Grk5 Modulators. WO2015022437 A1, February 19, 2015.
- (3) Sun, C. L.; Christensen, J. G.; McMahon, G. Discovery and Development of Sunitinib (SU11248): A Multitarget Tyrosine Kinase Inhibitor of Tumor Growth, Survival, and Angiogenesis. In *Kinase Inhibitor Drugs*; John Wiley & Sons, Ltd, 2009; pp 1–39. <https://doi.org/10.1002/9780470524961.ch1>.
- (4) Ngai, M. H.; So, C. L.; Sullivan, M. B.; Ho, H. K.; Chai, C. L. L. Photoinduced Isomerization and Hepatotoxicities of Semaxanib, Sunitinib and Related 3-Substituted Indolin-2-Ones. *ChemMedChem* **2016**, *11* (1), 72–80. <https://doi.org/10.1002/cmdc.201500475>.
- (5) Chu, T. F.; Rupnick, M. A.; Kerkela, R.; Dallabrida, S. M.; Zurakowski, D.; Nguyen, L.; Woulfe, K.; Pravda, E.; Cassiola, F.; Desai, J.; et al. Cardiotoxicity Associated with Tyrosine Kinase Inhibitor Sunitinib. *Lancet Lond. Engl.* **2007**, *370* (9604), 2011–2019. [https://doi.org/10.1016/S0140-6736\(07\)61865-0](https://doi.org/10.1016/S0140-6736(07)61865-0).
- (6) Gehringer, M.; Laufer, S. A. Emerging and Re-Emerging Warheads for Targeted Covalent Inhibitors: Applications in Medicinal Chemistry and Chemical Biology. *J. Med. Chem.* **2018**. <https://doi.org/10.1021/acs.jmedchem.8b01153>.
- (7) Tesmer, V. M.; Kawano, T.; Shankaranarayanan, A.; Kozasa, T.; Tesmer, J. J. G. Snapshot of Activated G Proteins at the Membrane: The Gαq-GRK2-Gβγ Complex. *Science* **2005**, *310* (5754), 1686–1690. <https://doi.org/10.1126/science.1118890>.
- (8) Harbeck, N.; Solca, F.; Gauler, T. C. Preclinical and Clinical Development of Afatinib: A Focus on Breast Cancer and Squamous Cell Carcinoma of the Head and Neck. *Future Oncol.* **2013**, *10* (1), 21–40. <https://doi.org/10.2217/fon.13.244>.
- (9) Keating, G. M. Afatinib: A Review of Its Use in the Treatment of Advanced Non-Small Cell Lung Cancer. *Drugs* **2014**, *74* (2), 207–221. <https://doi.org/10.1007/s40265-013-0170-8>.
- (10) Rowlands, R.; Cato, M. C.; Waldschmidt, H. V.; Bouley, R. A.; Chen, Q.; Avramova, L.; Larsen, S. D.; Tesmer, J. J. G.; White. Structure-Based Design of Selective, Covalent G Protein-Coupled Receptor Kinase 5 Inhibitors | ACS Medicinal Chemistry Letters <https://pubs.acs.org/doi/abs/10.1021/acsmchemlett.9b00365> (accessed Dec 23, 2019).
- (11) Baillie, T. A. Targeted Covalent Inhibitors for Drug Design. *Angew. Chem. Int. Ed.* **2016**, *55* (43), 13408–13421. <https://doi.org/10.1002/anie.201601091>.
- (12) Erian, A. W.; Sherif, S. M.; Gaber, H. M. The Chemistry of α-Haloketones and Their Utility in Heterocyclic Synthesis. *Mol. J. Synth. Chem. Nat. Prod. Chem.* **2003**, *8* (11), 793–865. <https://doi.org/10.3390/81100793>.
- (13) LoPachin, R. M.; Gavin, T.; DeCaprio, A.; Barber, D. S. Application of the Hard and Soft, Acids and Bases (HSAB) Theory to Toxicant–Target Interactions. *Chem. Res. Toxicol.* **2012**, *25* (2), 239–251. <https://doi.org/10.1021/tx2003257>.

- (14) Chaikuad, A.; Koch, P.; Laufer, S. A.; Knapp, S. The Cysteinome of Protein Kinases as a Target in Drug Development. *Angew. Chem. Int. Ed.* **2018**, *57* (16), 4372–4385. <https://doi.org/10.1002/anie.201707875>.
- (15) Kim, M.-S.; Zhong, J.; Pandey, A. Common Errors in Mass Spectrometry-Based Analysis of Post-Translational Modifications. *Proteomics* **2016**, *16* (5), 700–714. <https://doi.org/10.1002/pmic.201500355>.
- (16) Mann, M.; Jensen, O. N. Proteomic Analysis of Post-Translational Modifications. *Nat. Biotechnol.* **2003**, *21*, 7.
- (17) Posocco, B.; Buzzo, M.; Giodini, L.; Crotti, S.; D’Aronco, S.; Traldi, P.; Agostini, M.; Marangon, E.; Toffoli, G. Analytical Aspects of Sunitinib and Its Geometric Isomerism towards Therapeutic Drug Monitoring in Clinical Routine. *J. Pharm. Biomed. Anal.* **2018**, *160*, 360–367. <https://doi.org/10.1016/j.jpba.2018.08.013>.
- (18) Waldschmidt, H. V.; Homan, K. T.; Cato, M. C.; Cruz-Rodríguez, O.; Cannavo, A.; Wilson, M. W.; Song, J.; Cheung, J. Y.; Koch, W. J.; Tesmer, J. J. G.; et al. Structure-Based Design of Highly Selective and Potent G Protein-Coupled Receptor Kinase 2 Inhibitors Based on Paroxetine. *J. Med. Chem.* **2017**, *60* (7), 3052–3069. <https://doi.org/10.1021/acs.jmedchem.7b00112>.
- (19) Waldschmidt, H. V.; Homan, K. T.; Cruz-Rodríguez, O.; Cato, M. C.; Waninger-Saroni, J.; Larimore, K. M.; Cannavo, A.; Song, J.; Cheung, J. Y.; Kirchhoff, P. D.; et al. Structure-Based Design, Synthesis, and Biological Evaluation of Highly Selective and Potent G Protein-Coupled Receptor Kinase 2 Inhibitors. *J. Med. Chem.* **2016**, *59* (8), 3793–3807. <https://doi.org/10.1021/acs.jmedchem.5b02000>.
- (20) Petroff, M. G. V.; Kim, S. H.; Pepe, S.; Dessy, C.; Marbán, E.; Balligand, J.-L.; Sollott, S. J. Endogenous Nitric Oxide Mechanisms Mediate the Stretch Dependence of Ca²⁺ Release in Cardiomyocytes. *Nat. Cell Biol.* **2001**, *3* (10), 867–873. <https://doi.org/10.1038/ncb1001-867>.
- (21) Bers, D. M.; Perez-Reyes, E. Ca Channels in Cardiac Myocytes: Structure and Function in Ca Influx and Intracellular Ca Release. *Cardiovasc. Res.* **1999**, *42* (2), 339–360. [https://doi.org/10.1016/S0008-6363\(99\)00038-3](https://doi.org/10.1016/S0008-6363(99)00038-3).
- (22) Fearnley, C. J.; Roderick, H. L.; Bootman, M. D. Calcium Signaling in Cardiac Myocytes. *Cold Spring Harb. Perspect. Biol.* **2011**, *3* (11). <https://doi.org/10.1101/cshperspect.a004242>.
- (23) Meng, G.; Liu, C.; Qin, S.; Dong, M.; Wei, X.; Zheng, M.; Qin, L.; Wang, H.; He, X.; Zhang, Z. An Improved Synthesis of Sunitinib Malate via a Solvent-Free Decarboxylation Process. *Res. Chem. Intermed.* **2015**, *41* (11), 8941–8954. <https://doi.org/10.1007/s11164-015-1939-z>.
- (24) Zhang, L.; Zheng, Q.; Yang, Y.; Zhou, H.; Gong, X.; Zhao, S.; Fan, C. Synthesis and in Vivo SAR Study of Indolin-2-One-Based Multi-Targeted Inhibitors as Potential Anticancer Agents. *Eur. J. Med. Chem.* **2014**, *82*, 139–151. <https://doi.org/10.1016/j.ejmech.2014.05.051>.

Chapter 5. Future Directions in the Age of Covalent GRK5 Inhibitors

5.1 Expanding the SAR of the Indolinone Scaffold Could Offer New Insights

Herein, is described the current efforts towards making selective GRK5 inhibitors using a covalent strategy. It was proven that the indolinone scaffold, featured in CCG-273220, offers exceptional GRK5 affinity and selectivity. Additionally, the best pendants for the free phenyl ring, the benzylic position and the appropriate stereochemistry at the benzylic position were determined. These efforts are a strong start but there is still much that could be done. First, the SAR around the pyrrole linker and a combination of the SAR strategies for the other pendants has yet to be explored.

As this series has been developed to provide SAR around the phenyl ring and the benzylic positions, a combination strategy can be used to explore subtle synergistic effects. CCG-273563 and CCG-273564 were designed to address the potential metabolic liability of the benzylic position. GRK5 seems to prefer *para* pendants on the phenyl ring (as seen in CCG-273441, CCG-273443, and CCG-273583), thus by combining a benzylic pendant from CCG-273563 or CCG-273564 and one of the *para* pendants a greater level of activity could be achieved (Figure 5.1). As the 4-fluoro and 4-pyridyl pendants (273441 and 273423 respectively) have the best level of activity, these pendants serve as a good starting point for the next SAR campaign.

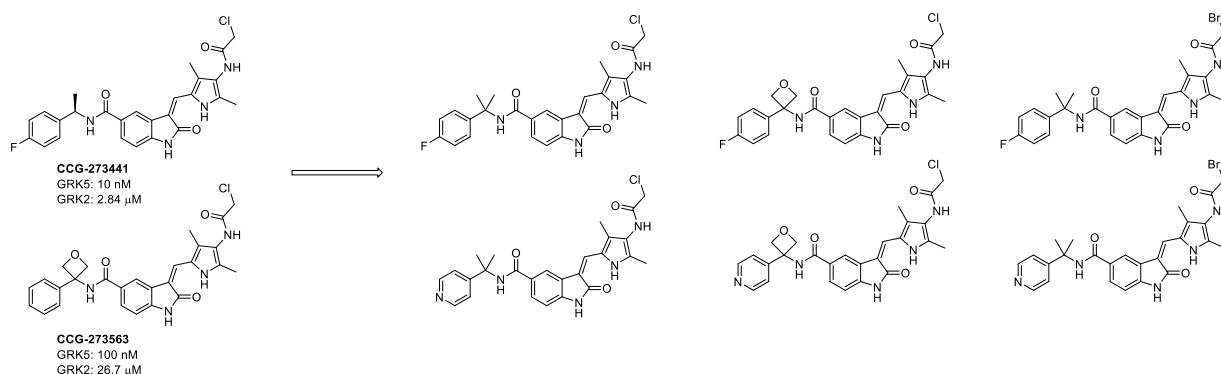


Figure 5.1 Design analogues which demonstrate a combined strategy for blocking metabolism and maintaining high levels of affinity for GRK5. Additional analogues can be designed but are not shown.

To further expand the SAR of this series, the pyrrole linker can be explored to understand the importance of the pseudo-seven membered ring on activity and solubility. The initial lead

compound, Sunitinib, contains this same pseudo-seven membered ring, and it has been suggested that this locked conformation leads to less isomerization, and more exposure to the active isomer of the compound.^{1,2} In order to validate this principal, other heterocycles could replace the pyrrole linker leading to either a loss of the pseudo-seven membered ring, or a weaker intramolecular interaction. Additionally, the 3-methyl and 5-methyl pendants can be removed from the pyrrole linker, as these too may be contributing to the overall locked conformation (Figure 5.2).^{3,4} This strategy provides a number of diverse new compounds which may not have a loss in activity, as our model suggests this linker is solvent exposed and therefore may not be critical to binding

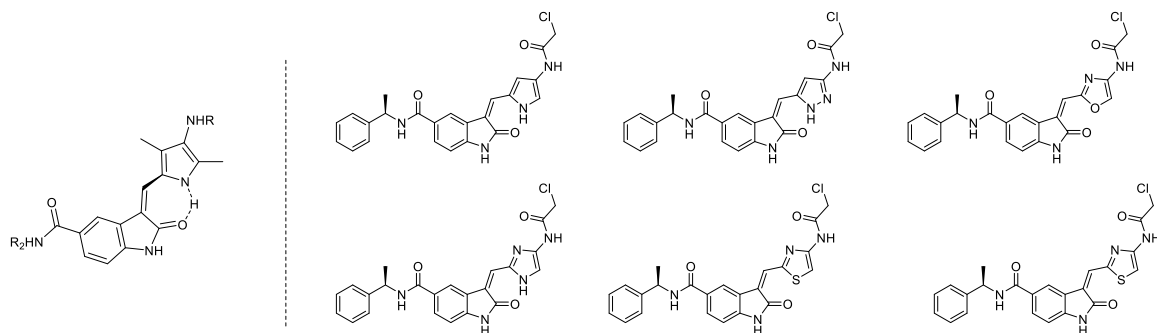


Figure 5.2 Pseudo-seven membered ring shown in the structure on the left. This pseudo-ring is what confers conformational restriction and stability to the inhibitors. To the right, compounds designed with various heterocyclic linkers. Some linkers can maintain the pseudo-seven membered ring, while others no longer have the hydrogen bond donor which allows the formation of this pseudo ring. Additional inhibitors can be designed with the pendants used in developing the SAR campaign in Chapter 4.

affinity. Such an SAR campaign would greatly expand the arsenal of GRK5 covalent selective compounds and facilitate elucidating the role of GRK5 in various disease states.

Perhaps one of the most interesting routes this project could take would be to explore reversibly covalent warheads. This idea was initially proposed in Chapter 2 but was not pursued due to the lack of potency of the initial pyrrolopyrimidine series. It is generally understood that the compounds carrying reversible covalent warheads need to have a high affinity for GRK5, as the experimental design dictates that such compounds undergo a “wash out” phase.^{5,6} With insufficient binding, the compounds could be washed out of the experiment before the covalent interaction can take place. However, the development of the indolinone scaffold offers a second chance at this avenue. So far, only one reversible covalent compound has been made, CCG-273240 (GRK5 IC_{50} = 250 nM). In initial mass spectrometry experiments, this compound was found to be non-covalent. However, this result is inconclusive because it cannot be determined whether or not the covalent interaction has not happened, or whether it has happened and then the reversible

disconnection has also occurred. In order to determine this, a wash-out experiment must be performed. As this wash-out experiment is highly dependent on the K_{on} rate of the compound, a

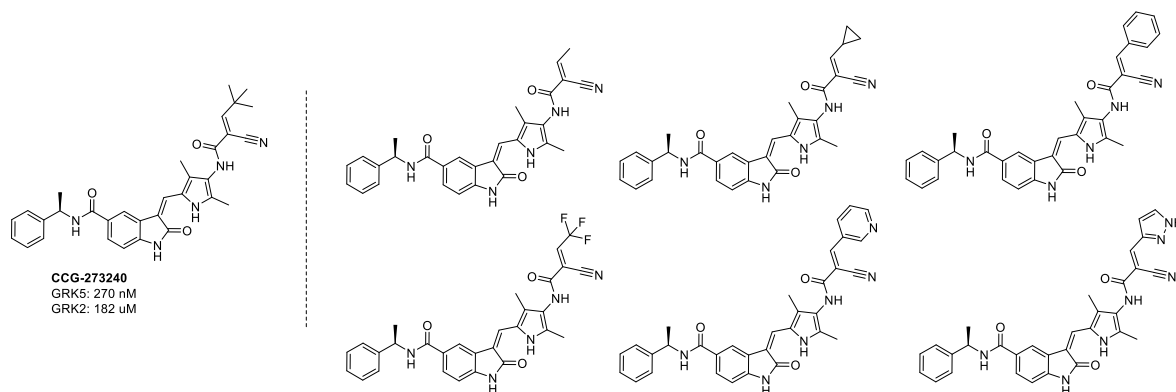


Figure 5.3 Reversible covalent inhibitor, CCG-273240, and designed analogues. A variety of pendants will need to be explored to gather an understanding variability of residence times for these analogues. Pendants are designed to increase aqueous solubility to balance the increase in lipophilicity that is observed in these analogues.

longer incubation for the initial covalent interaction will be needed. From the experiments with CCG-273182, it can be assumed that the incubation time will need to be around 3 h.

Recently, there has been a large amount of work concerning how to make tunable reversible covalent inhibitors.^{7,8} It is envisioned that this work could be translated to the indolinone series. Taunton et. al. have been able to develop a series of reversible warheads, that have demonstrated the ability to bind, and then come off the target residue with an increased residence time. It is possible to make a series of indolinones that contain these warheads, and have the optimized pendants explored in the initial campaign (Chapter 4). These reversible warheads would offer an avenue to avoid the potentially toxic side reactions that could arise from the reactive chloro-ketone warhead. Additionally, as the turnover time of GRK5 is not known, having an inhibitor with tunable residence time will provide another avenue to adequate inhibitor exposure if the turnover of GRK5 proves to be shorter than 24 h. Initially, there will have to be two classes of reversible warheads, as it is unknown whether an aliphatic or aromatic branch will be most beneficial for this series of inhibitors (Figure 5.3). Pleasingly, these compounds can be accessed through a common advanced intermediate, making rapid expansion of the series viable.

These new compounds can then be tested within the washout experiment parameters determined by Taunton et. al. to develop an understanding of how this strategy applies to GRK5 inhibitors. For further ways to avoid metabolic liability, it is envisioned that the strategy applied

to the indazole series, from which CCG-215022 is derived, can be applied to the indolinone series. In a new series of compounds, a fluorine walk can be performed around the indolinone ring, to limit metabolic liabilities on the core scaffold. The inclusion of the pendants from the initial SAR of the indazole series can further limit the metabolic liability of both the phenyl pendant and the benzylic position. However, metabolic stability cannot be so high as to prevent clearance of the compounds altogether. Rather, designed analogues must strike a balance between exposure and clearance to avoid cytotoxicity. As these inhibitors feature highly reactive warheads, limited cellular exposure is desired, as hitting multiple side targets can produce undesirable pharmacokinetic effects. Thus, only 1-2 metabolic strategies should be applied to avoid high cellular exposure, while also ensuring the inhibitors are not rapidly cleared thereby limiting efficacy.

Ultimately, this new series can give rise to a new arsenal of GRK5 selective inhibitors that feature warheads of variable reactivity and residence time. Once this has been achieved, additional biological assays can be performed to better understand the role of GRK5 in multiple disease states. This initial work will set a template for further work on GRK5 and indeed other kinase targets for which isoform selectivity remains a challenge.

5.2 Combining Linkers and Covalent Warheads can Rapidly Expand the Current Arsenal

As was laid out in the previous section, there are numerous ways to tune the residence time of a targeted covalent inhibitor, using reversible covalent warheads. While this is a valid approach, there are ways to tune the residence time of a targeted covalent inhibitor (TCI) through the use of irreversible warheads. Indeed, there have been numerous examples of FDA approved TCIs since the 1960s (although some compounds were not known to covalent at the time of approval). Perhaps one of the most interesting ways to introduce new warheads and linkers to the indolinone scaffold

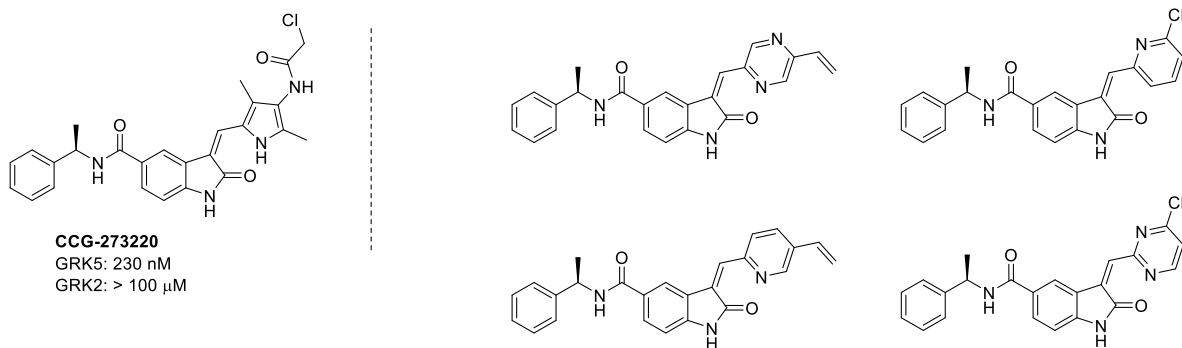


Figure 5.4 New analogues which possess a linker with a covalent element already in place.

is to combine the two elements together to form one linker, with a covalent element present. Examples of this approach are chloro-heterocycles and vinyl-heterocycles. Both use a different type of covalent engagement (S_NAr vs. Michael Addition, respectively), and have been used in various other examples of developing TCIs. In this case, the vinyl heterocycles offer the unique opportunity to tune the residence time of an irreversible covalent inhibitor.⁹ By making a few modifications to the current synthetic route, a larger variety of indolinone TCIs can be accessed quickly all of which would possess unique intellectual property (Figure 5.4).

Other approaches could include the issue of previously developed, but synthetically challenging warheads. As was demonstrated previously, the vinyl sulfone in **CCG-273182** can form a covalent engagement in 3 h. It would be interesting to see if the reactivity of the vinyl warheads could be increased to produce a covalent interaction within 30 min. One of the ways that this could be achieved would be to use the vinyl propellene warhead, which has a highly strained 1,1,1-propellane ring.¹⁰⁻¹² A free cysteine, Cys474 in this case, could open this highly strained ring, and therefore satisfy the enthalpic needs of the system, producing a rapid irreversible covalent engagement.

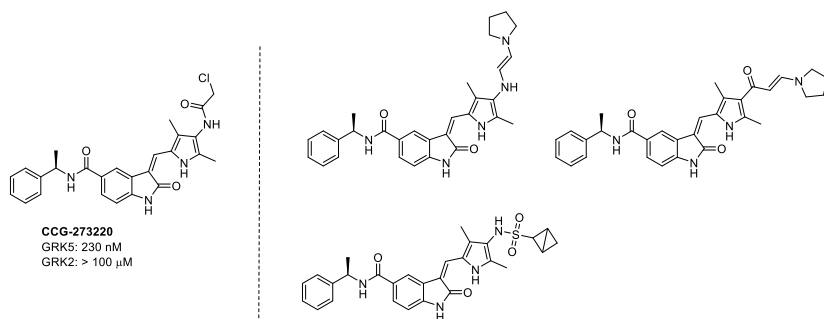


Figure 5.5 New enamine and sulfone warheads could be used to explore how to tune reactivity of a covalent warhead.

Additionally, using the information that has already been published by Ullrich and co-workers, redesign of covalent warheads to include crucial pieces of architecture that have validated activity is feasible. Of the options, the addition of a terminal amine appears to be the most important to include within the linker. Indeed, as demonstrated by **CCG-271421**, the terminal amine plays a crucial role in not only solubility of the compound, but also the activity, resulting in a low nanomolar compound. A terminal amine was included within this series of TCIs, see **CCG-273221**, but was not successful in retaining the level of activity seen in **CCG-271421**. This drop in potency is attributed to the ability of the highly flexible BI warhead to interact with the GRK5 P-loop. However, it is possible that the construction of a more constrained,

Additionally, using the information that has already been published by Ullrich and co-workers, redesign of covalent warheads to include crucial pieces of architecture that have validated activity is feasible. Of the options, the addition of a terminal amine

enamine Michael acceptor could regain that level of low anomolar activity while also increasing the solubility of the compound. Therefore, we propose the construction of enamine Michael acceptor linkers, with varying degrees of flexibility and varying levels of basicity (Figure 5.5). In these examples, both the original amide orientation and the reversed amide orientation are possible, allowing for exploration of the planar requirements for covalent action in this series. Additionally, the reactivity of each enamine will vary with either an electron sink (ketone) or an electron donor (amine) available in the γ -position.

5.3 Biological Evaluation of GRK5 Inhibitors Can Clarify Role of GRK5 in Cardiovascular Disease

Initial testing of these compounds indicates that GRK5 inhibitors do not affect cardiomyocyte contractility in the same fashion as GRK2 inhibitors. Rather, GRK5 inhibitors directly affect Ca^{2+} transience. As this is not a known function of GRK5, additional studies to understand how this relationship between calcium transience and GRK5 are needed.

5.4 Biological Evaluation of GRK5 Inhibitors Can Provide New Treatments for Cancer, and Neurodegenerative Diseases

In neurodegeneration, studies have shown that GRK5 hyperexpression is a hallmark of Parkinson's Disease. Meanwhile, GRK5 hypoexpression has been found to be detrimental in Alzheimer's Disease studies. Thus, the indolinone series can serve as an interesting probe for Parkinson's Disease. The indolinone series has not yet been designed to accommodate a central nervous system target, however, it is entirely possible to determine the effect of GRK5 inhibition in *ex vivo* studies. There is literature available on the effects of GRK5 genetic knockout on Parkinson's disease outcomes, and these probes provide an unexplored avenue for studying genetically unaltered systems to continue this work.¹³

Additionally, GRK5 plays an important role in migration of cancer cells, and furthermore, could impact the utility of currently marked cancer therapies. Sommer et. al. have shown that GRK5 plays a special role in the migration of breast cancer cells.¹⁴ Indeed, Sommer and coworkers were able to show that genetic downregulation of GRK5 hinders the migration of these cancerous cells. Such data indicates that these indolinone derived compounds could be used to produce a similar result. This effect also indicates that there could exist a synergistic effect between GRK5 inhibitors and standard-of-care breast cancer treatments. This does appear to be the case. Lagman et. al. have described the effect of genetic knockdown of GRK5 on the susceptibility of triple

negative breast cancer cells against paclitaxel. Lagman and co-workers found that when GRK5 is downregulated breast cancer cells are far more susceptible to paclitaxel.¹⁵ Therefore, it is envisioned that CCG-273463, CCG-271423 or CCG-359090, could be used to investigate whether a synergistic effect does occur when taken with paclitaxel.

5.5 Concluding Remarks

The initial intent of this project was to develop GRK5 inhibitors for the express purpose of investigating the role of GRK5 in cardiovascular disease, however, this project has grown to encompass several fields. The utility of selective GRK5 inhibitors spans from cardiovascular disease to neurodegenerative disease to cancer. As selective GRK5 inhibitors have been the missing piece in many biological studies in the past, it is fully expected these compounds will serve as useful probes in various systems to help uncover the underlying mechanism of several diseases. Meanwhile, this campaign serves as an excellent example of how to leverage a covalent strategy to achieve selectivity. Additionally, this work was able to establish a new covalent handle outside the kinase domain, Cys474, which was previously not utilized in the kinase drug discovery realm.

5.6 References

- (1) Ngai, M. H.; So, C. L.; Sullivan, M. B.; Ho, H. K.; Chai, C. L. L. Photoinduced Isomerization and Hepatotoxicities of Semaxanib, Sunitinib and Related 3-Substituted Indolin-2-Ones. *ChemMedChem* **2016**, *11* (1), 72–80. <https://doi.org/10.1002/cmdc.201500475>.
- (2) Posocco, B.; Buzzo, M.; Giodini, L.; Crotti, S.; D’Aronco, S.; Traldi, P.; Agostini, M.; Marangon, E.; Toffoli, G. Analytical Aspects of Sunitinib and Its Geometric Isomerism towards Therapeutic Drug Monitoring in Clinical Routine. *J. Pharm. Biomed. Anal.* **2018**, *160*, 360–367. <https://doi.org/10.1016/j.jpba.2018.08.013>.
- (3) Bissantz, C.; Kuhn, B.; Stahl, M. A Medicinal Chemist’s Guide to Molecular Interactions. *J. Med. Chem.* **2010**, *53* (14), 5061–5084. <https://doi.org/10.1021/jm100112j>.
- (4) Brameld, K. A.; Kuhn, B.; Reuter, D. C.; Stahl, M. Small Molecule Conformational Preferences Derived from Crystal Structure Data. A Medicinal Chemistry Focused Analysis. *J. Chem. Inf. Model.* **2008**, *48* (1), 1–24. <https://doi.org/10.1021/ci7002494>.
- (5) Lee, C.-U.; Grossmann, T. N. Reversible Covalent Inhibition of a Protein Target. *Angew. Chem. Int. Ed.* **2012**, *51* (35), 8699–8700. <https://doi.org/10.1002/anie.201203341>.
- (6) Smith, S.; Keul, M.; Engel, J.; Basu, D.; Eppmann, S.; Rauh, D. Characterization of Covalent-Reversible EGFR Inhibitors. *ACS Omega* **2017**, *2* (4), 1563–1575. <https://doi.org/10.1021/acsomega.7b00157>.
- (7) Bradshaw, J. M.; Mcfarland, J. M.; Paavilainen, V. O.; Bisconte, A.; Tam, D.; Phan, V. T.; Romanov, S.; Finkle, D.; Shu, J.; Patel, V.; et al. Prolonged and Tunable Residence Time Using Reversible Covalent Kinase Inhibitors. *Nat. Chem. Biol. Camb.* **2015**, *11* (7), 525–531. <http://dx.doi.org/10.1038/nchembio.1817>.

- (8) Miller, R. M.; Taunton, J. Chapter Four - Targeting Protein Kinases with Selective and Semipromiscuous Covalent Inhibitors. In *Methods in Enzymology*; Shokat, K. M., Ed.; Protein Kinase Inhibitors in Research and Medicine; Academic Press, 2014; Vol. 548, pp 93–116. <https://doi.org/10.1016/B978-0-12-397918-6.00004-5>.
- (9) Gehringer, M.; Laufer, S. A. Emerging and Re-Emerging Warheads for Targeted Covalent Inhibitors: Applications in Medicinal Chemistry and Chemical Biology. *J. Med. Chem.* **2018**. <https://doi.org/10.1021/acs.jmedchem.8b01153>.
- (10) Tetracyclo[5.1.0.01,6.02,7]octane, a [1.1.1]propellane derivative, and a new route to the parent hydrocarbon | Journal of the American Chemical Society <https://pubs.acs.org/doi/abs/10.1021/ja00308a053> (accessed Dec 31, 2019).
- (11) Lopchuk, J. M.; Fjelbye, K.; Kawamata, Y.; Malins, L. R.; Pan, C.-M.; Gianatassio, R.; Wang, J.; Prieto, L.; Bradow, J.; Brandt, T. A.; et al. Strain-Release Heteroatom Functionalization: Development, Scope, and Stereospecificity. *J. Am. Chem. Soc.* **2017**, *139* (8), 3209–3226. <https://doi.org/10.1021/jacs.6b13229>.
- (12) Gianatassio, R.; Lopchuk, J. M.; Wang, J.; Pan, C.-M.; Malins, L. R.; Prieto, L.; Brandt, T. A.; Collins, M. R.; Gallego, G. M.; Sach, N. W.; et al. Strain-Release Amination. *Science* **2016**, *351* (6270), 241–246. <https://doi.org/10.1126/science.aad6252>.
- (13) Nicoletti, G.; De Luca, V.; Tarantino, P.; Gagliardi, M.; Iannello, G.; Novellino, F.; Morelli, M.; Annesi, G.; Quattrone, A. Role of G-Protein Coupled Receptor Kinase 5 Gene in Cognitive Impairment in Parkinson's Disease. *Psychiatry Res.* **2015**, *230* (3), 975–977. <https://doi.org/10.1016/j.psychres.2015.11.026>.
- (14) Sommer, A.-K.; Falcenberg, M.; Ljepoja, B.; Fröhlich, T.; Arnold, G. J.; Wagner, E.; Roidl, A. Downregulation of GRK5 Hampers the Migration of Breast Cancer Cells. *Sci. Rep.* **2019**, *9* (1), 1–13. <https://doi.org/10.1038/s41598-019-51923-1>.
- (15) Lagman, J.; Sayegh, P.; Lee, C. S.; Sulon, S. M.; Jacinto, A. Z.; Sok, V.; Peng, N.; Alp, D.; Benovic, J. L.; So, C. H. G Protein-Coupled Receptor Kinase 5 Modifies Cancer Cell Resistance to Paclitaxel. *Mol. Cell. Biochem.* **2019**, *461* (1), 103–118. <https://doi.org/10.1007/s11010-019-03594-9>.